

UNIVERSITÀ DEGLI STUDI DI NAPOLI FEDERICO II



Scuola di Dottorato SCIENZE DELLA TERRA “GIUSEPPE DE LORENZO”

DOTTORATO IN SCIENZE ED INGEGNERIA DEL MARE (XXIV CICLO)

Tesi di Dottorato

**PHYTOPLANKTON ADAPTATION TO MARINE ECOSYSTEMS:
INSIGHTS INTO PHOTOPHYSIOLOGICAL FUNCTIONAL DIVERSITY**

Candidato

VASCO GIOVAGNETTI

Tutor

DR. VINCENZO SAGGIOMO

Co-Tutor

DR. CHRISTOPHE BRUNET

Coordinatore del Dottorato

PROF. ALBERTO INCORONATO

ANNO 2011

ABSTRACT

PHYTOPLANKTON ADAPTATION TO MARINE ECOSYSTEMS: INSIGHTS INTO PHOTOPHYSIOLOGICAL FUNCTIONAL DIVERSITY

The aim of this study was to investigate the diversity of the photoprotective responses activated by phytoplankton at short temporal scales, i.e. the non-photochemical quenching of Chl *a* fluorescence (NPQ) associated with the xanthophyll cycle (XC) activity. In this work, we tested the hypothesis that the process of photoprotection, in terms of modulation, extent and efficiency, might be considered as a functional trait in phytoplankton. This ecophysiological work has been performed on four species belonging to the *phylum* of Stramenopiles. The ecological diversity has been taken into account by studying the photoresponses of species isolated either in surface or deeper water layers, as well as of species adapted to grow either in oceanic or coastal or upwelling ecosystems. Species distinct photoresponses have been also assessed in relation to cell size constraints, using one microplanktonic and three picoplanktonic species.

The relation between phytoplankton ecophysiological functional diversity and ecological adaptation has been studied in three picoeukaryotes ($< 3.0 \mu\text{m}$) isolated from distinct ecosystems, through the analysis of the physiological response curves obtained by plotting a measured variable against a range of a factor (i.e. light) affecting that variable. The photophysiological flexibility as a functional trait has been discussed in relation to niche adaptation. Because of their peculiar set of biological and ecological features, related to their minute cell size, and because of their very narrow size range, picoeukaryotes are interesting model organisms to address (and answer) questions concerning the ecophysiology of algae.

The integrative physiological processes (i.e. photoacclimation, photoregulation, photosynthesis, growth), which are in part activated or modified in relation to changing light conditions, have been deeply investigated in the microplanktonic coastal diatom, *Pseudo-nitzschia multistriata* (Bacillariophyceae). A great plasticity in functioning and regulation has been shown to characterize the photoprotective/photoacclimative processes (XC and NPQ) of this diatom, in agreement with its ecological properties.

ACKNOWLEDGEMENTS

First of all, I am so thankful to “The Light”.

I would like to thank my tutor, Dr. Vincenzo Saggiomo, for his support and help during my PhD program.

Since the daily activity of work, I would like to deeply thank my co-tutor, Dr. Christophe Brunet. During these three years of PhD journey, many occasions of growth and many *stimuli* come from his guide. Actually, my refreshed passion and curiosity toward the scientific studies and questions are largely due to him. Thanks. Strictly related to this, an enormous *grazie* goes to my close laboratory colleagues (Fabio, Ferdinando, Maria Letizia, Serena): without your help, each single achievement would not have been possible.

Furthermore, all the L.E.E.P. and M.E.C.A. groups are greatly acknowledged for all the help, technical assistance, support, and inspiring talks that we had.

I'd like to deeply thank my external refer, Johann Lavaud, for all his valuable suggestions concerning this manuscript.

To my family (Fabrizio, Daniela, Elena), and to Agostina and family (you are so special)...no words can explain the love, the respect and the admiration I feel when I ‘think’ about you. The man, that I am, is just because of you. I feel so lucky about it. Seriously.

To all my extended family, to the brothers and sisters that I had the honor and pleasure to meet during my life path, either in my home town (Osimo) or in Naples. On purpose, I decided to mention no names, just because no ‘acknowledgement section’ could express all the gratitude, respect and love I feel. You know who you are. You guys are such a great source of inspiration, under private and professional life aspects.

Lastly, I cannot forget my ‘crates’. So many journeys. So much to experience.

Peace.

Abbreviations

α^B	Photosynthetic Efficiency
Ax	Antheraxanthin
ADP	Adenosine Diphosphate
ATP	Adenosine Triphosphate
CAB	Chlorophyll <i>a/c</i> -Binding Proteins
Chl	Chlorophyll
Cyt	Cytochrome
DCM	Deep Chlorophyll Maximum
Dd	Diadinoxanthin
DDE	Diadinoxanthin De-Epoxidase
DPS	De-Epoxidation State
Dt	Diatoxanthin
DEP	Diatoxanthin Epoxidase
DTT	Dithiotreitol
$_{abs}ETR_{max}$	Absolute Electron Transport Rate
$_{rel}ETR_{max}$	Relative Electron Transport Rate
Ek	Saturation Irradiance
FAD	Flavine Adenine Dinucleotide
FCP	Fucoxanthin Chlorophyll <i>a/c</i> -Binding Proteins
Fm	Maximal Fluorescence after dark acclimation
Fm'	Maximal Fluorescence in the light acclimated state
Fd	ferredoxin
FNR	Fd-NADP ⁺ -oxidoreductase
Fv	Variable Fluorescence after dark acclimation
Fv'	Variable Fluorescence in the light acclimated state
Fuco	Fucoxanthin
HL	High Light
LHC	Light Harvesting Complex
LL	Low Light

MGDG Monogalactosyldiacylglycerol
ML Moderate Light
NADH Nicotinamide Adenine Dinucleotide
NADPH Nicotinamide Adenine Dinucleotide Phosphate
NPQ Non-Photochemical Fluorescence Quenching
Neox Neoxanthin
PC Plastocyanin
PCP Peridinin Chlorophyll *a/c*-Binding Proteins
PFD Photon Flux Density
Pheo Pheophytin
PPC Photoprotective Carotenoids
PQ Photochemical Quenching
PQH₂ Plastoquinone Pool
PSI Photosystem I
PSII Photosystem II
PsbS PSII Subunit S Protein
PSU Photosynthetic Unit
Q Quinone
qE High-Energy-State Quenching
qI Photoinhibitory Quenching
qT Quenching Related to State Transitions
RC Reaction Center
RedCAP Red Lineage of Chl *a/b*-Binding like Proteins
RLC Rapid Light Curves
ROS Reactive Oxygen Species
RuBP Ribulose-1,5-Bisphosphate
Rubisco Ribulose-1,5-Bisphosphate Carboxylase Oxygenase
SL Sinusoidal Light
VDE Violaxanthin De-Epoxidase
Vx Violaxanthin
XC Xanthophyll Cycle

Y_z Tyrosine (D1-Tyr161; situated in the D1 protein)

ZEP Zeaxanthin Epoxidase

Zx Zeaxanthin

Table of contents

ABBREVIATIONS	i
TABLE OF CONTENTS	iv
LIST OF FIGURES	vii
LIST OF TABLES	xvi
CHAPTER 1 General introduction	2
CHAPTER 2 Introduction to photosynthesis and photoregulation	9
2.1 The photosynthetic process	10
2.2 Photoadaptation, photoacclimation and photoregulation	14
2.3 Photoacclimation	16
2.3.1 Chloroplast size, number, morphology and distribution	17
2.3.2 Light-harvesting complexes and thylakoid membranes	17
2.3.3 Pigments composition and function	21
2.4 Photoregulation and the xanthophyll cycle	23
2.4.1 State of art	24
2.4.2 Biochemical aspects of the xanthophyll cycle	27
2.4.2.1 Carotenoid biosynthesis	27
2.4.2.2 Localization of the xanthophyll cycle pigments	28
2.4.2.3 Properties of the enzymes involved in the xanthophyll cycle	30
2.4.3 Xanthophyll cycle functioning and non-photochemical fluorescence quenching	34
2.4.3.1 State of art	34
2.4.3.2 Function of the Vx cycle and NPQ mechanism	37
2.4.3.3 Function of the Dd cycle and NPQ mechanism	38
2.5 Xanthophyll cycle and ecophysiology of algae	41
CHAPTER 3 Biology and ecology of picoeukaryotes	45
3.1 Introduction	46
3.2 Ecological concept of small cell size	48

3.3 Biology of picoeukaryotes	51
3.4 Picoeukaryotes as model organisms picoeukaryotes	54
CHAPTER 4 Materials and methods	61
4.1 Algal models and culture maintenance	62
4.2 Determination of growth rate	63
4.3 Estimation of cell size and volume	65
4.4 Pigment analysis	65
4.5 Absorption spectrum analysis	66
4.6 Active chlorophyll <i>a</i> fluorescence and photosynthetic efficiency analysis	67
4.6.1 Chl <i>a</i> fluorescence	68
4.6.2 Principle of the Phyto-PAM Fluorometer	69
4.6.3 Determination of the photochemical efficiency of the Photosystem II (PSII)	70
4.6.4 Determination of non-photochemical fluorescence quenching (NPQ)	71
4.6.5 Determination of Rapid Light Curves (RLC)	74
4.7 Biochemical properties of cells	75
4.7.1 Determination of particulate organic carbon and nitrogen	75
4.7.2 Analysis of macromolecular pools and silica allocation	76
4.8 Environmental factors measurements	77
4.9 Statistical analysis	77
CHAPTER 5 Xanthophyll cycle ecophysiology in the context of photoacclimation processes: experimental approaches on <i>Pseudo-nitzschia multistriata</i>	78
5.1 Introduction	79
5.2 Algal model and culture conditions	81
5.3 Xanthophyll cycle functioning and non-photochemical fluorescence quenching	83
5.3.1 Experimental design, sampling strategy and analyzed parameters	83
5.3.2 Results	84
5.3.2.1 Pigment content changes and xanthophyll cycle activation	84
5.3.2.2 Variable fluorescence and non-photochemical fluorescence quenching	95
5.3.3 Discussion	98
5.4 Xanthophyll cycle ecophysiology in response to different kinetics of light change	104

5.4.1 Experimental design, sampling strategy and analyzed parameters	104
5.4.2 Results	106
5.4.2.1 Variable fluorescence measurements	106
5.4.2.2 Photoprotective responses	106
5.4.2.3 Photosynthetic and accessory pigment content changes	121
5.4.3 Discussion	125
5.5 Effect of light history on photoprotection	130
5.5.1 Experimental design, sampling strategy and analysed parameters	130
5.5.2 Results	132
5.5.2.1 Growth rate and photosynthetic parameters	132
5.5.2.2 Variable fluorescence measurements and photoprotective response	132
5.5.2.3 Photosynthetic and accessory pigments content changes	138
5.5.3 Discussion	140
CHAPTER 6 Functional relation between growth, photosynthetic rate and regulation in	144
the coastal picoeukaryote <i>Phaeomonas</i> sp. RCC503 (Pinguiphyceae, Stramenopiles)	
CHAPTER 7 Growth and photophysiological response curves of the two picoplanktonic	168
<i>Minutocellus</i> sp. RCC967 and RCC703 (Bacillariophyceae)	
CHAPTER 8 General discussion and conclusions	193
BIBLIOGRAPHY	201

List of Figures

Fig. 2.1: Scheme representing the organization of the photosystem II and the light-harvesting complex II in the thylakoid membrane of higher plants. CP24, CP26 and CP29 are minor light-harvesting proteins. CP43 and CP47 are internal antenna chlorophyll-protein complexes. D1 and D2 are the main components of the reaction center (RC) with binding sites for electron acceptor quinones (Q_A , Q_B). P680 is a chlorophyll dimer. Other cofactors associated with D1/D2: phaeophytin (Phe), non-haem iron (Fe), Mn-cluster. Accessory chlorophylls and β -carotene are not shown. Chl, chlorophyll; cyt b_6/f , cytochrome b_6/f complex; PQH_2 , plastoquinone pool; PsbS, PSII S subunit; Y_Z , D1-Tyr161. Arrows represent the electron flow along the photosynthetic chain. After Szábo *et al.* (2005). For a more detailed description, see Ferreira *et al.* (2004). 12

Fig. 2.2: Z-Scheme of electron transport in photosynthesis by Govindjee and Wilbert Veit (2010; gov@illinois.edu). The electron transport from H_2O to nicotinamide adenine dinucleotide ($NADP^+$) is traced from left to right on the diagram that uses the Photosystems II and I. This process is initiated by the simultaneous absorption of light by two antenna complexes, represented by clusters of colored balls. The absorbed energy is then transferred to the reaction center chlorophylls (Chl) P680 and P700 and this powers the entire process, during which 2 water molecules are split into 4 protons ($4H^+$), 4 electrons ($4e^-$) and 1 oxygen molecule (O_2). 13

Fig. 2.3: (a) Transversal cut of a diatom cell (*Phaeodactylum tricornutum*, Bacillariophyceae; Lavaud, 2007) showing the nucleus (N), the mitochondria (m) and the cell-wall silica valves (v). The chloroplast contains thylakoids grouped in three bands (t), surrounded by an inner “girdle lamella” of three thylakoids (gl), and by a four membranes envelope (e). Picture shows a pyrenoid (p). (b) Illustration representing Phaeophyceae and Bacillariophyceae chloroplast structure (after Taylor, 1976). 19

Fig. 2.4: Reaction sequences and enzymes involved in the violaxanthin (Vx) and diadinoxanthin (Dd) cycle (after Goss and Jakob, 2010). The cofactor requirements of the enzymes catalyzing the de-epoxidation reaction (VDE and DDE), and the epoxidation reaction (ZEP and DEP), are respectively shown. Symbols behind the cofactors indicate whether high (++) or low (+) concentrations of the respective substrates are needed for high enzyme activity. This figure also addresses the important observation that the proton gradient inhibits Dt epoxidation (high ΔpH control, ++), whereas Zx epoxidation is unaffected by the presence of the trans-membrane ΔpH (-). The pH range of the thylakoid lumen, where VDE and DDE activity occurs, is depicted. VDE, violaxanthin de-epoxidase; DDE, diadinoxanthin de-epoxidase; ZEP, zeaxanthin epoxidase; DEP diatoxanthin epoxidase; Asc, ascorbate; MGDG, monogalactosyldiacylglycerol. 25

Fig. 3.1. Scheme representing the interactions between phytoplankton cell size, elemental stoichiometry, marine food webs and biogeochemistry (after Finkel *et al.*, 2010). Organic matter fluxes in a future (i.e. warmer and more stratified) scenario, and in the actual (cooler and less stratified) scenario, are depicted in red and black arrows, respectively. 49

Fig. 4.1: Rapid light curves of electron transport rate (ETR) vs. irradiance. 75

Figure 5.1: *Pseudo-nitzschia multistriata* in culture (A, B: girdle band view, light microscope Axiophot x 10 x 40 x 1.25, image Zeiss Axiocam, resolution 2600 × 2060, Axiovision 3.1 software, scale bar 20 μm). After Sylvie V. M. Tesson O.U. PhD Thesis (2010). 81

Figure 5.2: The sine light (SL) climates applied during the pre-acclimation period of experiments (maximal PFD of 100 μmol photons m⁻² s⁻¹). 81

Figure 5.3: Scheme illustrating the illumination shift from low (grey bar) to high (red bar) irradiance intensity (37 and 300 μmol photons m⁻² s⁻¹, respectively), applied during the experiment. Low light dithiotreitol (DTT) incubation lasted 10 minutes before the high light shift. Arrows indicate sampling times, at 0, 1 and 10 minutes after the shift to high irradiance climate. 84

Fig. 5.4: Evolution of chlorophyll *a* cell⁻¹ content (a), β-carotene Chl *a*⁻¹ (b), diatoxanthin Chl *a*⁻¹ (c), the Dt : (Dt + Dd) DPS (d), and diadinoxanthin Chl *a*⁻¹ ratios (e), in function of time (minutes). Data are means with n = 3; error bars are SD. Relationship between diatoxanthin and diadinoxanthin Chl *a*⁻¹ ratio, in DTT-treated (f) and control cultures (g). DTT-treated culture: filled circles; control cultures: open circles. Numbers in figures f and g represent sampling time (in minutes). Chl *a*, chlorophyll *a*; β-Car, β-carotene; Dt, diatoxanthin; Dd, diadinoxanthin. Chl *a* cell⁻¹ content is expressed in 10⁻¹⁶ mol Chl *a* cell⁻¹; other pigment ratios are expressed in μg : μg Chl *a*. 85

Fig. 5.5: Evolution of violaxanthin (a) and zeaxanthin Chl *a*⁻¹ ratios expressed in μg : μg Chl *a* (b), in function of time (minutes). Data are means with n = 3; error bars are SD. Relationship between zeaxanthin and violaxanthin Chl *a*⁻¹, diatoxanthin and violaxanthin Chl *a*⁻¹, diadinoxanthin and violaxanthin Chl *a*⁻¹ ratios, in DTT-treated (c, e and g) and control cultures (d, f and h). DTT-treated culture: filled circles; control cultures: open circles. Chl *a*, chlorophyll *a*; Vx, violaxanthin; Zx, zeaxanthin; Dt, diatoxanthin; Dd, diadinoxanthin. 88

Fig. 5.6: Evolution of fucoxanthin (a) and *cis*-fucoxanthin Chl *a*⁻¹ ratios expressed in μg : μg Chl *a* (b), in function of time (minutes). Data are means with n = 3; error bars are SD. Relationship between fucoxanthin and *cis*-fucoxanthin Chl *a*⁻¹ ratios, in DTT-treated (c) and control cultures (d). DTT-treated culture: filled circles; control cultures: open circles. Chl *a*, chlorophyll *a*; Fuco, fucoxanthin; *Cis*-Fuco, *cis*-fucoxanthin. 90

Fig. 5.7: Relationship between diatoxanthin and fucoxanthin $\text{Chl } a^{-1}$, diadinoxanthin and fucoxanthin $\text{Chl } a^{-1}$, diatoxanthin and *cis*-fucoxanthin $\text{Chl } a^{-1}$, diadinoxanthin and *cis*-fucoxanthin $\text{Chl } a^{-1}$ ratios, in DTT-treated (**a**, **c**, **e** and **g**) and control cultures (**b**, **d**, **f** and **h**). DTT-treated culture: filled circles; control cultures: open circles. *Chl a*, chlorophyll *a*; *Dt*, diatoxanthin; *Dd*, diadinoxanthin; *Fuco*, fucoxanthin; *Cis-Fuco*, *cis*-fucoxanthin. 91

Fig. 5.8: Evolution of neoxanthin-? (**a**) and neoxanthin-like $\text{Chl } a^{-1}$ ratios expressed in $\mu\text{g} : \mu\text{g Chl } a$ (**b**), in function of time (minutes). Data are means with $n = 3$; error bars are SD. Relationship between neoxanthin-? and fucoxanthin $\text{Chl } a^{-1}$, neoxanthin-? and *cis*-fucoxanthin $\text{Chl } a^{-1}$ ratios, in DTT-treated (**a**, **c**, and **e**) and control cultures (**b**, **d**, and **f**). DTT-treated culture: filled circles; control cultures: open circles. *Chl a*, chlorophyll *a*; *Neox-?*, neoxanthin-?; *Neox-like*, neoxanthin-like. 92

Fig. 5.9: Relationship between diadinoxanthin and neoxanthin-? $\text{Chl } a^{-1}$, diatoxanthin and neoxanthin-? $\text{Chl } a^{-1}$ ratios, in DTT-treated (**a**, and **c**) and control cultures (**b** and **d**). DTT-treated culture: filled circles; control cultures: open circles. *Chl a*, chlorophyll *a*; *Dt*, diatoxanthin; *Dd*, diadinoxanthin; *Neox-?*, neoxanthin-?. . . . 93

Fig. 5.10: Relationship between neoxanthin-like and violaxanthin $\text{Chl } a^{-1}$, neoxanthin-like and zeaxanthin $\text{Chl } a^{-1}$ ratios, in DTT-treated (**a**, and **c**) and control cultures (**b** and **d**). DTT-treated culture: filled circles; control cultures: open circles. *Chl a*, chlorophyll *a*; *Dd*, diadinoxanthin; *Neox-like*, neoxanthin-like, *Vx*, violaxanthin; *Zx*, zeaxanthin. 94

Fig. 5.11: Evolution of non-photochemical fluorescence quenching (NPQ), in function of time (minutes; **a**). Data are means with $n = 3$; error bars are SD. Relationship between NPQ and diatoxanthin $\text{Chl } a^{-1}$, NPQ and the $\text{Dt} : (\text{Dt} + \text{Dd})$ ratios, in DTT-treated (**b** and **d**) and control cultures (**c** and **e**). DTT-treated culture: filled circles; control cultures: open circles. *Chl a*, chlorophyll *a*; *Dt*, diatoxanthin; *Dd*, diadinoxanthin. 96

Fig. 5.12: Evolution of photosystem II maximal photochemical efficiency ($\text{Fv} : \text{Fm}$), in function of time (minutes). Data are means with $n = 3$; error bars are SD. Relationship between the $\text{Dt} : (\text{Dt} + \text{Dd})$ ratio and $\text{Fv} : \text{Fm}$, $\text{Dt Chl } a^{-1}$ and $\text{Fv} : \text{Fm}$, NPQ and $\text{Fv} : \text{Fm}$, in DTT-treated (**b**, **d** and **f**) and control cultures (**c**, **e** and **g**). DTT-treated culture: filled circles; control cultures: open circles. *Chl a*, chlorophyll *a*; *Dt*, diatoxanthin; *Dd*, diadinoxanthin. 97

Fig. 5.13: Scheme of hypothetical relationships between xanthophyll-cycle pools and the biosynthetic pathway leading to photosynthetic accessory and accessory pigments in diatoms (from Lohr and Wilhelm, 1999; Bertrand, 2010, and our study). Red arrows represents high light-activated conversion steps. 101

Figure 5.14: Scheme of the five irradiance increases applied during the study, reaching the maximal PFD values of 100, 250, 350, 500, and 650 $\mu\text{mol photons m}^{-2} \text{s}^{-1}$, for the experimental kinetics of irradiance change of five (a), three (b) and two hours (c). Arrows indicate sampling times. 105

Fig. 5.15: Five hours kinetics experiment. Evolution of photosystem II maximal ($F_v : F_m$; a) and operating ($F_v' : F_m'$; b) photochemical efficiency, recovery ratio $\{[(F_v : F_m) - (F_v' : F_m')] : (F_v : F_m)\}$ (c), NPQ (d), and NPQ : Dt Chl a^{-1} ratio (f), over the irradiance range (PFD, $\mu\text{mol photons m}^{-2} \text{s}^{-1}$). Data are means with $n = 3$; error bars are SD. Relationship between NPQ and Dt Chl a^{-1} (e), NPQ and $[Dt : (Dt + Dd)]$ (DPS ratio; g), NPQ and $F_v : F_m$ (h). C100: filled circles; C250: filled square; C350: filled triangles; C500: open triangles; C650: open circles. Chl a , chlorophyll a ; Dt, diatoxanthin, Dd, diadinoxanthin; NPQ, non-photochemical fluorescence quenching. 108

Fig. 5.16: Three hours kinetics experiment. Evolution of photosystem II maximal ($F_v : F_m$; a) and operating ($F_v' : F_m'$; b) photochemical efficiency, recovery ratio $\{[(F_v : F_m) - (F_v' : F_m')] : (F_v : F_m)\}$ (c), NPQ (d), and NPQ : Dt Chl a^{-1} ratio (f), over the irradiance range (PFD, $\mu\text{mol photons m}^{-2} \text{s}^{-1}$). Data are means with $n = 3$; error bars are SD. Relationship between NPQ and Dt Chl a^{-1} (e), NPQ and $[Dt : (Dt + Dd)]$ (DPS ratio; g), NPQ and $F_v : F_m$ (h). C100: filled circles; C250: filled square; C350: filled triangles; C500: open triangles; C650: open circles. Chl a , chlorophyll a ; Dt, diatoxanthin, Dd, diadinoxanthin; NPQ, non-photochemical quenching. 109

Fig. 5.17: Two hours kinetics experiment. Evolution of photosystem II maximal ($F_v : F_m$; a) and operating ($F_v' : F_m'$; b) photochemical efficiency, recovery ratio $\{[(F_v : F_m) - (F_v' : F_m')] : (F_v : F_m)\}$ (c), NPQ (d), and NPQ : Dt Chl a^{-1} ratio (f), over the irradiance range (PFD, $\mu\text{mol photons m}^{-2} \text{s}^{-1}$). Data are means with $n = 3$; error bars are SD. Relationship between NPQ and Dt Chl a^{-1} (e), NPQ and $[Dt : (Dt + Dd)]$ (DPS ratio; g), NPQ and $F_v : F_m$ (h). C100: filled circles; C250: filled square; C350: filled triangles; C500: open triangles; C650: open circles. Chl a , chlorophyll a ; Dt, diatoxanthin, Dd, diadinoxanthin; NPQ, non-photochemical fluorescence quenching. 110

Fig. 5.18: Evolution of estimated Dd cycle dependent (a and b) and Dd cycle independent NPQ (c and d), and Dd cycle independent NPQ contribution (%; e and f), over the irradiance range (PFD, $\mu\text{mol photons m}^{-2} \text{s}^{-1}$). 112

Fig. 5.19: Five hours kinetics experiment. Evolution of diadinoxanthin (a), diatoxanthin Chl a^{-1} (b), and $[Dt : (Dt + Dd)]$ (DPS ratio; c), over the irradiance range (PFD, $\mu\text{mol photons m}^{-2} \text{s}^{-1}$). Data are means with $n = 3$; error bars are SD. Relationship between diatoxanthin and diatoxanthin Chl a^{-1} ratios (d), $F_v : F_m$ and diatoxanthin Chl a^{-1} (e), $F_v : F_m$ and DPS ratio (f). In chart a, C650 peak sample was not considered in the regression. C100: filled circles; C250: filled square; C350: filled triangles; C500: open triangles; C650: open circles. Chl a , chlorophyll a ; Dt, diatoxanthin; Dd, diadinoxanthin. 114

Fig. 5.20: Three hours kinetics experiment. Evolution of diadinoxanthin (**a**), diatoxanthin Chl a^{-1} (**b**), and [Dt : (Dt + Dd)] (DPS ratio; **c**), over the irradiance range (PFD, $\mu\text{mol photons m}^{-2} \text{s}^{-1}$). Data are means with $n = 3$; error bars are SD. Relationship between diatoxanthin and diatoxanthin Chl a^{-1} ratios (**d**), Fv : Fm and diatoxanthin Chl a^{-1} (**e**), Fv : Fm and DPS ratio (**f**). In chart **d**, filled dots represent C100 and C250 samples data, while open dots represent C350, C500 and C650 samples data. C100: filled circles; C250: filled square; C350: filled triangles; C500: open triangles; C650: open circles. Chl a , chlorophyll a ; Dt, diatoxanthin; Dd, diadinoxanthin. 115

Fig. 5.21: Two hours kinetics experiment. Evolution of diadinoxanthin (**a**), diatoxanthin Chl a^{-1} (**b**), and [Dt : (Dt + Dd)] (DPS ratio; **c**), over the irradiance range (PFD, $\mu\text{mol photons m}^{-2} \text{s}^{-1}$). Data are means with $n = 3$; error bars are SD. Relationship between diatoxanthin and diatoxanthin Chl a^{-1} ratios (**d**), Fv : Fm and diatoxanthin Chl a^{-1} (**e**), Fv : Fm and DPS ratio (**f**). In chart **a**, C500 and C650 peak samples were not considered in the regression. C100: filled circles; C250: filled square; C350: filled triangles; C500: open triangles; C650: open circles. Chl a , chlorophyll a ; Dt, diatoxanthin; Dd, diadinoxanthin. 116

Fig. 5.22: Five hours kinetics experiment. Evolution of violaxanthin (**a**), zeaxanthin (**b**), and β -carotene Chl a^{-1} (**f**), over the irradiance range (PFD, $\mu\text{mol photons m}^{-2} \text{s}^{-1}$). Data are means with $n = 3$; error bars are SD. Relationship between zeaxanthin and violaxanthin Chl a^{-1} (**c**), zeaxanthin and diatoxanthin Chl a^{-1} (**d**), violaxanthin and diadinoxanthin Chl a^{-1} (**e**), β -carotene and diadinoxanthin Chl a^{-1} (**g**), β -carotene and diatoxanthin Chl a^{-1} (**h**). In chart **d**, zeaxanthin Chl a^{-1} values equals to zero were not considered in the regression. In chart C100: filled circles; C250: filled square; C350: filled triangles; C500: open triangles; C650: open circles. Chl a , chlorophyll a ; Zx, zeaxanthin; Vx, violaxanthin; Dt, diatoxanthin; Dd, diadinoxanthin, β -Car, β -carotene. 118

Fig. 5.23: Three hours kinetics experiment. Evolution of violaxanthin (**a**), zeaxanthin (**b**), and β -carotene Chl a^{-1} (**f**), over the irradiance range (PFD, $\mu\text{mol photons m}^{-2} \text{s}^{-1}$). Data are means with $n = 3$; error bars are SD. Relationship between zeaxanthin and violaxanthin Chl a^{-1} (**c**), zeaxanthin and diatoxanthin Chl a^{-1} (**d**), violaxanthin and diadinoxanthin Chl a^{-1} (**e**), β -carotene and diadinoxanthin Chl a^{-1} (**g**), β -carotene and diatoxanthin Chl a^{-1} (**h**). C100: filled circles; C250: filled square; C350: filled triangles; C500: open triangles; C650: open circles. Chl a , chlorophyll a ; Zx, zeaxanthin; Vx, violaxanthin; Dt, diatoxanthin; Dd, diadinoxanthin, β -Car, β -carotene. 119

Fig. 5.24: Two hours kinetics experiment. Evolution of violaxanthin (**a**), zeaxanthin (**b**), and β -carotene Chl a^{-1} (**f**), over the irradiance range (PFD, $\mu\text{mol photons m}^{-2} \text{s}^{-1}$). Data are means with $n = 3$; error bars are SD. Relationship between zeaxanthin and violaxanthin Chl a^{-1} (**c**), zeaxanthin and diatoxanthin Chl a^{-1} (**d**), violaxanthin and diadinoxanthin Chl a^{-1} (**e**), β -carotene and diadinoxanthin Chl a^{-1} (**g**), β -carotene and diatoxanthin Chl a^{-1} (**h**). C100: filled circles; C250: filled square; C350: filled triangles; C500: open triangles;

C650: open circles. Chl *a*, chlorophyll *a*; Zx, zeaxanthin; Vx, violaxanthin; Dt, diatoxanthin; Dd, diadinoxanthin, β -Car, β -carotene. 120

Fig. 5.25: Five hours kinetics experiment. Evolution of chlorophyll *a* cell⁻¹ content (10^{-16} mol Chl *a* cell⁻¹; **a**), Chl *a* cell⁻¹ variation (%; **b**), chlorophyll *c*₁ (**c**), *c*₂ (**d**), and *c*₃ Chl *a*⁻¹ ratios (**e**), over the irradiance range (PFD, μ mol photons m⁻² s⁻¹). Data are means with n = 3; error bars are SD. Relationship between chlorophyll *a* and chlorophyll *c*₁ (**f**), chlorophyll *a* and chlorophyll *c*₂ (**g**), chlorophyll *a* and chlorophyll *c*₃ molar concentrations (10^{-11} mol pigment; **h**). C100: filled circles; C250: filled square; C350: filled triangles; C500: open triangles; C650: open circles. Chl *a*, *c*₁, *c*₂, and *c*₃: chlorophyll *a*, *c*₁, *c*₂, and *c*₃, respectively. 122

Fig. 5.26: Three hours kinetics experiment. Evolution of chlorophyll *a* cell⁻¹ content (expressed in 10^{-16} mol Chl *a* cell⁻¹; **a**), chlorophyll *c*₁ (**b**), *c*₂ (**c**), and *c*₃ Chl *a*⁻¹ ratios (**d**), over the irradiance range (PFD, μ mol photons m⁻² s⁻¹). Data are means with n = 3; error bars are SD. Relationship between chlorophyll *a* and chlorophyll *c*₁ (**e**), chlorophyll *a* and chlorophyll *c*₂ (**f**), chlorophyll *a* and chlorophyll *c*₃ molar concentrations (10^{-11} mol pigment; **g**). C100: filled circles; C250: filled square; C350: filled triangles; C500: open triangles; C650: open circles. Chl *a*, *c*₁, *c*₂, and *c*₃: chlorophyll *a*, *c*₁, *c*₂, and *c*₃, respectively. 123

Fig. 5.27: Two hours kinetics experiment. Evolution of chlorophyll *a* cell⁻¹ content (expressed in 10^{-16} mol Chl *a* cell⁻¹; **a**), chlorophyll *c*₁ (**b**), *c*₂ (**c**), and *c*₃ Chl *a*⁻¹ ratios (**d**), over the irradiance range (PFD, μ mol photons m⁻² s⁻¹). Data are means with n = 3; error bars are SD. Relationship between chlorophyll *a* and chlorophyll *c*₁ (**e**), chlorophyll *a* and chlorophyll *c*₂ (**f**), chlorophyll *a* and chlorophyll *c*₃ molar concentrations (10^{-11} mol pigment; **g**). C100: filled circles; C250: filled square; C350: filled triangles; C500: open triangles; C650: open circles. Chl *a*, *c*₁, *c*₂, and *c*₃: chlorophyll *a*, *c*₁, *c*₂, and *c*₃, respectively. 124

Figure 5.28: Illustration of the three sine light climates applied during the experiment, each with a different maximal PFD peak of 100 (ML), 350 (HL1), and 650 μ mol photons m⁻² s⁻¹ (HL2), respectively. Arrows indicate the five sampling times (per day). 131

Fig. 5.29: Evolution of photosystem II maximal (Fv : Fm; **a**, **b** and **c**) and operating (Fv' : Fm'; **d**, **e** and **f**) photochemical efficiency, and non-photochemical quenching (NPQ; **g**, **h** and **i**) over time, during the two days of the experiment (and one “dawn” sampling on the third day). Data are means with n = 3; error bars are SD. ML: filled circles; HL1: filled triangles; HL2: open circles. 133

Fig. 5.30: Evolution of the diatoxanthin (**a**, **b** and **c**) and diadinoxanthin Chl *a*⁻¹ ratios (**d**, **e** and **f**), and [Dt : (Dt + Dd)] ratio (DPS; **g**, **h** and **i**), over time, during the two days of the experiment (and one “dawn” sampling on the third day). Data are means with n = 3; error bars are SD. ML: filled circles; HL1: filled triangles; HL2: open circles. Chl *a*, chlorophyll *a*; Dt, diatoxanthin, Dd, diadinoxanthin; DPS, de-epox. state. 134

Fig. 5.31: Evolution of β -carotene (**a, b and c**), violaxanthin (**d, e and f**), zeaxanthin (**g, h and i**), and neoxanthin Chl a^{-1} ratios (**l, m and n**), over time, during the two days of the experiment (and one “dawn” sampling on the third day). Data are means with $n = 3$; error bars are SD. ML: filled circles; HL1: filled triangles; HL2: open circles. Chl a , chlorophyll a ; β -Car, β -carotene; Neox, neoxanthin; Vx, violaxanthin; Zx, zeaxanthin. 137

Fig. 5.32: Evolution chlorophyll a cell $^{-1}$ content (10^{-16} mol Chl a cell $^{-1}$; **a, b and c**), fucoxanthin (**d, e and f**), chlorophyll $c_1 + c_2$ (**g, h and i**), and chlorophyll c_3 Chl a^{-1} ratios (**l, m and n**), over time, during the two days of the experiment (and one “dawn” sampling on the third day). Data are means with $n = 3$; error bars are SD. ML: filled circles; HL1: filled triangles; HL2: open circles. Chl a , $c_1 + c_2$, and c_3 , chlorophyll a , $c_1 + c_2$, and c_3 ; Fuco, fucoxanthin. 139

Fig. 6.1: (**a**) The five sinusoidal light regimes applied during the study, with different maximal PFD peaks (10, 50, 100, 250 and 500 $\mu\text{mol photons m}^{-2} \text{s}^{-1}$, respectively). Arrows indicate sampling. (**b**) Evolution of growth rate of *Phaeomonas* sp. over the light conditions. Data are the average of three measurements per 3 days (corresponding to the exponential growth phase for HL and ML conditions); error bars are SD. 162

Fig. 6.2: Evolution of: chlorophyll a cell $^{-1}$ expressed in 10^{-16} mol Chl a cell $^{-1}$ (**a**), chlorophyll c_2 cell $^{-1}$ (white dots) and chlorophyll c_3 cell $^{-1}$ (black dots) expressed in 10^{-16} mol pigment cell $^{-1}$ (**b**), fucoxanthin cell $^{-1}$ (white squares), *cis*-fucoxanthin cell $^{-1}$ (white triangles) and β -carotene cell $^{-1}$ (grey dots) expressed in 10^{-16} mol pigment cell $^{-1}$ (**c**), and neoxanthin cell $^{-1}$ content in 10^{-17} mol pigment cell $^{-1}$ (**d**), over the five PFD conditions. Chl a , chlorophyll a ; Chl c_2 and c_3 , chlorophyll c_2 and c_3 ; Fuco, fucoxanthin; *cis*-Fuco, *cis*-fucoxanthin; β -Car, β -carotene; Neox, neoxanthin. Data are the average of three measurements per 3 days (corresponding to the exponential growth phase for HL and ML conditions); error bars are SD. 163

Fig. 6.3: Evolution of: cellular organic carbon (POC, white squares) and nitrogen (PON, black squares) concentrations (pg cell^{-1}) (**a**), Chl a : POC ratio expressed in 10^{-18} mol Chl $a^{-1} \text{pg C}^{-1}$ (**b**), and POC : PON ratio (**c**), over the five PFD conditions. Relationship between POC : PON ratio and growth rate ($R^2 = 0.98$; **d**). Data are the average of three measurements per 3 days (corresponding to the exponential growth phase for HL and ML conditions); error bars are SD. 164

Fig. 6.4: (**a**) Evolution of the maximal photosynthetic rate $\text{absETR}_{\text{max}}$ (in mol $e^{-} \text{g Chl } a^{-1} \text{h}^{-1}$) over the five PFD conditions. Relationship between growth rate and $\text{absETR}_{\text{max}}$ (**b**) or $\text{relETR}_{\text{max}}$ (**c**). Evolution of α^{B} (mol $e^{-} \text{g Chl } a^{-1} \text{h}^{-1} [\mu\text{mol photons m}^{-2} \text{s}^{-1}]^{-1}$; **d**), E_k (in $\mu\text{mol photons m}^{-2} \text{s}^{-1}$; **e**) and E_k : PFD ratio (**f**) over the five PFD conditions. Data are the average of three measurements per 3 days (corresponding to the exponential growth phase for HL and ML conditions); error bars are SD. 165

Fig. 6.5: Evolution of the maximal photochemical efficiency (Fv : Fm; **a**) and non-photochemical fluorescence quenching (NPQ; **b**) over the five PFD conditions. Data are the average of three measurements per 3 days (corresponding to the exponential growth phase for HL and ML conditions); error bars are SD. 166

Fig. 6.6: (a) Relationship between Zx : (Vx + Ax + Zx) and NPQ. (b) Evolution of zeaxanthin Chl a^{-1} (Zx Chl a^{-1} in 10^{-2} mol : mol Chl a) over the five PFD conditions. (c) Mean of zeaxanthin cell $^{-1}$ in the three samples of the dawn, irradiance peak and sunset under the HL1 and HL2 regimes. Data are the average of three measurements per 3 days (corresponding to the exponential growth phase for HL and ML conditions), error bars are SD. . . . 167

Figs. 7.1–7.6: Fig. 1. Scheme of the five sine irradiance conditions, peaking at maximal PFD of 10, 50, 100, 250 and 500 $\mu\text{mol photons m}^{-2} \text{s}^{-1}$ (arrows indicate sampling times). Figs 2-6. Evolution of the growth rate (d^{-1} ; Fig. 2), PSII maximal photochemical efficiency (Fv : Fm; Fig. 3), maximal absolute electron transport rate ($_{\text{abs}}\text{ETR}_{\text{max}}$, in $\text{mol e}^{-} \text{g Chl } a^{-1} \text{h}^{-1}$; Fig. 4), photosynthetic efficiency (α^{B} , in $\text{mol e}^{-} \text{g Chl } a^{-1} \text{h}^{-1} [\mu\text{mol photons m}^{-2} \text{s}^{-1}]^{-1}$; Fig. 5), and irradiance saturation index (E_k , in $\mu\text{mol photons m}^{-2} \text{s}^{-1}$; Fig. 6) in the two species. *Minutocellus* sp. RCC703: open circles; *Minutocellus* sp. RCC967: filled circles. Data are means with $n = 3$; error bars are SD. 186

Figs. 7.7–7.14: Evolution of chlorophyll a cellular content (10^{-16} mol Chl a cell $^{-1}$; Figs 7, 8), chlorophyll c_1 and c_2 Chl a^{-1} (Figs 9, 10), fucoxanthin and *cis*-fucoxanthin : Chl a (Figs 11, 12), and α - and β -carotene cellular content (10^{-16} mol pigment cell $^{-1}$; Figs 13, 14), over the irradiance conditions. Chl a , chlorophyll a ; Chl c_1 , chlorophyll c_1 ; Chl c_2 , chlorophyll c_2 ; Fuco, fucoxanthin; *cis*-Fuco, *cis*-fucoxanthin; α -Car, α -carotene; β -Car, β -carotene. *Minutocellus* sp. RCC703: open circles and triangles; *Minutocellus* sp. RCC967: filled circles and triangles. Data are means with $n = 3$; error bars are SD. 187

Figs. 7.15–7.20: Evolution of (Dt + Dd) cell $^{-1}$ (10^{-16} mol pigment Chl a cell $^{-1}$; Figs 15, 16), Dt and Dd cell $^{-1}$ (10^{-16} mol pigment cell $^{-1}$; Figs 17, 18), [Dt : (Dt + Dd)] DPS (DPS; Figs 19, 20), over the irradiance conditions. Chl a , chlorophyll a ; Dt, diatoxanthin; Dd, diadinoxanthin. *Minutocellus* sp. RCC703: open circles and triangles; *Minutocellus* sp. RCC967: filled circles and triangles. Data are means with $n = 3$; error bars are SD. 188

Figs 7.21–7.24: Figs 21, 22. Relationship between NPQ and Dt Chl a^{-1} . Figs 23, 24. Evolution of NPQ over the irradiance conditions. Data are means with $n = 3$; error bars are SD. NPQ, non-photochemical fluorescence quenching. *Minutocellus* sp. RCC703: open circles; *Minutocellus* sp. RCC967: filled circles. 189

Figs 7.25–7.32: Figs 25, 26. Evolution of particulate organic carbon (POC) and nitrogen (PON) concentrations (pg cell^{-1}) over the irradiance conditions. Data are means with $n = 3$; error bars are SD. Figs 27, 28. Relationship between POC and PON cell $^{-1}$. Figs 29, 30. Evolution of the POC : PON ratio over the irradiance conditions. Data

are means with $n = 3$; error bars are SD. Figs 31, 32. Relationship between growth rate (d^{-1}) and POC : PON ratio. *Minutocellus* sp. RCC703: open circles and triangles; *Minutocellus* sp. RCC967: filled circles and triangles. 190

Figs 7.33–7.38: Evolution of the protein : carbohydrate absorbance ratio (Figs 33, 34), lipid : carbohydrate absorbance ratio (Figs 35, 36), and protein : lipid over the irradiance conditions (Figs 37, 38). Data are means with $n = 3$; error bars are SD. *Minutocellus* sp. RCC703: black and grey bars; *Minutocellus* sp. RCC967: black and grey striped bars. Grey bars represent control samples, measured at $100 \mu\text{mol photons m}^{-2} \text{ s}^{-1}$ (ML condition). Crb, carbohydrate; Lp, lipid; Prt, protein. 191

Fig. 7.39: Relationship between maximal absolute electron transport rate ($_{\text{abs}}\text{ETR}_{\text{max}}$, expressed in $\text{mol e}^{-} \text{ g Chl } a^{-1} \text{ h}^{-1}$) and growth rate (d^{-1}), by pooling the data set of three picoeukaryotic species: *Minutocellus* sp. RCC703, RCC967, and *Phaeomonas* sp. RCC503 (data from Giovagnetti *et al.*, 2010). 192

List of Tables

Table 3.1: List of some relevant field and laboratory studies concerning picoeukaryotes ecology, biology and ecophysiology. Increase in the number of publications concerning picoeukaryotes over years (percentages have been estimated on the basis of the list presented in this chapter): before 1995 (14%), between 1995 and 2000 (12%), between 2000 and 2005 (32%), and after 2005 (42%).	59
Table 4.1: Algal models used in the studies conducted during the PhD project.	64
Table 4.2: Fluorescence parameters and their meaning. After Kromkamp and Forster (2003).	73
Table 5.1: Sampling times and parameters measured under three different sine climates, each with a different maximal PFD of 100 (ML), 350 (HL1), and 650 $\mu\text{mol photons m}^{-2} \text{s}^{-1}$ (HL2), respectively, during two days of experiment.	130
Table 5.2: Growth rate (d^{-1}) and photosynthetic parameters (retrieved through P-E curve measurements; $\text{absETR}_{\text{max}}$ in $\text{mol e}^{-1} \text{g Chl a}^{-1} \text{h}^{-1}$; α^{B} in $\text{mol e}^{-1} \text{g Chl a}^{-1} \text{h}^{-1} [\mu\text{mol photons m}^{-2} \text{s}^{-1}]^{-1}$; E_k in $\mu\text{mol photons m}^{-2} \text{s}^{-1}$) in <i>Pseudo-nitzschia multistriata</i> cells subjected for two days to different sine light climates set to peak at 100 (ML), 350 (HL1) and 650 $\mu\text{mol photons m}^{-2} \text{s}^{-1}$ (HL2), respectively. Data represent the second day of the experiment (i.e. after the first day of acclimation), and are means ($n = 3$) \pm SD.	132

CHAPTER 1

General introduction

Chapter 1

General introduction

A small ensemble of metabolic pathways has the ability to reduce inorganic carbon to organic matter. Due this metabolic capacity, such organisms are called ‘primary producers’ because they provide organic compounds for all the organisms in the ecosystem. All photosynthetic organisms are primary producers and photosynthesis represents the most efficient, and widespread, process to produce organic matter, but not all primary producers are photosynthetic (i.e. some bacteria and archaea accomplish this task through non-photochemical reactions; Falkowski and Raven, 2007).

Oxygenic photosynthesis is performed by photosynthetic eukaryotes, such as higher plants and phytoplankton, and by cyanobacteria (prokaryotes). In the last decades, numerous oceanographic studies investigated the role of phytoplankton on Earth’s global primary productivity (Platt *et al.*, 1977; Geider and MacIntyre, 2002; Behrenfeld *et al.*, 2004). In fact, despite representing only 0.2% of the global primary producer biomass, phytoplankton contribution (46.2%) to Earth’s primary productivity is similar to the contribution given by the terrestrial component (53.8%; Field *et al.*, 1998). Although their small size, the phytoplanktonic cells play a crucial role in the aquatic ecosystems (Fuhrman, 2003), vastly participating to the Earth’s ‘biological pump’ functioning, to climate regulation, food web structure and biogeochemical cycling (Moline, 1998; Laws *et al.*, 2000; Sterner and Elser, 2002; Katz *et al.*, 2004; Irwin *et al.*, 2006; Finkel *et al.*, 2010). In marine ecosystems, the main abiotic forces are nutrient concentrations, temperature, and light, the latter displaying the highest variability in amplitude and frequency, over daily and seasonal basis, to which other factors (e.g. cloud cover and water turbulence) might contribute (MacIntyre *et al.*, 2000; Raven and Geider, 2003; Dubinsky and Schofield, 2010). In most aquatic ecosystems, under many circumstances, light availability is the most limiting factor, driving the flux of carbon and other elements into cells, and thereby can determine the rate of nutrient use/acquisition of photoautotrophs, for growth (Dubinsky and Schofield, 2010).

To cope with short term (few seconds/minutes) light fluctuations, mainly when darkness and excessive photon flux densities occur, and regulate their photosynthetic rate,

phytoplankton evolved an array of physiological photoregulative mechanisms, such as the electron transfer cycle around photosystem (PS) II and I, the state transitions, and enzyme activities modulations (Raven and Geider, 2003; Lavaud, 2007; Dubinsky and Schofield, 2010; Suggett *et al.*, 2010). The xanthophyll cycle (XC) and the dependent thermal dissipation of the excessive light energy (i.e. the non-photochemical fluorescence quenching, NPQ) play a crucial role in the photoregulation (Lavaud, 2007; Brunet and Lavaud, 2010; Goss and Jakob, 2010). NPQ development is triggered by the formation of a trans-thylakoidal pH gradient upon exposure to high light, and is mediated by the XC functioning (Arsalane *et al.*, 1994; Olaizola *et al.*, 1994; Lavaud *et al.*, 2002b; Goss and Jakob, 2010). In some Stramenopiles classes (e.g. Bacillariophyceae and Pelagophyceae) and in Euglenophyceae, the xanthophyll cycle consists of diadinoxanthin (Dd) de-epoxidation in diatoxanthin (Dt) in response to high light, with NPQ response relying on Dt synthesis. As in vascular plants, in Chlorophyta, Phaeophyceae and in some Chrysophyceae (both belonging to Stramenopiles), the XC instead involves the de-epoxidation of violaxanthin (Vx) in zeaxanthin (Zx), through antheraxanthin (Ax). Vx cycle pigments have also been detected in species that display the Dd cycle (e.g. diatoms), with a role as intermediate products in the carotenoid biosynthetic pathway (Lohr and Wilhelm, 1999, 2001).

Differently, at longer time scales (hours to days), photoacclimative processes, concerning macromolecules net synthesis or breakdown (e.g. changes in pigment content, and in stoichiometry of cell components and cellular ultra-structure), are activated (Raven and Geider, 2003; Brunet and Lavaud, 2010; Suggett *et al.*, 2010). Photoregulative and photoacclimative processes are functionally related and affect each other function (Lavaud *et al.*, 2007; Brunet and Lavaud, 2010; see Chapter 2).

All phytoplankton groups have unicellular species whose size can vary by more than 9 orders of magnitude in body volume, from less than $1 \mu\text{m}^3$ (an equivalent spherical diameter (ESD) of $< 1 \mu\text{m}$), for instance for the cyanobacterium *Prochlorococcus* and the eukaryotic green alga *Ostreococcus* (Prasinophyceae), to over $10^9 \mu\text{m}^3$ (ESD $> 1 \text{mm}$) for *Ethmodiscus* (Sieburth *et al.*, 1978; Beardall *et al.*, 2008; Finkel *et al.*, 2010). Picophytoplankton cells are among the smallest-sized free-living cells. The smallest prokaryotic (*Prochlorococcus* spp, $\sim 0.6 \mu\text{m}$; Chisholm, 1992) and the smallest eukaryotic (*Ostreococcus tauri*, $\sim 0.9 \mu\text{m}$; Courties *et al.*, 1994) picophytoplankton have the

minimum possible size due to essential components non-scalability, such as genome and membranes thickness (Raven, 1998; Raven *et al.*, 2005).

Despite their lower abundance relative to prokaryote picoplankton, picoeukaryotes show a greater complexity/diversity as a group, and their relevance in terms of biomass and production (e.g. Li, 1994; Worden *et al.*, 2004; Pérez *et al.*, 2005; Jardillier *et al.*, 2010), as well as diversity (Díez *et al.*, 2001b; López-García *et al.*, 2001; Moon-van der Staay *et al.*, 2001; Le Gall *et al.*, 2008; Vaulot *et al.*, 2008; Lepere *et al.*, 2011), has been confirmed.

Their small cell size confers picoeukaryotes several physiological advantages (e.g. a higher pigment specific-absorption due to a lower package effect, greater acquisition and use of nutrients due to a higher surface area per unit volume, lower sinking rate, and generally higher maximum specific growth rate; Raven, 1998; Raven *et al.*, 2005), when compared to larger cells. At the same time, they are more sensitive to photo-saturation/inhibition processes. This set of ecological and biological features explains picoeukaryotes ability to dominate, in terms of biomass and primary production, in resources (nutrients and photons) poor, stratified water masses (see Chapter 3).

Phytoplankton size has been reported to affect many biological processes and ecophysiological functions of phytoplankton (Finkel *et al.*, 2010). The influence of cell size on photosynthesis regulation capacity, through the XC operation (Lavaud *et al.*, 2004; Dimier *et al.*, 2007b, 2009b), and physical constraints imposed on the energetic cost of photoacclimation (by determining the pigments pool and the architecture of PSII antenna; Finkel, 2001; Raven and Kübler, 2002; Litchman and Klausmeier, 2008; Key *et al.*, 2009), have been reported. The importance of the constraints set by cell size on phytoplankton metabolic rate (Brown *et al.*, 2004), and their consequent influence on photosynthesis regulation under changing light conditions, are aspects that make picoeukaryotes interesting model organisms to investigate photoacclimative strategies and niche adaptation. The high photophysiological plasticity of picoeukaryotes has been demonstrated both in laboratory (Dimier *et al.*, 2007a, 2009a; Six *et al.*, 2008, 2009; Giovagnetti *et al.*, 2010) and in field studies (Brunet *et al.*, 2006, 2007), possibly in relation to the fact that the light is the most limiting resource affecting their primary productivity (Timmermans *et al.*, 2005).

The knowledge of phytoplankton photophysiology is crucial to better understand the mechanisms driving population dynamics and species succession. Indeed, depending on species-specific different physiological acclimation abilities, light climate fluctuations might affect photosynthesis and biomass production of phytoplankton, resulting in changes

in the community size structure and marine food web, possibly altering the amount of carbon fixed and exported into the sea bottom (Beardall and Raven, 2004; Beardall and Stojkovic, 2006; Wagner *et al.*, 2006; Finkel *et al.*, 2010).

My PhD project aimed to investigate the ecophysiological (photoacclimative and photoregulative) functional diversity, both at the physiological level and in an ecological framework.

The diversity of photoprotective processes and kinetics were studied in four species belonging to the *phylum* of Stramenopiles (also known as Heterokonts). One of the main parameters used to assess the diversity in photoprotective capacity was cell size, using one microplanktonic and three picoplanktonic species.

Firstly, physiological processes (i.e. photoacclimation, photoregulation, photosynthesis, growth), which are in part activated or modified in relation to changing light conditions, have been investigated. To achieve such task, a series of experiments have been designed and conducted on the microplanktonic diatom, *Pseudo-nitzschia multistriata* (Takano) Takano (Bacillariophyceae, Stramenopiles). The choice of *P. multistriata* as model species reflects several aspects of interest: it is a temperate species, and in our case it has been isolated in the Gulf of Naples (Tyrrhenian Sea, Mediterranean Sea), its ecology and life cycle have been investigated (D'Alelio *et al.*, 2009, 2010; Tesson, 2010), and furthermore, many species of the genus *Pseudo-nitzschia* have been shown to be able to produce the neurotoxin domoic acid (DA; Fryxell and Hasle, 2003).

Then, the phytoplankton ecophysiological functional diversity, in relation to niche adaptation, has been studied in three picoeukaryotic species isolated from distinct ecosystems, through the analysis of the physiological response curves (PRC) obtained by plotting a measured variable against a range of a factor (in our case, light) affecting that variable (Peek *et al.*, 2002). Picoeukaryotes (< 3.0 μm) have been chosen as model organisms because of their peculiar array of biological and ecological properties, related to their minute cell size, and because of their very narrow size range.

Light climate conditions, photoperiod and (sine) curves, applied in the different experiments, have been chosen with respect to natural irradiance conditions, to obtain relevant data, concerning the functioning and regulation of physiological mechanisms, and ecological interpretations.

The photoresponses of pico- and micro-phytoplankton were investigated to better understand the link between the cell size and the photoprotective properties of species. In

addition, the relationship between photosynthesis regulation, through photoacclimative and photoregulative mechanisms, and growth rate was studied. Three (one micro- and two picoplanktonic) species belong to the class of Bacillariophyceae (i.e. diatoms), while one (picoplanktonic) species to the class of Pinguiphyceae (Kawachi *et al.*, 2002). The predominant inclination toward diatoms is explained by their biological and ecological success and relevance (in terms of biomass, primary production, taxonomic diversity, cells size range, etc.; Armbrust, 2009), as well as by the lack of studies conducted on picoplanktonic diatoms. Anyhow, despite the quite close phylogenetic relationship between the four species, both the Dd (Bacillariophyceae) and Vx cycles (Pinguiphyceae) were displayed in the chosen group, and it has been possible to study and compare both the XC types. The relationship between NPQ development and XC modulation, and their efficiency, were analyzed in different species, and compared between the two types of XC. The regulation of xanthophylls biosynthesis was particularly deepened, to dissect the contribution to the photoprotective mechanism, of the de-epoxidation modulation of both *de-novo* synthesized and pre-existing pigments. In this context, in the Dd cycle-containing species, the possible role of intermediate xanthophylls (Vx cycle representatives) in the photoprotective biosynthetic pathway was also tackled.

Finally, the ecological diversity was taken into account, by studying the photoresponses of species isolated either in surface or deeper water layers, as well as of species adapted to grow either in oceanic or coastal or upwelling ecosystems.

This thesis is presented in the shape of 8 chapters, and it begins (i.e. this chapter) with a general introduction regarding the topic dealt and the major aims of my PhD project. After an introduction on photosynthesis and photoregulation processes, the state of art of photoprotective mechanisms through a bibliographic synthesis concerning the biochemical, physiological and ecological functioning of the XC and NPQ, is reported in Chapter 2.

In Chapter 3, the biological and ecological features of picoeukaryotes are presented, while Chapter 4 describes the materials and methods used in the experiments conducted during this study.

The obtained results are reported and discussed in the four following chapters. Chapter 5 focused on the XC and NPQ ecophysiology and functioning of the diatom *Pseudo-nitzschia multistriata*, via three distinct experimental designs. NPQ dependence on the XC activation/modulation, and the role of Vx cycle pigments as intermediate xanthophylls in

the biosynthesis of Dd cycle pigments, are described in Section 5.3. The effect of light intensity and light increase velocity on the photoprotective response (through XC and NPQ), and the effect of light history of cells on photoacclimation/photoregulation mechanisms, are presented in Section 5.4 and Section 5.5, respectively.

Picoeukaryotes photophysiological plasticity and properties, in relation to ecological adaptation and cell size constraints, are reported and discussed in Chapters 6 and 7.

In Chapter 6, the relation between growth and photosynthetic rate capacity, and photoacclimative processes efficiency, has been studied in the picoeukaryote *Phaeomonas* sp. RCC503 (Pinguiphyceae, Stramenopiles), which underwent five sine-light conditions set to peak at different photon flux densities. In Chapter 7, the ecophysiological properties of two picoplanktonic diatoms (*Minutocellus* sp. RCC967 and RCC703), subjected to the same experimental design described in Chapter 6, have been investigated and compared.

The last chapter (Chapter 8) concerns a general conclusion. In this chapter, the results that have been achieved during my PhD are discussed in light of phytoplankton distinct ecophysiological and functional capacity. The photophysiological flexibility as a functional trait in algae is deepened in relation to ecological niche adaptation. In this context, new research inputs on XC ecophysiology, rising from the experiments conducted on *Pseudo-nitzschia multistriata*, are presented. Eventually, the relevance of cell size, as a potential ecophysiological functional trait in phytoplankton, is considered.

CHAPTER 2

Introduction to photosynthesis and photoregulation

Chapter 2

Introduction to photosynthesis and photoregulation

2.1 The photosynthetic process

Photosynthesis is the biological process responsible for the conversion of light energy to chemical bond energy, which is stored as organic compounds (Falkowski and Raven, 2007). Although terrestrial plants make up the vast majority of photosynthetic biomass on Earth, roughly 45% of the photosynthesis occurs each year in aquatic environments (Falkowski, 1994; Field *et al.*, 1998). Photosynthesis supplies the primary source of organic matter for growth and metabolism of upper trophic level organisms in almost all the aquatic ecosystems. Since less than 1% of the total photosynthetic biomass on our planet is represented by aquatic plants biomass, and although terrestrial plants are much more a part of the human experience, aquatic photosynthetic organisms play a crucial role and impact in structuring the ecology and biogeochemistry of Earth.

Photosynthetic organisms can be anaerobic or aerobic. ‘Anoxygenic’ photosynthesis is performed by phototrophic prokaryotes such as green sulfur bacteria, rhodospin-based bacteria (Béjà *et al.*, 2000) or bacteriochlorophyll-based bacteria (Kolber *et al.*, 2000). Anoxygenic photosynthesis is considered as an ancestral photosynthesis (Whitmarsh and Govindjee, 1999). ‘Oxygenic’ photosynthesis is performed by photosynthetic eukaryotes such as higher plants and algae, and by cyanobacteria (prokaryotes). According to the endosymbiotic theory, the oxygenic photosynthesis occurred to eukaryotes 2.3 billion years (*Giga annum*, Ga) ago because of the successive endosymbiosis of a cyanobacterium in an eukaryotic cell, giving rise to the plastid of algae and higher plants (Nisbet and Sleep, 2001). After their appearance, aquatic photosynthetic organisms permanently altered Earth’s atmosphere, enriching it with a highly reactive gas, oxygen (Farquhar *et al.*, 2000; Bekker *et al.*, 2004), ultimately permitting the evolution of multicellular animals, humans included (Knoll, 2003).

The photosynthetic processes of higher plants and eukaryotic algae occur in the chloroplasts. The chloroplasts contain the aqueous matrix called stroma and the large,

expanded membrane system, the thylakoid membranes. In prokaryote organisms, thylakoids are instead situated in the cytosol.

The photosynthetic pigment-protein complexes, the components of the photosynthetic electron transport chain and proton transport processes are embedded in the thylakoid membrane bilayers. The main components of the photosynthetic electron transport chain are photosystem II (PSII), the cytochrome b_6/f complex (cyt b_6/f), photosystem I (PSI) and the ATP-synthase. Between PSII and cyt b_6/f , the mobile plastoquinone (PQ) serves as electron carrier. During the process, energetic molecules such as adenosine triphosphate (ATP) and nicotinamide adenine dinucleotide phosphate (NADPH) are produced.

Photosystems are divided into two main structural and functional units: the antenna complexes, which bind the major parts of the light-harvesting pigments and where the light-harvesting processes occur, and the core complexes, where the photochemical reactions and the initiation of the electron transport processes take place.

Light energy is absorbed via two types of light-harvesting complexes (LHCI and LHCII), serving photosystems (PS) I and II. LHCII is the most abundant of these complexes in thylakoid membranes, and consists of pigments (chlorophylls and carotenoids) which are bound to chlorophyll-binding proteins (CBPs; Dittami *et al.*, 2010).

The photosynthetic antenna corresponds to an assemblage of chlorophyll *a*-binding proteins linking different types of chlorophylls and carotenoids. In Chlorobionts, the main peripheral antenna is composed of Light-Harvesting Complex (LHC) chlorophyll *a/b*-binding proteins (CABs; Green and Durnford, 1996). Heterokontophyta and Prymnesiophyta possess various carotenoids, among which fucoxanthin is usually the most important. For this reason, the light-harvesting antennae are called fucoxanthin chlorophyll *a/c*-binding proteins (FCPs; Büchel and Wilhelm, 1993; Hiller *et al.*, 1993). Dinophyta possess peridinin chlorophyll *a/c*-binding proteins (PCP) since they possess of the carotenoid peridinin, in addition to Chl *a* and *c* (Green and Durnford, 1996).

The photosystem center complex includes the Reaction Center (RC), and a minor internal antenna. The RC of PSII is mainly composed of two similar polypeptides, the D1 and D2 proteins, associated with pigments and cofactors (4 chlorophylls, 2 pheophitins, 2 plastoquinones and a non-heme iron; Xiong *et al.*, 1996) needed for the light-induced charge separation that initiates the transport of electrons across the thylakoid membrane (Diner and Babcock, 1996). The internal antenna contains two chloroplast-encoded proteins, CP43 and CP47, which are intrinsic light-harvesting proteins only binding Chl *a*. These two pigment-protein complexes serve as “core-antenna” to PSII, absorbing energy

from the major light-harvesting pigment-protein complexes, and transferring it directly to the RC (Vermaas, 1993; van Amerongen and Dekker, 2003).

In the photosynthetic process, photons are absorbed by antenna pigments, situated in the peripheral PSII light-harvesting antenna complexes (LHCII). Energy is then transferred from LHCII to CP43 and CP47 (i.e. the internal antenna; Fig. 2.1), or D1/D2 proteins (RC), through the minor light-harvesting proteins CP24 and CP26 (Nelson and Ben-Shem, 2004). The first electron donor of the PSII consists of a dimer of Chl *a* absorbing at 680 nm and linked to the D1 and D2 proteins: the P680 (Telfer, 2002). The light energy modifies the redox potential of Chl *a* (P680⁺) which gives an electron to the primary acceptor, the phaeophytin, yielding Pheo⁻. P680⁺ comes back to its initial level by receiving an electron from a tyrosine situated in the D1 protein and playing a key role in the oxidation of water (Diner and Babcock, 1996). After phaeophytin reduction, the electron is delivered to secondary quinone acceptors (Q_A and Q_B).

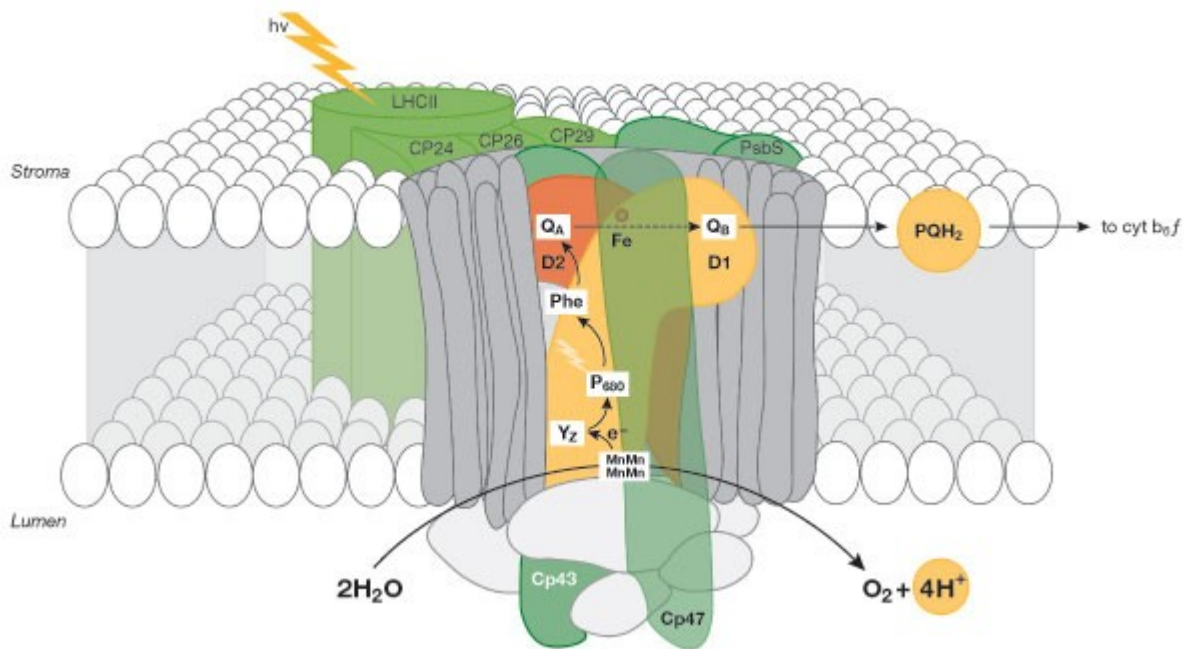


Fig. 2.1: Scheme representing the organization of the photosystem II and the light-harvesting complex II in the thylakoid membrane of higher plants. CP24, CP26 and CP29 are minor light-harvesting proteins. CP43 and CP47 are internal antenna chlorophyll-protein complexes. D1 and D2 are the main components of the reaction center (RC) with binding sites for electron acceptor quinones (Q_A, Q_B). P680 is a chlorophyll dimer. Other cofactors associated with D1/D2: phaeophytin (Phe), non-haem iron (Fe), Mn-cluster. Accessory chlorophylls and β -carotene are not shown. Chl, chlorophyll; cyt *b₆/f*, cytochrome *b₆/f* complex; PQH₂, plastoquinone pool; PsbS, PSII S subunit; Y_Z, D1-Tyr161. Arrows represent the electron flow along the photosynthetic chain. After Szábo *et al.* (2005). For a more detailed description, see Ferreira *et al.* (2004).

Then, the electron passes through the chain of electron carriers of the thylakoid membrane (ordered according to their redox potential) via plastoquinone, cytochrome b_6/f complex, plastocyanin (PC) or a soluble cytochrome c (cyt c), and finally PSI. In PSI, the first electron donor is a dimer of Chl a absorbing at 700 nm (P700). Two proteins (PsaA and PsaB), which are in the reaction center of the PSI, connect most of the pigments, donors and acceptors of electrons (Nelson and Ben-Shem, 2004).

In PSI, the primary photochemical reaction involves the oxidation of the Chl in the P700 reaction center thus producing $P700^+$. The liberated electron is transported towards $NADP^+$ through the primary acceptor A_0 (a Chl a molecule), A_1 (a phylloquinone molecule), ferredoxin (Fd) and the enzyme Fd- $NADP^+$ -oxidoreductase (FNR), which then catalyzes the reduction of $NADP^+$ to NADPH.

A schematic representation of the connection between the two photosystems, based on the apparent redox potentials of the two RC and the cytochromes, resembled the letter Z, and hence the two light reactions connected by an electron transport chain became a concept called ‘Z-scheme’ (Fig. 2.2).

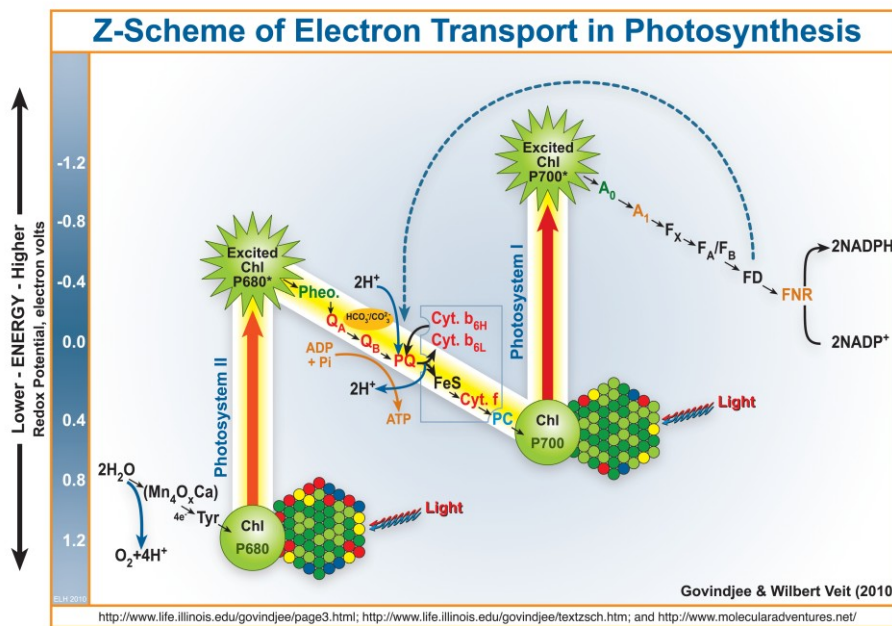


Fig. 2.2: Z-Scheme of electron transport in photosynthesis by Govindjee and Wilbert Veit (2010; gov@illinois.edu; Orr and Govindjee, 2010). The electron transport from H_2O to nicotinamide adenine dinucleotide ($NADP^+$) is traced from left to right on the diagram that uses the Photosystems II and I. This process is initiated by the simultaneous absorption of light by two antenna complexes, represented by clusters of colored balls. The absorbed energy is then transferred to the reaction center chlorophylls (Chl) P680 and P700 and this powers the entire process, during which 2 water molecules are split into 4 protons ($4H^+$), 4 electrons ($4e^-$) and 1 oxygen molecule (O_2).

The progression of electrons in the thylakoid membrane leads to the acidification of the lumen due to the oxidation of carriers such as plastoquinone, but also due to the photolysis of water. The net result of this process is the oxidation of water molecules, the production of molecular oxygen and the efficient reductant NADPH, and the generation of a proton gradient (ΔpH), which is exploited for ATP synthesis. In all oxygenic photoautotrophs, both NADPH and ATP are used in the photosynthetic dark reaction to incorporate CO_2 in the ribulose-1,5-bisphosphate (RuBP) thanks to the enzyme, Ribulose-1,5-Bisphosphate Carboxylase Oxygenase (Rubisco). This primary metabolic pathway responsible for carbon reduction occurs in the stroma of chloroplast and is called ‘Calvin cycle’ or ‘Calvin-Benson-Bassham cycle’ (Benson, 2002; Bassham, 2003), also known (erroneously) as the ‘dark reaction’ (being the Calvin cycle enzymes activated in the light, and also by products of the light-dependent reaction).

The light reactions of the photosynthesis are driven by light availability and light capture. According to the circumstances, light can be limiting, saturating or over-saturating with respect to the photosynthetic capacities of photosynthetic organisms. Thus, under variable irradiance, the photosynthetic electron rate needs to be regulated, to maintain/maximize photosynthesis, avoiding photo-damage.

2.2 Photoadaptation, photoacclimation and photoregulation

In their natural three-dimensional environment, aquatic photosynthetic organisms are exposed to a diverse and highly dynamic range of physical and chemical driving forces. High biodiversity and strong competition for resources characterize aquatic ecosystems where, in a few cubic mL of water, many phytoplankton species can grow, competing for light and nutrients to maintain photosynthetic and growth rates (Hutchinson, 1961; Liess *et al.*, 2009). Hence to be competitive, phytoplanktonic organisms must be able to quickly respond to any physical and chemical change encountered in their habitat.

The abiotic parameters of main influence for phytoplankton life are nutrient concentrations, temperature, salinity, and light. In this context, light is one of the most variable parameter in amplitude and frequency, over daily and annual cycles, and a key-factor ruling phytoplankton photosynthesis (MacIntyre *et al.*, 2000; Raven and Geider, 2003; Dubinsky and Schofield, 2010).

The light attenuation and dynamics of changes depend on the type of habitat occupied by planktonic and macrophytic algae. In oceanic offshore waters, the euphotic zone can be very deep and light conditions can be relatively stable, since the mixing of the water column would take several hours (MacIntyre *et al.*, 2000). Differently, estuarine habitats are characterized by a much stronger light attenuation than open ocean ones, and even moderate water mixing can cause phytoplankton to experience a change from complete darkness to high light throughout the day (Schubert and Forster, 1997). Coastal waters light climate can be seen as intermediate between oceanic and estuarine habitats (MacIntyre *et al.*, 2000).

Superimposed to this general classification of marine environments based upon their respective optical features, other factors, such as cloud cover and water bodies turbulence, add further unpredictability to light climate fluctuations.

Huisman and co-authors (2001) proposed that the diversity of life history and physiological capacities might promote the great biodiversity of phytoplankton. It has been proposed that the variability of physiological responses to light fluctuations would allow competitive exclusion, and thus spatial co-existence and/or temporal succession, of distinct species in both pelagic (Meyer *et al.*, 2000; Strzepek and Harrison, 2004; Dimier *et al.*, 2007b, 2009b; Lavaud *et al.*, 2007) and benthic ecosystems (Serodio *et al.*, 2005; van Leeuwe *et al.*, 2008). Indeed, in function of the phytoplanktonic groups/species (Litchman, 2000; Flöder and Kawabata, 2002; Mitrovic *et al.*, 2003; Wagner *et al.*, 2006) and of the photoacclimation capacity and light history of cells (Litchman and Klausmeier, 2001; van Leeuwe *et al.*, 2005; Wagner *et al.*, 2006; van de Poll *et al.*, 2007; Laurion and Roy, 2009), different growth rates are achieved in response to fluctuating light.

Three processes allow phytoplankton to cope with light climate changes: adaptation, acclimation and regulation (*sensu* Falkowski and LaRoche, 1991; Raven and Geider, 2003). As a result of genetic make up variations, different species are best suited for growth in different light environment (e.g. near the surface or at depth), and this is 'photoadaptation'. In function of light climate changes, a species adapted for growth in a given environment might need to modify its macromolecular composition (for instance, by increasing or decreasing the pigments content) to improve its growth efficiency or contrast potential photodamage (MacIntyre *et al.*, 2002): such process is termed 'photoacclimation'. Photoacclimation operates within the genetic constraints set by adaptation (i.e. no genetic changes occur), and responds at quite long time scales (from hours to days). It involves the net synthesis or breakdown of macromolecules, changing

the pigment quota, the stoichiometry of cell components and cellular ultra-structure. At shorter time scales (from seconds to minutes), a cell that is photoacclimated to a specific light regime may need to rapidly (and reversibly) regulate its photosynthetic efficiency, due to rapid fluctuations in the light climate: this is termed ‘photoregulation’. As opposed to photoacclimation, photoregulation does not require *de-novo* synthesis or breakdown of molecules, but involves the control of enzyme activities and energy dissipation pathways (Raven and Geider, 2003; Suggett *et al.*, 2010). These mechanisms include the Rubisco activity, the electron cycles of photosystem (PS) I and II, the state transitions, and the xanthophyll cycle (XC; Raven and Geider, 2003; Falkowski and Raven, 2007; Lavaud, 2007; Ruban and Johnson, 2009). Among these mechanisms, the XC and the mainly correlated thermal dissipation of the excessively-absorbed photons energy (i.e. the non-photochemical fluorescence quenching; NPQ) play a crucial role (Lavaud, 2007; Goss and Jakob, 2010; Brunet and Lavaud, 2010; Brunet *et al.*, 2011).

These two types of responses, regulative and acclimative, often act on synergy (Lavaud *et al.*, 2007; Brunet *et al.*, 2011). For instance, the content of photoprotective pigments involved in the XC activation, and the correlated modulation of NPQ development and kinetics, are influenced by the long-term photoacclimation occurring under a peculiar and prolonged (low or high, or intermittent) light climate (Lavaud *et al.*, 2003; van de Poll *et al.*, 2007; Gundermann and Büchel, 2008; Dimier *et al.*, 2009b).

The function and dynamics of long-term (photoacclimation) and short-term (photoregulation) processes are described in the following two sections (2.3 and 2.4, respectively). In the section 2.5 the ecophysiological variability of XC is reported.

2.3 Photoacclimation

Photoacclimation allows adjustment of the rate of light absorption relative to the maximal potential rate of energy utilization for photosynthetic carbon fixation and cells growth (Geider *et al.*, 1996). Photoacclimation is characterized by changes in the content and ratios of light-harvesting pigments and photoprotective carotenoids, in photosynthetic parameters, in enzymatic activities involved in photosynthesis and respiration, and eventually, in cell volume and chemical composition (Falkowski and LaRoche, 1991). In this section, we will focus on changes concerning chloroplasts, light-harvesting complexes, pigments composition and function.

2.3.1 Chloroplast size, number, morphology and distribution

The different phytoplankton classes and pigment-groups show huge differences in chloroplast size, numbers, morphology and distribution (Kirk and Tilney-Bassett, 1978; Larkum and Vesk, 2003). The chloroplast number is species-specific and varies from 1 to more than 100 chloroplasts per cell. An example can be given from the diatom genus *Chaetoceros*, where some species contain 1 chloroplast, while others, from 2 to more than 10 chloroplasts per cell. The species-specific differences in chloroplast size (typically 0.2–2 μm in length) and morphology (shape and structure) in a given species is also affected as a function of light climate (irradiance, the spectral composition of irradiance and day length). Light-induced chloroplast changes in a given species will especially affect light-harvesting and utilization (Raven and Geider, 2003), changing the intracellular self-shading (i.e. the package effect) and the optical signature of the chloroplast (colour, optical density, and *in vivo* fluorescence emission; Falkowski and Chen, 2003; Sakshaug and Johnsen, 2005; Johnsen and Sakshaug, 2007). Typically, low light-acclimated cells show chloroplasts evenly distributed within the cells (large light-harvesting surface), while high light-acclimated cells condensed ones (small light absorbing surface; Blatt *et al.*, 1981).

2.3.2 Light-harvesting complexes and thylakoid membranes

Phytoplankton pigment pools can be divided in two functional categories: pigments used for harvesting the light, and for photoprotection. Many accessory pigments constituting the light-harvesting complexes are photosynthetically active, which means they are able to transfer the energy absorbed to photosynthetic reaction centers (RC) of photosystems (PS) II and I. They are called light-harvesting pigments and include the photosynthetic carotenoids. However, some carotenoids are not involved in photosynthesis and do not transfer the absorbed energy to the RC. These non-photosynthetically active carotenoids are also called photoprotective carotenoids (PPC).

The majority of pigments in phytoplankton cells are situated inside the thylakoid membranes, in the form of light-harvesting complex (LHC), which are made of pigment-protein complexes. The thylakoid membrane organization and the energy regulation mechanisms of LHCs, of distinct phytoplankton classes, are distinct (Green *et al.*, 2003;

for a recent review on the evolution and function of PSII LHC in eukaryotes, refer to Ballottari *et al.*, 2011).

Most green algal thylakoids have both stacked and unstacked membrane regions (Bertos and Gibbs, 1998). Contrarily, the group of Stramenopiles (chlorophyll *c*-containing algae), comprising the classes Bacillariophyceae, Cryptophyceae, Dinophyceae, Pelagophyceae, Eustigmatophyceae, Chrysophyceae, Bolidophyceae, Pinguiphyceae, Raphidophyceae, Dictyochophyceae, Haptophyta, does not have grana stacking, so that the distribution of PSI and PSII is homogeneous along the membranes, with no segregation among stacked and external areas (stroma side; Green *et al.*, 2003; Lavaud, 2007; with the exception of Xanthophyceae; Büchel and Wilhelm, 1992). For some members of this algal group (e.g. Bacillariophyceae, Phaeophyceae and Chrysophyceae), a preferential concentration of PSI on the stroma side has been observed (Lichtlé *et al.*, 1992, 1995; Pyszniać and Gibbs, 1992).

In Rhodophyta and in most Chlorophyta, lateral segregation of PSI and PSII is related to their capacity of performing state transitions.

In addition to the aforementioned differences, Stramenopiles display a distinctive plastid ultrastructure and photosynthetic *apparatus* organization, when compared to vascular plants and green algae, due to their peculiar evolutionary origin (Pyszniać and Gibbs, 1992; Kroth and Strotmann, 1999; Falkowski *et al.*, 2004; Oudot-Le Secq *et al.*, 2007; Moustafa *et al.*, 2009). In Stramenopiles, thylakoids are organized in groups of parallel bands of three thylakoids (spaced by 2 nm) all along the plastid, which are surrounded by a band of three thylakoids, called the ‘girdle stack’ or ‘girdle lamella’, and by the chloroplast envelope, which consists of four membranes (Pyszniać and Gibbs, 1992; Lavaud, 2007; Fig. 2.3).

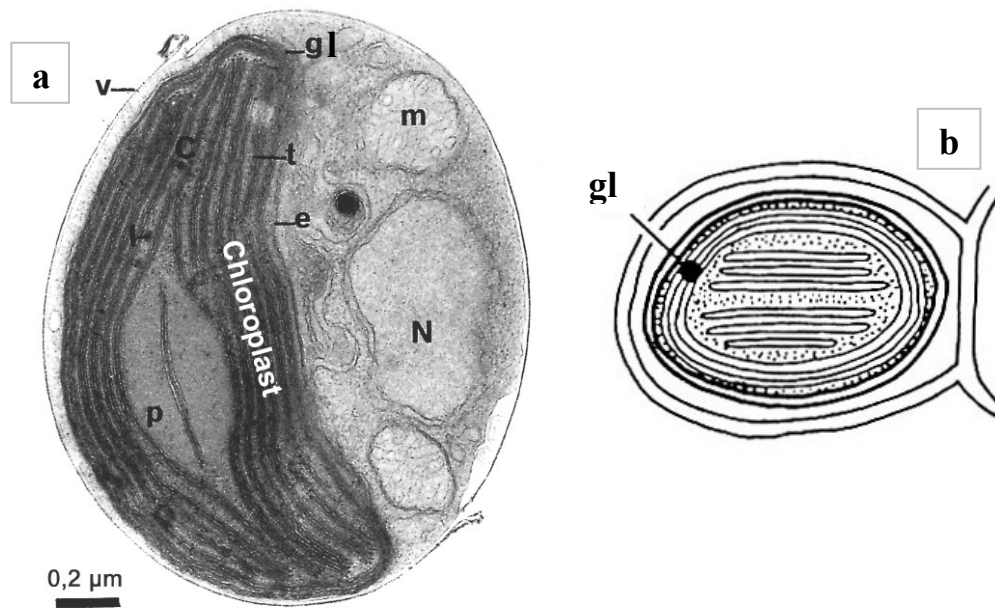


Fig. 2.3: (a) Transversal cut of a diatom cell (*Phaeodactylum tricornutum*, Bacillariophyceae; Lavaud, 2007) showing the nucleus (N), the mitochondria (m) and the cell-wall silica valves (v). The chloroplast contains thylakoids grouped in three bands (t), surrounded by an inner “girdle lamella” of three thylakoids (gl), and by a four membranes envelope (e). Picture shows a pyrenoid (p). (b) Illustration representing Phaeophyceae and Bacillariophyceae chloroplast structure (after Taylor, 1976).

Photoacclimation to changing light conditions lead to changes in the macromolecular composition and ultrastructure of the photosynthetic apparatus (Durnford and Falkowski, 1997; Raven and Geider, 2003). In general, high light-acclimated cells are usually characterized by a decrease in the size of the light-harvesting antenna and the associated pigments (Anderson *et al.*, 1995), such as accessory chlorophylls (Chl *c*) and photosynthetic carotenoids (Falkowski, 1981; Falkowski *et al.*, 1985; Mouget *et al.*, 1999), while an inverse relationship is found in low light-acclimated cells (Johnsen *et al.*, 1997; Stolte *et al.*, 2000; Falkowski and Chen, 2003; Rodriguez *et al.*, 2006).

Under high irradiance, the decrease in pigment content leads to a lower Chl *a* to carbon ratio (MacIntyre *et al.*, 2002), in relation with the decrease in light-harvesting efficiency per carbon biomass (Johnsen and Sakshaug, 1993).

The decrease in cellular Chl *a* (Geider *et al.*, 1997; Kana *et al.*, 1997) may be related to a decrease in size and/or number of the Photosynthetic Unit (PSU). Some algae modify the number but not the size of PSU (Perry *et al.*, 1981), while others the size of the PSU without any variation in number (Falkowski and Owens, 1980; Falkowski, 1983; Fisher *et al.*, 1989; Falkowski and LaRoche, 1991). The increase of the photoprotective carotenoids

(PPC) pool in response to high irradiance (Bidigare *et al.*, 1987; Harris *et al.*, 2005; Rodríguez *et al.*, 2006) results instead in a decrease of PSII functional absorption cross-section, since the light absorbed by PPC is not transferred to the reaction centers (Falkowski, 1981; Behrenfeld *et al.*, 2004). These processes have been described in many phytoplankton groups, such as diatoms (Mouget *et al.*, 1999; Anning *et al.*, 2000), dinoflagellates (Iglesias-Prieto and Trench, 1994), prymnesiophytes (Falkowski *et al.*, 1985; Harris *et al.*, 2005), prasinophytes (Buma *et al.*, 1993), chlorophytes (Durnford *et al.*, 2003) and cryptophytes (Goericke and Montoya, 1998).

Photoacclimation to low light conditions is a slower process than the transition from low to high light (Post *et al.*, 1984), since no damage effect occurs, at least at short term. Acclimation to low irradiance requires an increase in light-harvesting efficiency (photon absorbed per cell in a certain radiation field), which is achieved by photosynthetic pigment synthesis (Sukenik *et al.*, 1987), as well as some adjustments in the relative proportions of PSI and II, and synthesis of electron transport components (Falkowski and LaRoche, 1991). Shade-acclimation is accompanied by thylakoid membrane synthesis to accommodate the newly synthesized components of the photosynthetic apparatus (Falkowski and LaRoche, 1991).

In green algae and vascular plants, under low light conditions, an increase in grana stacks within the chloroplasts has been reported (Reger and Krauss, 1970, Anderson *et al.*, 1973, Lichtenthaler *et al.*, 1981). Since grana stacks are enriched in light-harvesting complexes associated with PSII (LHCII), but less PSII reaction centers, an increase in PSII antenna functional size and a lower PSII : PSI ratio, together with a decrease in the Chl *a* : Chl *b* ratio, occur under low light (Melis, 1991; Lepetit *et al.*, 2011). In addition, chloroplast membranes are highly packed and enriched in chlorophyll content, both features that enhance the package effect in the grana membranes and decrease the light-harvesting efficiency per unit of chlorophyll (i.e. low *in vivo* absorption coefficient, a_{ph}^* ; Berner *et al.*, 1989). Thus, in green algae low light-acclimated cells, the photosynthetic efficiency is not significantly enhanced compared to high light-acclimated cells (Lepetit *et al.*, 2011).

Differently, under high light conditions, the photosynthetic capacity (P_{max}) usually increases, mainly because of a greater capacity in electron transport chain and carboxylation reactions per absorption unit. Indeed, high light-acclimated cells tend to contain more cytochrome *f* and other enzymes catalyzing the CO₂ fixation in the Calvin cycle (Wilhelm, 1993).

In the green algae, the redox state of the plastoquinone (PQ) pool has been demonstrated to be functionally involved in mechanisms related to cellular response to changing light conditions, as: (i) the signal cascade inducing gene expression modifications, (ii) the direct or indirect activation of transcription factors encoding for protein complexes (Pesaresi *et al.*, 2009), and (iii) the regulation of short-term state transition mechanism (Pfannschmidt *et al.*, 2009).

In contrast to the green algal lineage, no change in number of membrane stacks has been described in Bacillariophyceae (*Thalassiosira weissflogii*), Eustigmatophyceae (*Nanochloropsis salina*), and in Dinophyceae (*Prorocentrum* sp.), in response to light changing conditions, remaining fixed to the number of three. No (or minor) changes have been found in Chl *a* : Chl *c* ratio (which is equivalent to Chl *a* : Chl *b* ratio in green algae), as well as in Chl *a* : fucoxanthin ratio. This indicates that, in contrast to green algae, no increase in the antenna size should be observed in Stramenopiles, an assumption that has been demonstrated by Dubinsky and co-authors (1986), showing no increase in PSII absorption cross-section under low light conditions, in Chl *c*-containing species.

Differently from what has been found in green algae, no sensing and control of light acclimation processes through PQ pool redox state was reported in diatoms. Indeed, in diatoms, no state transition mechanism was found (Owens, 1986), and a strong reduction of the PQ pool (via chlororespiration) has recently been reported in darkness (Grouneva *et al.*, 2009). Even if, a recent transcriptome study showed that in diatoms the genes encoding for the chlorophyll biosynthesis are down-regulated during the initial phase of high light-acclimation, whereas genes involved in photoprotection and ROS scavenging are up-regulated (Nymark *et al.*, 2009), the light sensors and the cascade of signals (related to these genes) are unknown.

2.3.3 Pigments composition and function

The high and specific differences between pigment-groups, in light harvesting and utilization, are a consequence of the great diversity of pigments within the light-harvesting complexes.

In most bloom-forming phytoplankton, some light harvesting pigments are of high importance; these are the peridinin, prasinoxanthin, violaxanthin and the fucoxanthins (including acyl-oxyderivatives). From the ratios between photosynthetic pigments, distinct

pigment-groups have been defined in prasinophyceae (e.g., Hooks *et al.*, 1988; Egeland *et al.*, 1995; Zingone *et al.*, 2002), or in haptophyta (e.g., Stolte *et al.*, 2000; Zapata *et al.*, 2004).

In most of the green algae and vascular plants, the chlorophylls (Chl) *a* and *b* represent the major pigments, while the carotenoids/xanthophylls, lutein, neoxanthin, violaxanthin (Vx) and β -carotene contribute to both light-harvesting and photoprotective functions, by being directly or indirectly converted into a closely-related pigments (e.g. Vx, as described later; Bassi and Caffarri, 2000).

In Stramenopiles (e.g. diatoms) Chl *b* is replaced by Chls *c* (Goedheer, 1970; Stauber and Jeffrey, 1988), and they show a set of specific pigments among which the xanthophylls are very abundant, giving them their characteristic brown-yellow color (Wilhelm, 1990).

Diatoms possess fucoxanthin (Fuco) chlorophyll (Chl) *a/c*-binding proteins (FCPs) as peripheral antennae of the photosystems. FCPs show high sequence similarity among the Stramenopiles (Green and Durnford, 1996), especially between the diatoms and the brown algae (Caron *et al.*, 1988; Apt *et al.*, 1995; de Martino *et al.*, 2000; Green, 2003). Fuco is an allenic xanthophyll only found in diatoms, other stramenopiles (like the brown algae) and in some Dinophytes (dinoflagellates; Takeshita *et al.*, 2004). In the Chl *c*-containing algae, the high amount of carotenoids associated with Chls *c* is believed to be an adaptation of the LHC, boosting the light absorption in the blue-green range of *spectrum*, which is crucial in aquatic environments (Richardson *et al.*, 1983; Macpherson and Hiller, 2003; Lavaud, 2007; Premvardhan *et al.*, 2010). Moreover, even Chls *c* (Jeffrey, 1969, 1972), replacing Chl *b*, are important both for light-harvesting (in the blue-green region), and for energy transfer to Chl *a* (Büchel, 2003).

Contrarily to higher plants, carotenoids/xanthophylls (especially Fuco) have a major role in harvesting light, in diatoms (Kirk, 1977). Even a part of the diadinoxanthin (Dd) pool seems to be able to absorb and efficiently transfer the light excitation energy to Chl *a*, despite Dd (and diatoxanthin; Dt) main role in the rapid regulation of the light absorption/dissipation (as described later; Wilhelm, 1990; Lavaud *et al.*, 2003). These xanthophylls, and especially Fuco, also have a structural role in the LHC within the thylakoid membrane (Pascal *et al.*, 1998), as it has already been reported for lutein, in organisms of the green lineage (Kuhlbrandt *et al.*, 1994).

Chl *a* is not an important pigment in light-harvesting function, since its major role is in the RC, receiving light energy from donor pigments inside the light-harvesting complex, and being a key molecule in the photochemical conversion of photons into chemical bond

energy. Pigment data are often normalized by Chl *a* as biomass indicator. Since the strict dependence of the cellular Chl *a* content on the experienced light, the particulate organic carbon (POC) can represent a less variable (and thus more accurate) indicator of biomass (Johnsen and Sakshaug, 1993; Brunet *et al.*, 1996; Rodriguez *et al.*, 2006). The interpretation of light harvesting pigments and photoprotective carotenoids (PPC), in high light (HL) and low light (LL) conditions, is therefore highly dependent on biomass normalization (Chl *a* : C ratio; Rodriguez *et al.*, 2006; Johnsen and Sakshaug, 2007). The Chl *a* : C ratio (w:w) is low under high light (and long day length) and high under low light. Thus, the Chl *a* : C (w:w) ratio indicates the photo-acclimation status, and is termed 'photoacclimation index' (Sakshaug *et al.*, 1997). The photo-acclimation index can be described as a function of absorbed quanta (Nielsen and Sakshaug, 1993). Averaged Chl *a* : C ratios for HL- and LL-acclimated cells of 10 phytoplankton classes were 0.020 and 0.043, respectively (Johnsen and Sakshaug, 2007).

In general, there are some common features of long-term photoacclimation. The faster the growth rate, the faster the acclimation process is, since cells can rapidly divide and respond to environmental changes. In addition, light history seems to clearly affect the photoacclimative response of cells (e.g., Anning *et al.*, 2000), affecting both the kinetics of photoprotective processes and the variations of pigment pools (Anning *et al.*, 2000; Dimier *et al.*, 2007b).

2.4 Photoregulation and the xanthophyll cycle

In addition to the long-term acclimation to light conditions, higher plants and algae have evolved a set regulatory mechanisms to rapidly acclimate their photosynthetic *apparatus* to sudden irradiance variations, thus avoiding the formation of reactive oxygen species (ROS) and photodamage (Gilmore, 1997; Demmig-Adams and Adams, 2000). These mechanisms include the rapid regulation of the enzymatic activities (e.g. Rubisco activity), state transitions mechanism (i.e. the changes in the relative absorption by the PSI and PSII antennae, via reversible dissociation of some pigment-protein complex from PSII, with or without reversible association to PSI), and the xanthophyll cycle (XC; Raven and Geider, 2003).

2.4.1 State of art

When the chlorophyll (Chl) *a* molecules of the light-harvesting complexes antenna absorb light, they enter a singlet-state excitation $^1\text{Chl } a^*$ from which energy is deactivated following several pathways. Most of the excitation energy is transferred through charge separation within the reaction centers of photosystems, and used to drive photochemistry. Part of the excitation energy leaks as energy re-emission via chlorophyll fluorescence and heat. Nevertheless, a significant part of the energy can be dissipated through the ‘triplet valve’, thereby forming triplet-state excitation: $\text{Chl } a + \text{light} \rightarrow ^1\text{Chl } a^* \rightarrow ^3\text{Chl } a^*$. Such a pathway depends on the lifetime of $^1\text{Chl } a^*$, which is related to other deactivation pathways. Under excessively-absorbed light pressure, the ability of the photosynthetic machinery to use the excitation energy via photochemistry reaches its maximal capacity, and the yield for Chl *a* fluorescence, together with the $^3\text{Chl } a^*$ formation probability, increase. This situation is critical since $^3\text{Chl } a^*$ can react with oxygen (O_2) within the PSII RC, producing ROS (such as singlet $^1\text{O}_2^{*-}$) – which are harmful to all the classes of biomolecules, including lipids, proteins, and DNA – and leading to a decrease in photosynthetic rate.

Photosynthetic organisms are able to maintain a low steady-state of $^3\text{Chl } a^*$ generation through several rapid photoprotective mechanisms, helping to minimize the production of ROS. The non-photochemical fluorescence quenching (NPQ) is believed to be one of the most important mechanisms for rapid (seconds to minutes) regulation of photochemistry, under excessive photon flux densities, and its development is strictly related to the xanthophyll cycle (XC) functioning (Demmig-Adams and Adams, 2006; Lavaud, 2007; Goss and Jakob, 2010; Brunet and Lavaud, 2010; Brunet *et al.*, 2011; Ruban *et al.*, 2011). The light-dependent conversion of xanthophylls has been discovered by Sapozhnikov and co-authors (1957), and the main features of the xanthophyll cycle were established in the 1960s and 1970s (e.g. Hager, 1969; Stransky and Hager, 1970; Yamamoto and Kamite, 1972).

Two groups of organisms can be distinguished on the basis of the pigments involved in the XC (Fig. 2.4). The first group consists of vascular plants, and green (Chlorophyta) and brown (Phaeophyceae) algae, and includes as the main XC the violaxanthin (Vx) cycle (Yamamoto *et al.*, 1962; Hager, 1967a; Stransky and Hager, 1970). The Vx cycle consists of a reversible reaction comprising two de-epoxidation steps, in which the di-epoxy xanthophyll Vx is converted into the epoxy-free zeaxanthin (Zx), through the mono-epoxy

antheraxanthin (Ax; Fig. 2.4). The conversions of Vx into Ax and Zx are catalyzed by the enzyme violaxanthin de-epoxidase (VDE), in response to high light intensities, while low light intensities or darkness stimulate the backward reaction, leading to the conversion of Zx back to Vx thanks to the enzyme zeaxanthin epoxidase (ZEP; Hager, 1967b).

The second group of photosynthetic organisms (i.e. the algal classes Bacillariophyceae, Xanthophyceae, Haptophyceae, and Dinophyceae) shows a second major XC, the diadinoxanthin (Dd) cycle (Stransky and Hager, 1970; Hager, 1980; Demers *et al.*, 1991). The reaction sequence includes the conversion of an epoxy-xanthophyll (Dd) into an epoxy-free carotenoid (diatoxanthin, Dt), catalyzed by the enzyme diadinoxanthin de-epoxidase (DDE) under high light conditions (Hager, 1969, 1980). The reverse reaction takes place under low light intensities or darkness, and it is catalyzed by the diatoxanthin epoxidase (DEP; Fig. 2.4). In addition to the light induced de-epoxidation of Dd into Dt, accumulation of Dt has also been observed in *Phaeodactylum tricorutum* cultures that have been exposed to periods of prolonged darkness (Jakob *et al.*, 1999), and in natural

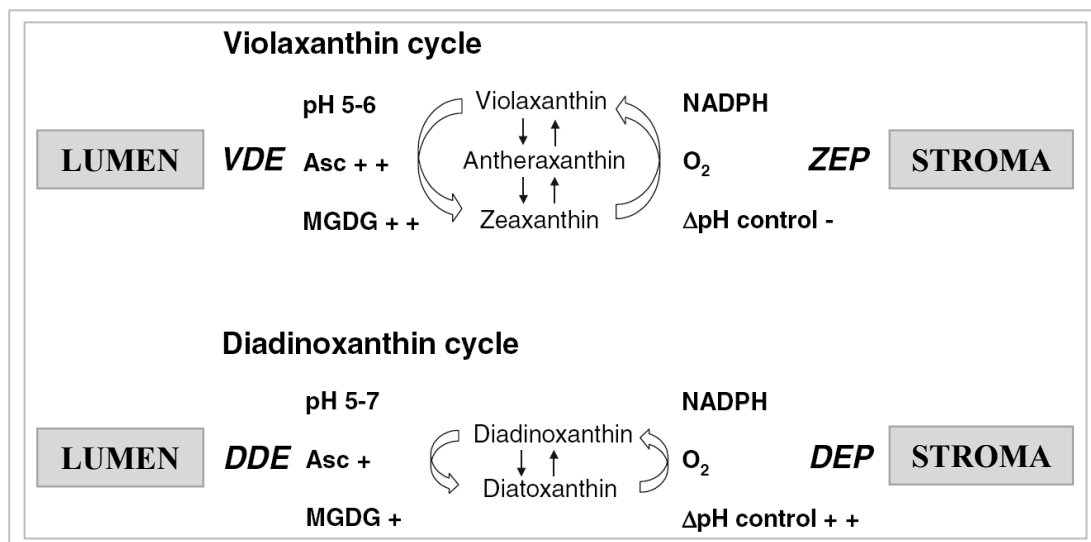


Fig. 2.4: Reaction sequences and enzymes involved in the violaxanthin (Vx) and diadinoxanthin (Dd) cycle (after Goss and Jakob, 2010). The cofactor requirements of the enzymes catalyzing the de-epoxidation reaction (VDE and DDE), and the epoxidation reaction (ZEP and DEP), are respectively shown. Symbols behind the cofactors indicate whether high (++) or low (+) concentrations of the respective substrates are needed for high enzyme activity. This figure also addresses the important observation that the proton gradient inhibits Dt epoxidation (high ΔpH control, ++), whereas Zx epoxidation is unaffected by the presence of the trans-membrane ΔpH (-). The pH range of the thylakoid lumen, where VDE and DDE activity occurs, is depicted. VDE, violaxanthin de-epoxidase; DDE, diadinoxanthin de-epoxidase; ZEP, zeaxanthin epoxidase; DEP diatoxanthin epoxidase; Asc, ascorbate; MGDG, monogalactosyldiacylglycerol.

phytoplankton populations under very low light conditions (Brunet *et al.*, 2006, 2007). Dd de-epoxidation into Dt in darkness, and probably under very low light, is driven by a proton gradient due to chlororespiration (Jakob *et al.*, 2001), and is further made possible by a change in the pH-dependent activation of DDE (Goss and Jakob, 2010).

A third group of organisms lack a XC, but show accumulation of Zx directly from β -carotene under high light exposure (while few species of red macroalgae show a XC; Raven and Geider, 2003). Within the first group, some prasinophytes have been shown to be unable to convert Vx further than Ax (Goss *et al.*, 1998), while some green macroalgae have no XC (Raven and Geider, 2003). A secondary type of XC, not with a less relevant role, has been reported in several plant species and in the green microalga *Chlamydomonas*, involving the de-epoxidation of lutein-epoxide into lutein, under peculiar circumstances (e.g. prolonged high light stress; Rascher and Nedbal, 2006). Additionally, in the green macroalga *Caulerpa*, a secondary XC, involving the conversion between lutein and siphonaxanthin (biosynthetically related to siphonein), has been reported (Raniello *et al.*, 2006).

Notably, within the second group, there are also some phyla in which the Vx cycle can be present, together with the main Dd cycle (Lohr and Wilhelm, 1999, 2001). They include some Heterokontophyta (Bacillariophyceae, Chrysophyceae, Xanthophyceae), Haptophyta and Dinophyta. However, in these algae, the Vx cycle pigments serve mainly as intermediate products in the biosynthetic pathway of carotenoids. It is still unclear whether the temporary accumulation of Zx under high light conditions is only an unavoidable consequence of the properties of the XC, or if it has a real physiological significance by enhancing the photoprotective ability of cells. Interestingly, among the Stramenopiles, some very close phyla kept the two-steps Vx cycle as the main XC (e.g. brown algae), while others evolved towards the one-step (and maybe more advantageous) Dd cycle (e.g. diatoms).

2.4.2 Biochemical aspects of the xanthophyll cycle

2.4.2.1 Carotenoid biosynthesis

Xanthophylls are pigments from the carotenoid group, composed of a C₄₀ hydrocarbon backbone absorbing light in the range 400-500 nm (Strzalka *et al.*, 2003). Fucoxanthin is the principal carotenoid in the golden-brown algae (Chrysophyceae, Bacillariophyceae, Prymnesiophyceae and Phaeophyceae), giving these algae their characteristic color (Lee, 1980). Carotenoids such as zeaxanthin, antheraxanthin, alloxanthin or neoxanthin are present in phycobilin-containing algae (Cyanophyta, Cryptophyta and Rhodophyta).

Lycopene is the precursor of all carotenoids and the successive formation of ionone-rings, followed by various hydroxylation and epoxidation reactions, yields to the molecule of β -carotene with one β -ionone ring at both sides (Sandmann and Boger, 1989; Huguene *et al.*, 1996). Hydroxylation of both β -ionone rings of β -carotene leads to the non-epoxidized xanthophyll Zx¹. In higher plants and green algae, Zx is then transformed to Vx (diepoxy)² by the introduction of two epoxide groups. This epoxidation, which proceeds through the intermediate Ax³ is catalyzed by the enzyme Zx epoxidase (ZEP; Lohr and Wilhelm, 2001). Under high light, Vx is de-epoxidized in Zx, thanks to the enzyme Vx de-epoxidase (VDE).

In chromophyte algae, the xanthophyll cycling pigments, Dd and Dt, are also synthesized from β -carotene (Björnland and Liaaen-Jensen, 1989; for a recent review concerning carotenoid biosynthesis in diatoms, see Bertrand, 2010). The Dd cycle involves the conversion of the mono-epoxy Dd⁴ in the epoxy-free Dt⁵. The presence of the three xanthophylls Vx, Ax and Zx has been revealed in the diatom *Phaeodactylum tricorutum* and in other algae possessing the Dd cycle (Lohr and Wilhelm, 1999). These authors demonstrated that Vx is an obligate precursor of Dd and is permanently present in small amount in cells. A putative role of Vx, Ax and Zx in thermal energy dissipation in chromophyte algae has not been demonstrated. The Dt mediates energy quenching less efficiently than Zx, but the lower efficiency may be compensated by a larger pool size of

¹ **Zx**: (3R, 3'R) - β , β - carotene - 3, 3' - diol.

² **Vx**: (3S, 5R, 6S, 3'S, 5'R, 6'S) - 5, 6; 5', 6' - diepoxy - 5, 6, 5', 6' - tetrahydro - β , β - carotene - 3, 3' - diol.

³ **Ax**: (3S, 5R, 6S, 3'R) - 5, 6 - epoxy - 5, 6 - dihydro - β , β - carotene - 3, 3' - diol.

⁴ **Dx**: (3S, 5R, 6S, 3'R) - 5, 6 - epoxy - 7', 8' - didehydro - 5, 6 - dihydro - β , β - carotene - 3, 3' - diol.

⁵ **Dt**: (3R, 3'R) - 7, 8 - didehydro - β , β - carotene - 3, 3' - diol.

the Dd cycle compared to the Vx cycle in higher plants (Lohr and Wilhelm, 1999). In *P. tricornutum*, under low light, Zx and Dt are epoxidized in Dd and Vx and then may be transformed into the light-harvesting carotenoid pigment fucoxanthin (Goericke and Welschmeyer, 1992; Lohr and Wilhelm, 1999, 2001). This conversion of photoprotective pigments in light-harvesting pigments could represent an advantage in term of metabolic cost (Lohr and Wilhelm, 1999).

2.4.2.2 Localization of the xanthophyll cycle pigments

In higher plants, xanthophyll-cycling pigments (Vx, Ax and Zx) are associated with all light-harvesting antenna components, including LHCI and PsbS (Ruban *et al.*, 1999). Those bound by the minor LHCII (CP24, CP26 and CP29) account for approximately 30% of the PSII-associated pool, while the remainder binds the major LHC (Ruban *et al.*, 1994; Ruban and Horton, 1999). Under high light, Vx is apparently converted into Zx in all complexes except in CP29, with a degree of de-epoxidation varying among the different LHCs (Ruban *et al.*, 1994; Croce *et al.*, 1996; Ruban and Horton, 1999). In the thylakoid membrane, one ionone ring of the Vx molecule is arranged into hydrophobic pocket formed by chlorophylls, hydrophobic residues of the protein and the membrane lipid phosphatidylglycerol (Yamamoto *et al.*, 1974; Latowski *et al.*, 2000). The opposite ionone ring of Vx sticks out of the binding pocket and faces the stromal side of the membrane. The ionone ring at the luminal side points to a cavity that might represent the docking site for VDE (Bugos *et al.*, 1998). Yamamoto and Bassi (1996), in agreement with Hager and Holocher (1994), observed that Vx in the lipid matrix, rather than the fraction bound to LHC proteins, is the substrate for VDE. It means that, in order to be de-epoxidized, Vx needs to diffuse out of its binding sites. After de-epoxidation, a part of Zx rebinds to CP26 and CP29 (minor antenna proteins), while another part is released in the lipid membrane and induces quenching by conformational change (Bassi and Caffari, 2000).

Compared to higher plants and green algae, diatoms have a different organization of the LHC. The organization of the thylakoid membranes differ significantly from that of Chlorophyta, with thylakoids arranged in groups of three and undifferentiated in grana and stromal lamellae (see above; Owens, 1988). No orthologs of CP26 and CP29 have been found in the genome of the diatom *Thalassiosira pseudonana* (Armbrust *et al.*, 2004), confirming that the light-harvesting proteins of diatoms are not differentiated into minor

and major complexes (Larkum and Veski, 2003). In diatoms, Dd was found in all the light-harvesting complex subunits (Lavaud *et al.*, 2003). Under intermittent light conditions, the size of the Dd pool increases compared to continuous light. The additional Dd molecules are bound in majority to the periphery of the LHC, while the LHC fraction associated with the reaction center is little enriched of Dd (Lavaud *et al.*, 2003).

New insights concerning diatoms organization of the antenna, pigment binding capacity and protein composition, have been achieved during the last years (see the recent reviews by Bertrand, 2010; Lepetit *et al.*, 2011).

The antenna of diatoms is organized in oligomeric complexes. In the centric diatom *Cyclotella meneghiniana*, a trimeric FCPa-complex, together with a hexameric or nonameric FCPb-complex have been described (Büchel, 2003; Beer *et al.*, 2006), whereas a trimeric organization of the antenna fraction, in the pennate diatom *Phaeodactylum tricorutum* (Lepetit *et al.*, 2007; Joshi-Deo *et al.*, 2010). By adjusting the solubilization conditions, higher oligomeric states have also been isolated in *P. tricorutum* (most probably hexameric complexes; Lepetit *et al.*, 2007), and in *C. meneghiniana*, both for FCPa and FCPb complexes (Lepetit *et al.*, 2010).

FCP-PSII supercomplexes, comparable to LHC-PSII supercomplexes of vascular plants, have not been yet isolated, and their presence still remains questionable (Lepetit *et al.*, 2011). Recent studies suggested the possible presence of such structures in *Chaetoceros gracilis*, even if they might be loosely bound to the PSII core complex (Nagao *et al.*, 2007, 2010).

The FCP complexes contain very high amounts of carotenoids, especially fucoxanthin (Fuco). Despite minor pigment contents differences in FCPs of different diatoms species or in distinct FCP complexes (FCPa or FCPb), a general model of FCP pigment organization have been recently described by Premvardhan and co-authors (2010). They reported strong evidences for the binding of 8 molecules of Chl *a* and of Fuco, and 2 molecules of Chl *c*₂ per FCP monomer (an 8 Chl *a* : 8 Fuco : 2 Chl *c*₂ stoichiometry). At least one molecule of Dd per FCP monomer should be added to the stoichiometry, since a minor amount of diadinoxanthin (Dd) has been lately found to be protein-bound to the FCP (Lepetit *et al.*, 2010).

Diatoms contain a peripheral antenna, delivering energy to both photosystems, and a PSI-specific antenna, whose function is still unclear (Lepetit *et al.*, 2010).

The protein composition of both peripheral and PSI-specific FCP has been recently revealed, in more details. Three different antenna protein families are encoded within

diatoms genome: (i) the light-harvesting proteins (Lhcf), (ii) the Lhcr proteins, related to the red algal LHCI proteins, and (iii) the ancient LI818 proteins (Lhcx; Eppard *et al.*, 2000; Green, 2007; Koziol *et al.*, 2007). In general, Lhcf and Lhcr proteins mainly constitute the FCP, together with other light-harvesting ones. Lhcr and Lhcf proteins have been confirmed to be present in comparable concentrations within diatom chloroplast, while Lhcx proteins are in much lower amount (Westermann and Rhiel, 2005). Lepetit and co-authors (2010) have been able to identify, within the FCP, 12 of the 15 Lhcf, and 7 of the 14 Lhcr proteins encoded in *P. tricornutum* genome, whereas, only Lhcx1 was present in FCPs isolated from cells grown under low irradiance. In addition, 4 FCP-related (and not further annotated) proteins, as well as the Lh11 protein (member of the lately discovered red lineage of Chl *a/b*-binding like proteins, RedCAP; Engelken *et al.*, 2010), have been detected. These results underline a huge diversity in FCP complexes, largely increasing the complexity of the peripheral LHC organization in diatoms, compared to higher plants.

As aforementioned, diatoms also contain a PSI-connected and specific FCP (Veith and Büchel, 2007; Veith *et al.*, 2009; Lepetit *et al.*, 2008, 2010). This specific FCP has significantly higher protein-bound Dd and lower Fuco amounts, than the major peripheral FCP. Furthermore, it is almost exclusively composed of Lhcr proteins, which are closely related to the PSI antenna of red algae and cryptophytes (Lepetit *et al.*, 2010).

2.4.2.3 Properties of the enzymes involved in the xanthophyll cycle

Like zeaxanthin epoxidase (ZEP), violaxanthin de-epoxidase (VDE) belongs to the lipocalin family of proteins (Bugos and Yamamoto, 1996; Bugos *et al.*, 1998; Hieber *et al.*, 2000). VDE is a water-soluble enzyme located in the thylakoid lumen of higher plants (Hager, 1969). This protein shows three important domains. The first domain is a cysteine-rich region where Dithiothreitol (DTT), inhibitor of de-epoxidase activity, acts (Yamamoto and Kamite, 1972). DTT reduces one or more disulfid-bonds formed by the cysteine rich N-terminal of the enzyme, thereby completely blocking VDE activity (Bugos and Yamamoto, 1996; Bugos *et al.*, 1998). The second one, is a domain signature typical of proteins belonging to the lipocalin family. The lipocalins mainly bind small lipophilic substrates (Bugos *et al.*, 1998). Their catalytic site forms a barrel-like structure. The binding site, located in this barrel, is a narrow cavity where the xanthophyll pigment is

inserted and de-epoxidized (Newcomer *et al.*, 1984; Holden *et al.*, 1987). Xanthophylls that do not have the appropriate configuration, i.e. 3-hydroxy and 5-6 epoxide groups (such as Zx and Dt), cannot be used as substrates for the VDE (Yamamoto and Higashi, 1978; Grotz *et al.*, 1999). Beside Vx and Ax, VDE can de-epoxidize other xanthophylls, such as Dd, Neoxanthin (Neox) and Lutein-epoxide (Yamamoto and Higashi, 1978; Holden *et al.*, 1987). The third relevant domain, located closed to the C-terminus of the protein, is a region containing a high concentration of glutamic acid residues (Bugos *et al.*, 1998). At low pH-values, the partial protonation of these residues may activate the VDE (Bugos and Yamamoto, 1996). A partial titration of the negative charges in this protein domain possibly increases the binding of VDE to the uncharged monogalactosyldiacylglycerol (MGDG)-rich regions of the thylakoid membrane (Yamamoto *et al.*, 1996).

The VDE enzyme is activated by the light-dependent acidification of the lumen and has an optimal pH activity ranging between 5 and 5.2 *in vivo* (Hager, 1969; Pfündel *et al.*, 1994). VDE requires the presence of ascorbate (Asc) as co-substrate to reduce the epoxy-group (Bratt *et al.*, 1995). Under high irradiances, increased ascorbate concentration resulting from lumen acidity allows optimal VDE activity (Logan *et al.*, 1996). The affinity of VDE for ascorbate is low (Grouneva *et al.*, 2006) and it is the acid form of ascorbate that binds VDE. Therefore, when the ascorbate level is decreased, the pH for optimal activity is shifted to lower values (pH < 5; Bratt *et al.*, 1995).

VDE activity also requires the presence of monogalactosyldiacylglycerol (MGDG; Yamamoto and Higashi, 1978). High concentration of MGDG could facilitate Vx solubilization in the membrane and make Vx accessible for VDE. The enzyme binds to region of the thylakoid membrane that are enriched in MGDG, where the actual de-epoxidation of Vx takes place (Hager and Holocher, 1994; Latowski *et al.*, 2002; Goss *et al.*, 2005). By creating hydrophobic insertion sites, MGDG facilitates the binding of VDE, allowing the enzyme to reach the epoxy-ring of the Vx located in the luminal side of the thylakoid membrane (Latowski *et al.*, 2002). The second reaction of de-epoxidation, i.e. conversion of Ax to Zx, also occurs in the MGDG-rich domain and is facilitated since Ax formed in such domains has an immediate access to VDE. Therefore, the conversion of Ax to Zx does not seem to be limited by a diffusion process (Latowski *et al.*, 2002), contrarily to the first de-epoxidation step of the cycle (from Vx to Ax).

The zeaxanthin epoxidase (ZEP) enzyme is localized in the stromal side of the thylakoid membrane where it epoxidizes xanthophylls having a 3-hydroxy-ionone rings in the 5-6

position (i.e. Zx and Dt; Hager, 1975; Siefermann and Yamamoto, 1975). The epoxidation of Zx to Vx through Ax has an optimal pH of activity between pH 7 and 7.5, close to stroma pH (Siefermann and Yamamoto, 1975). In Chlorophyta, epoxidation of Zx is not only observed under low-light conditions or in complete darkness after de-epoxidation, but also under high light (Siefermann and Yamamoto, 1975). Co-substrates for this reaction are oxygen (Takeguchi and Yamamoto, 1968), ferredoxin, ferredoxin-oxidoreductase and NADPH (Takeguchi and Yamamoto, 1968; Hager, 1975; Bouvier *et al.*, 1996). Another important co-factor, the flavine adenine dinucleotide (FAD), was found to enhance the epoxidase activity (Büch *et al.*, 1995).

Concerning the Dd cycle, studies dealing with the properties of the diadinoxanthin de-epoxidase (DDE) and the diatoxanthin epoxidase (DEP) are quite recent (Jakob *et al.*, 2001; Goss *et al.*, 2005, 2006b; Grouneva *et al.*, 2006).

Like VDE, the DDE is a water-soluble luminal protein that undergoes a conformational change when pH drops, allowing binding to the thylakoid membrane (Grouneva *et al.*, 2006). *In vitro*, isolated Dd de-epoxidase has a pH *optimum* at pH 5.5. However, enzyme activity has been observed at pH 7.2 (Jakob *et al.*, 2001), while VDE activity has not been observed at pH values higher than 6.5 (Hager, 1969; Pfündel *et al.*, 1994). In comparison to VDE, a reduced amount of negative charges in DDE would decrease the number of protons needed for neutralization, resulting in the activation and binding of the enzyme to the thylakoid membrane at higher pH-values (Jakob *et al.*, 2001). Activation of DDE at neutral pH values can influence the operation of the Dd cycle *in vivo*, since the de-epoxidation of Dd to Dt can be triggered by a weak lumen acidification (for instance, due to chlororespiratory electron flow; Jakob *et al.*, 1999, 2001). DDE has a higher affinity for ascorbate (Asc) than VDE of higher plants (Grouneva *et al.*, 2006). This feature allows the enzyme to convert Dd in Dt not only at a higher pH, but also at lower concentration of reduced Asc in the lumen of the thylakoid. The *optimum* of DDE activity was pH ~ 5 at low Asc concentration, while at high Asc concentration, its activity can be shifted to neutral pH values. In the latter condition, DDE has a very rapid and large response to small pH changes in the thylakoid lumen, compared to low Asc level conditions (Grouneva *et al.*, 2006). DDE requires the presence of the major thylakoid membrane lipid MGDG, which solubilizes Dd and provides a binding site (Goss *et al.*, 2005). Under low light, Dd and Vx are present in an aggregated form which limit their access to the de-epoxidase. To be effectively de-epoxidized, they need to be solubilized (Goss *et al.*, 2005). Although both DDE and VDE rely on the presence of MGDG, Dd is much more solubilized in

MGDG than is Vx of higher plants. A MGDG : xanthophyll ratio of 5 is enough for Dd de-epoxidation in diatoms, whereas VDE requires a lipid ratio MGDG : Vx, of almost 30 for optimal Vx de-epoxidation (Yamamoto and Higashi, 1978). Either the asymmetry of the Dd molecule, or its higher polarity might be responsible for such feature. This characteristic means that in diatoms experiencing high light, a larger number of Dd molecules can be released from the light-harvesting binding sites and diffuse to the lipid phase of the membrane. An efficient de-epoxidation of a large number of Dd molecules, and within a short time period, could thus provide a rapid photoprotection of the photosynthetic apparatus in these organisms (Goss *et al.*, 2005).

The diatoxanthin epoxidase (DEP) has the same co-substrate requirement as the ZEP of higher plants, using oxygen, FAD and NADPH (Büch *et al.*, 1995). Like ZEP, DEP is located in the chloroplast stroma and is active at pH values around 7.5 (Siefermann and Yamamoto, 1975).

A significant difference exists in the regulation of DEP and ZEP activity. Zx epoxidation proceeds with low rates in vascular plants and green algae (Siefermann and Yamamoto, 1975; Goss *et al.*, 2006a), normally taking place under conditions of low light or complete darkness. Under high light, the conversion of Zx to Vx is not inhibited, and even slightly increased rates of epoxidation can be observed (Siefermann and Yamamoto, 1975; Goss *et al.*, 2006a). On the other hand, DEP activity is thought to be completely inhibited under high light by the presence of the light-driven proton gradient (Mewes and Richter, 2002; Goss *et al.*, 2006b). The Δ pH-dependent regulation of DEP is necessary because of the enzyme significantly faster epoxidation rates than ZEP in Chlorophyta (Goss *et al.*, 2006b). Therefore, under high light conditions, both DEP inhibition and DDE activation ensure rapid and efficient de-epoxidation of Dd to Dt.

However, DEP activation during illumination has been recently reported by Dimier and co-authors (2009b). In their study, six algal species were exposed to gradually increasing light intensities, and a slow epoxidation of Dt was measured in three species (*Phaeocystis cordata*, *Pelagomonas calceolata* and *Mesopedinella arctica*), consistently with their ecological traits, once cells were acclimated to the new light conditions. Such a result might be due to cells photoacclimation to light conditions, causing a decrease in the transmembrane proton gradient, allowing DEP activity, and thus the visible Dt epoxidation. This finding clearly suggests that DEP can be activated under illumination.

For a recent review on photoprotective processes regulation/function in relation to xanthophyll cycle activation in algae, see Goss and Jakob (2010).

2.4.3 Xanthophyll cycle functioning and non-photochemical fluorescence quenching

2.4.3.1 State of art

The non-photochemical fluorescence quenching (NPQ) process takes place into the light-harvesting complex of PSII, when irradiance exceeds the photosynthetic capacity of the cell, and it dissipates part of the light energy absorbed in excess, thus decreasing the excitation pressure on PSII (Demmig-Adams and Adams, 2006; Lavaud, 2007; Li *et al.*, 2009; Goss and Jakob, 2010). NPQ reduces the lifetime of $^1\text{Chl } a^*$ and, as a consequence, the quantum yield of Chl *a* fluorescence as well as the quantum yield of photochemistry.

NPQ is composed of three components (qE, qT and qI) whose respective importance varies among the photosynthetic lineages (for reviews see Niyogi, 1999; Demmig-Adams and Adams, 2006; Goss and Jakob, 2010; Ruban *et al.*, 2011). qE, the energy-dependent quenching, is essential for most of the algal groups, and is regulated by the buildup of a trans-thylakoidal ΔpH and the xanthophyll cycle (XC) modulation. qT refers to the part of the quenching due to state transitions (allowing part of the absorbed energy reallocation from the PSII to the PSI), while qI is due to photoinhibition. qT is relevant in phycobilisome-containing organisms (i.e. cyanobacteria and red algae) and green microalgae, being not really significant under light conditions triggering maximal qE (Mullineaux and Emlin-Jones, 2004; Ruban and Johnson, 2009; Ruban *et al.*, 2011). Diatoms seem to lack a state-transitions mechanism (Owens, 1986). The origin of qI is not clearly defined except for some higher plants, in which it would require peculiar conditions, such as prolonged environmental stress (Demmig-Adams and Adams, 2006). In vascular plants, qI has been firstly attributed solely to photoinhibitory damage to the PSII reaction centers (Baker and Horton, 1987; Jahns and Krause, 1994). Then its major portion has been related to a sustained quenching in the LHCII antenna, through the photoprotective down regulation of PSII (i.e. zeaxanthin-dependent; Baker and Horton, 1987; Ruban *et al.*, 1993). Further studies on the zeaxanthin-dependent qI showed that it consists of two components: one is sensitive to uncouplers and persists for quite long periods in darkness (not being associated with the bulk ΔpH), while the other is not sensitive to uncouplers (Ruban and Horton, 1995). The modulation of qI by zeaxanthin seems to possibly originate from the same site and the same process underlying qE development.

The relationship between qE and the accumulation of de-epoxidized xanthophylls has been reported in many algal groups, with the first correlation between qE and the accumulation of de-epoxidized xanthophylls (under high light) observed in higher plants and green microalgae (see Demmig-Adams, 1990). Later it was also reported in diatoms and dinoflagellates (Sakshaug *et al.*, 1987; Demers *et al.*, 1991; Olaizola and Yamamoto, 1994), Chrysophyceae and Euglenophyta (Lichtlé *et al.*, 1995; Casper-Lindley and Björkman, 1998), red algae (Ritz *et al.*, 1999), and in cyanobacteria (Bailey *et al.*, 2005). Picoeukaryotes have lately showed to be interesting model organisms to tackle the functional relation between qE and XC modulation (Dimier *et al.*, 2007a, 2009a; Giovagnetti *et al.*, 2010), because of their high flexibility in PSII photoregulatory responses, in relation to a set of biological and ecological features linked to their small cell size (Raven, 1998; Raven *et al.*, 2005; Timmermans *et al.*, 2005). However, a clear understanding of the (mechanistic) functioning of qE in microalgae still lacks (with the exception of *Chlamydomonas reinhardtii* mechanism; Peers *et al.*, 2009), although few functioning conceptual models have been proposed (Lavaud, 2007; Goss and Jakob, 2010). In higher plants, qE has been largely investigated at the molecular level (Cogdell, 2006; Jahns and Holzwarth, 2011; Ruban *et al.*, 2011). An equally deep comprehension of qE complexity has not been reached in microalgae, in part because the XC molecular effectors for qE regulation, and their interactions, have not been fully identified. Furthermore, the effect on the functional relationship between qE and NPQ, relative to light exposure and light history of cells (especially under field-simulated light conditions, Dimier *et al.*, 2009a; Van de Poll *et al.*, 2010), deserves a deeper understanding (Brunet and Lavaud, 2010).

The red algae and cyanobacteria have extrinsic light-harvesting complexes system (i.e. phycobilisomes, PBS), and despite the presence of a weak qE quenching, the composition and organization of the antenna obviously support different type of qE mechanism (Wilson *et al.*, 2006; Kirilovsky, 2007; Bailey and Grossman, 2008). Despite a XC has been observed in some red algae species, no functional link with qE has been reported (Ursi *et al.*, 2003).

In cyanobacteria, a photoprotective mechanism has only recently been discovered (El-Bissati *et al.*, 2000). Contrarily to plants and eukaryotes, cyanobacteria lack both the pH-dependent quenching and the XC. NPQ in cyanobacteria is induced by blue-green light and mediated by a water-soluble orange carotenoid protein (OCP) (Wilson *et al.*, 2006, 2007; Karapetyan, 2007), and it has been reported in many species of cyanobacteria

(Boulay *et al.*, 2008). The OCP acts as a light sensor that, upon illumination with blue-green light, photo-converts from its dark stable (orange) form to the active (red) form, due to a marked red shift in the absorption spectrum (Wilson *et al.*, 2008).

A recent study by Gorbunov and co-workers (2011) demonstrates that the formation of the quenched state *in vivo* is a multistep process, involving both photo-induced and dark reactions. This reaction sequence has been described by the authors within the framework of the 3-state model: (i) under low light conditions the OCP is in the orange form (OCP^o) and is not attached (or weakly coupled) to PBS, (ii) upon actinic blue-green illumination the OCP converts into the red form (OCP^r), and finally conformational changes in the OCP and its attachment to the PBS core cause the quenched state (OCP^q; Gorbunov *et al.*, 2011).

It has been argued that qE in cyanobacteria would serve to adjust the energy transfer within the phycobilisomes of an already acclimated system to environmental stress(es) (high light, iron deficiency), but would not serve to cope with rapid fluctuations of irradiance, as in higher plants and eukaryotic algae. The weaker qE quenching in cyanobacteria than in other phytoplankton taxa (Lavaud, 2007) might be due to the lack of a finely regulated XC, but also to the activation of other preferential photoprotective processes (qT and/or the rapid repair of the D1 protein of PSII reaction centers; Wilson *et al.*, 2006; Six *et al.*, 2007). At the same time, the work of Gorbunov and co-authors (2011) reports that NPQ leads to a decrease in PSII functional absorption cross section of photochemistry, that reduces the flux of absorbed energy from PBS to reaction centers by ~52%.

A low qE quenching was also found in *Prochlorococcus* and its intrinsic Pcb antenna system (Bailey *et al.*, 2005), with qE being dependent on Zx accumulation under high light, instead of a XC activation.

Recently, Serôdio and Lavaud (2011) proposed a mathematical model to describe the light response of NPQ, providing a good fit to both experimental and published data. The model was further applied to quantitatively compare the light responses of NPQ and PSII electron transport rate (Serôdio and Lavaud, 2011).

2.4.3.2 Function of the V_x cycle and NPQ mechanism

In vascular plants, and green and brown algae, the de-epoxidation of V_x to Z_x leads to an enhanced dissipation of excess excitation energy in the photosystem II (PSII) antenna system, thereby preventing inactivation and damage in the photosynthetic *apparatus* (Demmig-Adams *et al.*, 1990; Horton and Ruban, 1992; Gilmore and Yamamoto, 1993). Excess excitation energy is dissipated as heat, through NPQ.

At present, despite the general agreement in the fact that NPQ would be related to a structural change of the PSII light-harvesting complex (LHCII), mechanistic details of the Z_x-dependent dissipation of excitation energy are still under debate.

Two main models have been proposed for the mechanism of energy dissipation by the violaxanthin-cycle: a direct (i) and an indirect (ii) quenching by Z_x (see Szábo *et al.*, 2005; Goss and Jakob, 2010; Jahns and Holzwarth, 2011 ; Ruban *et al.*, 2011).

The direct quenching mechanism, also called the “molecular gear-shift model” (Frank *et al.*, 1994, 2000) is based on a direct interaction of Z_x with a chlorophyll (Chl) *a* molecule in the excited state. According to this mechanism, Z_x would accept the excitation energy from a Chl *a* molecule in the singlet excited state (¹Chl *a**), dissipating this energy as heat after internal conversion to the ground state. This direct quenching mechanism depends on the possibility of energy transfer between a Chl *a* and a Z_x molecule, which in turn requires that the energy level of the first singlet excited state of the Z_x molecule to be lower than that of Chl *a*. The direct quenching mechanism still awaits final experimental verification, due to the complicated determination of the singlet excited state of carotenoid molecules, and the different results obtained by distinct measuring techniques (Polívka *et al.*, 1999; Josue and Frank, 2002).

According to Holt and co-authors (2005), Z_x would act as a direct quencher of excitation energy, with a charge separation between the Z_x and the Chl *a* molecules, and not a singlet–singlet energy transfer.

The indirect quenching mechanism is based on structural differences between the epoxidized and de-epoxidized xanthophyll cycle pigments. According to this model conversion of V_x to Z_x induces an aggregation of the peripheral LHCII (Horton *et al.*, 1991, 1996; for a recent modification of the model, see Horton *et al.*, 2005, 2008). The structural basis for the LHCII aggregation is the protonation of special amino acid residues of the LHCII apoproteins (Walters *et al.*, 1994), or the low lumenal pH sensing by the PsbS protein (Li *et al.*, 2000, 2002), and the different steric structure of the Z_x molecule.

The full induction of NPQ takes place in the presence of Zx which supports the establishment of the actual quenching site within the LHCII, which is composed of a Chl *a* homodimer or a Chl *a*/lutein heterodimer (Pascal *et al.*, 2005; Ruban *et al.*, 2007).

Recently, Holzwarth and co-authors (2009) proposed a new model for NPQ in vascular plants, according which, two different quenching sites are responsible for NPQ: (i) a quenching site consisting of PSII-detached and aggregated peripheral LHCII complexes (NPQ at this site depends on the presence of the PsbS protein), and (ii) a second quenching site, located in the minor PSII antenna proteins (NPQ at this site is instead related to the presence of Zx).

It has recently been reported that the LHCSR protein (formerly known as the LI818 protein) is essential for the qE component of NPQ in the green alga *Chlamydomonas reinhardtii* (Peers *et al.*, 2009). This protein represents an ancient member of the light-harvesting protein family, and orthologues are found in various taxa of eukaryotic algae (including diatoms). The fact that the LHCSR protein is missing in higher plants (but present in the prasinophyte *Ostreococcus tauri*), suggests the use of distinct proteins for the mechanism of NPQ in higher plants (PsbS protein), and at least in some green algal species (LHCSR protein).

Changes in the structure of XC pigments upon de-epoxidation may not only affect the aggregation of the LHCII, but may also the fluidity of the thylakoid membrane (Gruszecki and Strzalka, 1991). Zx and Ax seem to prevent lipid peroxidation under conditions of a highly reduced electron transport chain (Sarry *et al.*, 1994), and further evidence for such indirect photoprotective role of Zx came from studies conducted on *Arabidopsis thaliana* mutants (Havaux and Niyogi, 1999; Triantaphylideès and Havaux, 2009).

2.4.3.3 Function of the Dd cycle and NPQ mechanism

The Dd cycle represents the most important photoprotection mechanism of diatoms and leads to an efficient dissipation of excessively absorbed excitation energy as heat, which becomes visible as a strong NPQ (Olaizola *et al.*, 1994; Lavaud *et al.*, 2002a, 2002b; Lavaud, 2007; Goss *et al.*, 2006b).

In Dd cycle-containing algae, NPQ is not as heterogeneous as in vascular plants (Niyogi, 1999), and different mechanisms contribute to both qE and qI quenching components.

In diatoms, NPQ is closely correlated with Dt concentration (Lavaud *et al.*, 2002a), and the qT quenching is missing, since the absence of state transitions. This direct correlation between NPQ development and Dt can promote the development of extremely high values of NPQ, due to large pools of Dd cycle pigments (Lavaud *et al.*, 2002a; Ruban *et al.*, 2004; Goss *et al.*, 2006b), with a strong increase in Dd cycle pigment content when diatoms are subjected to high light conditions of growth (Schumann *et al.*, 2007). Furthermore, a very efficient conversion of Dt back to Dd ensures a rapid and effective switch from a photoprotective to a light-harvesting state of cells (Goss *et al.*, 2006b).

Goss and co-authors (2006b) proposed that NPQ solely depends on Dt concentration, once the quenching state has been formed (via ΔpH), and is independent of the proton gradient. Other studies have instead reported the necessity of a proton gradient for a Dt-dependent enhanced NPQ (Ruban *et al.*, 2004; Lavaud and Kroth, 2006). Concerning the results obtained in these studies, it seems that the trans-membrane proton gradient, together with the pH-dependent activation of the DDE, are needed to activate the quenching capacity of Dt, possibly through a protonation of special residues of the FCPs (Ruban *et al.*, 2004; Lavaud and Kroth, 2006).

Ruban and co-authors (2004) have proposed the occurrence of distinct events during the establishment of NPQ in diatoms. The formation of Dt and protonation of antenna proteins would lead to a conformational change of the antenna. The quenching state of the light-harvesting complex would involve the binding of Dt into hydrophobic regions of the protein, and the 'movement' of proton-binding domains, thus developing a stable NPQ. Such mechanism would prevent a fast relaxation of NPQ after the breakdown of the ΔpH , not differently to what Goss and co-authors (2006a, 2006b) observed (i.e. once Dt would be activated, the ΔpH would no longer be needed for effective NPQ).

Evidences of a conformational change of the antenna, in terms of an aggregation of FCPs, have been presented by a recent work of Miloslavina and co-authors (2009). In these experiments, a model describing the mechanistic basis of NPQ in the two diatoms *Phaeodactylum tricornutum* and *Cyclotella meneghiniana* predicts that two independent quenching sites are responsible for the steady-state NPQ in diatoms. One site is localized in FCPs, functionally detached from the PS core complexes, while the second quenching site is present in FCPs closely connected to the PSII core complex. Upon high light illumination, at the site one, PSII-detached FCPs aggregate and NPQ development is relatively independent of Dt, while at the second quenching site, NPQ development is Dt-

dependent. In vascular plants, a PSII-detached quenching has been reported for LHCII complexes, significantly contributing to total NPQ (Miloslavina *et al.*, 2008).

Supporting the relevance of binding sites of Dt in the regulation of the NPQ mechanism (Ruban *et al.*, 2004; Lavaud and Kroth, 2006), Gundermann and Büchel (2008) demonstrated differences of quenching capacity between Dt bound to the trimeric FCPa of the isolated FCP (strong fluorescence quenching), and Dt bound to the oligomeric FCPb (no quenching), in *C. meneghiniana*. These results are in agreement with the aforementioned evidence that NPQ can be allocated to two different quenching sites, in diatoms (Miloslavina *et al.*, 2009): a quenching site 1 (Q1), which is PSII-detached, relatively Dt-independent and based upon oligomeric complexes aggregation, and a quenching site 2 (Q2), attached to PSII and relying on Dt synthesis. Based on this hypothesis, it was suggested the possible identity of Q1 with the oligomeric FCPb complexes, and Q2 with the trimeric FCPa complexes, as described by Gundermann and Büchel (2008).

Besides the presence of different quenching sites within PSII and PSI, diatoms XC modulation might also be regulated by specific lipid domains in the thylakoid membrane (Goss and Wilhelm, 2009; Lepetit *et al.*, 2011).

Although the largest part of NPQ is composed by a Dt-dependent antenna quenching, recent results reported the existence of a reaction center (RC) type quenching, related to functional organization of the PSII RC (Eisenstadt *et al.*, 2008) and oxygen uptake in the photosynthetic machinery (Eisenstadt *et al.*, 2010), both contributing to energy dissipation. Notably, the Dd cycle containing algae do not possess the PsbS protein, which is essential for NPQ in vascular plants (Li *et al.*, 2000, 2002). No homolog of the PsbS protein was found in the genome of *Thalassiosira pseudonana* and *P. tricornutum* (Armbrust *et al.*, 2004; Montsant *et al.*, 2005; Bowler *et al.*, 2008), but homologues of the stress-related LHCSR/LI818 proteins, which very recently have been shown to be critical for NPQ in the green algae *Chlamydomonas reinhardtii* and *Ostreococcus tauri* (Peers *et al.*, 2009), are present in diatoms. In *C. meneghiniana* *fcp6* and *fcp7* were identified as *LI818* homologues (Beer *et al.*, 2006), while in *T. pseudonana* and *P. tricornutum* the *Lhcx* family showed homologies with the *LI818* gene (Zhu and Green, 2010; Nymark *et al.*, 2009).

Lhcx proteins clearly seem to play a crucial role on NPQ mechanism, as molecular effectors. Indeed, a correlation between the expression level of *fcp6-7* (*C. meneghiniana*) and of different Lhcx proteins (*T. pseudonana* and *P. tricornutum*) and NPQ development

in response to a low to high light transition, has been lately demonstrated (Bailleul *et al.*, 2010; Zhu and Green, 2010).

The diversity of stress-related proteins found in diatoms, compared to the single PsbS protein in higher plants, suggests different functions of these proteins. Furthermore, since the absence of acidic amino acids in LhcX proteins (as the ones described for the PsbS/LI818 protein), their possible pH-sensing function becomes uncertain (Bailleul *et al.*, 2010). Differently, LhcX proteins might play a structural role (for instance, in the binding of *de-novo* synthesized Dt), as suggested for fcp6-7 in *C. meneghiniana* (Beer *et al.*, 2006), and for LhcX6 in *T. pseudonana* (Zhu and Green, 2010). Differently, *lhcx1* expression level is correlated with NPQ development, even with no changes in Dt content, making its function in binding Dt molecules unlikely (Bailleul *et al.*, 2010). In such case, LhcX1 might regulate the NPQ mechanism, by inducing FCPs conformational changes, or by affecting the connectivity between antenna and photosystems.

2.5 Xanthophyll cycle and ecophysiology of algae

Each species of phytoplankton has a different combination of adaptative characteristics that defines (in many ways) its distribution in relation to ecological factors. Richardson and co-authors (1983) reviewed the adaptation of different taxa to light, showing broad differences between dinoflagellates, diatoms and green algae, that were generally consistent with their patterns of dominance in aquatic environments. On long time scale, from seasons to year, competition between, and succession of, phytoplankton species may in part depend on their respective photoacclimation and photoprotection capacities (Demers *et al.*, 1991; Falkowski and LaRoche, 1991). However, few data exist on the relationship between the photoprotective capacities of algal species and their ecology. Demers and co-authors (1991) first related the particularly active xanthophyll cycle of *Alexandrium excavatum* with light conditions representative of the ocean euphotic zone. Meyer and co-authors (2000) showed that differences in photoprotection capacities between *Phaeocystis globosa* and *Thalassiosira* sp. could be in part responsible for their succession in time in the North Sea. According to this study, *Phaeocystis globosa* out-competes *Thalassiosira* sp. at higher light intensities, since the slow xanthophyll acclimation and low light saturation level of the diatom.

Up to now, ecological studies dealing with xanthophyll cycle and photoprotection in marine phytoplankton have mainly focused on diatoms (Olaizola and Yamamoto, 1994; Fujiki and Taguchi, 2001; Lavaud *et al.*, 2002b, 2003; Lavaud *et al.*, 2007; Kashino and Kudoh, 2003). The occurrence and the success of these organisms in turbulent waters was related to their capacity to perform rapid and strong NPQ (compared to higher plants) under high light (Lavaud *et al.*, 2002b). Reports on other groups are less common (e.g. Chrysophyceae, Dinophyceae; Casper-Lindley and Björkman, 1998; Evens *et al.*, 2001). Casper-Lindley and Björkman (1998) clearly showed a high diversity of photoprotective responses among 4 algal groups containing different combination of light harvesting and xanthophyll cycle pigments, possibly related to their ecology. Under high irradiance, the bloom-forming prymnesiophyte *Emiliana huxleyi* increases the xanthophyll pigment pool and is able to quickly change its photosynthetic pigment content (Harris *et al.*, 2005). The prymnesiophyte *Phaeocystis antarctica* is numerically and structurally important in the Antarctic food web. During austral winter, water column mixing processes expose phytoplankton cells to a variety of irradiances. *P. antarctica* is able to tolerate sudden changes in irradiance by quickly activating the xanthophyll cycle through a stoichiometric conversion between Dd and Dt (Moisan and Mitchell, 1998, 1999). Recently the photophysiology of two strains of *P. antarctica* G. Karst (CCMP1374 and CCMP1871; Prymnesiophyceae) and one strain of *Fragilariopsis cylindrus* (Grunow) Willi Krieg (CCMP1102; Bacillariophyceae), populating the Ross Sea (Southern Ocean), have been investigated and compared under three dynamic irradiance regimes that simulated different mixed-layer depths (Mills *et al.*, 2010). In agreement with the results of Kropuenske and co-authors (2009), *F. cylindrus* CCMP1102 is better able to quench excess light energy through heat dissipation (XC), prioritizing photoprotection over rapid growth, while *P. antarctica* CCMP1871 maximizes growth and must continuously repair photodamage (Kropuenske *et al.*, 2009, 2010; Mills *et al.*, 2010). The photoacclimative strategies adopted by these two species might explain their capacity to grow in, and to exploit, different mixing and irradiance regimes (i.e. shallow mixed layers or sea ice for *F. cylindrus*, and deeply mixed water columns for *P. antarctica*; Kropuenske *et al.*, 2010; Mills *et al.*, 2010). These results underline the relevance of photosynthetic and photoacclimative diversity of distinct algal groups in affecting the phytoplankton community composition/distribution in the Ross Sea (Kropuenske *et al.*, 2010; Mills *et al.*, 2010). Further heterogeneity in photophysiological plasticity has been recently reported in

Antarctic microalgal communities and dominant diatom species (Petrou *et al.*, 2011a, 2011b).

The variability of physiological responses to light fluctuations seems to allow competitive exclusion, and thus spatial co-existence and/or temporal succession of species in both pelagic (Meyer *et al.*, 2000; Strzepek and Harrison, 2004; Dimier *et al.*, 2007b, 2009b; Lavaud *et al.*, 2007), and benthic environments (Serodio *et al.*, 2005; van Leeuwe *et al.*, 2008). Recent studies demonstrate how the XC activity and efficiency might be influenced by (and influence) the niche adaptation, in pelagic (Meyer *et al.*, 2000; Dimier *et al.*, 2007b, 2009a; Lavaud *et al.*, 2004, 2007; Giovagnetti *et al.*, 2010) and benthic species (Serodio *et al.*, 2005; van Leeuwe *et al.*, 2008; for a review on XC, see Brunet and Lavaud, 2010).

To simulate the different time scales of light variations, recent studies have been performed by subjecting algal cells to several fluctuating light regimes in order to look for a relationship between photoprotection and growth rate (Havelková-Dousová *et al.*, 2004; Wagner *et al.*, 2006). It has been showed that growth rate responds to fluctuating light in different ways in function of the phytoplankton groups/species (Litchman, 2000; Flöder and Kawabata, 2002; Mitrovic *et al.*, 2003; Wagner *et al.*, 2006) and of photoacclimation ability and light history of cells (Litchman and Klausmeier, 2001; van Leeuwe *et al.*, 2005; Wagner *et al.*, 2006; van de Poll *et al.*, 2007; Laurion and Roy, 2009).

Few *in situ* studies have tried to link the xanthophyll cycle functioning with the acclimation of natural phytoplankton populations to their hydrological environment. The first reports came from Bidigare *et al.* (1987), Olaizola *et al.* (1992), Brunet *et al.* (1993), and Claustre *et al.* (1994), where xanthophyll-cycling pigments were related to the hydrodynamic regime and the light history of algae. These studies were carried out just after the first ecophysiological data obtained on cultures (Sakshaug *et al.*, 1987; Demers *et al.*, 1991). It is known that the light history of phytoplankton influences the relationship between photosynthesis and irradiance by physiological and biochemical changes in cells (Steemann Nielsen and Hansen, 1959; Ryther and Menzel, 1959; Beardall and Morris, 1976). These processes were referred as 'light-shade adaptations', characterized by changes in photosynthetic responses accompanied by changes in chemical composition, fluorescence characteristics and cell volume (Falkowski and Owens, 1980; Falkowski, 1983; Falkowski and LaRoche, 1991; Falkowski *et al.*, 1994). Lewis *et al.* (1984) and Cullen and Lewis (1988) developed mathematical models linking vertical mixing and photoacclimation of phytoplankton. Some studies dealt with the relationship between the

vertical mixing velocity and the time scale of the photoresponse (e.g. Cullen and Lewis, 1988; Lewis *et al.*, 1984; Claustre *et al.*, 1994; Dusenberry *et al.*, 1999). If the time scale of photoacclimation is shorter than that for vertical mixing, phytoplankton would exhibit a vertical gradient associated with acclimation to light intensities. If mixing occurs with a time scale shorter than photoacclimation, the photo-properties in the mixed layer will be uniform.

Water masses can also be well-marked by photoprotective pigments as noticed in the coastal English Channel and in the Mediterranean Sea (Brunet *et al.*, 1993, 2003, 2006). Vertical distributions of photoprotective pigments can be used to establish the rate of vertical mixing of the upper mixed layer (Brunet *et al.*, 2003). Using the Dd : Chl *a* ratio, Claustre and co-authors (1994) determined advection velocities in a frontal system of the Mediterranean Sea.

However, the xanthophyll cycle also depends on environmental factors other than light intensity. Brunet *et al.* (1992) described a decrease in Dd + Dt content in phytoplankton cells trapped in a tidal frontal region of the Eastern English Channel. This decrease could be due to environmental changes (e.g. nutrients or temperature). Indeed, some reports documented the effect of nutrient starvation on the accumulation of xanthophyll pigments in cultures (Geider *et al.*, 1993; Staehr *et al.*, 2002). The production of xanthophyll pigments under nutrient-starved conditions is thought to be analogous to responses of phytoplankton to high light, i.e. an increase in photoprotection by non-photochemical quenching (Moline, 1998). An alternative explanation to the decrease of Dd + Dt in the tidal front could be related to an exportation of the coastal biomass to open sea during the tide. In this case, the acclimation (through xanthophyll pigment synthesis) of exported phytoplankton cells to open sea light conditions (stable and high irradiance) may be a long term process, or cells were dying (Brunet *et al.*, 1992).

In natural populations of Antarctic phytoplankton, low temperature is thought to slow down enzymatic activities and *de novo* synthesis of the xanthophyll pool (Moline, 1998). Continuous light activates the xanthophyll cycle (Brunet *et al.*, 1996) with respect to a light : dark cycle. Bertrand *et al.* (2001) reported an inhibition of Dt epoxidation in diatoms in response to cadmium poisoning.

Casotti *et al.* (2005) showed an increase in Dt in response to algal aldehydes. At this level, Dt may act as an antioxidant and therefore be synthesized without any light increase but in response to an unfavorable and/or harmful environment. This role has already been hypothesized for Zx in vascular plants (Strzalka *et al.*, 2003).

CHAPTER 3

Biology and ecology of picoeukaryotes

Chapter 3

Biology and ecology of picoeukaryotes

3.1 Introduction

Photosynthetic single-celled eukaryotes (i.e. protists) are often referred to as phytoplankton or algae, despite the existence of unicellular and multicellular algae. Heterotrophic protists are instead called protozoa, even though some eukaryotic phytoplanktonic taxa are mixotrophic (Worden and Not, 2008).

Since protistan cell diameter can range from less than one micrometre (μm) to several hundreds, microbial eukaryotes are grouped in size fractions (i.e. cell diameter) and discerned in: pico- (0.2–2.0 μm), nano- (2.0–20 μm), and micro-phytoplankton (20–200 μm ; Sieburth *et al.*, 1978). Picoeukaryotes are formally identified as the smallest cell size fractions (0.2–2.0 μm), despite their size range have been often extended to 3 μm , because of field studies using 3 μm -pore size filters to separate small phytoplanktonic cells from larger ones (e.g. Moon-van der Staay *et al.*, 2001; Brunet *et al.*, 2006, 2007).

Despite some picoplanktonic species have been described in the early 19th century (e.g. the green alga *Stichococcus bacillaris*; Nägeli, 1849), the number of new small species (both prokaryotic and eukaryotic phytoplankton) increased in the 1960s (Butcher, 1952; Manton and Parke, 1960; Bailey-Watts *et al.*, 1968). In the late 1970s and 1980s, small cell size organisms gained *momentum* as a consequence of both methodological progress (e.g. the use of epifluorescence microscopy; Hobbie *et al.*, 1977) and relevant scientific discoveries, such as the description of small prokaryotic (*Synechococcus*, Waterbury *et al.*, 1979; *Prochlorococcus*, Chisholm *et al.*, 1988) and eukaryotic producers (Johnson and Sieburth, 1982), and the formulation of the concept ‘microbial loop’ (Azam *et al.*, 1983).

The application of molecular tools in gene sequences analysis of field samples (Giovannoni *et al.*, 1990) improved the poorly-resolved picture of the picoplanktonic diversity, until then based solely on ‘batch culture’ approaches. In addition, the recent and powerful genomic and metagenomic tools have been successfully used to sequence genomes of important and cultivated species (e.g. *Prochlorococcus*; Dufresne *et al.*, 2003; Rocap *et al.*, 2003), as well as to assess the phylogenetic diversity of unknown natural populations (Béjà *et al.*, 2000; Venter *et al.*, 2004).

However, while the marine microbiology developed, the eukaryotic component of picophytoplankton (i.e. the picophytoeukaryotes) received much less attention than the prokaryotic one, partially due to picoeukaryotes lower abundance, but greater complexity/diversity as a group. Indeed, despite some early publications dating back to the 1950s (Knight-Jones and Walne, 1951; Butcher, 1952), the importance of picoeukaryotes in terms of both biomass and production (e.g. Li, 1994; Worden *et al.*, 2004; Pérez *et al.*, 2005; Jardillier *et al.*, 2010), and diversity (Díez *et al.*, 2001b; López-García *et al.*, 2001; Moon-van der Staay *et al.*, 2001; Le Gall *et al.*, 2008; Vaulot *et al.*, 2008; Lepere *et al.*, 2011), has been revealed quite recently.

Picophytoplanktonic organisms evolved from larger ancestors, in both cyanobacteria and in eukarya, being in the latter polyphyletically derived (Raven, 1998; Raven *et al.*, 2005). Picoeukaryotes are known to live by photoautotrophy and heterotrophy, but in this chapter we will only focus on the photoautotrophic component (i.e. the picophytoeukaryotes), to which we will simply refer as 'picoeukaryotes'.

Most of picoeukaryotes are found in three divisions of major ecological interest (Vaulot *et al.*, 2008; Worden and Not, 2008). The first division is the Chlorophyta, a group at the base of the green lineage origin, with many picoeukaryotic species belonging to the order of Mamiellales, within the polyphyletic class Prasinophyceae (Guillou *et al.*, 2004). Field abundances data show the ecological importance of Mamiellales, particularly in coastal waters (Worden and Not, 2008). Well-studied species are *Micromonas pusilla* (one of the first picoplanktonic species to be described; Knight-Jones and Walne, 1951), and *Ostreococcus tauri* (i.e. the smallest - 0.9 μm cell size - free-living eukaryote; Courties *et al.*, 1994).

The second division is the Heterokontophyta, also known as Stramenopiles, with picoplanktonic representatives found in classes such as Pelagophyceae (e.g. *Pelagomonas calceolata*; Andersen *et al.*, 1993), Bacillariophyceae (with the genera *Minidiscus*, *Minutocellus*, *Skeletonema*), Pinguiophyceae (Kawachi *et al.*, 2002) and Bolidophyceae (e.g. *Bolidomonas mediterranea* and *B. pacifica*, which are closely related to diatoms, for pigment content and 18S rRNA gene sequences; Guillou *et al.*, 1999a).

Haptophyta is the third major division that contains photosynthetic picoeukaryotes, few of which are cultured species (e.g. *Imantonia rotunda* and *Phaeocystis cordata*; Vaulot *et al.*, 2004).

In this chapter, the 'microbial loop' components in marine ecosystems, and the distribution and abundance of picoeukaryotes are described in the section 3.2. Picoeukaryotes

biological features and implications of their hallmark (i.e. the minute cell size), as well as their possible role as model organisms are reported in sections 3.3 and 3.4, respectively.

3.2 Ecological concept of small cell size

In the 1970s, interactions between non-living organic matter and microbial plankton were only hypothetically considered (Pomeroy, 1974). Later, Azam and co-workers (1983) coined the concept of ‘microbial loop’, which he later transformed into ‘microbial food web’, emphasizing the ecological role of microbes in the water-column. Originally, the microbial loop described the path of dissolved organic matter (DOM), taken up by heterotrophic prokaryotes and converted into living particulate organic matter (POM), which is then grazed upon by protists. Through the conversion of DOM into bacterial biomass, organic carbon, otherwise inaccessible to metazoa, becomes available to higher trophic levels (Herndl *et al.*, 2008). Even though all trophic levels (not only primary producers) release copious amounts of organic matter, in dissolved or colloidal form (Lignell, 1990; Stoderegger and Herndl, 1998, 1999; Nagata, 2000; Conan *et al.*, 2007), phytoplankton primary production fuels the activity of heterotrophic prokaryotes either directly (extracellular release), or indirectly (grazing losses; Marañón, 2005).

Both the quality (elemental and biochemical composition) and the quantity of primary production that is transferred up the food web, exported to the deep ocean, and buried in the seafloor are strictly related to the eco-physiological features of the phytoplankton community (Finkel *et al.*, 2010; Fig. 3.1). The process responsible for the export of carbon dioxide (CO₂), other gases, and nutrients to the bottom of the ocean as sinking organic matter (including also dead large phytoplanktonic cells and fecal pellets), is called ‘biological pump’ (Volk and Hoffert, 1985).

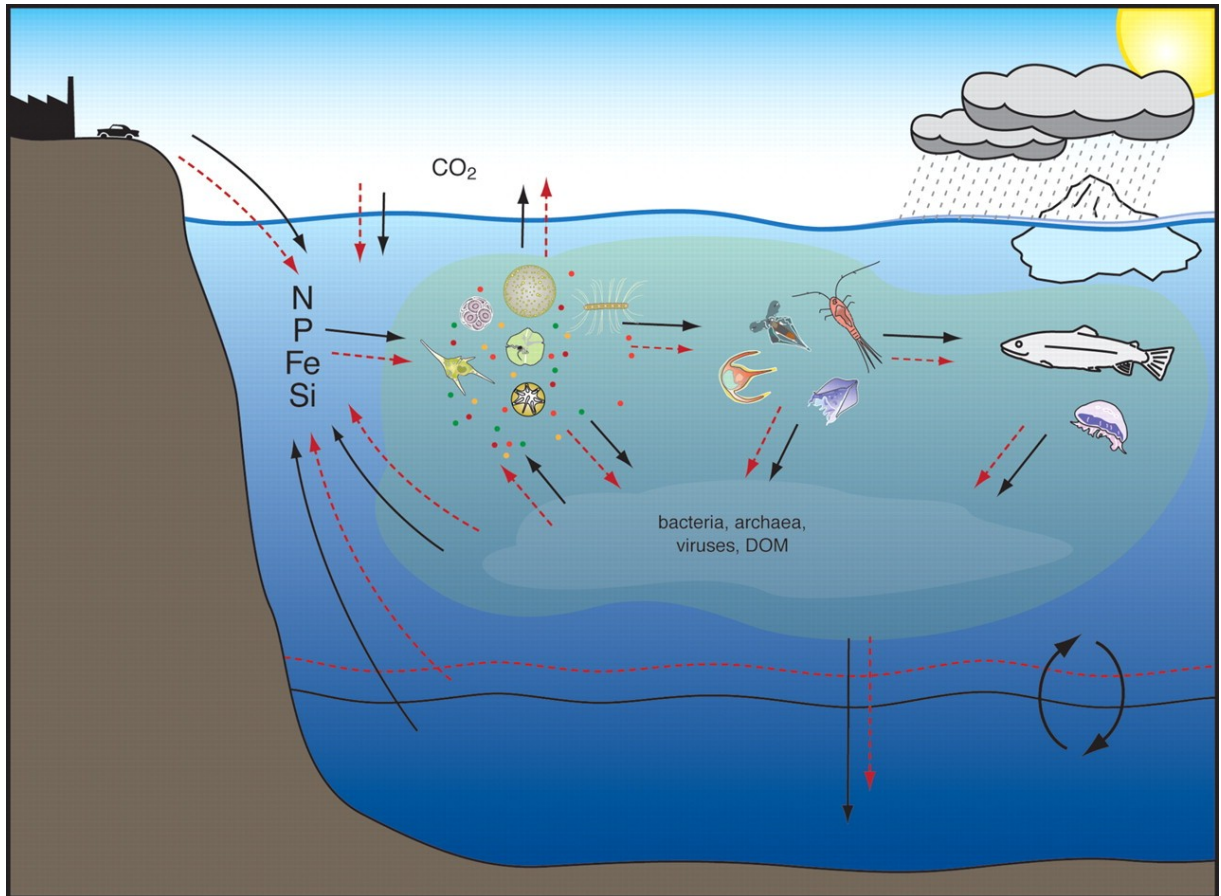


Fig. 3.1. Scheme representing the interactions between phytoplankton cell size, elemental stoichiometry, marine food webs and biogeochemistry (after Finkel *et al.*, 2010). Organic matter fluxes in a future (i.e. warmer and more stratified) scenario, and in the actual (cooler and less stratified) scenario, are depicted in red and black arrows, respectively.

Phytoplankton eco-physiological traits, such as cell size, and elemental requirement and stoichiometry, link growth rate, nutrient and light-harvesting capacities, thus dramatically affecting food web dynamics and biogeochemical cycles (Finkel *et al.*, 2010). Hypothetically, a dominance shift in the phytoplankton community might alter both the size structure and the elemental composition of phytoplankton, and consequently affect the microbial loop, in terms of concentration of organic matter transferred to higher trophic levels or exported into the deep sea (Pomeroy, 1974; Azam *et al.*, 1983; Laws *et al.*, 2000), as well as the amount and stoichiometry of future upwelling nutrient fluxes (Finkel *et al.*, 2010).

Phytoplankton cells span over nine orders of magnitude in cell volume (Irwin *et al.*, 2006; Beardall *et al.*, 2008), but in general, many field data suggest that in terms of biomass,

small cell-sized phytoplankton dominate in stable and oligotrophic environments (open ocean), whereas larger-sized ones in variable and eutrophic environments (coastal areas; Sprules and Munawar, 1986; Ahrens and Peters, 1991; Chisholm, 1992; Li, 2002). In the literature, different hypotheses concerning the relationship between abundance and organism size (see Irwin *et al.*, 2006), as well as food web models (Moloney and Field, 1991; Moloney *et al.*, 1991; Kerr and Dickie, 2001) including several trophic levels (often autotrophs, herbivores, and detritivores) and size-dependent processes (e.g. uptake, respiration, sinking rate, grazing rate), have not been able to successfully explain size structure changes of phytoplankton communities in relation to nutrient availability and eco-physiological mechanisms (see Irwin *et al.*, 2006). Several models have suggested that ‘grazing’ would be responsible of phytoplankton community size structure (Armstrong, 2003; Irigoien *et al.*, 2004; Morin and Fox, 2004). However, in the investigation of the relationship between abundance and organisms size, cell size physical constraints, superimposed to phytoplankton metabolic rate and resource acquisition ability, have been often poorly-considered. A general and synthetic theory, called ‘Metabolic Theory of Ecology’ (MTE) have been recently developed for structure and function of plants and animals communities, and integrated from cells to ecosystems (Brown *et al.*, 2004; Price *et al.*, 2010). Brown and co-workers (2004) hypothesized that size- and temperature-dependent metabolic rates explain biomass-size distributions (even if they did not consider the size effects on resources acquisition/requirements; Irwin *et al.*, 2006). For all these reasons, a clear understanding of the community structure of both large (nano or micro) and small cell-sized (pico) planktonic fractions is of major interest to better comprehend temporal and spatial fluctuations in the food web structure. Furthermore, in the impelling climate change *panorama*, the study of plankton size structure and elemental stoichiometry can be a very useful tool to partially predict the response of the entire phytoplankton community to environmental changing conditions, and improve the knowledge on the biological pump potential and the long-term CO₂-sinking ability of the ocean (Watson and Liss, 1998; Sarmiento and Wofsy, 1999; Kohfeld *et al.*, 2005; Finkel *et al.*, 2010).

Picophytoplankton dominate in oligotrophic waters, in which they reach up to 50% of total biomass and primary production, while they are less represented in eutrophic waters (Agawin *et al.*, 2000; Worden and Not, 2008). Although in nutrient-poor environments, picoeukaryotes have been found to prefer higher nitrate concentrations (Blanchot and Rodier, 1996; Shalapyonok *et al.*, 2001; Matsumoto *et al.*, 2004). Their cellular concentration might range between ~ 1000 (in oligotrophic waters) and 5000 cells mL⁻¹ (in

coastal waters), occasionally reaching more than 20000 cells mL⁻¹ (Worden and Not, 2008).

In the open ocean, despite being an important component of primary producers biomass (in the pico size fraction), picoeukaryotes are much less abundant than *Prochlorococcus* (up to two orders of magnitude of difference), while they are similarly or (slightly) less abundant than *Synechococcus* (Li *et al.*, 1992; Campbell and Vaulot, 1993; Li, 1994; Binder *et al.*, 1996; Blanchot and Rodier, 1996; Blanchot *et al.*, 2001; Landry *et al.*, 1996; Zubkov *et al.*, 1998; Brown *et al.*, 1999; Partensky *et al.*, 1999), even if covariance of picoeukaryotes with *Synechococcus* does not always occur (Worden and Not, 2008). In general, both the covariance of their abundance with *Synechococcus* (mainly at surface water layers), and their increase in concentration with depth, especially in correspondence of the deep chlorophyll maximum (DCM; Iriarte and Purdie, 1993; Raven, 1994; Veldhuis and Kraay, 2004; Timmermans *et al.*, 2005), are peculiar trends of picoeukaryote distribution (Worden and Not, 2008).

3.3 Biology of picoeukaryotes

This section aims to examine the phytoplankton biological and ecological features (advantages and disadvantages) related to a very small cell size, relative to larger cells.

Among photolithotrophs, picophytoplanktonic cells can be considered as the closest approximation to the physicochemical behaviour of single molecules rather than macroscopic structures (Newton and Liss, 1990; Raven, 1998). A small cell size relates to the concept of ‘non-scalable essential components’ (Haldane, 1928; Pirie, 1964, 1973; Koch, 1996; Raven, 1986, 1998). In picophytoplankton non-scalability applies to genome and membranes thickness (Raven, 1986, 1994a, 1994b, 1998), meaning that as cell size decreases, their biomass fraction cannot be maintained constant. The proportion of cell volume, taken up by components to which non-scalability applies (i.e. genome needed for photolithotrophic growth and membranes thickness), is higher as cell and genome size decreases (Raven, 1986, 1994a, 1994b, 1998; Raven *et al.*, 2005). Furthermore, the volume requirement in a photolithotrophic mode (i.e. photosynthetic and core metabolic machineries needed to channel the photosynthesis products into cell growth) is higher than in phagotrophic (i.e. heterotrophs which essentially engulf particulate food) and saprotrophic modes (i.e. those organisms that obtain their nutrition by secreting digestive

juices onto dead and decaying organic matter, and absorb the nutrients from it; Raven, 1998).

Cell size have been shown to affect phytoplankton physiological rates and ecological functions, from metabolic rate (growth, photosynthesis, respiration), to resources (photons and nutrient) use and requirements, to sinking and grazing rates (for a selection of some of the major physiological and ecological processes that scale with size, see Finkel *et al.*, 2010), even if exceptions to these ‘size rules’ are known. These physiological and ecological processes/parameters can be expressed as the power-law relationship between maximum metabolic rates (R) and organism size (M):

$$R = a \cdot e^{-E_a/kT} M^b \quad (3.1)$$

where a is a constant, E_a the activation energy for the metabolic machinery, k the Boltzmann’s constant, b the size scaling exponent and T the temperature (see, Finkel *et al.*, 2010).

In general, a three-fourth ($3/4$) size scaling of metabolic rates (constant b) has been observed for many organisms under favourable growth conditions (Kleiber, 1947; Hemmingsen, 1960; López-Urrutia *et al.*, 2006). At the same time, many (laboratory and field) studies on the size scaling of phytoplankton growth and other metabolic rates, reported a wide range of size scaling slopes and intercepts. Different reasons can explain such a variability in the size scaling exponent. Size-independent taxonomic differences in metabolic rate (Banse, 1976; Taguchi, 1976; Schlesinger *et al.*, 1981; Moloney and Field, 1989; Sommer, 1989; Finkel, 2001; Finkel *et al.*, 2004; Irwin *et al.*, 2006; Raven *et al.*, 2005; Mei *et al.*, 2009), and un-favourable environmental conditions (e.g. sub-optimal growth temperatures, irradiances and nutrient concentrations; Finkel and Irwin, 2000; Finkel, 2001; Gillooly *et al.*, 2001; Finkel *et al.*, 2004; Irwin *et al.*, 2006; López-Urrutia *et al.*, 2006; Marañón, 2008) have been reported to alter both the slope and intercept of the equation (3.1). In addition, to compare size scaling patterns in phytoplankton and other organisms, appropriate measurements of organism sizes and metabolic rates are fundamental (Finkel *et al.*, 2010).

The maximum specific growth rate of organisms, μ_m (e.g. biomass increase per unit biomass per unit time), has been predicted to be greater in smaller cells, which means that small cells would have a higher rate of biomass production per unit cell energy and nutrient concentrations, than larger ones (Altabet, 1990; Raven, 1998). On the other hand,

evidences of taxonomic and experimental variations in μ_m estimates were found, with higher maximum growth rates normalized by cell volume in larger cells, instead of smaller ones (Raven *et al.*, 2005).

Due to their tiny size, picoplankton have low Reynolds numbers (Re), indicating that their movement is dominated by viscous forces, rather than inertial forces (Aris, 1989), because of their large surface area : volume (SA/V) ratio (Fogg, 1986; Raven, 1986, 1998; Raven *et al.*, 2005). The greater SA/V ratio and the minimal diffusion boundary layer thickness enable cells of an enhanced capacity of nutrient solute influxes from bulk phase concentrations relative to growth needs, and lower half-saturation constants, than larger cells (Raven, 1986; Aksnes and Egge, 1991; Chisholm, 1992; Hein *et al.*, 1995). Energetic considerations, taking into account the greater efficiency in photons absorption in small than in large cells, suggest minor energy costs of extra leakage of solutes, and of excessive influxes of Na^+ and Ca^{2+} from sea water (Raven, 1986, 1999). However, this higher potential for solutes loss might reduce the energetic efficiency of photosynthetic inorganic carbon concentrating mechanisms (CCMs), since the greater rate constant for efflux of accumulated CO_2 (Raven 1986, 1998; Giordano *et al.* 2005).

The small cell size of picoeukaryotes also results in a lower package effect than in nano- or microphytoplankton, affecting the light-harvesting capacity of cells because of lower resource (energy, C, N, Fe, Mn, Cu) costs and a higher efficiency in the harvest and photochemical transformation of light energy (via a more effective absorption of photons per pigment molecule, and a faster excitation energy transfer in pigment-protein complexes; Raven 1984, 1998; Finkel *et al.* 2004; Raven *et al.*, 2005). The overall result of such a feature is a more effective acquisition of photosynthetically active radiation (PAR), and possibly a higher specific growth rate (μ_m) at low photon flux densities, in smaller than in larger cells (Fogg 1986, Raven, 1986, Chisholm 1992, Raven 1998). Picoplankton also show greater diversity of photosynthetic pigments than larger organisms do (Raven, 1999; Larkum & Kühl, 2005; Miller *et al.*, 2005), a feature that has been related to niche partitioning of different picoplanktonic species (Stomp *et al.* 2005), despite being less relevant on larger evolutionary scales (Falkowski *et al.*, 2004a, 2004b). At the same time, the smaller package effect involves a greater potential for energy saturation, hence a high risk of photo-inhibition/damage (and resource costs for mechanisms of repair) due to photosynthetically active radiation (PAR), and a weak capacity of UV-B radiation screening (Raven, 1998, 1999).

Several processes regarding cells loss are also influenced by cell size. For instance, for tiny (non-motile) cells, characterized by a low sinking rate, the possibility of sinking out of the euphotic zone is greatly reduced than for nano- or microphytoplankton (Fogg, (1986; Raven, 1986, 1998), even if cells coagulation can increase sinking velocities (Stemmann *et al.*, 2004a). While no eukaryotic parasites (i.e. parasitoids) of picophytoplankton has been reported so far, due to energetic constraints (Raven, 1998; Raven and Waite, 2004; Raven *et al.*, 2005), both viral attack either for cyanobacterial (Sullivan *et al.* 2005) and eukaryotic picophytoplankton (Wilson *et al.* 2005), and grazing, are widespread top-down factors that control picoplankton community structure. Both viruses and grazers are considered to significantly and almost equally affect pico-, as well as nano- and microphytoplankton productivity (Raven, 1998; Raven *et al.*, 2005).

Small cell-sized phytoplankton are advantaged in nutrient-limited environmental conditions over larger phytoplanktonic cells, since their more effective acquisition and use of resources (thus the predicted, even if not always observed, higher specific growth rates in smaller than in larger cells; Raven *et al.*, 2005). However, several disadvantages characterize small cells, either the lack of storage ability, or the higher leakage of solutes and excessive cations influxes, or the greater light (PAR and UV-B) sensitivity. All these biological “pros and cons” might in part explain picoeukaryotes distribution, and dominance in terms of biomass and primary production, in oligotrophic (nutrients-poor) and low-irradiance (DCM) environments, and their influence in phytoplankton community size-structure.

3.4 Picoeukaryotes as model organisms

During the last decade, different studies concerning the ecophysiological properties of picoeukaryotes have supported their importance as model organisms, either in batch cultures or *in situ* experiments (several examples are listed below; see Table 3.1). A strict adaptation to the physicochemical properties of the water mass of growth (i.e. ‘ecological niche’) has been often reported for picoeukaryotes, and possible explanations may reside in peculiar biological features related to their cell size (see above). In picoeukaryotes, being the mesoscale distribution more strongly determined by passive lateral advection and vertical mixing events (Hamilton *et al.*, 2008), a more strict adaptation to the water column abiotic properties might be expected, than in larger cells. Furthermore, picoplankton

genomes streamlining and minute cell size have also been considered as properties which might have increased their rate of evolution (Raven, 1998; Moreira and López-García, 2002; Vaultot *et al.*, 2002; Dufresne *et al.*, 2005; Giovannoni *et al.*, 2005; Raven *et al.*, 2005).

The first taxonomic overview of marine picoeukaryotes is dated 1986 (Thomsen, 1986). Nowadays, picoeukaryotes are known to be characterized by an extremely wide phylogenetic diversity (Le Gall *et al.*, 2008; Vaultot *et al.*, 2008; Lepere *et al.*, 2011). Early studies of picoeukaryotes diversity in the open ocean were mostly based on pigment analysis, and suggested haptophytes and pelagophytes as significant components of the pico-size fraction (Ondrusek *et al.*, 1991; Letelier *et al.*, 1993; Andersen *et al.*, 1996). Green algae and other groups were reported as less abundant, despite some exceptions (e.g. prasinophytes; Suzuki *et al.*, 2002). A greater resolution in picoeukaryotes phylogenetic diversity was achieved by applying molecular tools (11 years after these techniques have been proved highly successful on the prokaryotic component diversity, see Giovannoni *et al.*, 1990; López-García *et al.*, 2001; Moon-van der Staay *et al.*, 2001). The use of classical and molecular approaches clearly revealed the importance of picoeukaryotes in terms of biomass and production (e.g. Li, 1994; Worden *et al.*, 2004; Pérez *et al.*, 2005; Jardillier *et al.*, 2010), and diversity (Simon *et al.*, 1994; Veldhuis *et al.*, 1997a; Díez *et al.*, 2001b; López-García *et al.*, 2001; Moon-van der Staay *et al.*, 2001; Le Gall *et al.*, 2008; Vaultot *et al.*, 2008; Lepere *et al.*, 2011).

Picoeukaryotes high molecular phylogenetic diversity was demonstrated in distinct open marine systems, including the equatorial Pacific Ocean (Moon-van der Staay *et al.*, 2001), the Antarctic Polar Front (López-García *et al.*, 2001), the Arctic Ocean (Not *et al.*, 2005; Hamilton *et al.*, 2008), the Mediterranean (Brunet *et al.*, 2006, 2007) and Scotia Sea, as well as the North Atlantic Ocean (Díez *et al.*, 2001b; Marie *et al.*, 2010). In the Atlantic Ocean picoeukaryotes have been described to represent a large portion of the primary producers biomass of the pico size fraction (Li, 1994; Marañón *et al.*, 2001; Zubkov *et al.*, 1998; Pérez *et al.*, 2005), even if less important than the picocyanobacteria in terms of cells number (Li *et al.*, 1992; Li, 1994). Similar evidences were also found in other regions, such as the Arabian Sea (Shalapyonok *et al.*, 2001), and the Sargasso Sea (Li *et al.*, 1992; Durand, 2001; Not *et al.*, 2007a). Molecular approaches revealed the prominent contribution of chrysophyte and prymnesiophyte algae in the Arabian Sea (Fuller *et al.*, 2006a, 2006b), and the diversity of microbial eukaryotic assemblages was recently investigated in a subtropical Indian Ocean gyre (Not *et al.*, 2008).

In coastal environments, similar levels of diversity (Massana *et al.*, 2004; Romari and Vaultot, 2004; Worden *et al.*, 2004; Worden, 2006; Jing *et al.*, 2010), and first insights into the abundance and distribution of specific taxa (i.e. *Micromonas pusilla*, Prasinophyceae; Biégala *et al.*, 2003; Not *et al.*, 2004; Countway and Caron, 2006), have been revealed. At a coastal Pacific Ocean site, Worden and co-authors (2004) reported that, even if picoeukaryotes were not numerically dominant (in comparison with *Prochlorococcus* and *Synechococcus*), they were the greatest in terms of standing stock carbon, net carbon produced and carbon consumed.

Two emblematic species, such as *Micromonas pusilla* (Knight-Jones and Walne, 1951), and *Ostreococcus tauri* (Courties *et al.*, 1994; Chrétiennot-Dinet *et al.*, 1995), both belonging to the order Mamiellales (Prasinophyceae), have been largely studied, and their genomes have been quite recently deciphered (Derelle *et al.*, 2006; Palenik *et al.*, 2007; Worden *et al.*, 2009). Their oceanic distribution has been mapped using techniques such as fluorescent *in situ* hybridization (Not *et al.*, 2005) or quantitative PCR (Marie *et al.*, 2006). At the same time, a large number of novel picoeukaryote phylogenetic groups, some without clear affiliations (Moreira and López-García, 2002), and a new division of photosynthetic eukaryotes (i.e. ‘picobiliphytes’; Not *et al.*, 2007), have been discovered. Many phylogenetic groups are only known from their sequences (e.g. *Chrysochromulina*-related clades within prymnesiophytes, Moon-van der Staay *et al.*, 2000; Prasinophyceae clade VII B, Guillou *et al.*, 2004), due to the difficulty of maintaining in culture representatives of species isolated in open ocean oligotrophic regions, because of low nutrient and competition constrains (Le Gall *et al.*, 2008).

After the ecological and biological importance of picoeukaryotes, and their peculiar ability to exploit resources paucity (as low nutrient concentrations and low light conditions) have been established *in situ*, the biochemical and physiological properties of these small photosynthetic organisms were investigated in laboratory approaches (Veldhuis *et al.*, 2005; Timmermans *et al.*, 2005).

Thanks to their wide distribution in marine ecosystems (e.g. open ocean, costal and upwelling water masses), the consequent adaptation of picoeukaryotes to a large range of irradiance conditions (i.e. from high light in superficial/sub-superficial layers, to low light in DCM, to highly fluctuating light climate in turbulent coastal waters), and their biological properties (e.g. low sinking rate and package effect, high pigment diversity), the interest in studying picoeukaryotes photophysiology raised. Their great photophysiological potential and ability in photoacclimation and photosynthesis regulation, in response to

light changes, have been demonstrated in different species, either isolated from surface (*Picochlorum* RCC237, Trebouxiophyceae, Chlorophyta; Dimier *et al.*, 2007a), DCM (*Pelagomonas calceolata*, Pelagophyceae, Stramenopiles; Dimier *et al.*, 2009a), or coastal waters (*Phaeomonas* sp. RCC503, Pinguiphyceae, Stramenopiles; Giovagnetti *et al.*, 2010, see Chapter 6). Such a high plasticity of PSII photoregulatory responses was also supported by *in situ* data (Brunet *et al.*, 2006, 2007).

Rodríguez and co-workers (2005) reported distinct adaptation to environmental conditions in 12 *Ostreococcus* strains isolated from distinct marine environments and depths, supporting the validity of the ‘ecotype’ concept also for eukaryotes, and lately, the genomic sequences of three *O.* ecotypes became available (Derelle *et al.*, 2006; Palenik *et al.*, 2007). After distinct photoacclimation strategies were found in two *O.* strains, the *O. tauri* (strain OTH95, isolated from Thau Lagoon, France) and *O.* sp. RCC809 (isolated at the depth of 105 m, in the tropical Atlantic Ocean; Cardol *et al.*, 2008; Six *et al.*, 2008), Six and co-authors (2009) investigated and compared the photophysiology of three ecotypes of *Ostreococcus* (i.e. *O. tauri* OTH95, *O.* sp. RCC809 and *O. lucimarinus* CCMP2514, isolated from surface water of the California Current) and of a larger prasinophyte, *Pyramimonas obovata* (strain CCMP722, isolated from surface water of the Sargasso Sea), in response to a sudden increase in light. Results from this work proved cell size to be highly influent in prasinophytes response to light changes, being *Ostreococcus* spp. photophysiological properties and responses shaped in function of their tiny size (almost negligible package effect and relatively high PSII repair rates, to deal with a higher risk of photo-inactivation than larger cells).

Since cell size might strongly affect the regulation of photosynthetic and photoacclimative/ photoprotective processes, and because physiological acclimation to light changes requires a heavy cost (Finkel, 2001; Raven and Kübler, 2002; Litchman and Klausmeier, 2008; Key *et al.*, 2009), picoeukaryotes can be considered as interesting model organisms (Dimier *et al.*, 2007a, 2009a; Six *et al.*, 2008, 2009) to explore the influence of cell size on cellular metabolism (MTE; Brown *et al.*, 2004). Indeed, Dimier and colleagues (2009a) suggested that the energetic cost of an enhanced photoregulation in response to high light fluctuations might explain the decrease of growth rate, in the shade-adapted species *P. calceolata*.

Despite the fact that almost 20 species of the class Bacillariophyceae belong to the picoplankton fraction (besides being one of the most prominent group of nano- and microplankton; Vaulot *et al.*, 2008), physiological studies on picoplanktonic diatoms are lacking. In Chapter 7, the results obtained from the study of two picoplanktonic diatoms

adapted to different ecological niches (i.e. *Minutocellus* sp. RCC967 isolated from an upwelling ecosystem in the Pacific Ocean, whereas *Minutocellus* sp. RCC703 from oceanic waters in the Indian Ocean), are presented and discussed in the light of functional relations between ecological niche adaptation, and photosynthetic regulation capacity and efficiency. The fact that, the genome of the species *M.* sp. RCC703 is currently sequenced at Genoscope (Centre National de Séquençage, France; www.sb-roscoff.fr/Phyto/RCC/), is a further proof of the growing scientific interest in picoeukaryotes.

Species/Communities	Field Studies	Laboratory Studies	References
<i>Micromonas pusilla</i>	First description		Knight-Jones and Walne, 1951
<i>Pelagomonas calceolata</i>	First description		Andersen <i>et al.</i> , 1993
<i>Ostreococcus tauri</i>	First description		Courties <i>et al.</i> , 1994
<i>Bolidomonas pacifica</i> , and <i>B. mediterranea</i>	New class and two species description		Guillou <i>et al.</i> , 1999a
Pinguiophyceae	New class description		Kawachi <i>et al.</i> , 2002
Picobiliphytes	New marine algal group		Not <i>et al.</i> , 2007
Communities	Taxonomic overview		Thomsen, 1986
Communities	Atlantic Ocean		Li, 1994; Andersen <i>et al.</i> , 1996; Zubkov <i>et al.</i> , 1998; Diez <i>et al.</i> , 2001b; Marañón <i>et al.</i> , 2001; Not <i>et al.</i> , 2004; Romari and Vaulot, 2004; Pérez <i>et al.</i> , 2005; Marie <i>et al.</i> , 2006; Jardillier <i>et al.</i> , 2010
Communities	Pacific Ocean		Ondrusek <i>et al.</i> , 1991; Letelier <i>et al.</i> , 1993; Andersen <i>et al.</i> , 1996; Moon-van der Staay <i>et al.</i> , 2000, 2001; Suzuki <i>et al.</i> , 2002; Worden <i>et al.</i> , 2004; Worden, 2006; Countway and Caron, 2006; Le Gall <i>et al.</i> , 2008; Lepere <i>et al.</i> , 2011
Communities	Indian Ocean		Veldhuis <i>et al.</i> , 1997b; Not <i>et al.</i> , 2008; Jing <i>et al.</i> , 2010
Communities	Antarctic Ocean		López-García <i>et al.</i> , 2001; Moreira and López-García, 2002
Communities	Arctic Ocean		Not <i>et al.</i> , 2005; Hamilton <i>et al.</i> , 2008
Communities	Mediterranean Sea		Massana <i>et al.</i> , 2004; Brunet <i>et al.</i> , 2006, 2007
Communities	Sargasso Sea		Li <i>et al.</i> , 1992; Durand, 2001; Not <i>et al.</i> , 2007a

Communities	Arabian Sea		Shalapyonok <i>et al.</i> , 2001; Fuller <i>et al.</i> , 2006a, 2006b
Communities	Different Areas		Simon <i>et al.</i> , 1994; Andersen <i>et al.</i> , 1996; Díez <i>et al.</i> , 2001b; Guillou <i>et al.</i> , 2004; Not <i>et al.</i> , 2007
Picoeukaryotic Species		Biochemical composition and photosynthetic properties	Veldhuis <i>et al.</i> , 2005
<i>Pelagomonas calceolata</i> (CCMP1756)		Physiological responses to nutrient and light limitation	Timmermans <i>et al.</i> , 2005
<i>Prasinomonas capsulatus</i> (CCMP1617)			
<i>Ostreococcus</i> 12 strains		Ecotypes adaptation and diversity	Rodríguez <i>et al.</i> , 2005
<i>Ostreococcus tauri</i> (OTH95), <i>O. sp.</i> RCC809, and <i>O. lucimarinus</i> (CCMP2514)		Genomes, and photophysiology	Derelle <i>et al.</i> , 2006; Palenik <i>et al.</i> , 2007; Cardol <i>et al.</i> , 2008; Six <i>et al.</i> , 2008, 2009
<i>Picochlorum</i> RCC237		Photophysiology	Dimier <i>et al.</i> , 2007a
<i>Pelagomonas calceolata</i>		Photophysiology	Dimier <i>et al.</i> , 2009a
<i>Phaeomonas sp.</i> RCC503		Photophysiology	Giovagnetti <i>et al.</i> , 2010
Communities	Review	Review	Raven, 1998; Raven <i>et al.</i> , 2005; Worden and Not, 2008; Vaultot <i>et al.</i> , 2008; Finkel <i>et al.</i> , 2010

Table 3.1: List of some relevant field and laboratory studies concerning picoeukaryotes ecology, biology and ecophysiology. Increase in the number of publications concerning picoeukaryotes over years (percentages have been estimated on the basis of the list presented in this chapter): before 1995 (14%), between 1995 and 2000 (12%), between 2000 and 2005 (32%), and after 2005 (42%).

CHAPTER 4

Materials and methods

Chapter 4

Materials and methods

4.1 Algal models and culture maintenance

Non-axenic strains of *Phaeomonas* sp. RCC503, *Minutocellus* sp. RCC967 and RCC703 were provided by the Roscoff Culture Collection (France; Vaultot *et al.*, 2004). Non-axenic strains of *Pseudo-nitzschia multistriata* SY416 was provided by Diana Sarno (Taxonomy and Identification of Marine Phytoplankton, TIMP, Stazione Zoologica "Anton Dohrn", Naples, Italy). The four species were semi-continuously grown at 20° C in 225 cm² polystyrene canted-neck flasks (Corning® Flask, Corning Inc., NY, USA). *Phaeomonas* sp. RCC503 and *P. multistriata* SY416 cultures were cultivated in locally obtained, and sterilized seawater amended with f/2 nutrients (Guillard and Ryther, 1962), while the two *Minutocellus* sp. RCC967 and RCC703 in Keller medium (Keller *et. al*, 1987).

The taxonomic position, size, growth medium, "ecological habitat", and origin of the different species are presented in Table 4.1.

Irradiance was provided by the light system consisting of the ACLS (Advanced Control Lighting System) and Infinity XR4 (Aquarium Technologies, Sfiligoi S.r.l., Bassano del Grappa, Italy), simulating light–dark sine cycles, reproducing dawn and sunset. The Infinity XR4 was equipped with HQI metal halide lamps (10000 K).

Cultures were grown with a 11 : 13 light : dark photoperiod, at moderate sine light (ML, 100 $\mu\text{mol photons} \cdot \text{m}^{-2} \cdot \text{s}^{-1}$), measured with a PAR 4 π sensor (QSL 2101, Biospherical Instruments Inc., San Diego, CA, USA). Under this condition, cultures pre-acclimation lasted for two weeks before the experiments started.

Algae were continuously bubbled with filtered air, gently agitated twice a week (to prevent the cells to accumulate at the flask bottom), and maintained in exponential phase by daily and semicontinuous dilution with fresh medium.

4.2 Determination of growth rate

Cell concentration of the three picoeukaryotic species was estimated on culture triplicate non-fixed sub-samples. An aliquot of 120 μL was used to fill a Neubauer ruling haemocytometer (0.1 mm depth, Preciss, France), and cells were counted using a Zeiss Axioskop 2 Plus light microscope (Carl Zeiss, Göttingen, Germany).

P. multistriata SY416 cell concentration was estimated on sub-samples fixed with formaldehyde to reach a 1.5 % (v/v) final concentration. An aliquot of 1 mL was used to fill a Sedgewick Rafter counting cell chamber, and cells counts were performed using a Zeiss Axioskop 2 Plus microscope.

The growth rate was daily estimated from cell abundance measurements using the following equation:

$$\mu = \ln [N_{t_2} : N_{t_1}] : [t_2 - t_1] \quad (4.1)$$

where μ is the growth rate (day^{-1}) and N_t is the mean cell concentration at time t , and t_1 and t_2 correspond to the morning sampling time of Days 1 and 2, respectively. From the growth rate, the number of cell divisions (n) per day was estimated with the following equation:

$$n = \mu : [\ln (2)] \quad (4.2)$$

where n is the number of cell divisions per day and μ is the growth rate.

Species	Division	Class	Growth Medium	Size (μm)	Ecological habitat	Origin
<i>Phaeomonas</i> sp. RCC503	Heterokontophyta	Pinguiophyceae	f/2	3.27 ± 0.07	Mediterranean Sea, coastal species (0 m)	Roscoff Culture Collection, France
<i>Minutocellus</i> sp. RCC967	Heterokontophyta	Bacillariophyceae	K	2.88 ± 0.19	Pacific Ocean, upwelling species (40 m)	Roscoff Culture Collection, France
<i>Minutocellus</i> sp. RCC703	Heterokontophyta	Bacillariophyceae	K	2.83 ± 0.18	Indian Ocean, oceanic species (100 m)	Roscoff Culture Collection, France
<i>Pseudo-nitzschia multistriata</i> SY416	Heterokontophyta	Bacillariophyceae	f/2	40.6 ± 0.29	Mediterranean Sea, coastal species (LTER-MC)	Stazione Zoologica A. Dohrn, Italy

Table 4.1: Algal models used in the studies conducted during the PhD project.

4.3 Estimation of cell size and volume

Cell size and volume measurements of the three picoeukaryotic species were carried out by Coulter Multisizer II counter analysis (Beckman Coulter Inc., Brea, CA, USA). In order to adequately resolve small cells, a 30 μm orifice was used.

After machine was warmed up, the orifice was flushed twice with filtered seawater (FSW), after which particles in FSW were estimated for blank value subtraction. Considering the cultures density, 0.5 mL of sample were diluted in FSW up to a final volume of 25 mL. Analysis were conducted in triplicate, avoiding measurements of the same sample by using three independent dilutions.

Cell size of *P. multistriata* was estimated by microscope observation.

4.4 Pigment analysis

Pigment analysis was conducted by HPLC (High Performance Liquid Chromatography). An aliquot of algal culture (from 8 to 10 mL) was taken with a syringe and immediately filtered on 25 mm - GF/F glass-fiber filter (Whatman, Maidstone, UK) and immediately stored in liquid nitrogen until further analysis. Pigments were extracted by mechanical grinding during 3 minutes in 3 mL of a 100% methanol solution. Successively, the homogenate was filtered onto Whatman 25-mm GF/F filters and the volume of the extract accurately measured. Prior to injection into the HPLC, 500 μL of an Ion Pairing Agent (ammonium acetate $1 \text{ mol} \cdot \text{L}^{-1}$, final concentration $0.33 \text{ mol} \cdot \text{L}^{-1}$) were added to 1 mL of the pigment extract and incubated for 5 minutes in darkness at 4°C . The ion pairing agent was used to increase pigments hydrophobicity so that they were better retained on the column and peaks quality was improved (Mantoura and Llewellyn, 1983). This extract was then injected in the 200 μL loop of the Hewlett Packard series 1100 HPLC (Hewlett-Packard, Wilmington, NC, USA). The reversed-phase column (3 μm diameter C_8 BDS column; $100 \text{ mm} \times 4.6 \text{ mm}$; ThermoHypersil, Runcorn, UK) corresponds to an apolar stationary phase composed of silica beads possessing aliphatic chains of 8 carbon atoms (C_8). The temperature of the column was steadily maintained at 20°C and the flow rate of the mobile phase was set up at $1 \text{ mL} \cdot \text{min}^{-1}$. The mobile phase was composed of two solvents mixture: A, methanol : aqueous ammonium acetate (70 : 30, v/v) and B, methanol. During the 20-minutes elution, the gradient between the solvents was

programmed as in Vidussi *et al.* (1996): 75% A (0 min), 50% A (1 min), 0% A (15 min), 0% A (18.5 min), 75 % A (19 min). Pigments were detected at 440 nm using a Hewlett Packard photodiode array detector model DAD series 1100 which gives the 400-700 nm spectrum for each detected pigment. A fluorometer (Hewlett Packard standard FLD cell series 1100) with excitation at 407 nm and emission at 665 nm allowed the detection of fluorescent molecules (chlorophylls and degraded products). Identification of pigments was carried out according to their retention time and by comparing the on-line-collected pigment spectra with the database established with standards from the D.H.I. Water & Environment (Hørsholm, Denmark). These standards allowed the quantification of the most common chlorophylls and carotenoids. For the other minor pigments, the quantification was done according to extinction coefficients obtained from the literature.

4.5 Absorption spectrum analysis

The analysis of the absorption spectrum was performed on a spectrophotometer Hewlett Packard HP-8453E equipped with an inverted Labsphere integrating sphere (RSA-HP-53 Reflectance Spectroscopy Accessory). Filtration of 10 mL samples of algal culture was carried out on 25-mm GF/F filter (Whatman, Buckinghamshire, UK) and filters were immediately stored in cell culture plates (Corning Inc., NY, USA) in the dark at -20° C. Filters were thawed just prior to analysis and moistened with FSW, together with a Whatman GF/F blank filter. For absorbance measurement, the filter (sample and blank) was placed on a glass slide and scanned for 4 seconds between 400 and 800 nm with a 1-nm slit width. The absorption due to the filter, estimated from the spectrum done on a blank Whatman GF/F filter, was removed from the phytoplankton spectrum. A correction factor of 0.72 was applied on the absorbance values due to the use of Hewlett Packard diodes (as recommended by the Ocean Optics Protocol Version 2.0 - 2000). Before calculating the absorption coefficient, all particulate absorption spectra were corrected for scattering by subtracting the average absorption between 790 and 800 nm from the entire spectrum. Since the strong diffusivity of the filter, the measurements of absorption spectrum need to be corrected by applying a β -correction. To convert the absorption obtained for phytoplankton particles on the filter (A_s) to particles in suspension (A_{sus}), the Tassan and Ferrari (1995) equation was applied:

$$A_{\text{sus}}(\lambda) = 0.406 \cdot A_s(\lambda) + 0.519 \cdot A_s^2(\lambda) \quad (4.3)$$

The absorption of particles in suspension was then converted to an absorption coefficient using the relationship of Cleveland and Weidemann (1993):

$$a_{\text{ph}}(\lambda) = 2.3 \cdot A_{\text{sus}} \cdot (\lambda) / (V / A) \quad (4.4)$$

where $a_{\text{ph}}(\lambda)$ is the absorption coefficient (m^{-1}) of particulate organic material at a fixed wavelength, V is the volume of culture filtered (in m^3) and A is the clearance area of the filter (m^2 , “clearance rate”).

The absorption coefficient $a_{\text{ph}}(\lambda)$ was then transformed to the total absorption coefficient of cells *in vivo* (a_{ph}) by calculating the mean absorption between 400 and 700 nm with the following equation:

$$a_{\text{ph}} = \left[\sum_{\lambda=400\text{nm}}^{700\text{nm}} a_{\text{ph}}(\lambda_i) \right] / (700 - 400) \quad (4.5)$$

Finally, a_{ph} was converted to a_{ph}^* by the following equation:

$$a_{\text{ph}}^* = a_{\text{ph}} / \text{Chl } a \quad (4.6)$$

where a_{ph}^* is the Chl a specific absorption coefficient ($\text{m}^2 \cdot \text{mg Chl } a^{-1}$) with Chl a expressed in $\text{mg} \cdot \text{m}^{-3}$.

4.6 Active chlorophyll a fluorescence and photosynthetic efficiency analysis

To assess the photosynthetic capacities and the physiological state of phytoplankton cells, measurements of active Chl a fluorescence were performed using a Phyto-PAM fluorometer (Heinz Walz GmbH, Effeltrich, Germany). The first fluorometer was constructed by Waltz (Waltz, GmbH, Effeltrich, Germany) and designed by Dr. Ulrich Schreiber (Wuerzburg, Germany) in 1984. This method was originally developed for research purposes regarding higher plants physiology, and it was thus applied to study phytoplankton.

Advantageously, PAM fluorometer performs non-invasive measurements of photosynthetic efficiency, it can be applied during *in vivo* experiments without any incubation and used at high time-frequency.

4.6.1 Chl *a* fluorescence

The pulse amplitude modulation (PAM) measurement is based on the selective amplification of the fluorescence signal emitted by the Chl *a* after excitation by an intense and very short light pulse. At room temperature, most of the fluorescence measured comes from the photosystem II (PSII), whilst PSI contributes to only 1 to 5 % to the signal fluorescence (Kirk, 1983).

When the molecules of Chl *a* of the light harvesting complexes (LHC) antenna absorb a photon of light, they enter to an excited singlet-state ($\text{Chl } a + \text{light} \rightarrow {}^1\text{Chl } a^*$) where an electron has been moved to a higher orbital from a ground state in which all their electrons occupy a low stable orbital (Brunet *et al.*, *in press*). This Chl *a* excited state is transient and to return each again the ground state, light energy can undergo one of these three fates:

1. it can be re-emitted as a photon of lower energy (longer wavelength) either by fluorescence or luminescence;
2. it can be transmitted to non-specific molecules and dissipated in the form of heat;
3. and mostly important in photosynthesis, it can drive a chemical reaction by transmission of the excited electron to the photosynthetic electron transport chain (photochemistry).

These processes occur in competition ($1 + 2 + 3 = 100\%$), such that any increase in the efficiency of one will result in a decrease in the yield of the other two. Therefore, by measuring the yield of Chl *a* fluorescence, information about changes in the efficiency of photochemistry and heat dissipation can be gained.

Each process' occurrence is determined by physical properties (rate constants or lifetime) which, in turn, are linked to the physiological state of cells and thus to the environmental conditions. The fluorescence yield is defined as:

$$\Phi_f = k_f / (k_f + k_d + A \cdot k_p) \quad (4.7)$$

where A is the fraction of open reaction centers and k_f , k_d and k_p correspond to the first-order rate constant of fluorescence, heat dissipation and photochemistry, respectively.

Since this equation links quantitatively the fluorescence yield to the number of open reaction centers, the quantum yield of fluorescence reflects the capacity of PSII reaction centers to drive photochemistry (Genty *et al.*, 1989) and is generally used as a proxy for the photochemical efficiency.

4.6.2 Principle of the Phyto-PAM Fluorometer

The Phyto-PAM allows the differentiation of 3 groups of algae in a mixed sample. This apparatus can generate excitation at four different wavelengths thanks to a light-emitting diode array cone (PHYTO-ML) constituted by 25 LEDs peaking at 470 nm (blue), 520 nm (green), 645 nm (orange) and 665 nm (red) with 12 additional red LEDs (peaking at 655 nm) for actinic illumination (maximum intensity: $600 \mu\text{mol photons} \cdot \text{m}^{-2} \cdot \text{s}^{-1}$). Actinic light is defined as the light able to produce an identifiable or measurable change while interacting with matter. The goal behind the Phyto-PAM functioning is that the above-mentioned four excitation wavelengths do not excite directly the Chl *a* but rather the photosynthetic accessory pigments. For green algae, the excitation wavelengths absorbed by Chl *b* are 470 and 645 nm. In cyanobacteria, Chl *a* is mostly excited through 645-nm wavelength which is absorbed by phycocyanin and allophycocyanin. For brown algae such as diatoms or dinoflagellates, blue (470 nm) and green (520 nm) excitations are preferentially absorbed by Chl *c*, fucoxanthin and other carotenoids (e.g. peridinin, diadinoxanthin, etc.).

The different-colour pulses are applied successively at high velocity in order to obtain quasi-simultaneous information on chlorophyll fluorescence, when excited by the four different wavelengths. The fluorescence signal emitted by Chl *a* is detected at wavelengths ≥ 710 nm by a photomultiplier detector PM-101P with a high red sensitivity (type H6779-01). Through the Phyto Win-program a deconvolution of the 4-channels signal is applied to assess the contribution of the corresponding algal classes. The deconvolution of the signal is based on a “Reference Excitation Spectrum” which gives the relative fluorescence response of a species when subjected to the four excitation wavelengths.

Before performing any measurement of fluorescence, the reference spectrum was measured for each species studied at the beginning of the experiment. The gain of the

photomultiplier was adjusted to the algal sample concentration in order to have a suitable measurement of variable fluorescence values.

The contribution of the background signal to the fluorescence measurement was estimated by measuring the fluorescence of a culture sample filtered onto 0.22 μm filters (MILLEX-GS, Millipore, Carrigtwohill, Co. Cork, Ireland), i.e. without algal cells.

To avoid variations of light due to apparatus variability, the irradiance was recalibrated before each experiment thanks to a Spherical Micro Quantum Sensor US-SQS. Calibration was performed at the same temperature as the experiment.

4.6.3 Determination of the photochemical efficiency of the Photosystem II (PSII)

Measurements of the PSII photochemical efficiency were performed on two kinds of samples: 15-minutes dark-acclimated and light-acclimated algal samples.

After dark-acclimation, all irradiance energy has been removed from the photosynthetic electron transport chain. The reaction centers are “open” and the limiting step for energy transfer is the oxidation/reduction reactions regarding the electron acceptors in the photosynthetic pathway, downstream of PSII, notably the plastoquinone pool (particularly Q_A ; Consalvey *et al.*, 2005). When all reaction centers are “open” ($A = 1$, in the equation 4.7), Q_A is completely oxidized and the level of fluorescence is minimal (F_0):

$$F_0 = E \cdot [k_f / (k_f + k_p + k_d)] \quad (4.8)$$

where E is the light received by the PSII. The measurement of F_0 is done using light of low intensity ($1 \mu\text{mol photons} \cdot \text{m}^{-2} \cdot \text{s}^{-1}$) and low frequency (approximately 25 Hz).

The measurement of F_m is done by applying a short flash of actinic light which completely reduces

Q_A . In our case, the saturation flash of bright red light (655 nm) was applied at an intensity of $2000 \mu\text{mol photons} \cdot \text{m}^{-2} \cdot \text{s}^{-1}$ for a duration of 450 ms. Once all reaction centers are “closed” ($A = 0$), Q_A is reduced (Q_A^-) and the fluorescence level is maximal (F_m):

$$F_m = E \cdot [k_f / (k_f + k_d)] \quad (4.9)$$

The photochemical efficiency of the PSII (F_v / F_m , Table 4.2), defined as the quantum yield of photochemistry, corresponds to the quantum yield of electron transfer from the PSII (P680) to the plastoquinone pool (Q_A). It is estimated by:

$$\Delta\Phi_m = (F_m - F_o) / F_m = F_v / F_m \quad (4.10)$$

where F_v is the variable fluorescence ($F_v = F_m - F_o$; Table 4.2). For the dark-acclimated cells, F_v / F_m corresponds to the maximal photochemical efficiency of the PSII (or the maximal light utilization efficiency of PSII).

Different durations of dark-acclimation have been tested. In agreement with similar studies, it has been accepted that 15 minutes was a reasonable time to get reliable measurements of F_v / F_m (Honeywill, 2001). When cells photosynthetic machinery is exposed to high light, some of the reaction centers are “closed” due to the photosynthetic activity. The PSII photochemical efficiency depends on the proportion of “open” reaction centers but also on their efficiency to transmit energy (Consalvey *et al.*, 2005).

The light utilization efficiency of the PSII is calculated by:

$$\Delta\Phi = F_v' / F_m' = (F_m' - F') / (F_m') \quad (4.11)$$

where F_v' / F_m' is the PSII operating efficiency with $F_v' = F_m' - F'$. F_m' is the maximum fluorescence in the light-acclimated state and F' is the steady-state fluorescence level in the light obtained with the measuring light. With increasing light, F_v' / F_m' decreases due to the progressive closure of the reaction centers. The more light-acclimated is the sample, the slower is the decrease of the F_v' / F_m' .

4.6.4 Determination of non-photochemical fluorescence quenching (NPQ)

Under excess light, a part of the incident light is diverted away from the reaction centers and dissipated as heat (i.e., non-photochemical quenching, NPQ). The dissipation of light energy as heat induces a fluorescence down-regulation and the yield (F_v / F_m or F_v' / F_m') decreases due to lower F_m' or F_m (White and Critchley, 1999).

Estimation of the non-photochemical quenching is given by the qN coefficient, calculated as follows:

$$qN = 1 - [(Fm' - Fo') / (Fm - Fo)] \quad (4.12)$$

Since the determination of Fo' (minimum light-acclimated fluorescence level) is difficult, a proxy for NPQ (Consalvey *et al.*, 2005) is calculated by the Stern-Volmer expression (Bilger *et al.*, 1989):

$$NPQ = (Fm - Fm') / Fm' = (Fm / Fm') - 1 \quad (4.13)$$

This equation derives a parameter proportional to the level of NPQ employed by the cells at any particular light level. Indeed, the decrease of Fm to Fm' is proportional to the level of NPQ when expressed as a fraction of the maximum fluorescence at a certain light level (Consalvey *et al.*, 2005).

As proposed by some authors (Villareal, 2004; Dimier *et al.*, 2007b, 2009a), NPQ can also be estimated on the rapid light curves (see Sec. 4.6.5).

Parameter	Meaning
F _o	Minimal fluorescence after dark acclimation
F _o '	Minimal fluorescence in the light acclimated state
F'	Steady-state fluorescence in the light (RLC)
F _m	Maximum fluorescence after dark acclimation and then measurement using single turnover flash
F _m '	Maximum fluorescence in the light acclimated state using single turnover flash
F _v	Variable fluorescence after dark acclimation using single turnover flash (F _v = F _m – F _o)
F _v / F _m (ΔΦ _m)	Maximum PSII photochemical efficiency measured using a single turnover flash
F _v '	Variable fluorescence in the light acclimated state using a single turnover flash (F _v ' = F _m ' – F _o ')
F _v ' / F _m ' (ΔΦ)	Effective PSII photochemical efficiency measured using a single turnover flash
qN	Photochemical quenching coefficient (qN = 1 – [(F _m ' – F _o ') / (F _m – F _o)])
NPQ	Stern-Volmer non-photochemical quenching coefficient NPQ = (F _m - F _m ') / F _m '
ETR	Electron Transport Rate (RLC)
_{abs} ETR _{max}	Absolute Electron Transport Rate (RLC)
_{rel} ETR _{max}	Relative Electron Transport Rate (RLC)
α ^B	Photosynthetic efficiency in limiting light conditions (RLC)
E _k	Light saturation parameter (RLC)

Table 4.2: Fluorescence parameters and their meaning. After Kromkamp and Forster (2003).

4.6.5 Determination of Rapid Light Curves (RLC)

The photosynthetic capacity of cells was estimated by studying the relationship between irradiance and photosynthesis. Rapid light curves of electron transport rate (ETR) vs. irradiance were determined on the 15-minutes dark-acclimated samples by applying a series of 10 increasing actinic light treatments lasting 2 minutes each (from 1 to 1600 $\mu\text{mol photons} \cdot \text{m}^{-2} \cdot \text{s}^{-1}$).

The first measurement performed on the 15-min dark-acclimated sample corresponds to the maximal PSII photochemical efficiency of the algal sample (F_v / F_m). Then, light treatment (E) automatically increases and at the end of each 2-minutes actinic light step, the steady-state level of fluorescence in the light (F') is measured as well as the F_m' after the saturating flash. The quantum yield is determined using Eq. 4.11.

Determination of photosynthetic parameters is based on the Electron Transport Rate (ETR) measurements. The relative electron transport rate of the photosynthetic apparatus can be estimated based on the measurement of PSII photochemical efficiency (Genty *et al.*, 1989). According to Hofstraat *et al.*, (1994) and Schreiber *et al.*, (1994), the relative ETR ($_{\text{rel}}\text{ETR}$) is defined as:

$$_{\text{rel}}\text{ETR} = F_v' / F_m' \cdot E \cdot 0.5 \quad (4.14)$$

where $_{\text{rel}}\text{ETR}$ is expressed in $\text{mol e}^- \cdot \text{m}^{-2} \cdot \text{s}^{-1}$. E is irradiance, and a factor of 0.5 is applied since it is assumed that half of the incident light is absorbed by the PSI and half by the PSII. The absolute ETR, taking into account the part of incident light energy effectively absorbed by the photosystem (Genty *et al.*, 1989; Kolber and Falkowski, 1993), has been calculated as follows:

$$_{\text{abs}}\text{ETR} = F_v' / F_m' \cdot E \cdot 0.5 \cdot a_{\text{ph}}^* \quad (4.15)$$

where a_{ph}^* is the Chl *a* specific absorption coefficient expressed in $\text{m}^2 \cdot \text{mg Chl } a^{-1}$. The absolute ETR is expressed in $\text{mol e}^- \cdot \text{g Chl } a^{-1} \cdot \text{h}^{-1}$.

From the $_{\text{abs}}\text{ETR}$ vs E curve, the photosynthetic parameters (α^{B} , $_{\text{abs}}\text{ETR}_{\text{max}}$ and E_k ; Fig. 4.1) were retrieved according to the equation of Eilers and Peeters (1988):

$$_{\text{abs}}\text{ETR} = E / [(a \cdot E^2) + (b \cdot E) + c] \quad (4.16)$$

where $\alpha^B = 1/c$, ${}_{\text{abs}}\text{ETR}_{\text{max}} = 1 / [b + 2(ac)]$ and $E_k = c / [b + 2(ac)]$.

The α^B parameter represents the slope of the initial linear increase of the ${}_{\text{abs}}\text{ETR}$ vs E curve (Fig. 4.1). The ${}_{\text{abs}}\text{ETR}_{\text{max}}$ is the apparent saturated electron transfer rate and E_k represents the light value at which photosynthesis becomes saturated (Fig. 4.1).

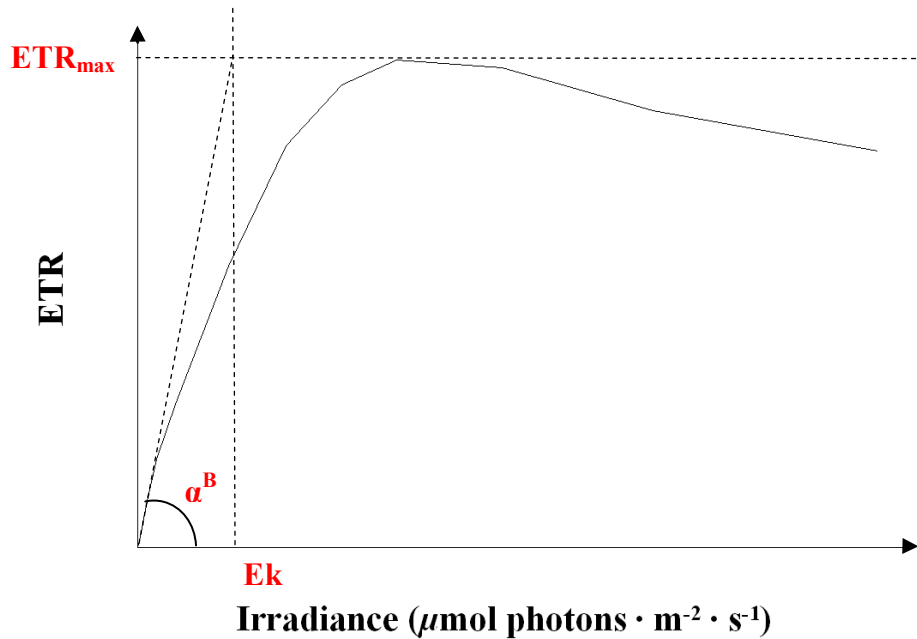


Fig. 4.1: Rapid light curves of electron transport rate (ETR) vs. irradiance.

4.7 Biochemical properties of cells

4.7.2 Determination of particulate organic carbon and nitrogen

Ten mL aliquots for the determination of particulate organic carbon (POC) and particulate organic nitrogen (PON) were filtered on pre-combusted (450°C , 5 hours) glass fiber filters (Whatman GF/F), conserved in cell culture plates (Corning Inc., NY, USA), and immediately stored at -20°C . The analyses were performed with a Thermo Scientific FlashEA 1112 automatic elemental analyzer (Thermo Fisher Scientific, MA, USA), following the procedure described by Hedges and Stern (1984). Filters were thawed just prior to analysis and allowed to dry at 60°C through a desiccator. Then filters were loaded in small tin cups which were crimped closed and transferred to the CHN analyzer. A set of

empty filters were processed as ordinary samples to accomplish the blank determination. Cyclohexanone 2,4-dinitrophenylhydrazone (C% 51.79, N% 20.14, H% 5.07) was used as standard.

4.7.1 Analysis of macromolecular pools and silica allocation

Fourier transform infrared (FTIR) spectroscopy analysis were performed to investigate the macromolecular pools and silica allocation in the three picoeukaryotic species.

Preliminary trials were performed to determine the density of cell suspensions necessary to produce spectra with an optimal signal-to-noise ratio without band saturation ($\sim 4 \times 10^6$ cells mL⁻¹). Cells were harvested by centrifugation at 1800 · g for 15 minutes with a ALC 4235A Centrifuge (ALC International, Milan, Italy). Cells were then washed twice with an iso-osmotic solution of ammonium formate to minimize seawater carryover and optical scattering effects due to salt crystals. Cells were fixed by the addition of 3 μL of Lugol's solution per milliliter of algal suspension. Samples were immediately stored at 4° C for further analysis which were conducted at Prof. M. Giordano's Laboratorio di Fisiologia delle Alghe (Dipartimento di Scienze del Mare, Università Politecnica delle Marche). Prior to analysis, cells underwent the last wash and a suitable number of cells was resuspended in 50 μL of an iso-osmotic solution of ammonium formate. This volume was deposited on silicon windows (Crystran Ltd., Poole, UK) and desiccated for 3 hours in a desiccator at 60° C (samples were kept in the desiccator until analyzed). Blank samples were prepared depositing 50 μL of ammonium formate solution on the windows which were subjected to the same treatment described for the samples. No trace of ammonium formate was detected in the blank spectra.

Spectra were acquired with a Bruker Tensor 27 FTIR spectrometer (Bruker Optik, Ettlingen, Germany), following the procedure by Domenighini and Giordano (2009). Band attribution was performed according to Giordano *et al.* (2001). The sum of the integrals of the absorption bands at 1160 cm⁻¹ and 1220 cm⁻¹ was used as a proxy for carbohydrates. The amide I 1656 cm⁻¹ peak was used in the calculations as an indicator of protein relative abundance, the feature at 1740 cm⁻¹ was used for lipids, while the absorption band at 1075 cm⁻¹ was used for silica (Giordano *et al.*, 2001). Relative ratios of carbohydrates, lipids, protein, and silica were calculated from the peaks' integrals using the software OPUS 6.5 (Bruker Optik). The calculation of the band integrals was performed after deconvolution of

the spectrum from 1800 cm^{-1} to 1000 cm^{-1} with the “peak fit” function of OPUS 6.5; to minimize subjective assessments, the main peaks on which deconvolution was based were identified by the application to each spectrum of a second derivative, with nine smoothing points. FT-IR measurements were conducted in triplicate on samples taken during the exponential growth phase for each irradiance condition, and at the beginning of exponential growth phase for control samples (ML condition acclimated cells).

4.8 Environmental factors measurements

Irradiance was measured in the culture flasks with a laboratory PAR sensor equipped with a Teflon 4π spherical optical collector (QSL 2101, Biospherical Instruments Inc., San Diego, CA, USA).

The pH and temperature of the culture were monitored at each sampling time thanks to a microprocessor pH/Temperature meter (HI-9214, Hanna Instruments, Woonsocket, RI, USA).

4.9 Statistical analysis

Descriptive statistics, correlation and multivariate analysis were conducted using the software Systat 7 (Systat Software, Inc., IL, USA).

CHAPTER 5

**Xanthophyll cycle ecophysiology in the context of
photoacclimation processes: experimental
approaches on *Pseudo-nitzschia multistriata***

Chapter 5

Xanthophyll cycle ecophysiology in the context of photoacclimation processes: experimental approaches on *Pseudo-nitzschia multistriata*

5.1 Introduction

Pseudo-nitzschia multistriata (Takano) Takano is a microplanktonic raphid pennate diatom. Cells are between 38–50 μm long and 2.8–3.8 μm wide (Sarno and Dahlman, 2000), and can form chains to give stepped colonies (D’Alelio *et al.*, 2009b). According to distribution ranges illustrated in Hasle (2002), *P. multistriata* is a temperate species that occurs closest towards the tropics, being observed generally in the warmer temperate waters. It is found in the Gulf of Naples (Tyrrhenian Sea, Mediterranean Sea), and the genus *Pseudo-nitzschia* has gained considerable attention over the last decade because many of its species have been shown to be able to produce the toxin domoic acid (DA), causing amnesic shellfish poisoning (Fryxell and Hasle, 2003). *P. multistriata*, is considered as a mildly toxic species.

In order to obtain a clearer knowledge on the xanthophyll cycle (XC) ecophysiology and functioning, *P. multistriata* has been chosen as model species to investigate the efficiency in the photoprotective and photoacclimative responses of a toxic diatom. Toxic species photobiology has been in part investigated in prymnesiophytes and dinoflagellates (Johnsen *et al.*, 1992, 1997, 1999; Johnsen and Sakshaug, 1993).

The main questions addressed by this study are herein divided in four groups in order to tackle different aspects of the XC ecophysiology during the photoacclimative state of cells.

- i. Is non-photochemical fluorescence quenching (NPQ) only dependent on the XC activation? Can we infer any role of Vx cycle pigments as intermediate xanthophylls in the biosynthesis of Dd cycle pigments?

These questions were addressed on the section *Xanthophyll cycle functioning and non-photochemical fluorescence quenching* (Sec. 5.3).

- ii. Is the photoprotective response through XC and NPQ linearly correlated to light intensity? How does the relation time/light affect XC functioning and NPQ development?
- iii. What is the effect of light increase velocity on the photoprotective response? How is XC and NPQ modulation regulated in function of the light increase velocity? Is photoprotection similarly enhanced when cells are subjected to same irradiance peaks but reached with different velocities?

Both light intensity and increase velocity are crucial factors in photosynthesis and photoprotective response regulation of cells. Regarding the velocity of light changes, we would expect it to affect XC and NPQ functioning, since the light stress difference.

These questions (ii and iii) were addressed on the section *Xanthophyll cycle ecophysiology in response to different kinetics of light change* (Sec. 5.4).

- iv. Does light history affect photoacclimation and regulation (XC and NPQ)?

We expect that the higher is growth irradiance condition, the greater would be the pool of XC pigments stored by cells, and the lower the photosynthetic pigment content. It has been observed that high light acclimated cells developed lower NPQ values if compared to cells grown at lower irradiance climate (Dimier *et al.*, 2007b).

From the general question, may therefore arise many specific questions, such as:

- How is the relation between photoprotection and light intensity (for instance, see Sec. 5.4) influenced by the light history?
- Which components of the photoprotective mechanism (XC and NPQ functioning, or the relation between them) are sensibly affected by light history?
- Is there a light threshold after which the light history effect would play a role on photosynthesis regulation?
- How long the light history effect would act and how much time is needed to develop it?

These questions were addressed on the section *Effect of light history on photoprotection* (Sec. 5.5).

5.2 Algal model and culture conditions

The non-axenic strain SY416 of *Pseudo-nitzschia multistriata* (Bacillariophyceae) was isolated at the Long-Term Ecological Research station MareChiara (LTER-MC) in the Gulf of Naples (40° 48.5' N, 14° 15' E, Tyrrhenian Sea, Mediterranean Sea). The strain was isolated by Sylvie V. M. Tesson, from a net sample collected during September 2009, and provided by Diana Sarno (Taxonomy and Identification of Marine Phytoplankton, TIMP). Cultures were cultivated at 20° C, in locally obtained, and sterilized seawater amended with f/2 medium (Guillard and Ryther, 1962) using 225 cm² polystyrene canted-neck flasks (Corning® Flask, Corning Inc., NY, USA).

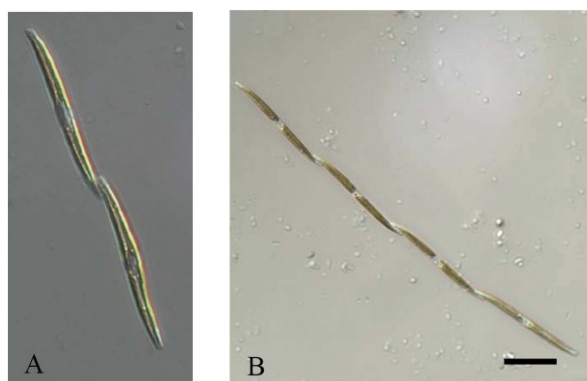


Figure 5.1: *Pseudo-nitzschia multistriata* in culture (A, B: girdle band view, light microscope Axiophot x 10 x 40 x 1.25, image Zeiss AxioCam, resolution 2600 × 2060, Axiovision 3.1 software, scale bar 20 μm). After Sylvie V. M. Tesson O.U. PhD Thesis (2010).

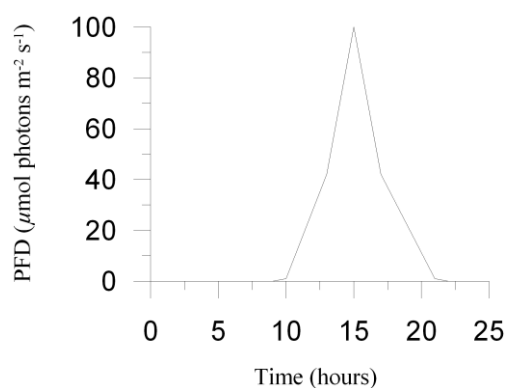


Figure 5.2: The sine light (SL) climates applied during the pre-acclimation period of experiments (maximal PPFD of 100 μmol photons m⁻² s⁻¹).

During the two weeks before the experiments started, cells were subjected to a pre-acclimation period.

Pre-acclimation was conducted under a sine light (SL) climate set to peak at a maximal photon flux density (PFD) of $100 \mu\text{mol photons} \cdot \text{m}^{-2} \cdot \text{s}^{-1}$, with a 11 : 13 hours light : dark photoperiod (Fig. 5.2).

Irradiance measurements were achieved by using a laboratory PAR 4π sensor (QSL 2101, Biospherical Instruments Inc., San Diego, CA, USA).

Daily and semicontinuous dilution with fresh medium (50% of the total volume), over a period of more than two weeks before the experiments, assured nutrient repletion and maintenance of cells in the exponential growth phase. Cultures were continuously bubbled with filtered air.

Before performing experiments, we checked the light condition pre-acclimation state of the strain, by assessing stability of pigment content and growth rate.

5.3 Xanthophyll cycle functioning and non-photochemical fluorescence quenching

5.3.1 Experimental design, sampling strategy and analysed parameters

This experiment was done on cells acclimated to a SL climate set to peak at a maximal PFD of $100 \mu\text{mol photons} \cdot \text{m}^{-2} \cdot \text{s}^{-1}$ (Fig. 5.2). The day of experiment, cells were subjected to five hours of illumination at $37 \mu\text{mol photons} \cdot \text{m}^{-2} \cdot \text{s}^{-1}$. At the end of this period, an aqueous solution of dithiothreitol (DTT) was injected into the culture to a final concentration of $500 \mu\text{mol} \cdot \text{L}^{-1}$ (Lohr and Wilhelm, 2001), largely enough to block the synthesis of the photoprotective pigment diatoxanthin (Dt; Lavaud *et al.*, 2002b). Cells were incubated for 10 minutes with the inhibitor before the shift to high light ($300 \mu\text{mol photons} \cdot \text{m}^{-2} \cdot \text{s}^{-1}$; Fig. 5.3). The experiment was conducted in triplicate (+DTT) and results were compared to the three control culture flasks (-DTT), which followed the same light shift as the three DTT-treated culture flasks.

Light was provided by the light system ACLS and Infinity XR4 (Aquarium Technologies, Sfiligoi S.r.l., Bassano del Grappa, Italy). XR4 was equipped with HQI metal halide lamps (10000 K).

Fifteen mL of culture were immediately taken as the flasks were shifted to the high light condition (t_0), and after 1 (t_1) and 10 (t_{10}) minutes *post* shift, to measure variable fluorescence, NPQ, and for further pigments analysis.

A ten mL aliquot was filtered onto GF/F glass fibre filters (Whatman, UK), and immediately stored in liquid nitrogen until further pigment analysis. Triplicate samples were taken during each sampling time. Pigment analysis was carried out following the procedure described in chapter 4 (Sec. 4.4).

Triplicate measurements of variable fluorescence were performed on both light- and dark-acclimated samples. NPQ triplicate measurements were conducted in 15 minutes dark-acclimated samples. Active Chl *a* fluorescence and NPQ were obtained following the procedures described in chapter 4 (Sec. 4.6).

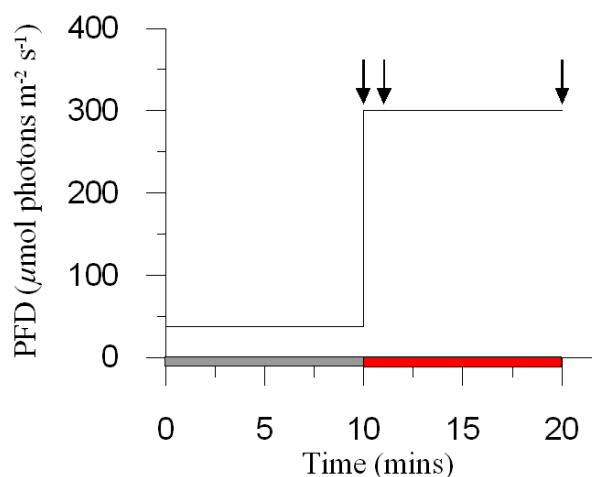


Figure 5.3: Scheme illustrating the illumination shift from low (grey bar) to high (red bar) irradiance intensity (37 and $300 \mu\text{mol photons m}^{-2} \text{s}^{-1}$, respectively), applied during the experiment. Low light dithiotreitol (DTT) incubation lasted 10 minutes before the high light shift. Arrows indicate sampling times, at 0, 1 and 10 minutes after the shift to high irradiance climate.

5.3.2 Results

5.3.2.1 Pigment content changes and xanthophyll cycle activation

The content of the photosynthetic pigments, as chlorophyll (Chl) a , did not show any significant variation in time and in both control (-DTT) and inhibitor-treated cultures (+DTT, Fig. 5.4 a). The same result was obtained for the other chlorophylls detected in the species (Chl c_2 and c_3 , data not shown).

Such result was expected since the short time scale experiment (10 mins) that prevented any changes of photosynthetic pigment content due to longer-term photoacclimation responses.

On the contrary, accessory pigments related to small-time scale photoprotective responses varied during the light shift and between control and inhibitor-treated cultures.

β -carotene (β -Car) Chl a^{-1} ratio was also quite stable in function of time, and did not change in function of the inhibitor presence-absence, besides a very small increase at 10 mins in the control compared to the DTT-treated cultures (Fig. 5.4 b). No significant correlation was found between β -Car and the accessory photosynthetic or photoprotective pigments, either in control or DTT-treated cultures.

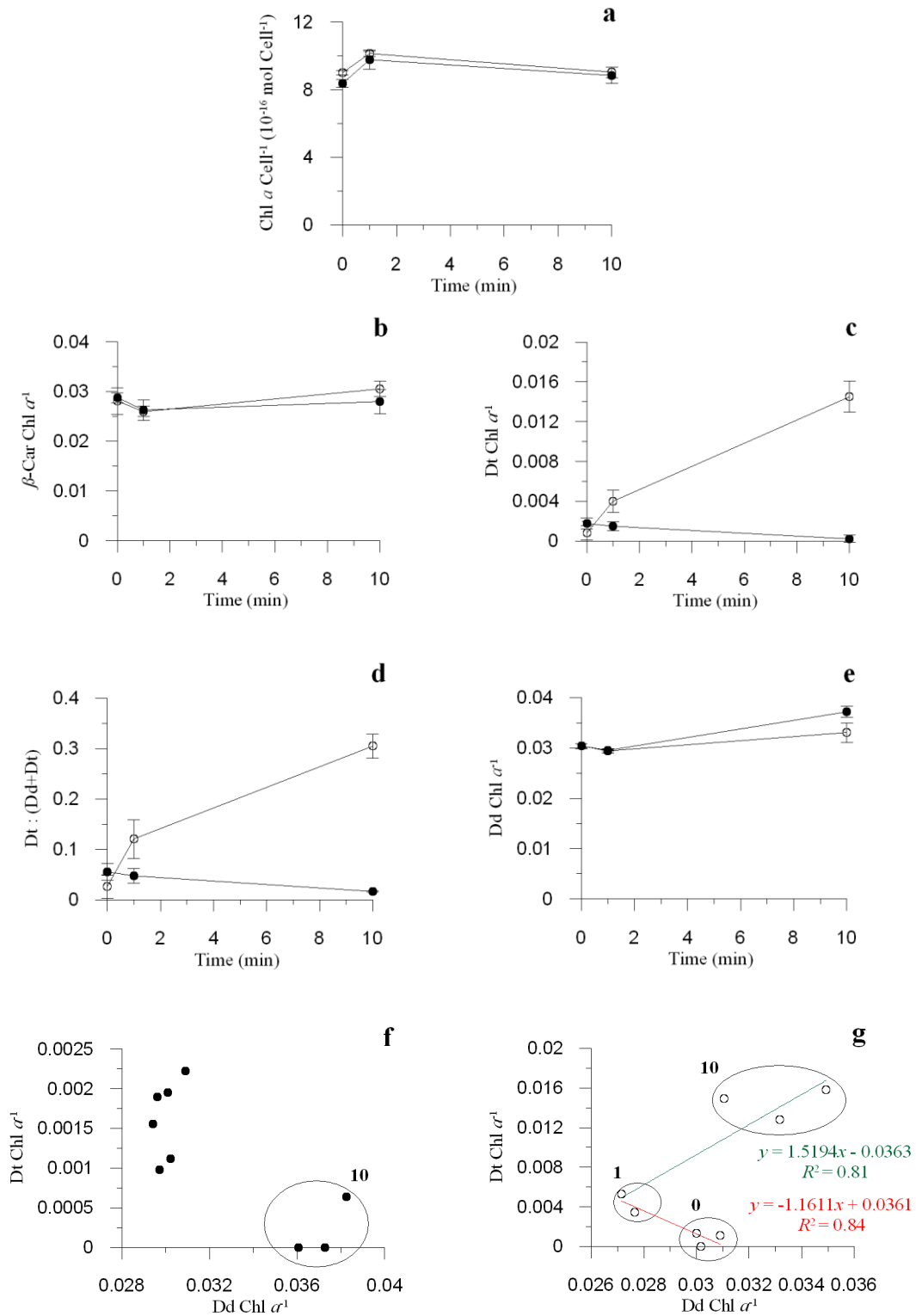


Fig. 5.4: Evolution of chlorophyll *a* cell⁻¹ content (a), β-carotene Chl *a*⁻¹ (b), diatoxanthin Chl *a*⁻¹ (c), the Dt : (Dt + Dd) DPS (d), and diadinoxanthin Chl *a*⁻¹ ratios (e), in function of time (minutes). Data are means with n = 3; error bars are SD. Relationship between diatoxanthin and diadinoxanthin Chl *a*⁻¹ ratio, in DTT-treated (f) and control cultures (g). DTT-treated culture: filled circles; control cultures: open circles. Numbers in figures f and g represent sampling time (in minutes). Chl *a*, chlorophyll *a*; β-Car, β-carotene; Dt, diatoxanthin; Dd, diadinoxanthin. Chl *a* cell⁻¹ content is expressed in 10⁻¹⁶ mol Chl *a* cell⁻¹; other pigment ratios are expressed in μg : μg Chl *a*.

In response to the high irradiance shift, Dt Chl a^{-1} ratio and the de-epoxidation state of cells (DPS, [Dt : (Dt + Dd)] ratio) strongly increased (Figs. 5.4 c and d). In the control cultures, DPS reached $\sim 30\%$ after 10 mins, while no Dt increase was revealed in the inhibitor-treated cultures, as expected, since the action of DTT (Figs. 5.4 c and d). On the contrary, the small quantity of Dt present in the cells under low light decreased in the DTT-treated cultures, in relation with the inhibition of the diadinoxanthin (Dd) de-epoxidase (DDE). This means that the Dt epoxidase (DEP) was active in these cells, since this small decrease in Dt Chl a^{-1} ratio was related to the increase in Dd Chl a^{-1} after 10 minutes (Figs. 5.4 e and f). The Dd Chl a^{-1} ratio increased after 1 minute in control condition (Fig. 5.4 e), in relation with the activation of the photoprotective biosynthetic pathway as suggested by the correlation between Dt and Dd Chl a^{-1} ratios (Fig. 5.4 g). Indeed, one minute after the shift to high light, Dt and Dd Chl a^{-1} ratios were significantly and positively correlated ($p < 0.05$), while in the first minute these pigments were significantly and negatively correlated ($p < 0.05$). The initial increase of Dt was related to the depletion of the available Dd content, and then the further increase of Dt was due to Dd *de-novo* synthesis (Fig. 5.4 g).

Together with the Dd cycle main photoprotective xanthophylls, two pigments of the Vx-cycle, violaxanthin (Vx) and zeaxanthin (Zx), were detected in *P. multistriata*, while the intermediary mono-epoxy carotenoid antheraxanthin (Ax) was not (Figs. 5.5 a and b). The Vx Chl a^{-1} ratio was higher than Zx Chl a^{-1} (Figs. 5.5 a and b). Injection of DTT led to an increase in Vx Chl a^{-1} ratio as shown by Fig. 5.5 a. This increase was activated during the first minute of the high light shift, while in the control culture the Vx Chl a^{-1} ratio decreased during the same time period, and later increased (Fig. 5.5 a). The Zx Chl a^{-1} ratio did not show any variation in control cultures, while in DTT-treated cultures it decreased from 0 to 1 min and then increased (Fig. 5.5 b).

A significant and negative correlation was found between Vx and Zx in DTT-treated cultures ($p < 0.05$; Fig. 5.5 c), underlining that the Zx epoxidase (ZEP) was not inhibited by high light, as already observed in other organisms (Siefermann and Yamamoto, 1975; Goss *et al.*, 2006a). This feature was not observable in control cultures due to the functioning of the Vx de-epoxidase (converting Vx to Zx, through Ax). In the DTT-treated cultures, the Vx Chl a^{-1} ratio was significantly correlated with Dd Chl a^{-1} ($p < 0.05$), and it showed a negative trend with Dt Chl a^{-1} (Figs. 5.5 e and g). Despite a likely positive trend between Vx and Zx Chl a^{-1} , and Dd Chl a^{-1} (Figs. 5.5 d and f), no significant

correlation was found in control cultures, highlighting the fact that many biosynthetic processes were linked to the Dd de-epoxidation.

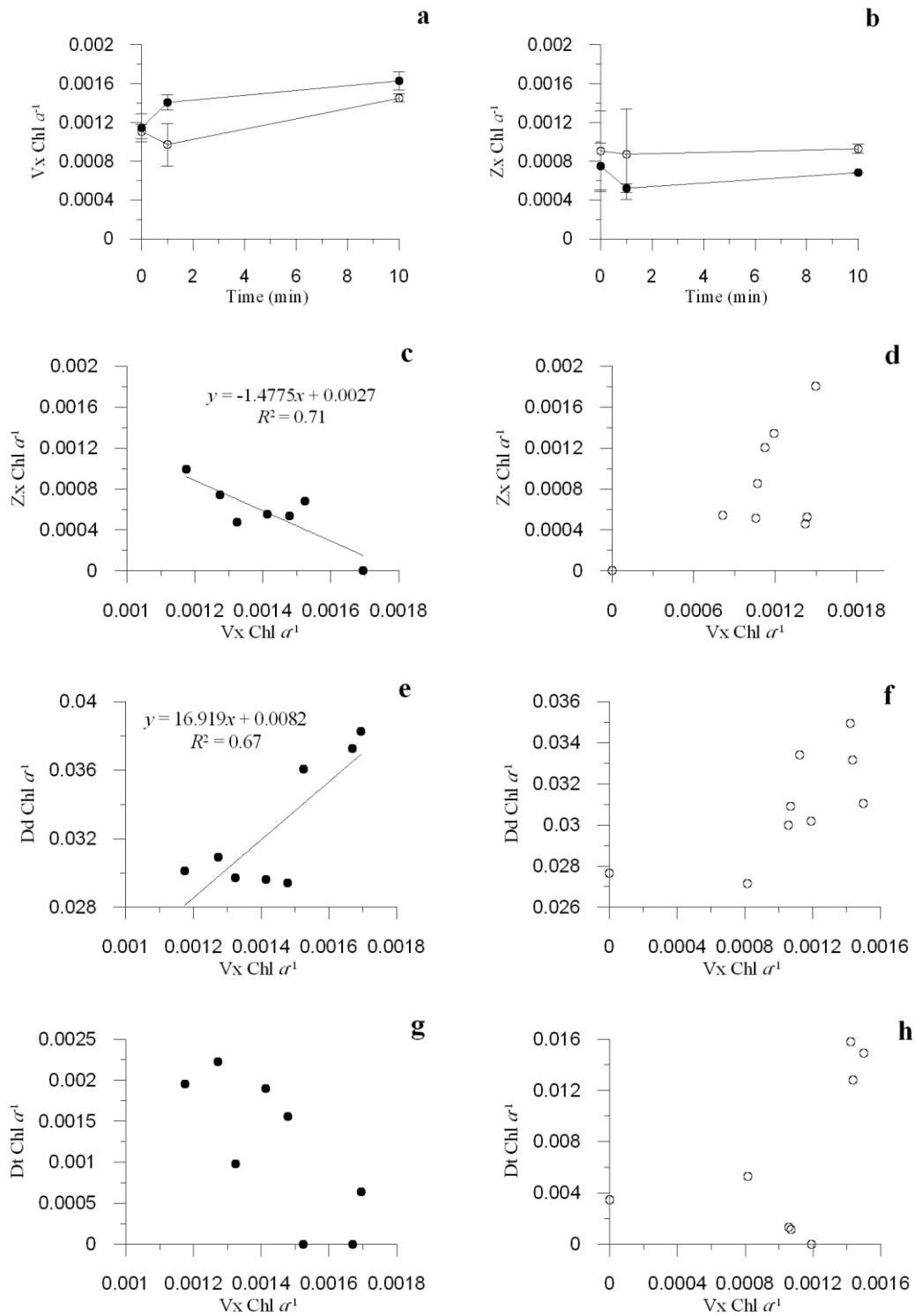


Fig. 5.5: Evolution of violaxanthin (a) and zeaxanthin $\text{Chl } a^{-1}$ ratios expressed in $\mu\text{g} : \mu\text{g Chl } a$ (b), in function of time (minutes). Data are means with $n = 3$; error bars are SD. Relationship between zeaxanthin and violaxanthin $\text{Chl } a^{-1}$, diatoxanthin and violaxanthin $\text{Chl } a^{-1}$, diadinoxanthin and violaxanthin $\text{Chl } a^{-1}$ ratios, in DTT-treated (c, e and g) and control cultures (d, f and h). DTT-treated culture: filled circles; control cultures: open circles. Chl *a*, chlorophyll *a*; Vx, violaxanthin; Zx, zeaxanthin; Dt, diatoxanthin; Dd, diadinoxanthin.

Variations of fucoxanthin (Fuco) and *cis*-fucoxanthin (*cis*-Fuco) Chl a^{-1} ratios reflected rapidly regulated biochemical responses, also linked to the xanthophyll cycle functioning. The Fuco Chl a^{-1} ratio increased in both conditions, with higher values in the control cultures than in the DTT-treated cultures (Fig. 5.6 a). Differently, the *cis*-Fuco Chl a^{-1} ratio decreased in control and increased in DTT-treated cultures (Fig. 5.6 b). The relationship between these two pigments was revealed by the significant and negative correlation in control cultures ($p < 0.025$; Fig. 5.6 d), a correlation that was not visible when the inhibitor was injected (Fig. 5.6 c). Fuco Chl a^{-1} was significantly correlated with Dt Chl a^{-1} ($p < 0.01$; Fig. 5.7 b), while showed a positive trend with Dd Chl a^{-1} (Fig. 5.7 d). The stronger correlation obtained between Dt Chl a^{-1} and Fuco Chl a^{-1} relatively to Dd Chl a^{-1} was probably due to the fact that Dd is a transient pigment, which is rapidly de-epoxidated to Dt in response to high light (Fig. 5.4 f).

A negative trend between *cis*-Fuco and Dd Chl a^{-1} ratios was observable (Fig. 5.7 h). These results highlighted how under high irradiance Fuco increased at the expense of *cis*-Fuco, and such increase was related to the enhancement of XC photoprotective response.

Accessory xanthophylls neoxanthin-? (Neox-?) and neoxanthin-like (Neox-like) were detected in *P. multistriata* pigment pool. Since these pigments were detected close to the elution time of neoxanthin and had similar absorption spectra, we decided to add to the name of this pigment the suffixes “-like” and “-?” due to discrimination uncertainty.

Both Neox-? and Neox-like Chl a^{-1} ratios were greater in DTT-treated rather than in control cultures (Figs. 5.8 a and b). Neox-? Chl a^{-1} decreased from 0 to 1 min, and then remained stable in control cells, whereas it increased in DTT-treated cells (Fig. 5.8 a). Neox-like Chl a^{-1} gradually decreased in control cultures, whereas it showed the opposite trend in DTT-treated cultures (Fig. 5.8 b).

In control cultures, Neox-? Chl a^{-1} was strongly correlated with Fuco and *cis*-Fuco Chl a^{-1} ratios, underlining a possible involvement of Neox-? in the regulation of XC ($p < 0.005$ and 0.025 , respectively; Figs. 5.8 d and f). This feature was confirmed by the Neox-? Chl a^{-1} negative trend with Dd Chl a^{-1} , and the significant and negative correlation between Neox-? and Dt Chl a^{-1} ($p < 0.01$; Figs. 5.9 b and d).

Neox-like seemed to be linked to the Vx-cycle, as revealed by the significant and positive correlation with Vx Chl a^{-1} ($p < 0.025$), and by the presence of a negative trend with Zx Chl a^{-1} (Figs. 5.10 a and c). These correlations were absent in control cultures (Figs. 5.10 b and d).

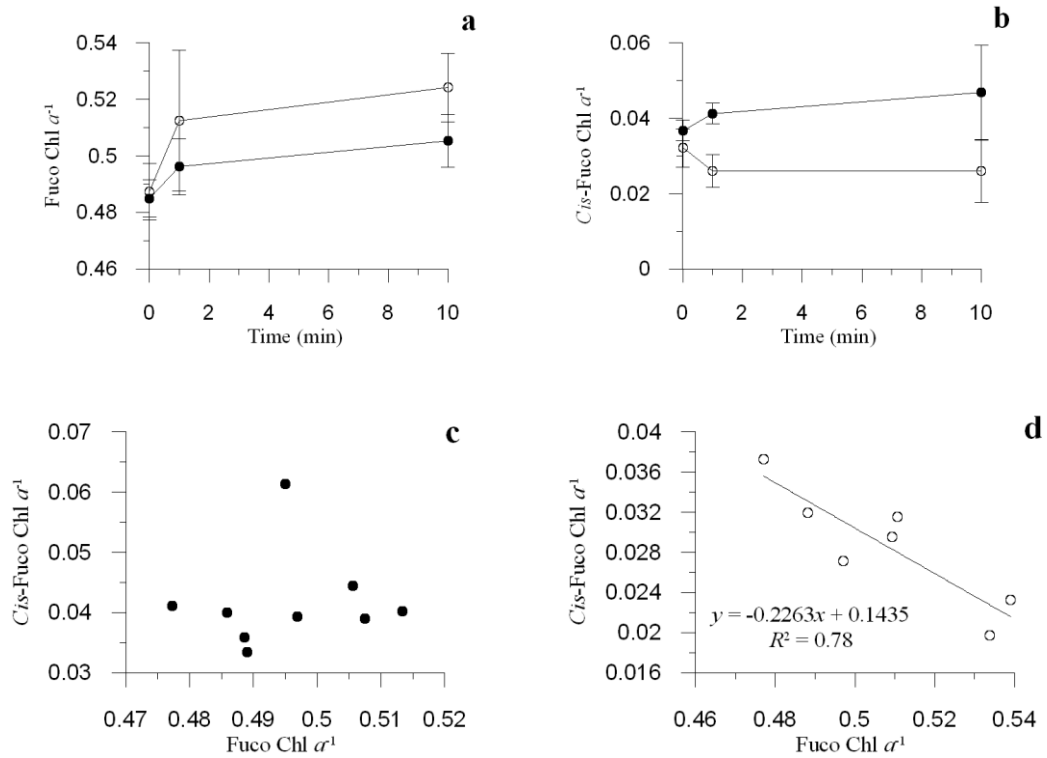


Fig. 5.6: Evolution of fucoxanthin (a) and *cis*-fucoxanthin Chl a^{-1} ratios expressed in $\mu\text{g} : \mu\text{g Chl } a$ (b), in function of time (minutes). Data are means with $n = 3$; error bars are SD. Relationship between fucoxanthin and *cis*-fucoxanthin Chl a^{-1} ratios, in DTT-treated (c) and control cultures (d). DTT-treated culture: filled circles; control cultures: open circles. Chl a , chlorophyll a ; Fuco, fucoxanthin; *Cis*-Fuco, *cis*-fucoxanthin.

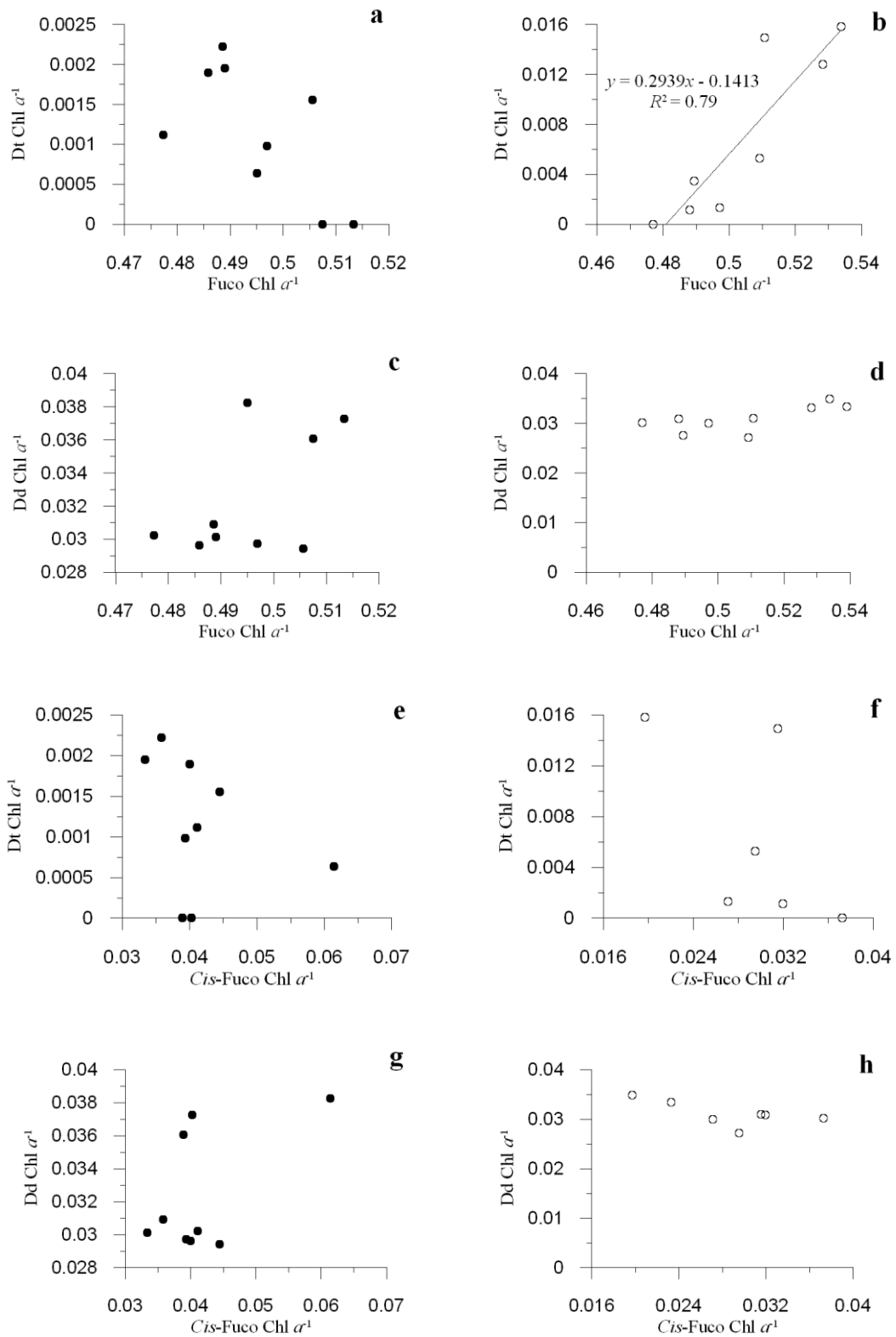


Fig. 5.7: Relationship between diatoxanthin and fucoxanthin $\text{Chl } a^{-1}$, diadinoxanthin and fucoxanthin $\text{Chl } a^{-1}$, diatoxanthin and *cis*-fucoxanthin $\text{Chl } a^{-1}$, diadinoxanthin and *cis*-fucoxanthin $\text{Chl } a^{-1}$ ratios, in DTT-treated (a, c, e and g) and control cultures (b, d, f and h). DTT-treated culture: filled circles; control cultures: open circles. Chl *a*, chlorophyll *a*; Dt, diatoxanthin; Dd, diadinoxanthin; Fuco, fucoxanthin; *Cis*-Fuco, *cis*-fucoxanthin.

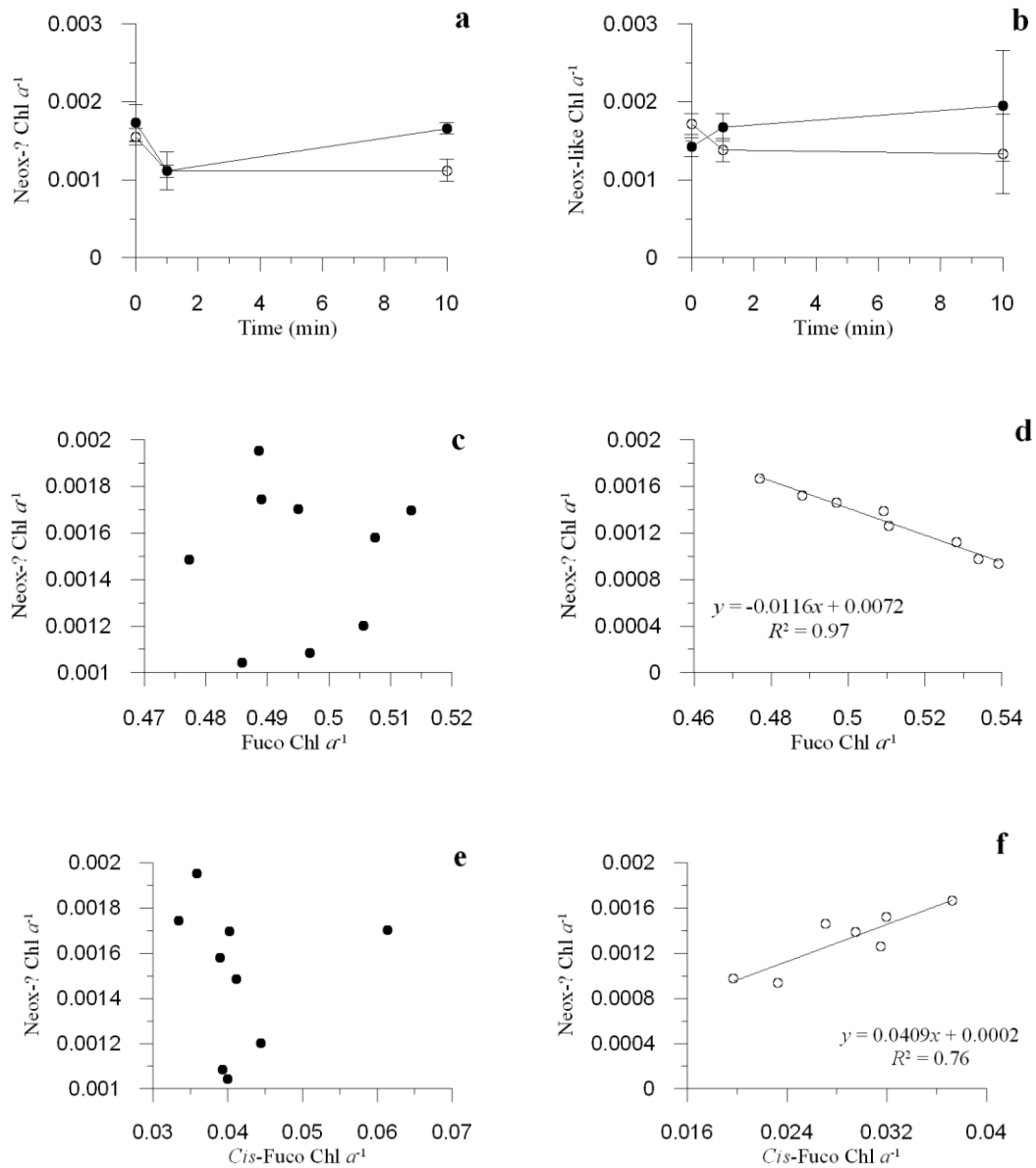


Fig. 5.8: Evolution of neoxanthin-? (a) and neoxanthin-like Chl a^{-1} ratios expressed in $\mu\text{g} : \mu\text{g}$ Chl a (b), in function of time (minutes). Data are means with $n = 3$; error bars are SD. Relationship between neoxanthin-? and fucoxanthin Chl a^{-1} , neoxanthin-? and *cis*-fucoxanthin Chl a^{-1} ratios, in DTT-treated (a, c, and e) and control cultures (b, d, and f). DTT-treated culture: filled circles; control cultures: open circles. Chl a , chlorophyll a ; Neox-?, neoxanthin-?; Neox-like, neoxanthin-like.

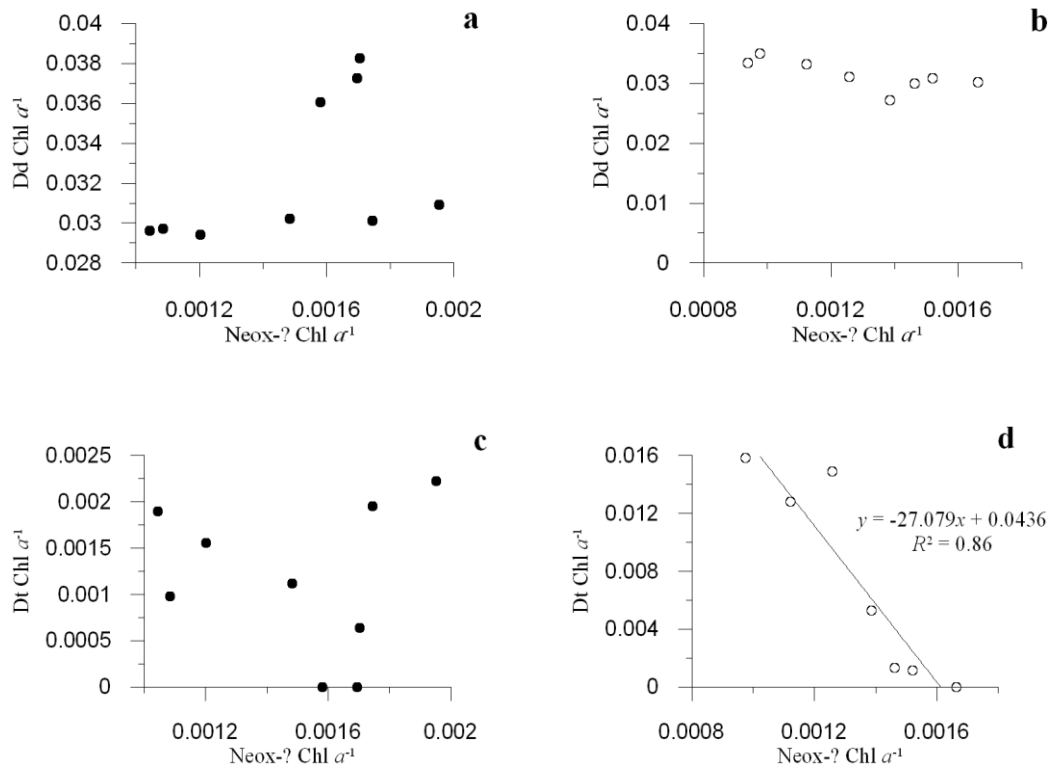


Fig. 5.9: Relationship between diadinoxanthin and neoxanthin-? Chl a^{-1} , diatoxanthin and neoxanthin-? Chl a^{-1} ratios, in DTT-treated (a, and c) and control cultures (b and d). DTT-treated culture: filled circles; control cultures: open circles. Chl a , chlorophyll a ; Dt, diatoxanthin; Dd, diadinoxanthin; Neox-?, neoxanthin-?.

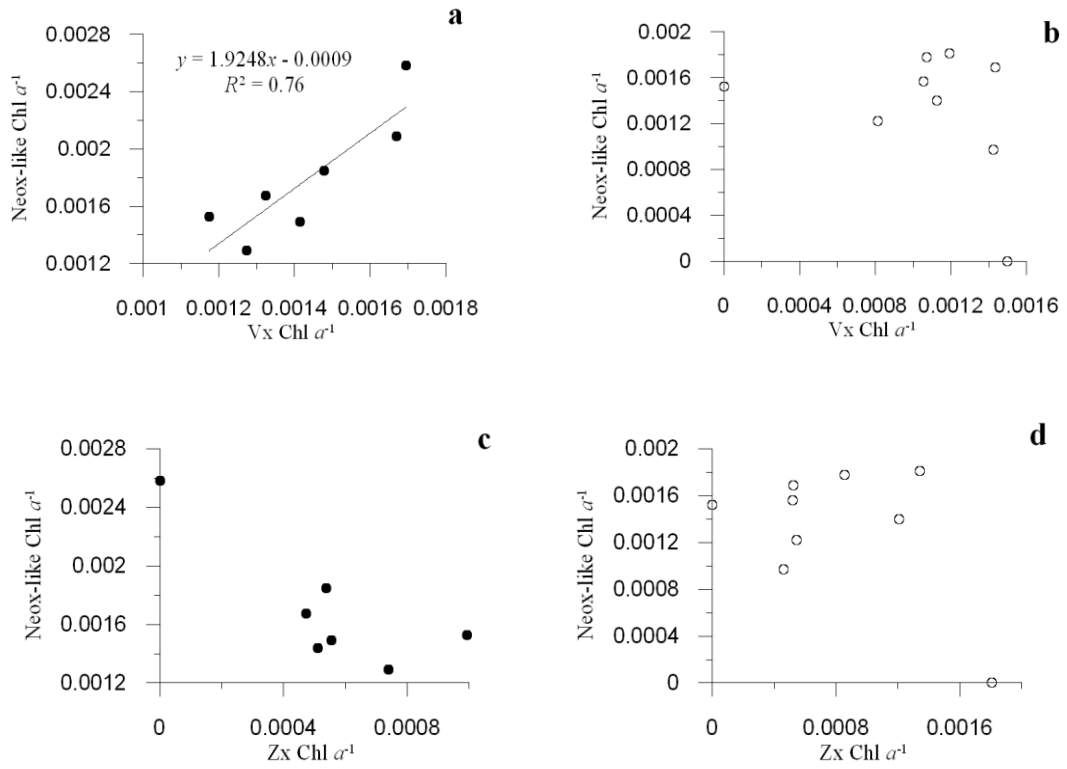


Fig. 5.10: Relationship between neoxanthin-like and violaxanthin Chl a^{-1} , neoxanthin-like and zeaxanthin Chl a^{-1} ratios, in DTT-treated (a, and c) and control cultures (b and d). DTT-treated culture: filled circles; control cultures: open circles. Chl a , chlorophyll a ; Dd, diadinoxanthin; Neox-like, neoxanthin-like, Vx, violaxanthin; Zx, zeaxanthin.

5.3.2.2 Variable fluorescence and non-photochemical fluorescence quenching

The lack of Dd de-epoxidation limits the development of non-photochemical fluorescence quenching (NPQ, Fig. 5.11). NPQ was developed and identical at t_0 in both DTT-treated and control cultures, probably in relation with the basal presence of Dt at this time (Fig. 5.4 c). NPQ strongly and gradually increased in control cultures, while it slightly decreased after 1 minute of high light, then being stable, in DTT-treated cultures (Fig. 5.11 a).

As expected, a strong correlation was found between NPQ and Dt Chl a^{-1} , and DPS ratios, in control conditions (in both correlations $p < 0.005$; Figs. 5.11 c and e), revealing that the NPQ development mainly relied on the rapid de-epoxidation of Dd to Dt. However, the small amount of NPQ developed in DTT-treated cells seemed to be not related to Dt content. In fact, the NPQ value of DTT-treated cultures was the 34% of the NPQ developed in control cultures at 10 mins (0.19 and 0.54, respectively). This value of 0.19 agreed with the value 0.14 found as b-constant value ($y = a \cdot x + b$) in the linear regression equation between NPQ and DPS ratio (Fig. 5.11 e).

The photosystem II (PSII) maximal photochemical efficiency ($F_v : F_m$) of cells decreased in both condition as the result of the high light effect. The lack of Dt synthesis led to a stronger decrease of $F_v : F_m$ (Fig. 5.12 a). The $F_v : F_m$ in control cultures was significantly and negatively correlated with the DPS ratio ($p < 0.025$; Fig. 5.12 c) and Dt Chl a^{-1} ratio ($p < 0.025$, Fig. 5.12 e), as it was also with NPQ ($p < 0.025$; Fig. 5.12 g). These significant relationships demonstrated the link between photoprotective responses and the decrease in $F_v : F_m$, the latter decreasing more in DTT-treated cells due to the lack of photoprotection activation. A 7.6% of the $F_v : F_m$ decrease caused by the lack of Dt synthesis was estimated as the difference between the lowest $F_v : F_m$ value in control and DTT-treated cultures (i.e. 0.66 and 0.61, respectively; Fig. 5.12 a).

In DTT-treated cultures a significant and positive correlation occurred between $F_v : F_m$, DPS and Dt Chl a^{-1} ratio ($p < 0.005$ and 0.01, respectively; Figs. 5.12 b and d), result of the little decrease in Dt content with DTT injection.

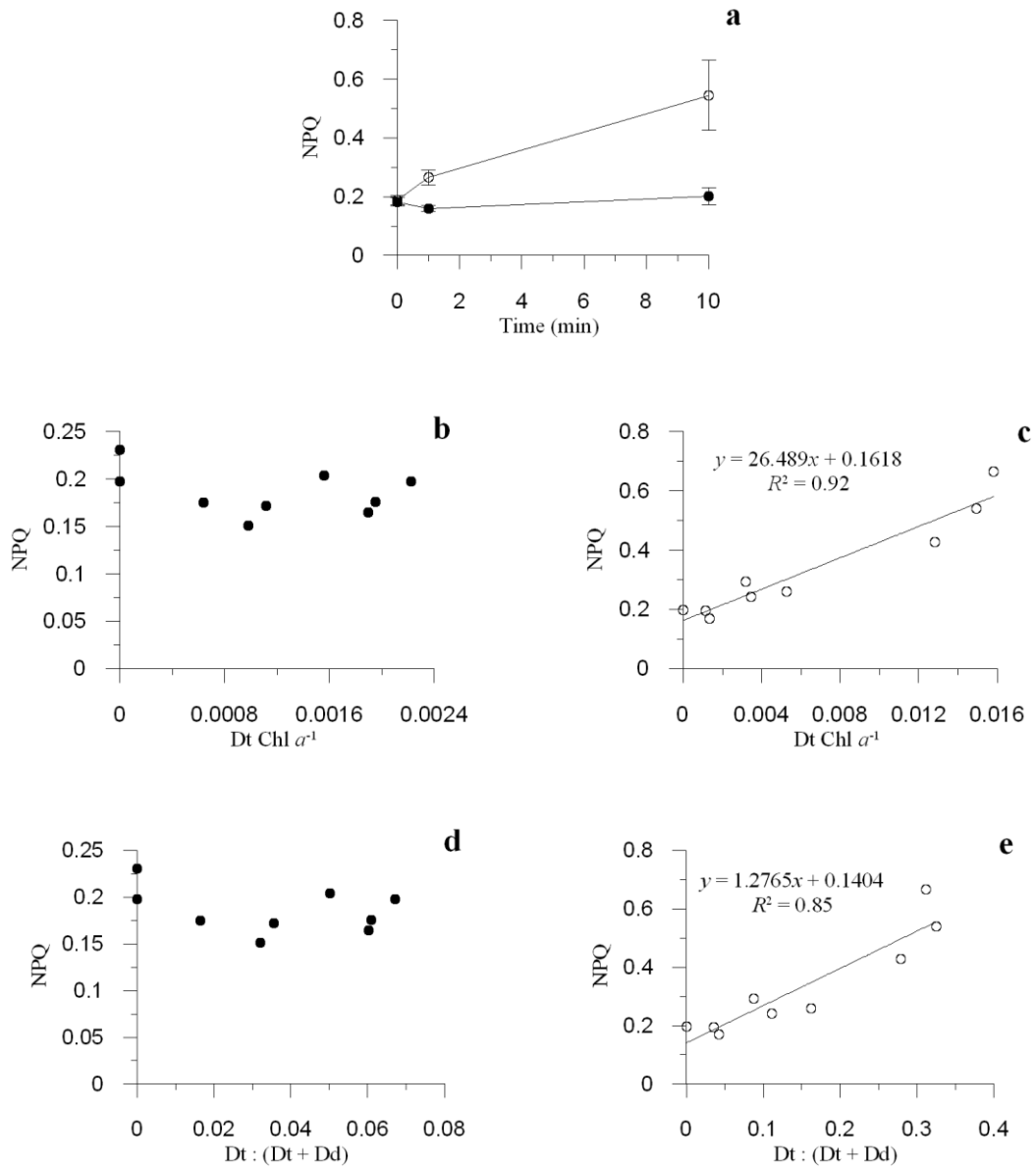


Fig. 5.11: Evolution of non-photochemical fluorescence quenching (NPQ), in function of time (minutes; **a**). Data are means with $n = 3$; error bars are SD. Relationship between NPQ and diatoxanthin Chl a^{-1} , NPQ and the Dt : (Dt + Dd) ratios, in DTT-treated (**b** and **d**) and control cultures (**c** and **e**). DTT-treated culture: filled circles; control cultures: open circles. Chl a , chlorophyll a ; Dt, diatoxanthin; Dd, diadinoxanthin.

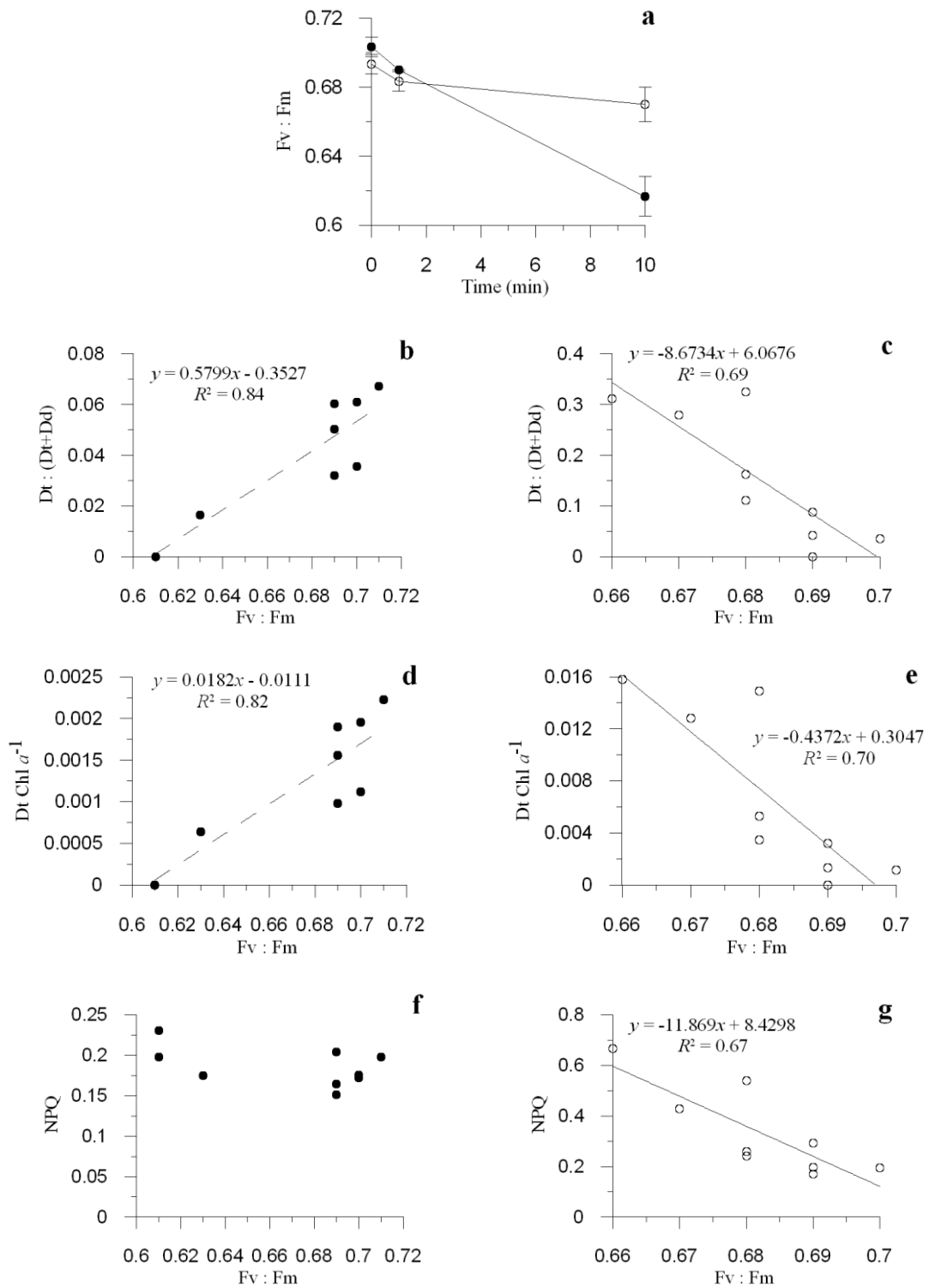


Fig. 5.12: Evolution of photosystem II maximal photochemical efficiency (Fv : Fm), in function of time (minutes). Data are means with $n = 3$; error bars are SD. Relationship between the Dt : (Dt + Dd) ratio and Fv : Fm, Dt Chl a^{-1} and Fv : Fm, NPQ and Fv : Fm, in DTT-treated (**b**, **d** and **f**) and control cultures (**c**, **e** and **g**). DTT-treated culture: filled circles; control cultures: open circles. Chl a , chlorophyll a ; Dt, diatoxanthin; Dd, diadinoxanthin.

5.3.3 Discussion

The present study was conducted to investigate the short-time scale regulation processes activating the xanthophyll cycle (XC) and the consequent non-photochemical fluorescence quenching (NPQ) in response to the shift from low to high irradiance climate (from 37 to 300 $\mu\text{mol photons} \cdot \text{m}^{-2} \cdot \text{s}^{-1}$; Fig. 5.3). The disulfide reductant dithiotreitol (DTT), an inhibitor of the de-epoxidation activity of the enzyme DDE (and VDE; Yamamoto and Kamite, 1972) responsible for the light-induced conversion of Dd to Dt (and Vx to Zx, through Ax), has been used as a tool to better elucidate (i) the involvement of the photoprotective epoxy-free xanthophylls in the NPQ development, and (ii) to eventually grasp a clearer view regarding some of the players involved in the biochemical steps of the xanthophylls biosynthetic pathway, in the diatom *Pseudo-nitzschia multistriata*.

Many authors have described the Dt-dependent NPQ - called qE - as the main photoprotective mechanism in diatoms (Olaizola *et al.*, 1994; Goss *et al.*, 1999, 2006b; Lavaud *et al.*, 2002a, 2002b; for recent reviews, see Goss and Jakob, 2010; Lepetit *et al.*, 2011). In *P. multistriata*, in response to high light, the NPQ development is tightly dependent on the fast Dd de-epoxidation to Dt, as demonstrated by the correlation occurred between NPQ and Dt as well as the stable and lower NPQ values in DTT-treated cultures compared to the stronger increase in NPQ in control cultures.

Strikingly, despite the inhibitor treatment, NPQ development is not completely prevented, and a small but still relevant NPQ values (34% of the maximal value obtained in the control culture) have been measured in DTT-treated cultures. This NPQ is thus a Dd cycle activation uncoupled quenching, as it has been previously described to occur in *Phaeodactylum tricorutum* (Ruban *et al.*, 2004; Lavaud and Kroth, 2006).

The NPQ development that is immediately measured upon the onset of illumination can be explained by the presence of an initial pool of Dt, generating a transient-like NPQ component, as recently described only in the diatom *Cyclotella meneghiniana* (Grouneva *et al.*, 2008). Maybe, a chlororespiratory proton gradient might be involved in this initial accumulation of Dt (Jakob *et al.*, 1999, 2001). The presence in *P. multistriata* of an initial Dt pool, whose accumulation in this species seems to be light-independent (since cells came from low light condition), is similar to what Grouneva and co-authors (2008) found while subjecting *C. meneghiniana* to different experimental irradiance conditions. The authors of the aforementioned study reported that in *C. meneghiniana* the NPQ mechanism is composed of three sequential components, respectively called transient, steady-state, and

fast relaxing NPQ component. The transient NPQ component has been described to be an antenna-based reaction mechanism, Δ pH-dependent and modulated by the initial Dt cellular content. Such a definition ('transient') is because of its slow relaxation soon after having reached its maximal value (in ~ 1 minute). This NPQ component has been compared to the transient component found in vascular plants and also localized within the LHCII complexes (Kalituho *et al.*, 2007). It is also worth to note that while in *C. meneghiniana* the transient NPQ component increased with irradiance intensities, in vascular plants it occurred at non-saturating irradiance intensities, and actually no information is present about its eventual light-dependence, since the adopted experimental design (Kalituho *et al.*, 2007).

Despite the relative distance in phylogeny between *C. meneghiniana* (centric diatom, Thalassiosirales) and *P. multistriata* (raphid pennate diatom, Bacillariales; Kooistra *et al.*, 2007), our results suggest that *P. multistriata* might adopt the same initial transient NPQ modulation found in *C. meneghiniana*, but not as the unique immediate mechanism developed upon the illumination shift. In fact, if that would have been the case, we would have also measured a decrease of this NPQ contribute in function of time, as the Dt content decreased. The small NPQ increase at 10 mins despite the Dt decrease might be related to the interactions between PSII-detached fucoxanthin chlorophyll *a/c*-binding protein (FCP) complexes (Miloslavina *et al.*, 2009). In the study conducted by Miloslavina and co-authors (2009) the fluorescence decay kinetics of the diatoms *P. tricornutum* and *C. meneghiniana* have been compared in quenched and unquenched state, and a model describing their NPQ mechanism has been proposed. The presence of two different quenching locations responsible for the steady-state NPQ in diatoms has been supported, and according to this model, a portion of NPQ would be Dt-independent and rely on the aggregation of specific FCP antennae, functionally detached from PSII during high light adaptation. This quenching mechanism can therefore support the NPQ increase occurring after one minute of high irradiance exposure, in *P. multistriata*.

On the basis of these results, we propose that in *P. multistriata* the damage related to energy excess absorption is avoided/limited by finely regulating both the XC and an efficient multi-component NPQ mechanism. Together with the major Dd cycle dependent NPQ contribute, the photoprotective response is functionally related to the concomitant activation of an instantaneous transient NPQ component (relying on the initial Dt pool) coupled with the quenching caused by the aggregation of PSII-detached FCP antennae.

Notably, changes within the PSII core center might also contribute to the basal NPQ, as it has been recently reported in *P. tricornutum* (Eisenstadt *et al.*, 2008).

One third of the total NPQ might rely on these mechanisms and limit the physiologically damaging stress of high light. At the same time, the activation of these two Dd cycle independent mechanisms does not result in an efficient photoprotective state of cells, which is only provided when the XC is optimally functioning and thus NPQ modulation can rely on a strong Dt conversion, as demonstrated by the greater decrease of PSII maximal photochemical efficiency (7.6 %) in DTT-treated cultures compared to control cultures.

The efficient XC regulation is based on two kinetics of Dd de-epoxidation. The Dt Chl a^{-1} ratio initially increases by depleting the available Dd cellular pool (between 0 and less than 10 minutes), then both photoprotective xanthophylls content increases (Dd *de-novo* synthesis). The sampling strategy prevented us to determine the precise moment during which the Dd *de-novo* synthesis started, after the first minute cells experienced high light. With respect to other studies (Dimier *et al.*, 2007b; Lavaud *et al.*, 2004), the Dd *de-novo* synthesis activation time is quite short, revealing a great potential for fast and powerful photoprotection in this species.

This could be due to the high enzymatic activity of this species. Indeed, the decrease of Dt in favour of Dd content in DTT-treated cells demonstrates the activity of the Dt epoxidase (DEP) even when cells experience high light conditions, as it was also suggested by the recent study of Dimier and co-authors (2009b) in different marine phytoplanktonic (non-diatom) species, while other authors did not find such result (Mewes and Richter 2002; Goss *et al.*, 2006b). Discrepancies between those studies are probably due to specific diversity, related to the higher or lower sensibility of the enzyme to light climate. This increasing kinetics of epoxidation from Dt to Dd could be an ecological competitive advantage enabling the species to limit the loss of energy when light becomes less excessive, and thus rapidly increase the photosynthetic quantum yield. Under our experimental light condition, the lack of 'high light'-inhibition of DEP activity is also accompanied by the parallel Zx epoxidase (ZEP) activity, demonstrated by the significant and negative correlation between Zx and Vx Chl a^{-1} ratios in DTT-treated cultures. The ZEP slope-constant value of the linear regression (i.e. -1.4775) is similar to the DDE slope-constant values of the negative and positive regressions (i.e. -1.1611 and 1.5194),

suggesting that the epoxidation of Zx to Vx and the de-epoxidation of Dd to Dt have similar reaction kinetics.

The results obtained from this experiment allow us to hypothesize a conceptual model of the biosynthetic photoprotective pathway during the xanthophyll cycle activation (Fig. 5.13).

Under high irradiance condition, the increase in Fuco content, formed from *cis*-Fuco content, is related to the enhancement of XC photoprotective response, by replenishing the Dt content, through Dd. In *P. tricornutum* cells, subjected to prolonged low light conditions, the Dd formed from Vx has been described to be the precursor of Fuco (Lohr and Wilhelm, 1999). These authors proposed that in diatoms the di- and mono-epoxy xanthophylls, Vx and Dd, are fundamental pigments not only because of their photo-

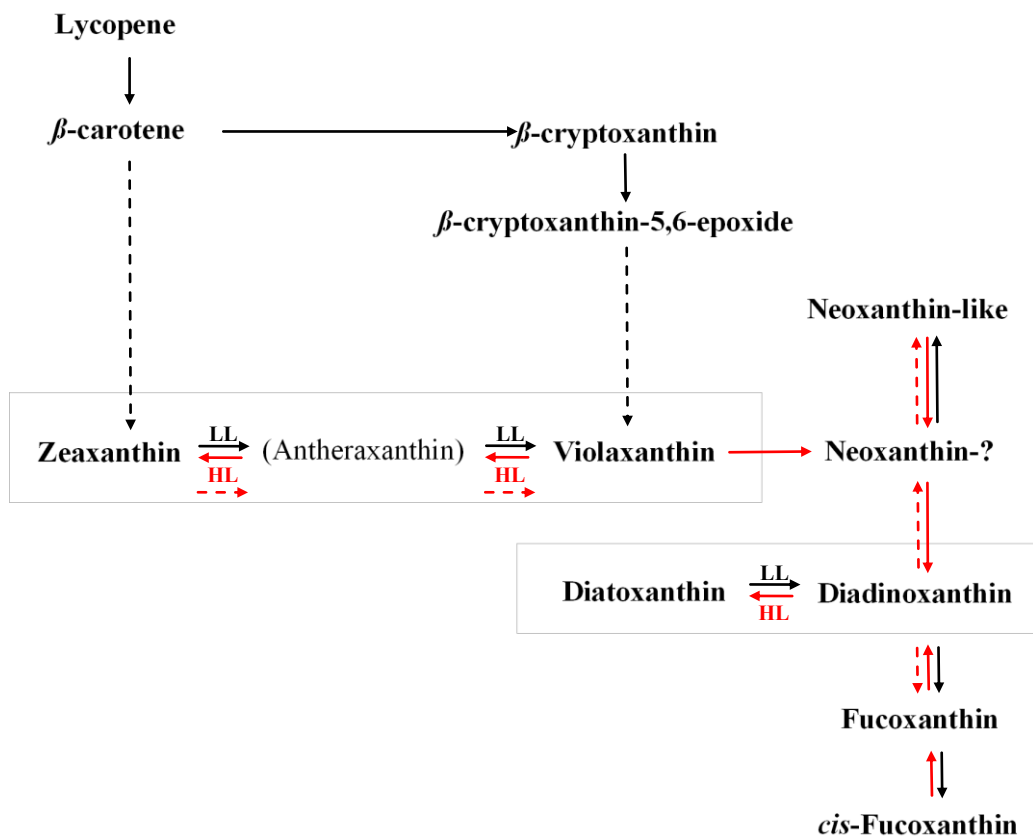


Fig. 5.13: Scheme of hypothetical relationships between xanthophyll-cycle pools and the biosynthetic pathway leading to photosynthetic accessory and accessory pigments in diatoms (from Lohr and Wilhelm, 1999; Bertrand, 2010, and our study). Red arrows represents high light-activated conversion steps.

protective role, but also because they represent a source of xanthophylls that could be eventually converted in light-harvesting pigments during low light periods. Our data support the presence of inter-conversion between Dd and Fuco occurring in function of the light intensity the cells would experience. The conversion of Fuco to Dd might be a biosynthetic step activated in *P. multistriata* in conjunction with Dd *de-novo* synthesis, when a strong photoprotection is needed. Additionally, since Dd does not seem to be an obligate precursor of Fuco in diatoms and other species (Phaeophyceae and Chrysophyceae groups) displaying it as the major light-harvesting accessory pigment (Lohr and Wilhelm, 1999), we propose that *cis*-Fuco might be involved as precursor pigment in the biosynthesis of Fuco.

As the case of green algae and higher plants, in which the accessory pigment neoxanthin (Neox) has been thought to form from Vx, a Neox-? precursor role for Vx might be reliable, under high light conditions, in *P. multistriata*. Neox-? might represent an intermediate step of conversion between Vx and Dd.

Neox-like plays also an important role in this scheme of interactions as suggested by its content variations measured during the experiment, as well as by its significant correlation with Vx and negative trend with Zx content. Moreover, a potential function of Neox-like in preventing PSII photo-oxidation and membrane lipids disruption can be hypothesized, as it has been recently suggested for Neox in the picoeukaryote *Phaeomonas* sp. (Giovagnetti *et al.*, 2010) and higher plants (Dall'Osto *et al.*, 2007; Fig. 5.13).

Our data support the presence of a dual flow of Dd cycle precursor pigments functionally related to Vx (through Neox-?) and Fuco (from *cis*-Fuco) under high irradiance conditions. While the Dd replenishment from Fuco content is continuously enhanced, the Dd accumulation due to Vx seems less strong and dependent on the feedback-response of the XC activation. The fact that the lack of Dt synthesis (due to the inhibitor injection) weakened the biosynthetic step from Vx to Dd might reflect a possible inhibition of the enzymatic activity responsible for the conversion of Neox-? to Dd. These results are preliminary and further studies are requested to better clarify the role of these photosynthetic and accessory pigments in the photoprotective pathway of diatoms.

We conclude that *P. multistriata* is armed with an effective photoprotective pathway of biosynthesis and a related NPQ development, part of a multi-component NPQ, which enable this diatom to efficiently and rapidly cope with high irradiance climate. This multi-component NPQ consists of an initial transient mechanism based upon the Dt content present in cells, coupled with an FCP antennae aggregation mechanism, both of which are

strengthened by a stronger XC-dependent mechanism. All the three components must act in synergy to efficiently protect the photosystems from photo-damage and maximize the photosynthetic efficiency.

5.4 Xanthophyll cycle ecophysiology in response to different kinetics of light change

5.4.1 Experimental design, sampling strategy and analysed parameters

Pseudo-nitzschia multistriata cultures underwent three distinct time courses (kinetics) of irradiance increase, during which the photon flux density (PFD) peak of each irradiance condition was reached in 5, 3 and 2 hours (Fig. 5.14). To be clearer, we termed these three experiments as 5, 3 and 2 hours kinetics, respectively.

During each experiment, cells in exponential growth phase were subjected to five irradiance increases set to peak at maximal PFD of 100, 250, 350, 500, and 650 $\mu\text{mol photons} \cdot \text{m}^{-2} \cdot \text{s}^{-1}$, respectively termed as C100, C250, C350, C500 and C650 (Fig. 5.14). Cells were subjected to two weeks of pre-acclimation under a sine light (SL) climate set to peak at a maximal PFD of 100 $\mu\text{mol photons} \cdot \text{m}^{-2} \cdot \text{s}^{-1}$ (Fig. 5.2).

The three experiments were performed in triplicate for each irradiance condition.

Flasks were illuminated by the light system ACLS and Infinity XR4 (Aquarium Technologies, Sfiligoi S.r.l., Bassano del Grappa, Italy), simulating light–dark sine climate, reproducing dawn and sunset. XR4 was equipped with HQI metal halide lamps (10000 K). The PFD was measured by using a laboratory PAR 4 π sensor (QSL 2101, Biospherical Instruments Inc., San Diego, CA, USA).

Cultures were sampled three times during the irradiance increase (Fig. 5.14). The first sampling was carried out at dawn, when cells were still in dark, 15 minutes before the irradiance increase started. The second sampling time occurred after 3, 2, and 1.5 hours the irradiance increase started for the 5, 3, and 2 hours kinetics of irradiance change, respectively (Fig. 5.14). The second sampling was taken at PFD values of 42, 123, 150, 164, and 280 $\mu\text{mol photons} \cdot \text{m}^{-2} \cdot \text{s}^{-1}$, for the condition C100, C250, C350, C500 and C650 $\mu\text{mol photons} \cdot \text{m}^{-2} \cdot \text{s}^{-1}$, respectively. The third sampling corresponded to irradiance peaks.

Temperature and pH were controlled daily with an HI-9214-Stick pH meter (Hanna Instruments, Woonsocket, RI, USA).

Twenty mL of culture were rapidly taken during each sampling time, for measuring variable fluorescence, NPQ, and for further analysis of pigments. A ten mL aliquot was filtered onto GF/F glass fibre filters (Whatman, UK), and immediately stored in liquid nitrogen until further pigment analysis. Triplicate samples were taken during each

sampling time. Pigment analysis was carried out following the procedure described in chapter 4 (see Sec. 4.4).

Triplicate measurements of variable fluorescence were performed on both light- and dark-acclimated samples. Non-photochemical fluorescence quenching (NPQ) triplicate measurements were performed on dark-acclimated samples. Active Chl *a* fluorescence and NPQ analysis were carried out following the procedures described in chapter 4 (see Sec. 4.6).

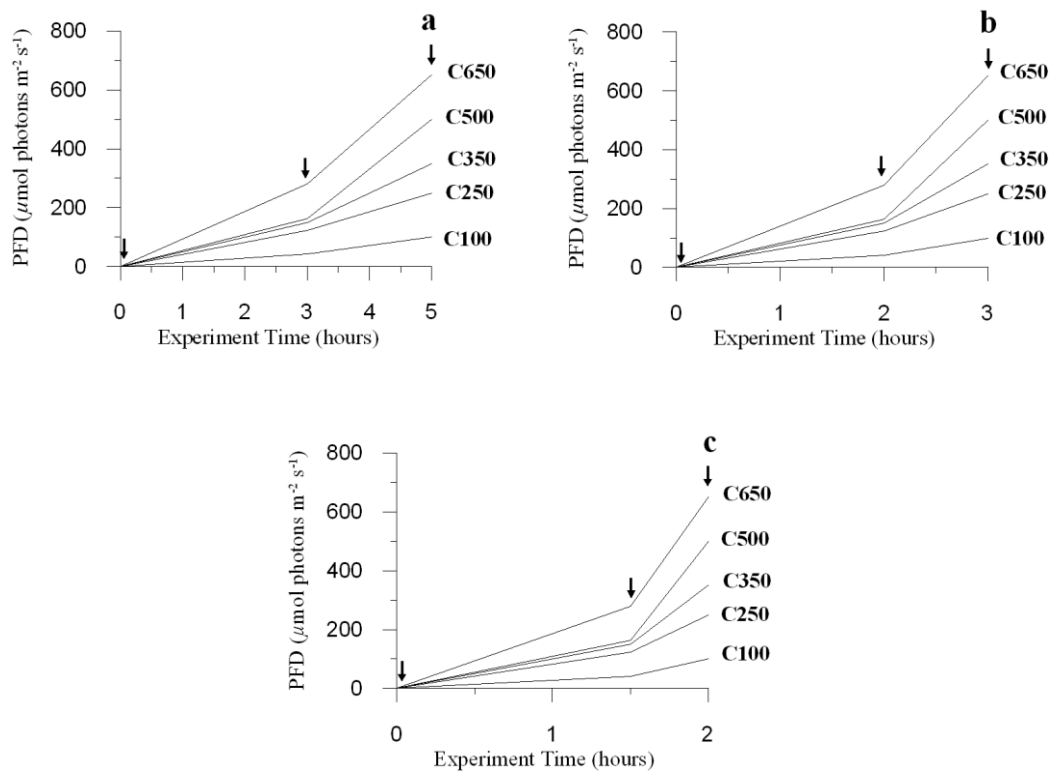


Figure 5.14: Scheme of the five irradiance increases applied during the study, reaching the maximal PFD values of 100, 250, 350, 500, and 650 $\mu\text{mol photons m}^{-2} \text{s}^{-1}$, for the experimental kinetics of irradiance change of five (a), three (b) and two hours (c). Arrows indicate sampling times.

5.4.2 Results

5.4.2.1 Variable fluorescence measurements

A similar range of variation was found in PSII maximal ($F_v : F_m$) and operating ($F_v' : F_m'$) photochemical efficiencies, during the three kinetics of irradiance increase (Figs. 5.15 a and b, 5.16 a and b, and 5.17 a and b). Both $F_v : F_m$ and $F_v' : F_m'$ linearly decreased over the irradiance gradient ($p < 0.005$), with a greater and steeper decrease in $F_v' : F_m'$ than in $F_v : F_m$ (Figs. 5.15 a and b, 5.16 a and b, and 5.17 a and b). The higher was the irradiance, the stronger was the decrease in $F_v : F_m$ and $F_v' : F_m'$. The only exception was the quite similar $F_v : F_m$ values measured at the (intermediate) 164 and 280, and (peak) 500 and 650 $\mu\text{mol photons} \cdot \text{m}^{-2} \cdot \text{s}^{-1}$ irradiance conditions, during the 2 hours kinetics (Fig. 5.17 a). The lowest $F_v' : F_m'$ value was reached at 650 $\mu\text{mol photons} \cdot \text{m}^{-2} \cdot \text{s}^{-1}$ in 5 and 3 hours kinetics, while at 280 $\mu\text{mol photons} \cdot \text{m}^{-2} \cdot \text{s}^{-1}$ in the 2 hours kinetics (Fig. 5.17 b), in agreement with cells experiencing the most intense and rapidly-reached PFD condition (i.e. 280 $\mu\text{mol photons} \cdot \text{m}^{-2} \cdot \text{s}^{-1}$ in 1.5 hour), and with the highest NPQ value (Fig. 5.17 d).

The recovery of fluorescence yield was estimated by using the ratio $\{[(F_v : F_m) - (F_v' : F_m')] : (F_v : F_m)\}$, and it gradually increased in function of the irradiance ($p < 0.005$, in Figs. 5.15 c, and 5.16 c; $p < 0.05$, in Fig. 5.17 c). During the three kinetics, an almost absence of recovery occurred at 42 and 123 $\mu\text{mol photons} \cdot \text{m}^{-2} \cdot \text{s}^{-1}$ (and 150 $\mu\text{mol photons} \cdot \text{m}^{-2} \cdot \text{s}^{-1}$ in the 5 hours kinetics), being consistent with no $F_v' : F_m'$ decrease since the low irradiance intensities (Figs. 5.15 c, 5.16 c, and 5.17 c).

5.4.2.2 Photoprotective responses

The non-photochemical fluorescence quenching (NPQ) increased over the irradiance range during the three time courses, with the exception of the almost stable NPQ values under 100 $\mu\text{mol photons} \cdot \text{m}^{-2} \cdot \text{s}^{-1}$ (Figs. 5.15 d, 5.16 d, and 5.17 d).

The observed decrease in fluorescence yield was in agreement with the NPQ response (and Dd cycle modulation), as suggested by the negative trend between NPQ and $F_v : F_m$ in the three kinetics (Figs. 5.15 h, 5.16 h, and 5.17 h).

The slowest kinetics of irradiance increase (i.e. 5 hours) caused the lowest NPQ development (Fig. 5.15 d), while the most enhanced NPQ response occurred in the 3 hours kinetics (Fig. 5.16 d). The highest NPQ values were reached under 500 $\mu\text{mol photons} \cdot \text{m}^{-2} \cdot \text{s}^{-1}$ (0.81 ± 0.17 ; Fig. 5.15 d), 164 $\mu\text{mol photons} \cdot \text{m}^{-2} \cdot \text{s}^{-1}$ (1.05 ± 0.09 ; Fig. 5.16 d), and 280 $\mu\text{mol photons} \cdot \text{m}^{-2} \cdot \text{s}^{-1}$ (0.88 ± 0.14 ; Fig. 5.20 d) PFD intensities, in the 5, 3 and 2 hours kinetics, respectively.

NPQ increase was linear in the 5 and 2 hours kinetics of irradiance increase ($p < 0.005$; Fig. 5.15 d, and Fig. 5.17 d), while it was not in the 3 hours kinetics (Fig. 5.16 d). A disruption in the trend of NPQ increase occurred at PFD thresholds of 164 and 280 $\mu\text{mol photons} \cdot \text{m}^{-2} \cdot \text{s}^{-1}$, in the 3 and 2 hours kinetics, respectively. Then, NPQ decreased in the 3 hours kinetics (Fig. 5.15 d), while remaining quite stable in the 2 hours one (Fig. 5.16 d).

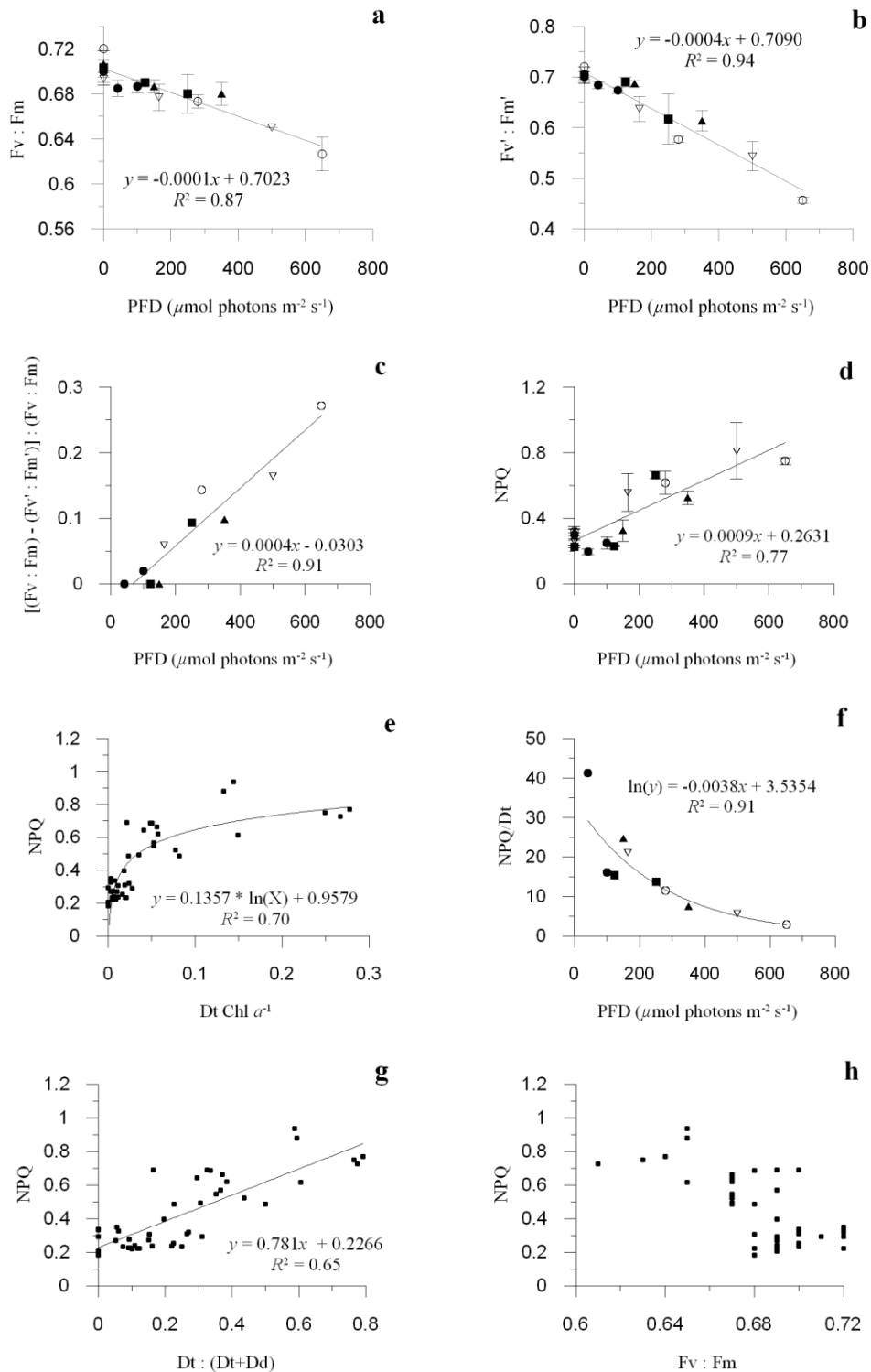


Fig. 5.15: Five hours kinetics experiment. Evolution of photosystem II maximal ($F_v : F_m$; **a**) and operating ($F_v' : F_m'$; **b**) photochemical efficiency, recovery ratio $\{[(F_v : F_m) - (F_v' : F_m')] : (F_v : F_m)\}$ (**c**), NPQ (**d**), and NPQ : Dt Chl a^{-1} ratio (**f**), over the irradiance range (PFD, $\mu\text{mol photons m}^{-2} \text{s}^{-1}$). Data are means with $n = 3$; error bars are SD. Relationship between NPQ and Dt Chl a^{-1} (**e**), NPQ and $[Dt : (Dt + Dd)]$ (DPS ratio; **g**), NPQ and $F_v : F_m$ (**h**). C100: filled circles; C250: filled square; C350: filled triangles; C500: open triangles; C650: open circles. Chl a , chlorophyll a ; Dt, diatoxanthin, Dd, diadinoxanthin; NPQ, non-photochemical fluorescence quenching.

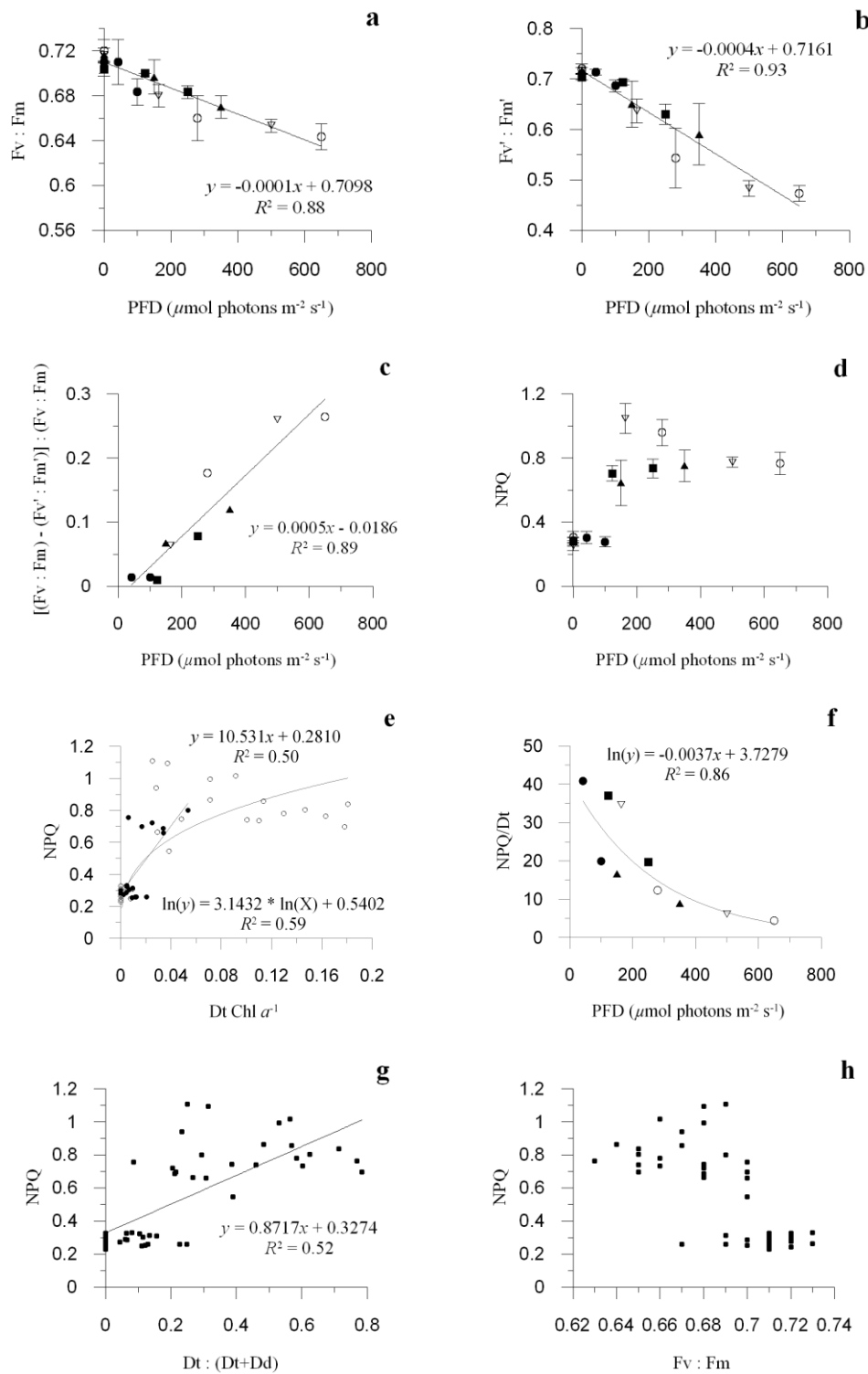


Fig. 5.16: Three hours kinetics experiment. Evolution of photosystem II maximal ($F_v : F_m$; **a**) and operating ($F_v' : F_m'$; **b**) photochemical efficiency, recovery ratio $\{[(F_v : F_m) - (F_v' : F_m')] : (F_v : F_m)\}$ (**c**), NPQ (**d**), and NPQ : Dt Chl a^{-1} ratio (**f**), over the irradiance range (PFD, $\mu\text{mol photons m}^{-2} \text{s}^{-1}$). Data are means with $n = 3$; error bars are SD. Relationship between NPQ and Dt Chl a^{-1} (**e**), NPQ and $[Dt : (Dt + Dd)]$ (DPS ratio; **g**), NPQ and $F_v : F_m$ (**h**). C100: filled circles; C250: filled square; C350: filled triangles; C500: open triangles; C650: open circles. Chl a , chlorophyll a ; Dt, diatoxanthin, Dd, diadinoxanthin; NPQ, non-photochemical quenching.

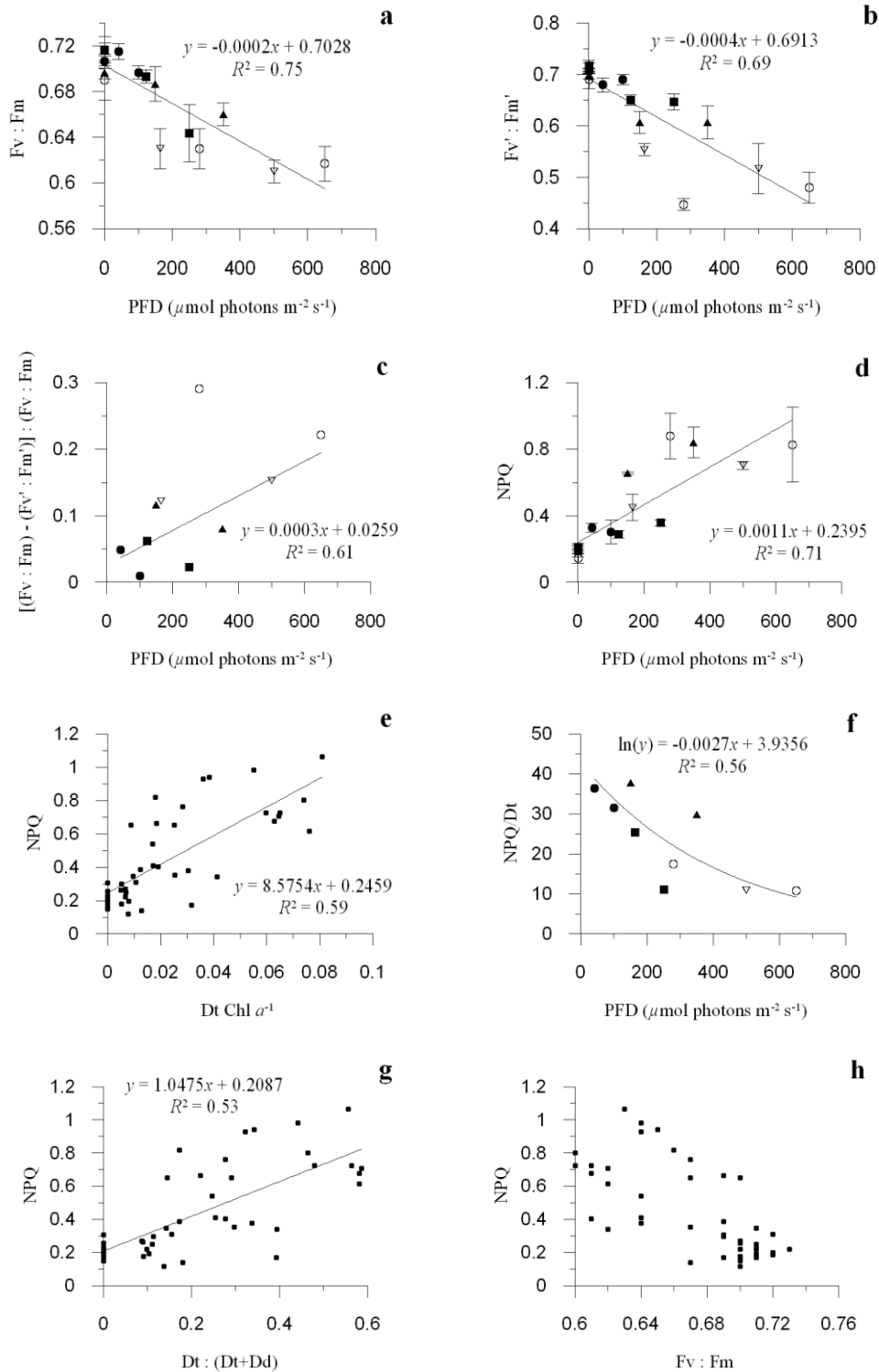


Fig. 5.17: Two hours kinetics experiment. Evolution of photosystem II maximal ($F_v : F_m$; **a**) and operating ($F_v' : F_m'$; **b**) photochemical efficiency, recovery ratio $\frac{[(F_v : F_m) - (F_v' : F_m')]}{(F_v : F_m)}$ (**c**), NPQ (**d**), and NPQ : Dt Chl a^{-1} ratio (**f**), over the irradiance range (PFD, $\mu\text{mol photons m}^{-2} \text{s}^{-1}$). Data are means with $n = 3$; error bars are SD. Relationship between NPQ and Dt Chl a^{-1} (**e**), NPQ and $[\text{Dt} : (\text{Dt} + \text{Dd})]$ (DPS ratio; **g**), NPQ and $F_v : F_m$ (**h**). C100: filled circles; C250: filled square; C350: filled triangles; C500: open triangles; C650: open circles. Chl a , chlorophyll a ; Dt, diatoxanthin, Dd, diadinoxanthin; NPQ, non-photochemical fluorescence quenching.

In the 5 hours-lasting experiment, the NPQ development was significantly correlated to Dt Chl a^{-1} ($R^2 = 0.70$; Fig. 5.15 e). In the 3 hours-lasting experiment, only for low irradiance conditions (C100 and C250), NPQ development was linearly correlated with Dt Chl a^{-1} ($p < 0.025$; Fig. 5.16 e). All data pooled together were instead described by a power function. In the 2 hours-lasting experiment, NPQ development was linearly correlated to Dt Chl a^{-1} ($p < 0.005$; Fig. 5.17 e).

In the three kinetics, the NPQ : Dt Chl a^{-1} ratio was significantly correlated to PFD, with R^2 decreasing with the time course of PFD increase ($R^2 = 0.91, 0.86$ and 0.56 , in the 5, 3 and 2 hours kinetics, respectively; Figs. 5.15 f, 5.16 f, and 5.17 f). The linear correlation between NPQ and DPS was also stronger in the 5 hours than in the 3 and 2 hours kinetics ($p < 0.005$; Figs. 5.15 g, 5.16 g, and 5.17 g), suggesting an NPQ development more strictly dependent on the Dd cycle activation.

Since the aforementioned results, we made the assumption that under the slowest kinetics of irradiance increase, the NPQ development was almost exclusively dependent on the Dd cycle activation, and hence the NPQ *surplus* found in the faster kinetics possibly corresponded to distinct NPQ components, independent from the Dd cycle modulation (see Sec. 5.3.3).

Dd cycle dependent and independent NPQ components have been estimated using the logarithmic equation found for the correlation between NPQ and Dt Chl a^{-1} in the 5 hours kinetics (Fig. 5.15 e), and applying it the 3 and 2 hours kinetics. Thus, the Dt synthesis dependent NPQ development was estimated (Figs. 5.18 a and b), and subtracting these values to the NPQ values measured under the 3 and 2 hours kinetics, it was possible to calculate the Dd cycle independent NPQ component (Figs. 5.18 c and d).

The Dd cycle dependent NPQ significantly increased over the irradiance range in both kinetics ($R^2 = 0.78$ and 0.67 , in the 3 and 2 hours kinetics, respectively; Figs. 5.18 a and b). In the 3 hours kinetics, Dd cycle dependent NPQ reached a greater maximal value (0.73; Fig. 5.18 a) than the maximal value of the 2 hours kinetics (0.62; Fig. 5.18 b).

The Dd cycle independent NPQ response was mainly enhanced under moderate PFD, with a greater development in the 3 rather than in the 2 hours kinetics (Figs. 5.18 c and d). The highest contribution of the estimated Dd cycle independent NPQ component to the total NPQ development occurred at 123 (65%) and 150 $\mu\text{mol photons} \cdot \text{m}^{-2} \cdot \text{s}^{-1}$ (52%), in the 3 and 2 hours kinetics, respectively (Figs. 5.18 e and f). In the 3 hour kinetics, the maximal Dd cycle independent NPQ value was reached under 164 (0.65; Fig. 5.18 c), while under 350 $\mu\text{mol photons} \cdot \text{m}^{-2} \cdot \text{s}^{-1}$ in the 2 hours kinetics (0.42; Fig. 5.18 d).

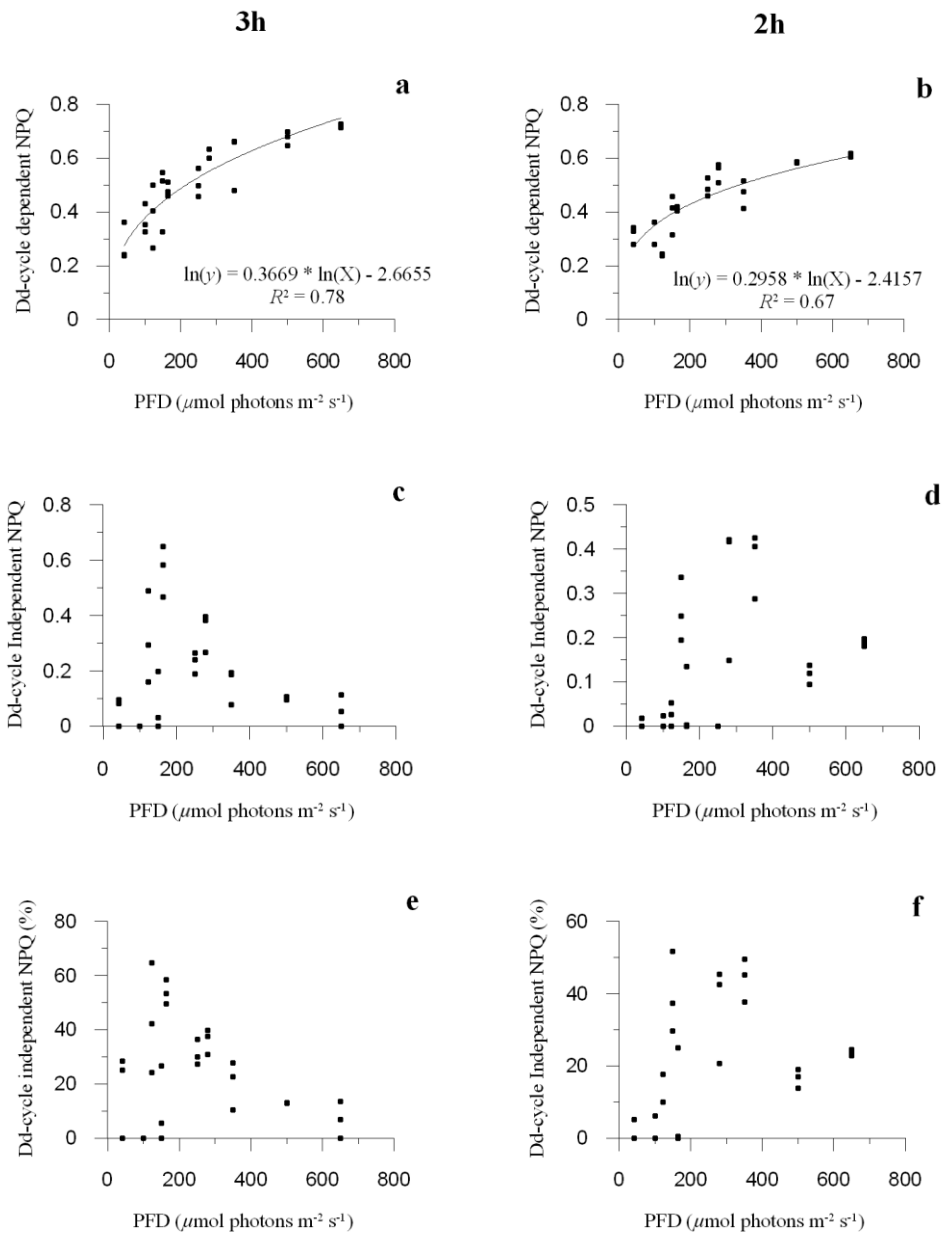


Fig. 5.18: Evolution of estimated Dd cycle dependent (**a** and **b**) and Dd cycle independent NPQ (**c** and **d**), and Dd cycle independent NPQ contribution (%; **e** and **f**), over the irradiance range (PFD, $\mu\text{mol photons m}^{-2} \text{s}^{-1}$).

In the three experiments, the diadinoxanthin (Dd) Chl a^{-1} ratio linearly increased over the irradiance range ($p < 0.005$ for Fig. 5.19 a, and $p < 0.025$ for Fig. 5.20 a and Fig. 5.21 a), but under the highest PFD (and also under $500 \mu\text{mol photons} \cdot \text{m}^{-2} \cdot \text{s}^{-1}$ in the 2 hours kinetics). These data were thus not considered in the linear regression. Such a decrease in Dd Chl a^{-1} was in agreement with a high de-epoxidation rate demand.

Dd Chl a^{-1} variations were not significantly different between the 5 and the 3 hours kinetics (Figs. 5.19 a, and 5.20 a). Slightly lower Dd Chl a^{-1} ratios were found in the 2 hours kinetics, than in the slower ones (Fig. 5.21 a). Dd Chl a^{-1} ranged between 0.044 and 0.097 (Fig. 5.19 a), 0.047 and 0.099 (Fig. 5.20 a), and 0.044 and 0.078 (Fig. 5.21 a), in the 5, 3 and 2 hours kinetics, respectively.

Differently, the increase in diatoxanthin (Dt) Chl a^{-1} over the irradiance range was higher the slower was the irradiance increase, reaching the maximal values of 0.26 ± 0.01 (Fig. 5.19 b), 0.17 ± 0.01 (Fig. 5.20 b), and 0.08 ± 0.004 (Fig. 5.21 b), in the 5, 3 and 2 hours kinetics, respectively.

The [Dt : (Dt + Dd)] ratio (DPS) linearly increased over the irradiance gradient ($p < 0.005$), and reached 78 (Fig. 5.19 c), 76 (Fig. 5.20 c) and 58% (Fig. 5.21 c), in the 5, 3 and 2 hours kinetics, respectively. In the 5 and 3 hours kinetics, in response to PFD increases of $100 \mu\text{mol photons} \cdot \text{m}^{-2} \cdot \text{s}^{-1}$, DPS increased of $\sim 10\%$, whereas in the 2 hours kinetics of $\sim 8\%$.

In the 5 and 3 hours kinetics, a linear correlation between Dd and Dt Chl a^{-1} ratios was found by pooling the C100 and C250 data set ($p < 0.005$; Figs. 5.19 d, and 5.20 d), whereas it was not in the 2 hours kinetics (Fig. 5.21 d). In all the three kinetics, higher irradiance conditions prevented the occurrence of a linear correlation between the Dt and Dd.

In all the three experiments, the Fv : Fm was significantly and negatively correlated with both Dt Chl a^{-1} and DPS ratios ($p < 0.005$; Figs. 5.19 e and f, Figs. 5.20 e and f, and Figs. 5.21 e and f).

The violaxanthin (Vx) and zeaxanthin (Zx) Chl a^{-1} ratios were quite stable over the irradiance gradient in the 3 and 2 hours kinetics (Figs. 5.23 a and b, and Figs. 5.24 a and b). In the 5 hours kinetics, a clear break in both pigment ratios occurred under moderate PFD, with Vx and Zx Chl a^{-1} increasing after the PFD of 250 and $164 \mu\text{mol photons} \cdot \text{m}^{-2} \cdot \text{s}^{-1}$, respectively (Figs. 5.22 a and b).

Vx Chl a^{-1} ratios ranged between 0.003 and 0.007 (Fig. 5.22 a), 0.003 and 0.005 (Fig. 5.23 a), and 0.004 and 0.006 (Fig. 5.24 a), in 5, 3 and 2 hours kinetics, respectively.

$Zx \text{ Chl } a^{-1}$ ratios ranged between 0.002 and 0.007 (Fig. 5.22 b), 0.002 and 0.007 (Fig. 5.23 b), and 0.004 and 0.005 (Fig. 5.24 b), in 5, 3 and 2 hours kinetics, respectively. $Zx \text{ Chl } a^{-1}$ linearly increased over the irradiance range in the 5 hours kinetic ($p < 0.005$; Fig. 5.22 b). During the 3 hours kinetics, $Zx \text{ Chl } a^{-1}$ was quite stable, only increasing at $650 \mu\text{mol photons} \cdot \text{m}^{-2} \cdot \text{s}^{-1}$ (Fig. 5.23 b), whereas no Zx synthesis occurred during the 2 hours kinetics, with the exception of the highest PFD conditions (Fig. 5.24 b).

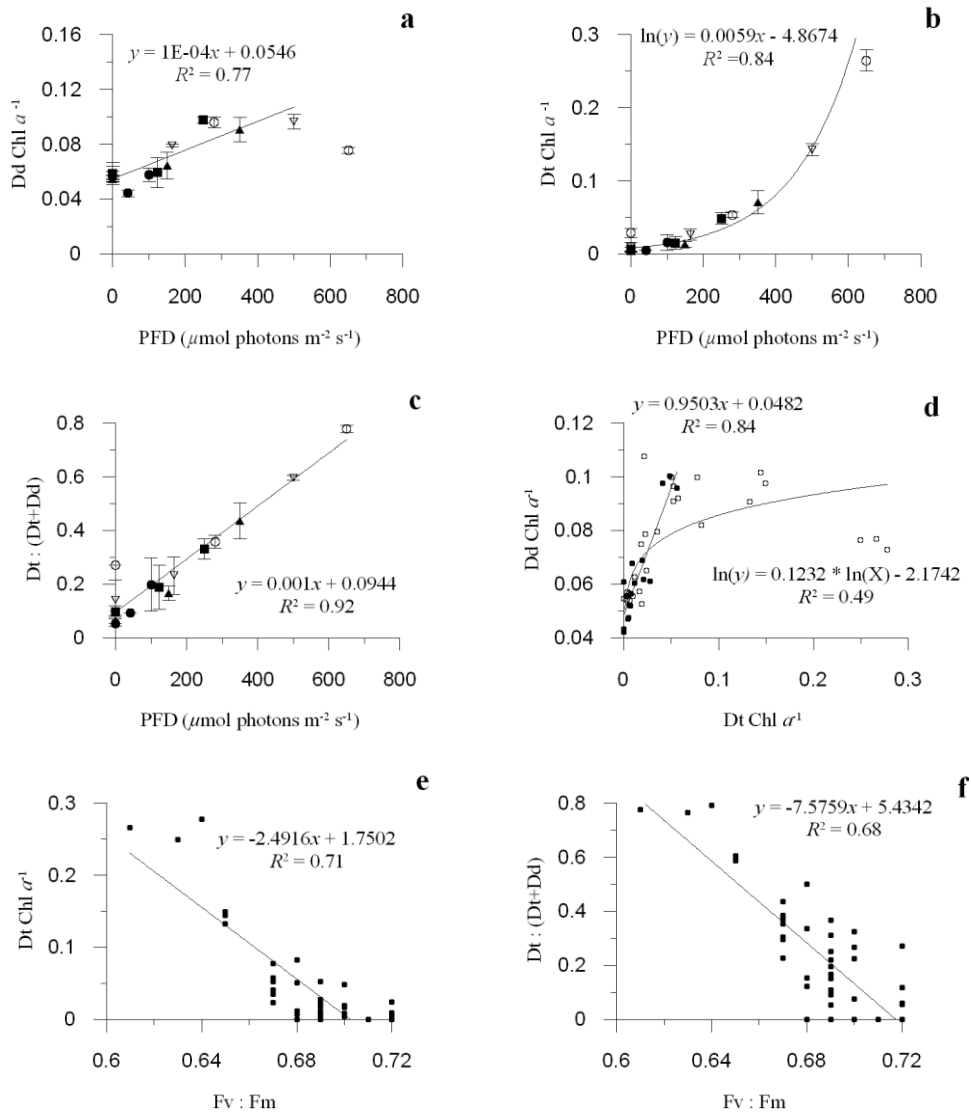


Fig. 5.19: Five hours kinetics experiment. Evolution of diadinoxanthin (a), diatoxanthin Chl a^{-1} (b), and [Dt : (Dt + Dd)] (DPS ratio; c), over the irradiance range (PFD, $\mu\text{mol photons m}^{-2} \text{s}^{-1}$). Data are means with $n = 3$; error bars are SD. Relationship between diatoxanthin and diatoxanthin Chl a^{-1} ratios (d), Fv : Fm and diatoxanthin Chl a^{-1} (e), Fv : Fm and DPS ratio (f). In chart a, C650 peak sample was not considered in the regression. C100: filled circles; C250: filled square; C350: filled triangles; C500: open triangles; C650: open circles. Chl a , chlorophyll a ; Dt, diatoxanthin; Dd, diadinoxanthin.

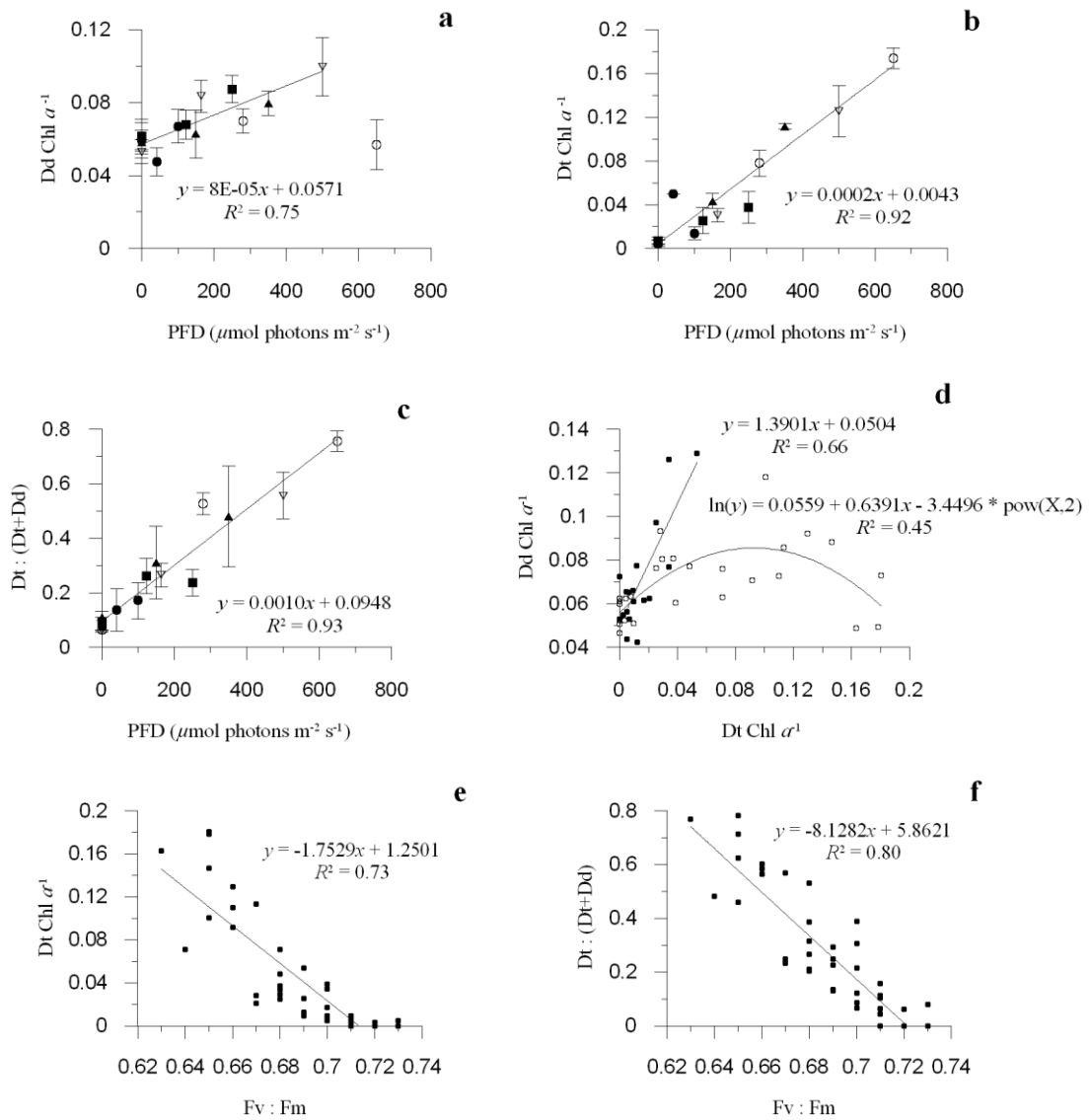


Fig. 5.20: Three hours kinetics experiment. Evolution of diadinoxanthin (a), diatoxanthin Chl a^{-1} (b), and [Dt : (Dt + Dd)] (DPS ratio; c), over the irradiance range (PFD, $\mu\text{mol photons m}^{-2} \text{s}^{-1}$). Data are means with $n = 3$; error bars are SD. Relationship between diatoxanthin and diatoxanthin Chl a^{-1} ratios (d), Fv : Fm and diatoxanthin Chl a^{-1} (e), Fv : Fm and DPS ratio (f). In chart d, filled dots represent C100 and C250 samples data, while open dots represent C350, C500 and C650 samples data. C100: filled circles; C250: filled square; C350: filled triangles; C500: open triangles; C650: open circles. Chl a , chlorophyll a ; Dt, diatoxanthin; Dd, diadinoxanthin.

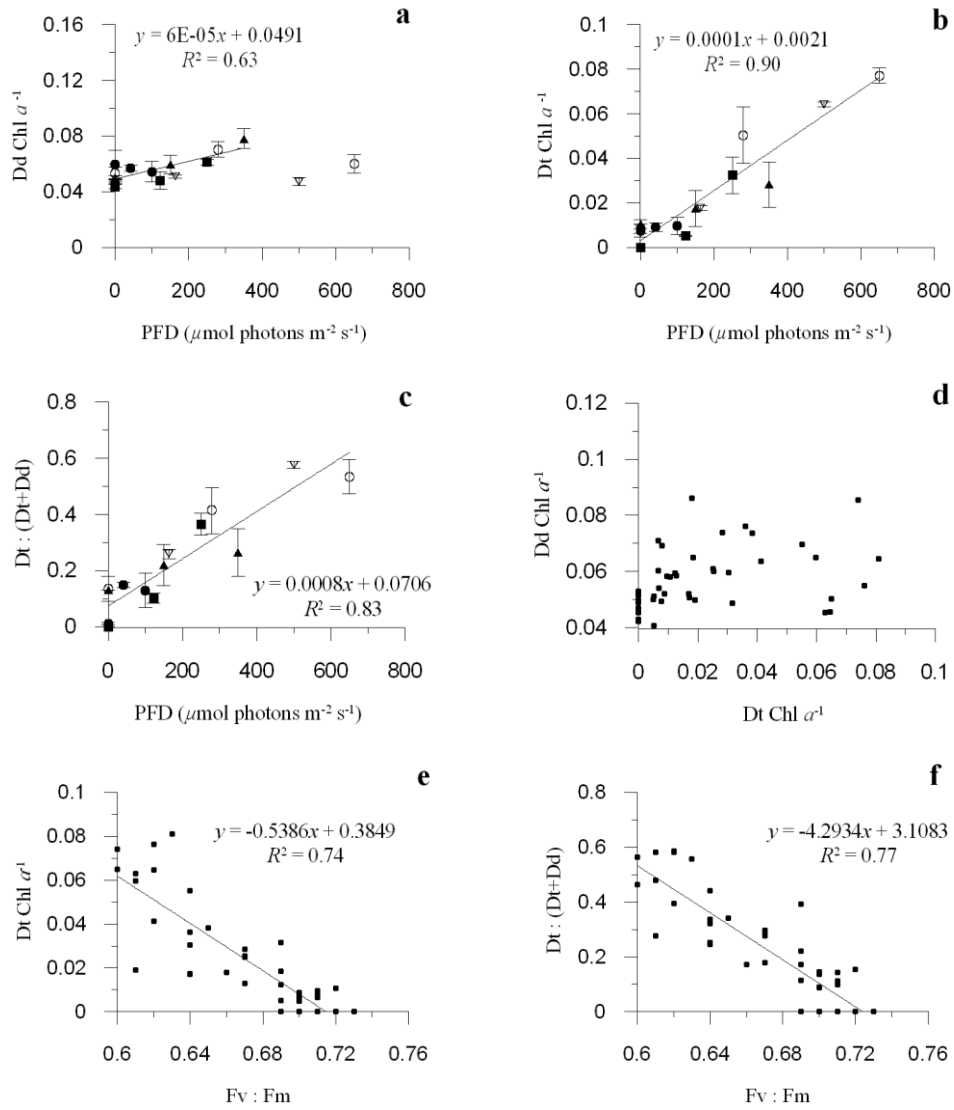


Fig. 5.21: Two hours kinetics experiment. Evolution of diadinoxanthin (**a**), diatoxanthin Chl a^{-1} (**b**), and [Dt : (Dt + Dd)] (DPS ratio; **c**), over the irradiance range (PFD, $\mu\text{mol photons m}^{-2} \text{s}^{-1}$). Data are means with $n = 3$; error bars are SD. Relationship between diatoxanthin and diatoxanthin Chl a^{-1} ratios (**d**), Fv : Fm and diatoxanthin Chl a^{-1} (**e**), Fv : Fm and DPS ratio (**f**). In chart **a**, C500 and C650 peak samples were not considered in the regression. C100: filled circles; C250: filled square; C350: filled triangles; C500: open triangles; C650: open circles. Chl a , chlorophyll a ; Dt, diatoxanthin; Dd, diadinoxanthin.

In all the three experiments, no significant correlation occurred between V_x and Z_x (Figs. 5.22 c, 5.23 c, and 5.24 c).

A significant correlation was found between Z_x and $Dt \text{ Chl } a^{-1}$, in the 5 hours kinetics ($p < 0.05$; Fig. 5.22 d), while no other significant correlations occurred between Z_x and $Dt \text{ Chl } a^{-1}$ (Fig. 5.23 d, and Fig. 5.24 d), or V_x and $Dd \text{ Chl } a^{-1}$ ratios (Figs. 5.22 e, 5.23 e, and 5.24 e).

β -carotene (β -Car) $\text{Chl } a^{-1}$ linearly increased ($p < 0.005$) over the irradiance gradient, during the 5 hours kinetics (Fig. 5.22 f). Instead, the increase in β -Car $\text{Chl } a^{-1}$ over the irradiance gradient was described by a power ($R^2 = 0.71$; Fig. 5.23 f) and a logarithmic function ($R^2 = 0.45$; Fig. 5.24 f), in the 3 and 2 hours kinetics, respectively. A significant linear correlation between β -Car and $Dd \text{ Chl } a^{-1}$ was only found in the 5 hours kinetics ($p < 0.005$; Fig. 5.22 g), while β -Car and $Dt \text{ Chl } a^{-1}$ ratios were significantly correlated ($p < 0.005$) only in the 5 and 3 hours kinetics ($R^2 = 0.51$, Fig. 5.22 h; $R^2 = 0.40$, Fig. 5.23 h).

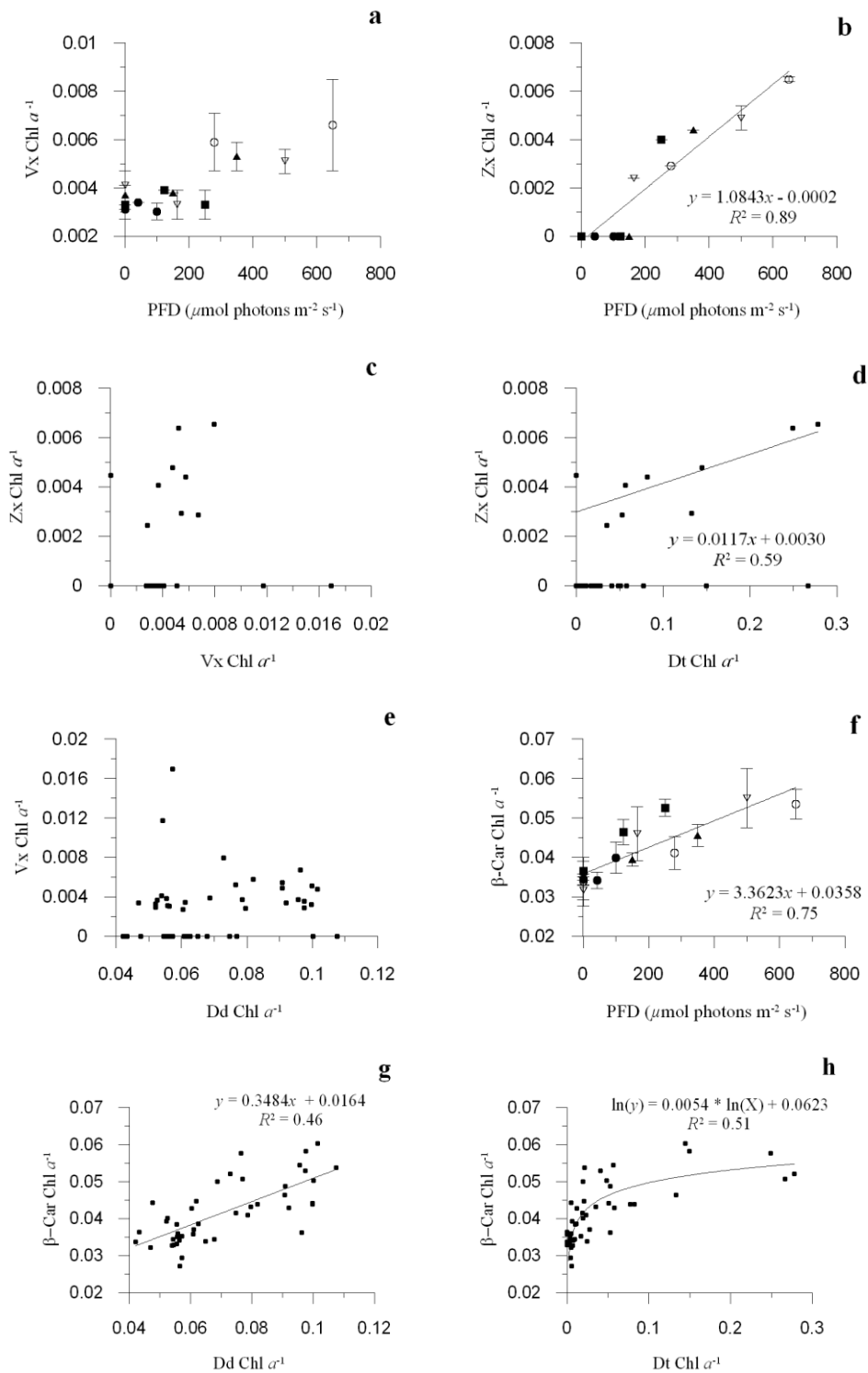


Fig. 5.22: Five hours kinetics experiment. Evolution of violaxanthin (a), zeaxanthin (b), and β -carotene Chl a^{-1} (f), over the irradiance range (PFD, $\mu\text{mol photons m}^{-2} \text{s}^{-1}$). Data are means with $n = 3$; error bars are SD. Relationship between zeaxanthin and violaxanthin Chl a^{-1} (c), zeaxanthin and diatoxanthin Chl a^{-1} (d), violaxanthin and diadinoxanthin Chl a^{-1} (e), β -carotene and diadinoxanthin Chl a^{-1} (g), β -carotene and diatoxanthin Chl a^{-1} (h). In chart d, zeaxanthin Chl a^{-1} values equals to zero were not considered in the regression. In chart C100: filled circles; C250: filled square; C350: filled triangles; C500: open triangles; C650: open circles. Chl a , chlorophyll a ; Zx, zeaxanthin; Vx, violaxanthin; Dt, diatoxanthin; Dd, diadinoxanthin, β -Car, β -carotene.

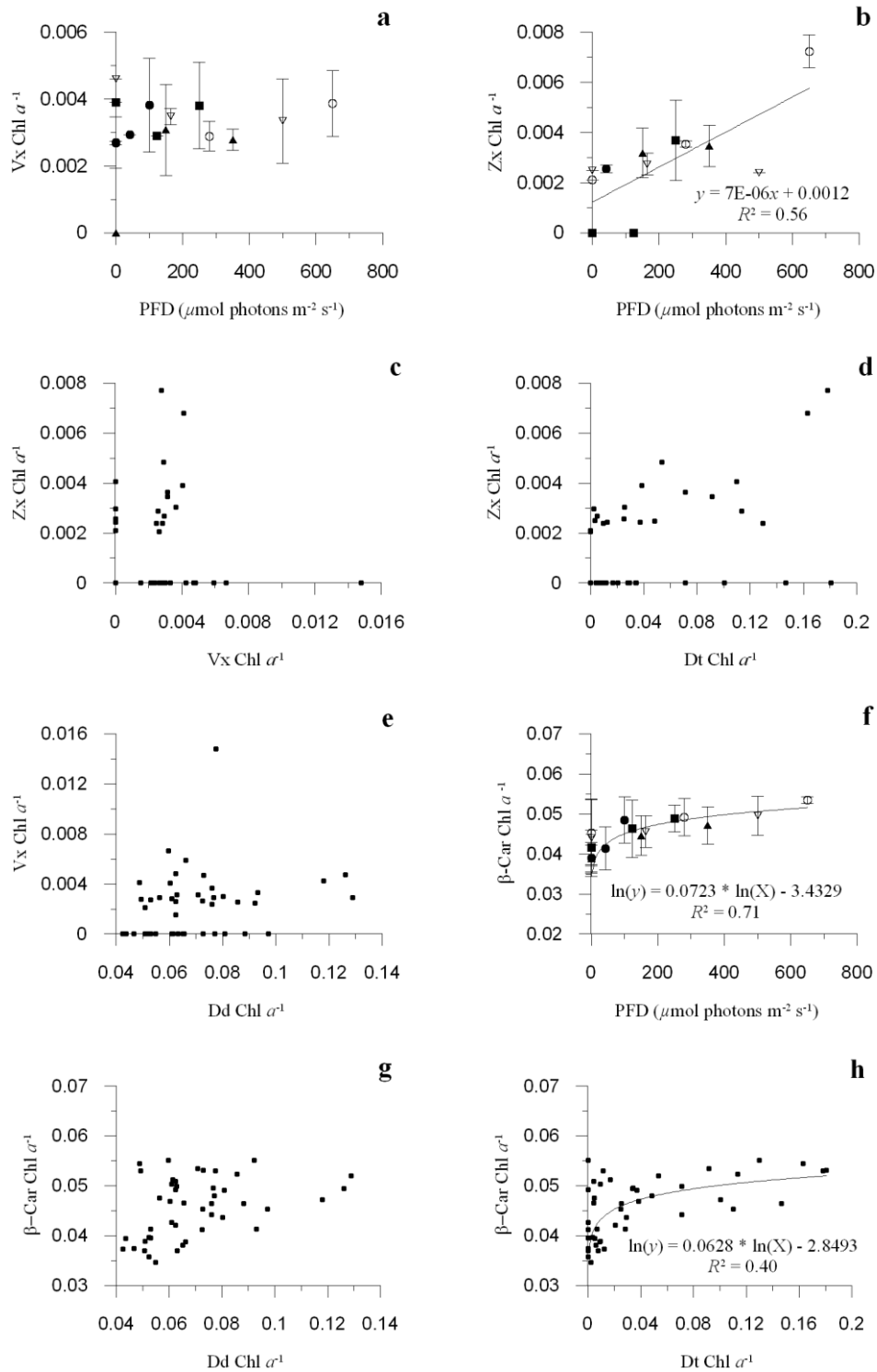


Fig. 5.23: Three hours kinetics experiment. Evolution of violaxanthin (a), zeaxanthin (b), and β -carotene Chl a^{-1} (f), over the irradiance range (PFD, $\mu\text{mol photons m}^{-2} \text{s}^{-1}$). Data are means with $n = 3$; error bars are SD. Relationship between zeaxanthin and violaxanthin Chl a^{-1} (c), zeaxanthin and diatoxanthin Chl a^{-1} (d), violaxanthin and diadinoxanthin Chl a^{-1} (e), β -carotene and diadinoxanthin Chl a^{-1} (g), β -carotene and diatoxanthin Chl a^{-1} (h). C100: filled circles; C250: filled square; C350: filled triangles; C500: open triangles; C650: open circles. Chl a , chlorophyll a ; Zx, zeaxanthin; Vx, violaxanthin; Dt, diatoxanthin; Dd, diadinoxanthin, β -Car, β -carotene.

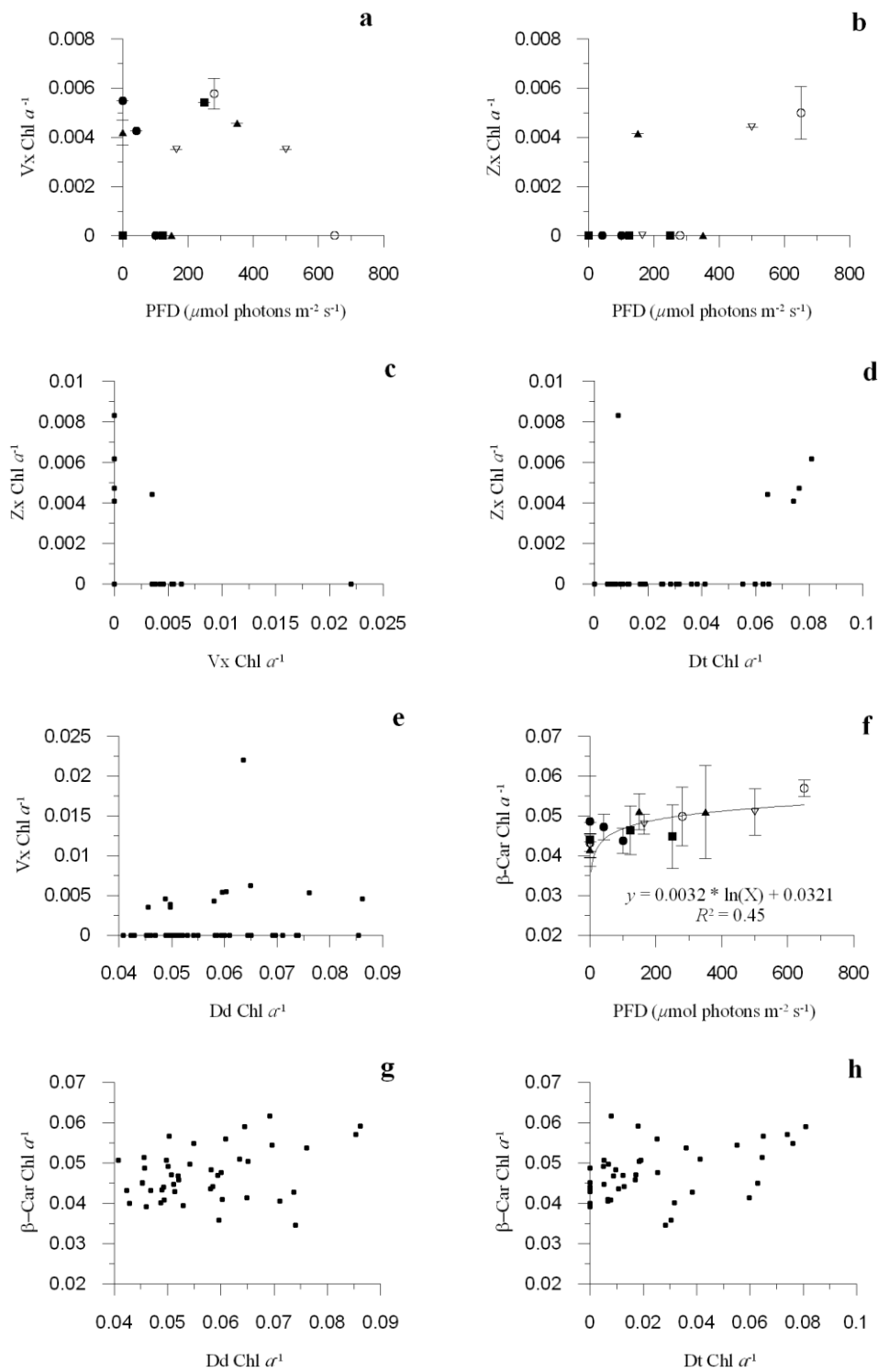


Fig. 5.24: Two hours kinetics experiment. Evolution of violaxanthin (a), zeaxanthin (b), and β -carotene Chl a^{-1} (f), over the irradiance range (PFD, $\mu\text{mol photons m}^{-2} \text{s}^{-1}$). Data are means with $n = 3$; error bars are SD. Relationship between zeaxanthin and violaxanthin Chl a^{-1} (c), zeaxanthin and diatoxanthin Chl a^{-1} (d), violaxanthin and diadinoxanthin Chl a^{-1} (e), β -carotene and diadinoxanthin Chl a^{-1} (g), β -carotene and diatoxanthin Chl a^{-1} (h). C100: filled circles; C250: filled square; C350: filled triangles; C500: open triangles; C650: open circles. Chl a , chlorophyll a ; Zx, zeaxanthin; Vx, violaxanthin; Dt, diatoxanthin; Dd, diadinoxanthin, β -Car, β -carotene.

5.4.2.3 Photosynthetic and accessory pigment content changes

The chlorophyll (Chl) *a* cellular content was quite stable and similar in the three experimental conditions, in agreement with the relatively short duration of experiments.

The Chl *a* cell⁻¹ content ranged between 3.05 and 5.23×10^{-16} mol Chl *a* cell⁻¹ (Figs. 5.25 a and b), in the 5 hours kinetics, between 3.37 and 5.37×10^{-16} mol Chl *a* cell⁻¹, in the 3 hours kinetics (Fig. 5.26 a).

In the 2 hours kinetics, the Chl *a* cell⁻¹ content was slightly higher than in the 5 and 3 hours kinetics, ranging between 4.33 and 7.24×10^{-16} mol Chl *a* cell⁻¹ (Fig. 5.27 a). Besides the small increase under $100 \mu\text{mol photons} \cdot \text{m}^{-2} \cdot \text{s}^{-1}$, the Chl *a* cell⁻¹ content slightly decreased over the irradiance gradient.

During the three experiments, chlorophyll *c* pigments ratios were also quite stable over the irradiance gradient, especially Chl *c*₃ Chl *a*⁻¹ (Figs. 5.25, 5.26, and 5.27). The Chl *c*₂ Chl *a*⁻¹ ratio was greater than the Chl *c*₁ and Chl *c*₃ Chl *a*⁻¹ ones (~ ten-fold). Higher Chl *c*₃ Chl *a*⁻¹ ratios were found for shorter irradiance increases (Figs. 5.25 e, 5.26 d, and 5.27 d). Lower Chl *c*₁ and *c*₂ Chl *a*⁻¹ ratios occurred in the 2 hours rather than in the 5 and 3 hours kinetics.

In the three experiments, the molar concentrations of Chl *a* and Chl *c* were significantly and positively correlated ($p < 0.005$; Figs. 5.25, 5.26, and 5.27). Only in 2 hours kinetics, no significant correlation was found between Chl *a* and Chl *c*₁ molar concentrations (Fig. 5.27 e), underlining that the fast irradiance increase was “stressful” for cells acclimation.

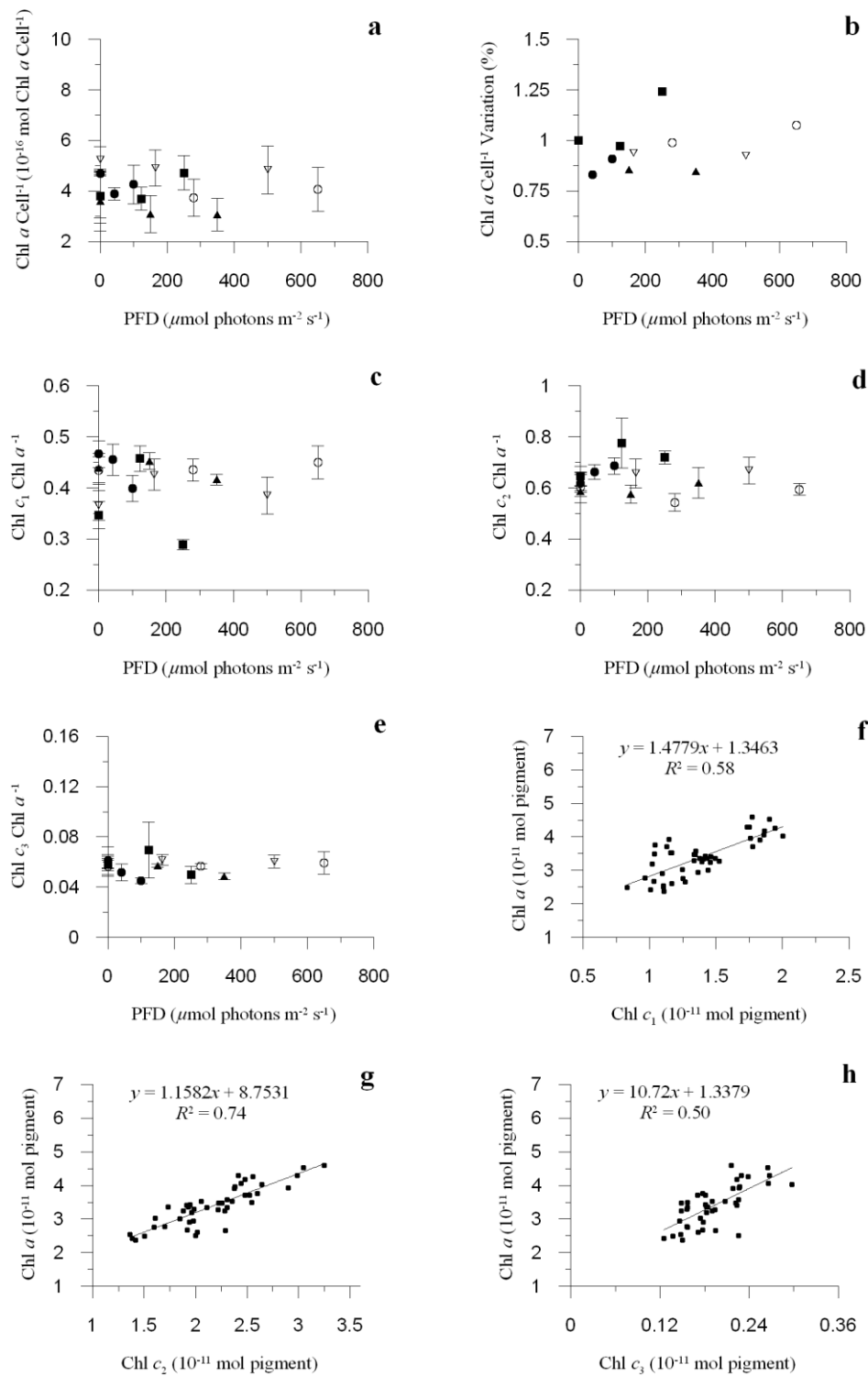


Fig. 5.25: Five hours kinetics experiment. Evolution of chlorophyll a cell $^{-1}$ content (10^{-16} mol Chl a cell $^{-1}$; **a**), Chl a cell $^{-1}$ variation (%; **b**), chlorophyll c_1 (**c**), c_2 (**d**), and c_3 Chl a $^{-1}$ ratios (**e**), over the irradiance range (PFD, $\mu\text{mol photons m}^{-2} \text{s}^{-1}$). Data are means with $n = 3$; error bars are SD. Relationship between chlorophyll a and chlorophyll c_1 (**f**), chlorophyll a and chlorophyll c_2 (**g**), chlorophyll a and chlorophyll c_3 molar concentrations (10^{-11} mol pigment; **h**). C100: filled circles; C250: filled square; C350: filled triangles; C500: open triangles; C650: open circles. Chl a , c_1 , c_2 , and c_3 : chlorophyll a , c_1 , c_2 , and c_3 , respectively.

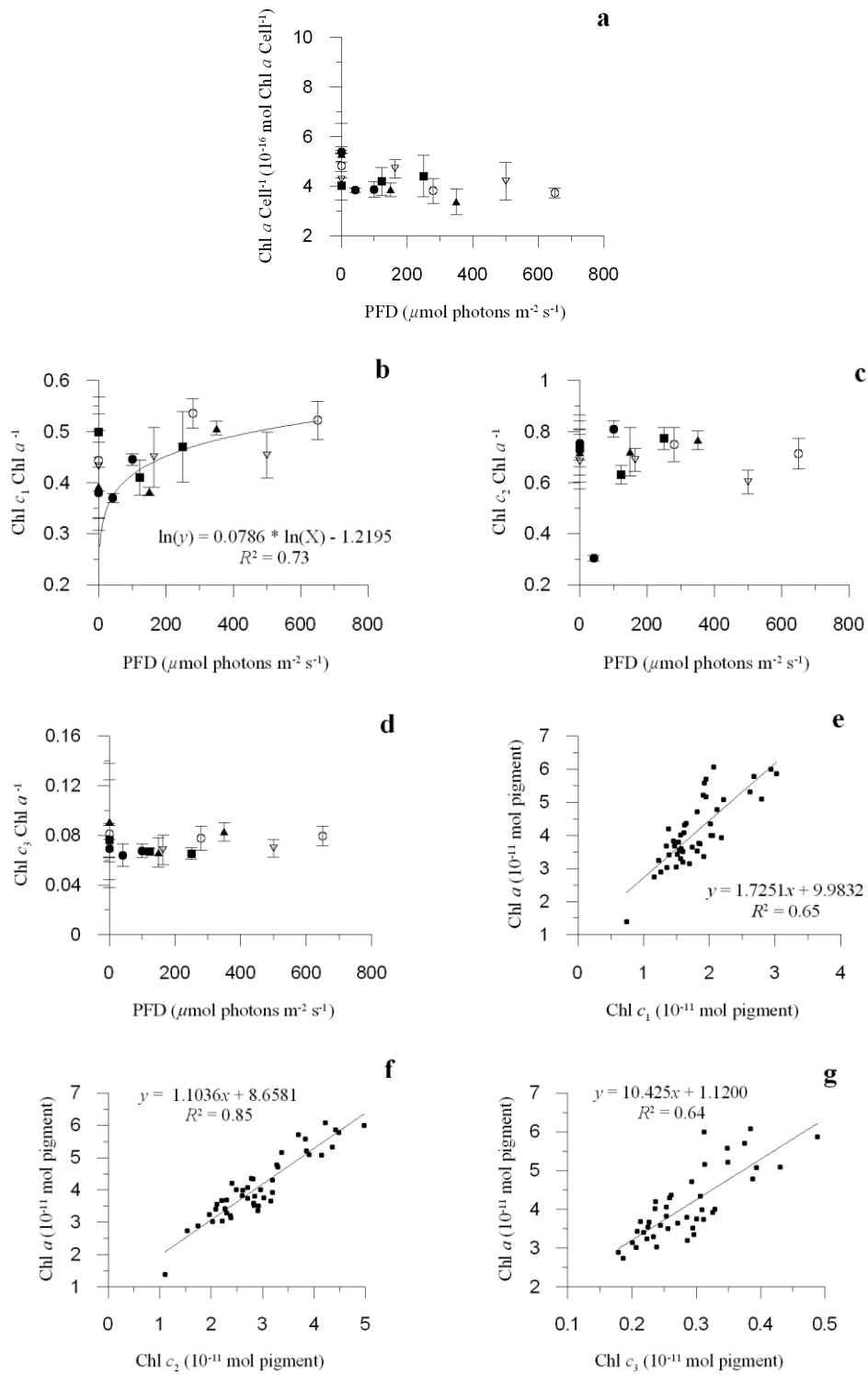


Fig. 5.26: Three hours kinetics experiment. Evolution of chlorophyll a cell $^{-1}$ content (expressed in 10^{-16} mol Chl a cell $^{-1}$; **a**), chlorophyll c_1 (**b**), c_2 (**c**), and c_3 Chl a^{-1} ratios (**d**), over the irradiance range (PFD, μ mol photons $m^{-2} s^{-1}$). Data are means with $n = 3$; error bars are SD. Relationship between chlorophyll a and chlorophyll c_1 (**e**), chlorophyll a and chlorophyll c_2 (**f**), chlorophyll a and chlorophyll c_3 molar concentrations (10^{-11} mol pigment; **g**). C100: filled circles; C250: filled square; C350: filled triangles; C500: open triangles; C650: open circles. Chl a , c_1 , c_2 , and c_3 : chlorophyll a , c_1 , c_2 , and c_3 , respectively.

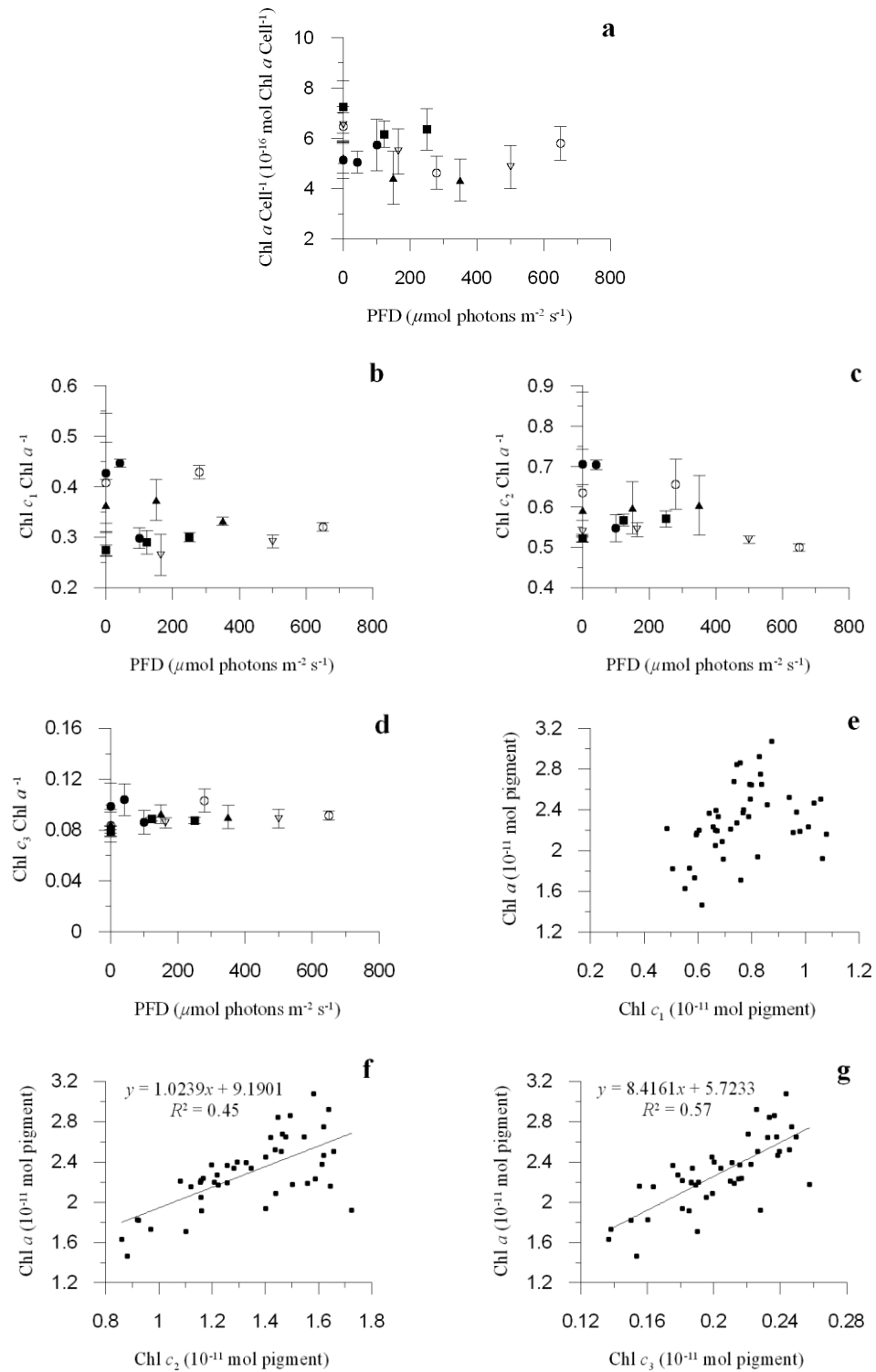


Fig. 5.27: Two hours kinetics experiment. Evolution of chlorophyll a cell⁻¹ content (expressed in 10⁻¹⁶ mol Chl a cell⁻¹; **a**), chlorophyll c_1 (**b**), c_2 (**c**), and c_3 Chl a ⁻¹ ratios (**d**), over the irradiance range (PFD, $\mu\text{mol photons m}^{-2} \text{ s}^{-1}$). Data are means with $n = 3$; error bars are SD. Relationship between chlorophyll a and chlorophyll c_1 (**e**), chlorophyll a and chlorophyll c_2 (**f**), chlorophyll a and chlorophyll c_3 molar concentrations (10⁻¹¹ mol pigment; **g**). C100: filled circles; C250: filled square; C350: filled triangles; C500: open triangles; C650: open circles. Chl a , c_1 , c_2 , and c_3 : chlorophyll a , c_1 , c_2 , and c_3 , respectively.

5.4.3 Discussion

The slow shift from low (LL) to high light (HL; 5 hours), the fast shift from LL to HL (3 hours), and the very fast shift from LL to HL (2 hours kinetics), represent three ecological conditions of light change to which cells differently respond.

Xanthophyll cycle functioning

Activation and functioning of the photoprotective processes (xanthophyll cycle – XC – and non-photochemical fluorescence quenching – NPQ) have been investigated in response to the 5 hours kinetics of irradiance increase.

Since the relatively short period of irradiance increase, regulative – and not acclimative - processes mainly occur. No significant correlation between irradiance and photosynthetic or accessory pigments is found, as demonstrated by the quite stable Chl *a* and photosynthetic accessory pigments cellular content. The significant correlation between the different Chl pools indicate that the photosystem II (PSII) can efficiently cope with the irradiance increase, being able to maintain its light harvesting capacity and properties.

During the slowest kinetics of irradiance increase, the XC response is strongly enhanced, with the Dt : (Dt + Dd) ratio (DPS) reaching 79%. Diatoxanthin (Dt) exponentially increases, while the linear increase in diadinoxanthin (Dd) Chl a^{-1} is only disrupted under $650 \mu\text{mol photons} \cdot \text{m}^{-2} \cdot \text{s}^{-1}$, due to the higher need for Dt exceeding the rate of Dd replenishment.

PFD higher than $250 \mu\text{mol photons} \cdot \text{m}^{-2} \cdot \text{s}^{-1}$ prevent linearity in the correlation between Dt and Dd : Chl *a* ratios, and the Vx-cycle pigments trend over the irradiance gradient breaks under moderate PFD, with violaxanthin (Vx) and zeaxanthin (Zx) Chl a^{-1} clearly increasing after the PFD of 250 and $164 \mu\text{mol photons} \cdot \text{m}^{-2} \cdot \text{s}^{-1}$, respectively. Thus, an enhanced carotenoid biosynthesis is required after a moderate PFD ($\sim 250 \mu\text{mol photons} \cdot \text{m}^{-2} \cdot \text{s}^{-1}$) threshold is exceeded, in this slow shift from LL to HL. These results, together with the significant correlation between Zx and Dt Chl a^{-1} , are consistent with a functional involvement in the *de novo* xanthophyll biosynthesis of Vx-cycle pigments as intermediate reaction products, where Vx plays a role of putative precursor of Dd (Lohr and Wilhelm, 1999, 2001; see Sec. 5.3.3). The intense activation of the cascade of biosynthetic reactions is additionally supported by the linear increase of the carotenoids precursor β -carotene (β -Car) Chl a^{-1} over the irradiance range, and by the significant correlation between Dd and β -Car Chl a^{-1} .

The 5 hours kinetics of irradiance increase causes the strongest and most efficient enhancement of XC response, when compared to faster kinetics. The greatest significance of the correlation between NPQ and XC modulation indicates the strong role of XC efficient and functional adjustments. Indeed, relatively low velocities of irradiance increase would confer sufficient time to progressively increase the dissipation of excessively absorbed energy in the PSII. These changes are achieved by finely regulating the xanthophylls biosynthetic pathway, also taking advantage of Dd accumulation from Vx (a step probably dependent on the feedback-response of the XC activation; see Sec. 5.3.3). Such a strong XC modulation results in the highest amount of photoprotective pigments of the three experimental conditions.

NPQ linearly increases over the irradiance range, being mostly enhanced under HL and largely related to the high rate of Dt synthesis, as demonstrated by the significant correlations with Dt Chl a^{-1} , and DPS ratios. Despite the high Dt content, NPQ development is moderate and less strong (0.81 ± 0.17) than in the faster kinetics of irradiance increase (1.05 ± 0.09 and 0.88 ± 0.14 , in the 3 and 2 hours kinetics, respectively).

This finding highlights that: (i) a slow light increase does not require a strong NPQ development, (ii) the XC modulation-dependent NPQ development is effective to cope with a slow light increase, (iii) the sufficiently long time course of light increase enables cells to adequately manage the photoprotective response over time, and lastly (iv) the slow kinetics of irradiance change (thus the quite low amount of photon per time) might cause a modest lumen acidification and, consequently a moderate capacity in switching all the Dt molecules into an ‘activated state’ (Lavaud and Kroth, 2006). The protonation of the LHC antenna sites has been recently proposed to explain such a switch into a quenching-promoting state of Dt molecules (Goss *et al.*, 2006b).

Mixing event effect on photoprotection

The photoacclimation to the two fast kinetics of irradiance increase ensures photosynthetic pigment stability, with no significant differences in Chl a and photosynthetic accessory pigments cellular content.

Since our previous assumption that NPQ development almost exclusively (or at least largely) relies on XC modulation in the slow shift from LL to HL, Dd cycle dependent and independent NPQ responses are estimated and discerned in the faster shifts. We cannot

exclude that a small portion of Dd cycle independent quenching might also be a part of the photoprotective response of cells subjected to the slow shift of light change.

During the 3 hours kinetics, XC response is differently regulated than in the 5 hours kinetics, despite the similar DPS (76 *versus* 78%, in the 3 and 5 hours kinetics, respectively).

Dt Chl a^{-1} linearly increases over the irradiance gradient, but Dt synthesis is lower than in the 5 hours kinetics. However, a greater NPQ development is achieved, especially enhanced under moderate (instead of high) PFD (NPQ is maximal under $164 \mu\text{mol photons} \cdot \text{m}^{-2} \cdot \text{s}^{-1}$). This result is consistent with the greater Dt Chl a^{-1} values measured under moderate PFD in the fast kinetics (0.033 ± 0.006) rather than in the slow one (0.022 ± 0.001), together with the Dd cycle independent quenching strong response. In fact, while the Dd cycle dependent NPQ gradually increases over the irradiance range upon Dt synthesis, the Dd cycle independent component peaks under moderate PFD (65% of the total NPQ development), then decreasing when PFD are higher than $164 \mu\text{mol photons} \cdot \text{m}^{-2} \cdot \text{s}^{-1}$. Interactions between PSII-detached fucoxanthin chlorophyll *a/c*-binding protein (FCP) complexes (Miloslavina *et al.*, 2009), as well as the PSII electron cycle (Lavaud *et al.*, 2002b, 2007), might be responsible for the Dd cycle independent quenching. This hypothesis agrees with the multi-component NPQ mechanism observed in *P. multistriata* (see Sec. 5.3.3).

These results demonstrate a clear effect of the velocity of light change on the dynamics of photoprotection and NPQ requirement. Even if PFD conditions seemingly are not stressful, the higher integrated irradiance intensity per unit of time requires a more rapid and intense NPQ development in conditions simulating a fast mixing event than in a slow one.

The Dd cycle independent NPQ is clearly related to the excessive integrated irradiance quantity per unit of time, due to shift velocity, representing a functional and very efficient response. Its activation is greater under moderate PFD ($164 \mu\text{mol photons} \cdot \text{m}^{-2} \cdot \text{s}^{-1}$) and gradually decreases under HL, hence causing the lower NPQ *plateau* under HL. To efficiently cope with both HL peaks and the excessive flux of photons per time, both the Dd cycle dependent and independent NPQ components are required.

The fast light increase prevents the Vx-cycle pigments participation to the carotenoids biosynthesis, as demonstrated by the quite stable Vx Chl a^{-1} over the irradiance range and the lower Zx Chl a^{-1} than in the slow kinetics (excluding the $650 \mu\text{mol photons} \cdot \text{m}^{-2} \cdot \text{s}^{-1}$ value). The weak increase in β -Car Chl a^{-1} over the irradiance range, and the lack of

correlations between β -Car and Dd cycle pigments Chl a^{-1} ratios, furthermore underline the scarce activation of xanthophylls biosynthesis.

On the other hand, a very fast shift from LL to HL (i.e. 2 hours) gives the strongest effect on the modulation of the photoprotective response.

Dt synthesis and DPS (56%) are the least enhanced of the three experimental conditions, as the very rapid increase of irradiance precludes an efficient activation of the biosynthetic pathway of carotenoids. In fact, Dd increase is low, and Vx-cycle pigments (when detected) and β -Car Chl a^{-1} are stable over the irradiance range.

Both the Dd cycle dependent and independent responses are lower than in the fast kinetics, explaining the moderate NPQ development.

The low amount of Dt molecules determines the lower increase of the Dd cycle dependent NPQ over the irradiance gradient, compared to the fast kinetics. The highest NPQ response occurs after the PFD of $280 \mu\text{mol photons} \cdot \text{m}^{-2} \cdot \text{s}^{-1}$ is reached, mostly due to the Dd cycle independent NPQ response. As the integrated irradiance stress per unit of time increases, the Dt synthesis-independent quenching is prolonged over the irradiance range (from 150 to $350 \mu\text{mol photons} \cdot \text{m}^{-2} \cdot \text{s}^{-1}$).

This very fast mixing-simulation event results in a stressful condition, under which the severe pressure of photons per time prevents cells to effectively and strongly respond to HL. We can infer that this kind of mixing event does not occur in the natural environment.

The different regulation of the dynamics of photoprotection of the diatom *P. multistriata* in response to three mixing event simulations can be resumed as follows.

During the slow shift from LL to HL (the 5 hours kinetics), the sufficiently low velocity of irradiance increase enables the photoprotective response to largely rely upon a strong activation of XC, hence resulting in a high accumulation of xanthophylls. The efficient regulation of the photoprotective biosynthetic pathway is also achieved through the involvement of Vx-cycle pigments as intermediary products, causing functional changes in the PSII. NPQ development largely relies upon Dt synthesis, without the necessity for a strong enhancement. Relatively long-term modifications of photoprotective processes dynamics ensure an efficient photo-regulation under slowly-increasing irradiances. This condition can be considered equal to the diel cycle of light.

During the fast shift from LL to HL (the 3 hours kinetics), the XC response is less strong than in the slow kinetics, due to a less activated xanthophyll biosynthesis. The higher the velocity of irradiance increase is, the greater is the need for a multi-component NPQ

mechanism. The Dd cycle independent quenching and the Dt synthesis are strongly enhanced under moderate PFD, mainly responding to the integrated irradiance quantity excess per unit of time, rather than PFD intensity. Probably, the fact that this fast light increase would not be “perceived” by cells as potential diel cycle of light, might have induced an enhancement of the photoprotective processes.

The very fast shift from LL to HL (2 hours kinetics) causes the least enhanced XC modulation, preventing an efficient NPQ development (both the Dd cycle dependent and independent components). The explanation of such weak photoresponse might reside in the highest (and excessive) integrated irradiance quantity per unit of time of such a stressful condition of light change that overcomes the capacity of cells to efficiently respond.

5.5 Effect of light history on photoprotection

5.5.1 Experimental design, sampling strategy and analysed parameters

The experiment lasted two days and it was performed in triplicate for each irradiance condition. For a two weeks-long period, cultures were pre-acclimated to a sine light (SL) climate set to peak at a maximal photon flux density (PFD) of $100 \mu\text{mol photons} \cdot \text{m}^{-2} \cdot \text{s}^{-1}$ (Fig. 5.2). During the exponential growth phase, cells were then shifted under three different SL regimes, each with a different maximal PFD of 100 (ML), 350 (HL1), and $650 \mu\text{mol photons} \cdot \text{m}^{-2} \cdot \text{s}^{-1}$ (HL2), respectively (Fig. 5.28).

Flasks were illuminated by the light system ACLS and Infinity XR4 (Aquarium Technologies, Sfiligoi S.r.l., Bassano del Grappa, Italy), simulating light–dark sine climate, reproducing dawn and sunset. XR4 was equipped with HQI metal halide lamps (10000 K). Temperature and pH were controlled daily with an HI-9214-Stick pH meter (Hanna Instruments, Woonsocket, RI, USA).

Cultures were sampled five times per day (Table 5.1; Fig. 5.28). The first sampling (“dawn”) was carried out when cells were in the dark, 15 minutes before the irradiance increase started. The second sample (“morning”) was taken after three hours of irradiance increase, while the third sample (“peak”) corresponded to the irradiance peaks. The fourth (“afternoon”) sample was taken three hours after the PFD peak was reached, while the fifth sample (“sunset”) soon before dark (Table 5.1; Fig. 5.28).

Sampling Time	PFD			Parameters
	ML	HL1	HL2	
Dawn	0	0	0	Growth rate (μ), pigment analysis
Morning	42	150	280	Pigment analysis, active Chl <i>a</i> fluorescence
Peak	100	350	650	Pigment analysis, active Chl <i>a</i> fluorescence, P-E curves
Afternoon	42	150	280	Pigment analysis, active Chl <i>a</i> fluorescence
Sunset	5	16	30	Pigment analysis, active Chl <i>a</i> fluorescence

Table 5.1: Sampling times and parameters measured under three different sine climates, each with a different maximal PFD of 100 (ML), 350 (HL1), and $650 \mu\text{mol photons m}^{-2} \text{s}^{-1}$ (HL2), respectively, during two days of experiment.

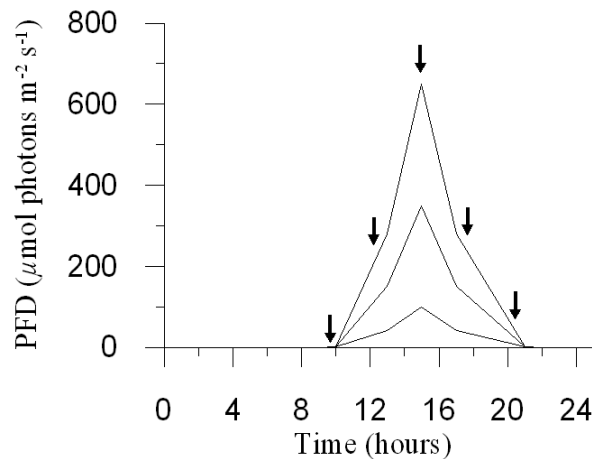


Figure 5.28: Illustration of the three sine light climates applied during the experiment, each with a different maximal PFD peak of 100 (ML), 350 (HL1), and 650 $\mu\text{mol photons m}^{-2} \text{s}^{-1}$ (HL2), respectively. Arrows indicate the five sampling times (per day).

Fifteen to twenty mL of culture were rapidly taken during each sampling time to measure active Chl *a* fluorescence, NPQ, photosynthetic rate through P-E curve, and for further analysis of pigments, and cell concentration (by microscopic counts).

The growth rate (μ) and the number of cell divisions (n) per day were daily estimated from cell abundance measurements as described in chapter 4 (Sec. 4.2).

A ten mL aliquot was filtered onto GF/F glass fibre filters (Whatman, UK), and immediately stored in liquid nitrogen until further pigment analysis. Triplicate samples were taken during each sampling time. Pigment analysis was carried out following the procedure described in chapter 4 (Sec. 4.4).

Triplicate measurements of active Chl *a* fluorescence were performed on both light- and dark-acclimated samples. NPQ triplicate measurements were conducted in 15 minutes dark-acclimated samples. P-E curves were conducted in 15 minutes dark-acclimated samples. Active Chl *a* fluorescence, NPQ and P-E curves were obtained following the procedures described in chapter 4 (Sec. 4.6).

5.5.2 Results

5.5.2.1 Growth rate and photosynthetic parameters

In response to the shift under the three irradiance conditions, after the first day of acclimation, the growth rate increased over the irradiance range, reaching the highest value under HL2 condition (1.16 ± 0.15), being two-fold higher than the ML value (i.e. the pre-acclimation irradiance condition; Table 5.2).

During the second day of the experiment, the absolute electron transport rate ($_{\text{abs}}\text{ETR}_{\text{max}}$) was greater under ML and HL2 conditions than under HL1, while the photosynthetic efficiency (α^{B}) was the highest under moderate irradiance condition, underlining the low light acclimation of cells (Table 5.2).

The saturation irradiance value (E_k ; Table 5.2), measured during the second day of the experiment, did not change much in the three irradiance conditions.

Light Conditions	Growth Rate	$_{\text{abs}}\text{ETR}_{\text{max}}$	α^{B}	E_k
100 (ML)	0.64 ± 0.21	0.35 ± 0.05	0.008 ± 0.001	431.9 ± 112.1
350 (HL1)	1.05 ± 0.01	0.16 ± 0.03	0.005 ± 0.001	359.1 ± 81.9
650 (HL2)	1.16 ± 0.15	0.38 ± 0.10	0.005 ± 0.001	388.3 ± 190.5

Table 5.2: Growth rate (d^{-1}) and photosynthetic parameters (retrieved through P-E curve measurements; $_{\text{abs}}\text{ETR}_{\text{max}}$ in $\text{mol e}^{-1} \text{ g Chl } a^{-1} \text{ h}^{-1}$; α^{B} in $\text{mol e}^{-1} \text{ g Chl } a^{-1} \text{ h}^{-1} [\mu\text{mol photons m}^{-2} \text{ s}^{-1}]^{-1}$; E_k in $\mu\text{mol photons m}^{-2} \text{ s}^{-1}$) in *Pseudo-nitzschia multistriata* cells subjected for two days to different sine light climates set to peak at 100 (ML), 350 (HL1) and 650 $\mu\text{mol photons m}^{-2} \text{ s}^{-1}$ (HL2), respectively. Data represent the second day of the experiment (i.e. after the first day of acclimation), and are means ($n = 3$) \pm SD.

5.5.2.2 Variable fluorescence measurements and photoprotective response

The decrease over time, during daylight, in the photosystem II (PSII) maximal ($F_v : F_m$), and especially, operating ($F_v' : F_m'$) photochemical efficiencies, was stronger under HL2 than under ML and HL1 conditions (Fig. 5.29). Such a decrease of (maximal and operating) fluorescence yields was greater during the first day of the experiment compared

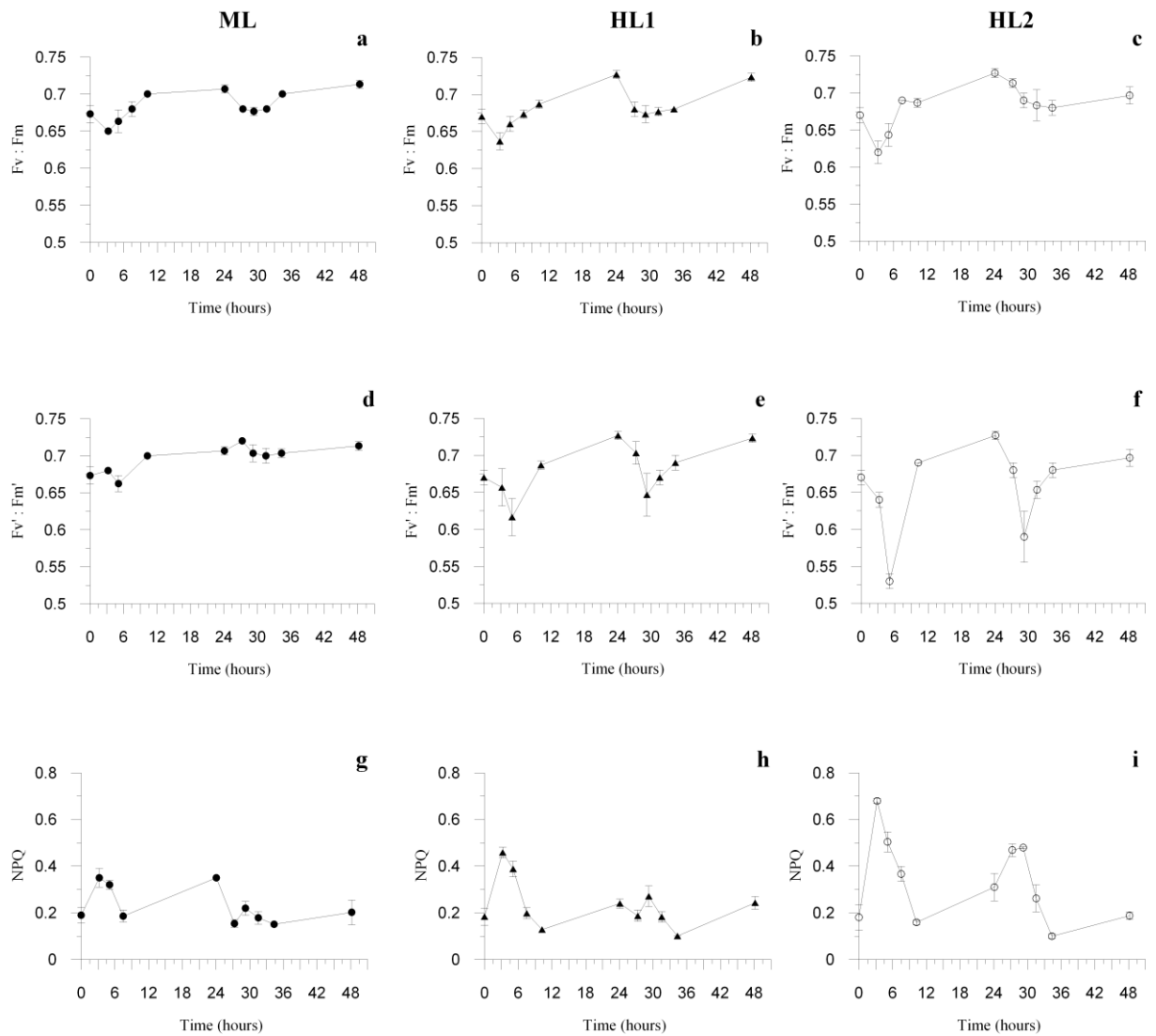


Fig. 5.29: Evolution of photosystem II maximal ($F_v : F_m$; **a**, **b** and **c**) and operating ($F_v' : F_m'$; **d**, **e** and **f**) photochemical efficiency, and non-photochemical quenching (NPQ; **g**, **h** and **i**) over time, during the two days of the experiment (and one “dawn” sampling on the third day). Data are means with $n = 3$; error bars are SD. ML: filled circles; HL1: filled triangles; HL2: open circles.

to the second one, revealing an acclimation to the high irradiance conditions, in the second day of the experiment. The fluorescence values measured at “dawn” (first) and “sunset” (fifth sampling time of the day) were not significantly different in the three irradiance conditions, suggesting that an efficient recovery occurred during the dark hours, despite the high irradiance conditions.

For all the three irradiance conditions, the highest non-photochemical fluorescence quenching (NPQ) values were reached during the morning sampling time of the first day

of the experiment, showing a rapid and maximal photoprotective response to HL before the PFD peak was reached. The higher was the irradiance condition, the greater was the NPQ development, with the highest NPQ value reached under HL2, during the first day of the experiment (0.68 ± 0.01 ; Figs. 5.29 g, h and i). Contrarily, on the second day of the experiment, HL1 and HL2 maximal NPQ values were lower than the values of the first day, and shifted to the peak sampling time, suggesting HL acclimation of cells (Figs. 5.29 h and i).

The higher was the irradiance condition, the greater was the diatoxanthin (Dt) Chl a^{-1} ratio, reaching the highest value at the HL2 peak of the second day of the experiment

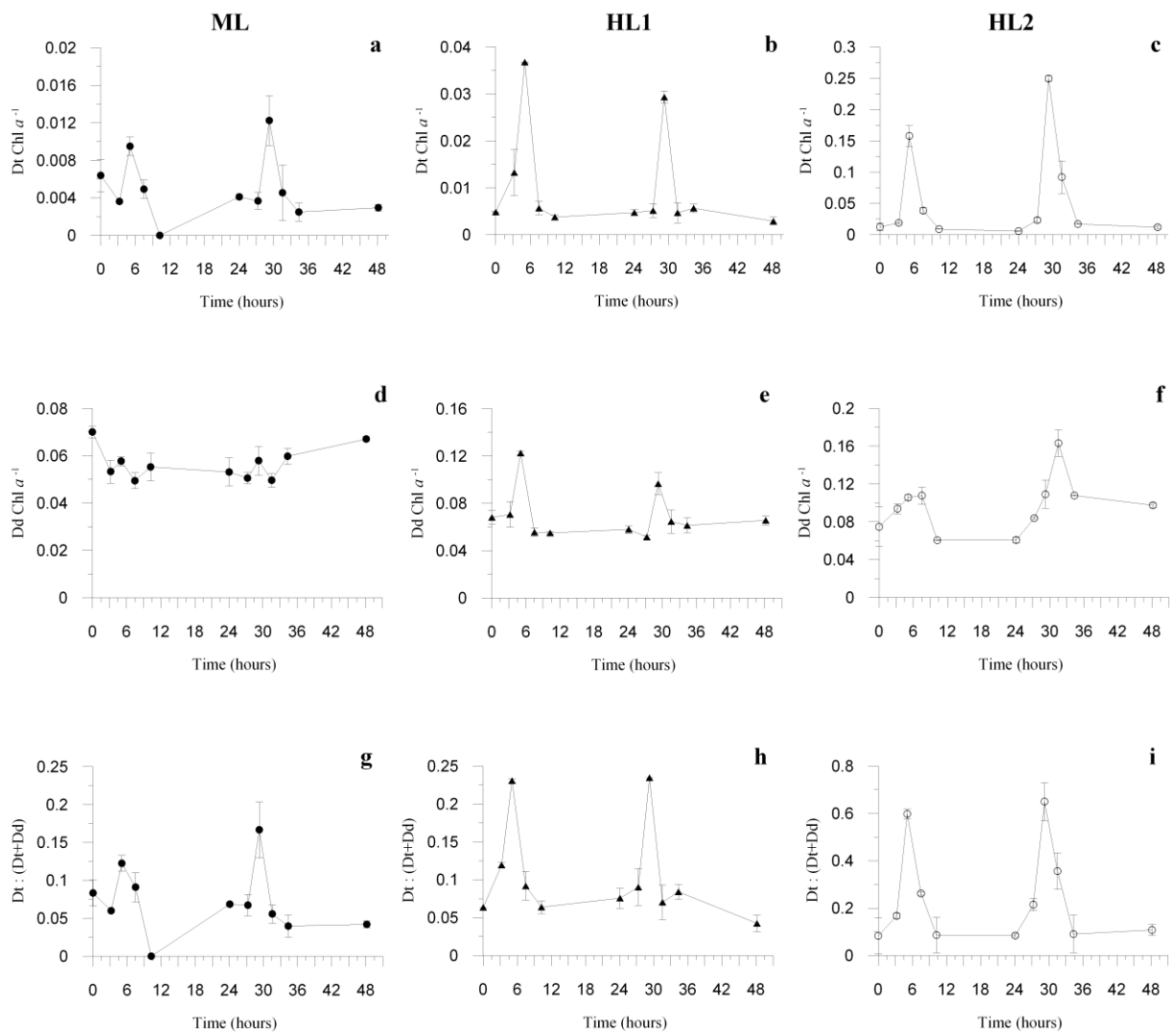


Fig. 5.30: Evolution of the diatoxanthin (a, b and c) and diadinoxanthin Chl a^{-1} ratios (d, e and f), and [Dt : (Dt + Dd)] ratio (DPS; g, h and i), over time, during the two days of the experiment (and one “dawn” sampling on the third day). Data are means with $n = 3$; error bars are SD. ML: filled circles; HL1: filled triangles; HL2: open circles. Chl a , chlorophyll a ; Dt, diatoxanthin, Dd, diadinoxanthin; DPS, de-epox. state.

(0.249 ± 0.005 , ~ 8 fold greater than HL1 maximal Dt Chl a^{-1} value; Figs. 5.30 a, b and c). The Dt Chl a^{-1} ratio followed a diel cycle pattern under the three irradiance conditions, with maximal values reached at peak sampling times (Figs. 5.30 a, b and c).

The fact that the HL1 highest Dt Chl a^{-1} ratio was measured at the peak of the first day of the experiment supported the xanthophyll cycle (XC) rapid activation as a regulation process, while no structural acclimative changes at the level of the photosystem II (PSII) occurred.

On the other hand, under HL2 condition, after the fast XC regulation of the first day of the experiment, the Dt Chl a^{-1} ratio further increased in the second day, indicating a structural acclimation. The enhanced Dt synthesis to afford a structural photoprotective response (PSII rearrangement) could explain the lower NPQ value measured during the second day rather than the first day of the experiment (Fig. 5.29 i).

The diadinoxanthin (Dd) Chl a^{-1} ratio increased over the irradiance range, consistently with the photoacclimative strategies adopted by cells, reaching the highest value on the second day of the experiment under HL2 (Fig. 5.30 f), while on the first day under HL1 (at peak; Fig. 5.30 e), in agreement with the Dt Chl a^{-1} evolution over time and photoprotective response, in the three irradiance conditions. A diel cycle periodicity was found in Dd Chl a^{-1} ratio under HL1 and HL2 conditions, with the highest values measured at peak sampling time for HL1 (Fig. 5.30 e), while at peak and afternoon sampling times for HL2 condition (Fig. 5.30 f), since the higher need of Dt synthesis. Dd Chl a^{-1} was instead quite stable under ML condition (Fig. 5.10 d).

Under HL1 and HL2, the [Dt : (Dt + Dd)] (DPS) ratio values measured at peaks were almost similar between the first and the second day of the experiment (Figs. 5.30 h and i), differently from Dt and Dd Chl a^{-1} evolution over time (Fig. 5.30). This result suggested a strong relation between Dt and Dd, and an equal rate of Dt replenishment from Dd, either during regulation or acclimation responses. DPS increased over the irradiance range, reaching $\sim 65\%$ on HL2 peak sampling, almost three-fold higher than the HL1 percentage ($\sim 23\%$; Figs. 5.30 g, h and i). For all the irradiance conditions, the maximal DPS ratios occurred at peak sampling times, while similar values ($\sim 10\%$) were found at dawn and sunset sampling times for HL1 and HL2 conditions, underlining an efficient epoxidation of Dt into Dd, during the dark and non-saturating PFD periods (Figs. 5.30 h and i).

The β -carotene (β -Car) : Chl a ratio increased under HL conditions (mainly HL2), following a diel cycle pattern, with maximal values reached at peaks (Figs. 5.31 a, b and c), while being stable under ML condition (Fig. 5.31 a). As for Dt and Dd Chl a^{-1} ratios,

the highest β -Car Chl a^{-1} value (0.087 ± 0.002) was also found on HL2 second day peak, in relation with its involvement during the activation of the photoprotective biosynthetic pathway.

The violaxanthin (Vx) Chl a^{-1} ratio increased over the irradiance range, following a diel cycle pattern under the three irradiance conditions, with maximal values reached at peak sampling times (Figs. 5.31 d, e and f).

For all the irradiance conditions, the highest Vx Chl a^{-1} values were measured on the first day of the experiment, suggesting the involvement of this xanthophyll in the fast photoprotective response related to XC modulation, during the early regulative process of cells.

Also, the zeaxanthin (Zx) Chl a^{-1} ratio followed a similar trend as Vx Chl a^{-1} , in relation with its involvement in the photoprotective biosynthetic pathway activation (Figs. 5.31 g, h and i).

Interestingly, the accessory pigment neoxanthin (Neox) was detected, showing a diel cycle pattern, but with the highest Neox Chl a^{-1} ratio values measured at HL1 and HL2 afternoon sampling times (Figs. 5.31 l, m and n). In agreement with the hypothesized conceptual model for the biosynthetic photoprotective pathway (Sec. 5.3.3), the Neox increase might be the outcome of the Dt epoxidation into other xanthophylls, with decreasing PFD.

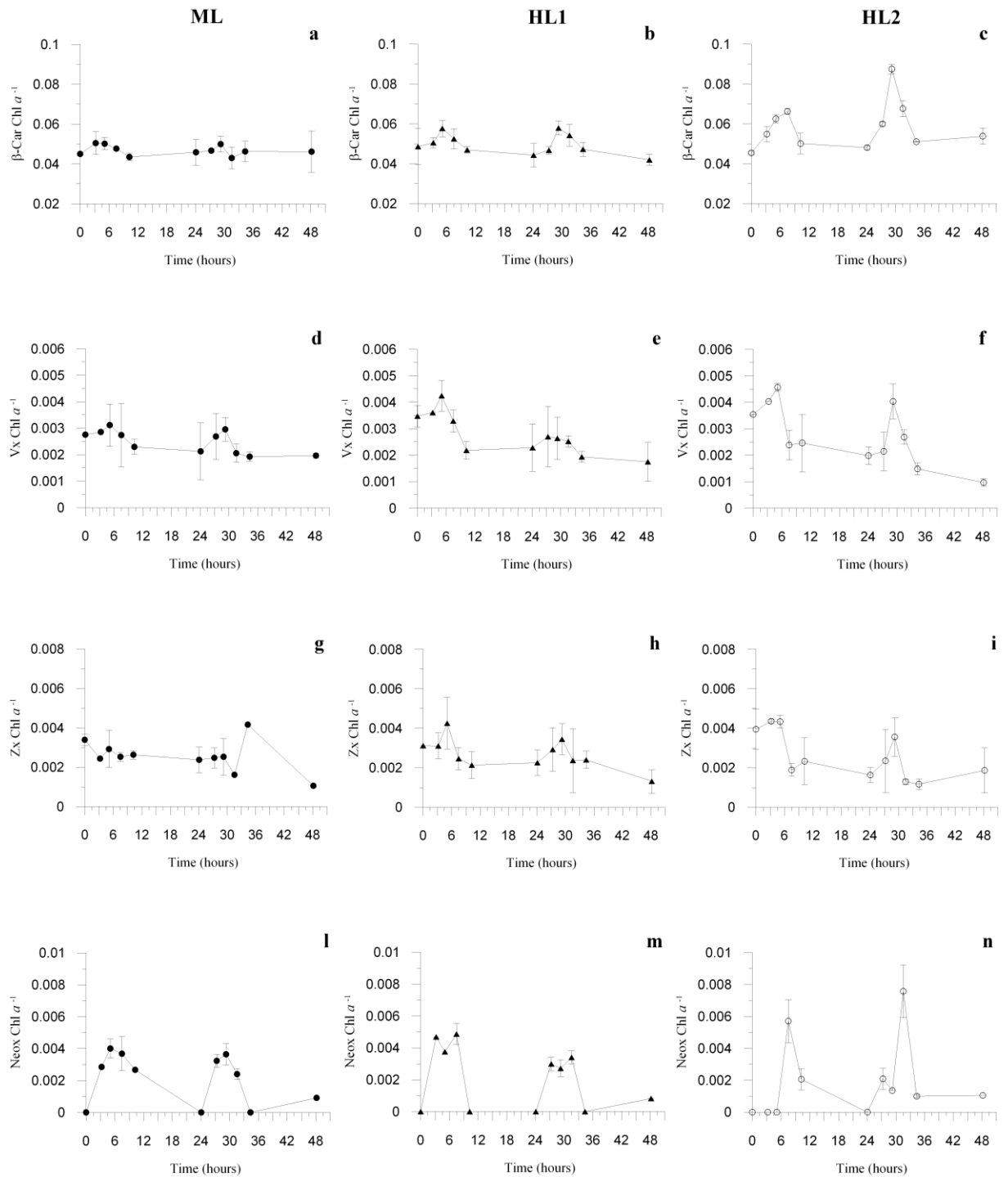


Fig. 5.31: Evolution of β -carotene (a, b and c), violaxanthin (d, e and f), zeaxanthin (g, h and i), and neoxanthin Chl a^{-1} ratios (l, m and n), over time, during the two days of the experiment (and one “dawn” sampling on the third day). Data are means with $n = 3$; error bars are SD. ML: filled circles; HL1: filled triangles; HL2: open circles. Chl a , chlorophyll a ; β -Car, β -carotene; Neox, neoxanthin; Vx, violaxanthin; Zx, zeaxanthin.

5.5.2.3 Photosynthetic and accessory pigments content changes

The cellular chlorophyll (Chl) *a* content was lower under HL2 condition (ranging between 3.56 and 7.91×10^{-16} mol cell⁻¹; Fig. 5.32 c), than ML and HL1 conditions (both with similar values ranging between 4.68 and 11.40×10^{-16} mol cell⁻¹; Figs. 5.32 a and b). Under HL2 condition, a decrease in Chl *a* cell⁻¹ content was found between the first and the second day of the experiment (Fig. 5.32 c). The similar Chl *a* cell⁻¹ contents of ML and HL1 conditions demonstrated that HL1 condition did not induce an acclimative response of cells aimed at decreasing their light harvesting capacity.

The fucoxanthin (Fuco) and chlorophylls *c*₁ + *c*₂ (Chl *c*₁ + *c*₂) Chl *a*⁻¹ ratios were not significantly different between the irradiances conditions, with slightly variable ratios under HL intensities, while quite stable under ML condition (Fig. 5.32). The highest Fuco and Chl *c*₁ + *c*₂ Chl *a*⁻¹ ratios were measured on HL2 second day of the experiment (Figs. 5.32 f and i). The increase in Fuco Chl *a*⁻¹ on HL2 second day at the afternoon sampling time might be a consequence of Dt epoxidation into Dd and other carotenoids, while PFD decreases.

Under HL2 condition, the increase in photosynthetic accessory pigments content might be related to the enhanced Dt synthesis, responsible for decreasing the photon flux pressure (but also the light harvesting capacity) in PSII LHC antenna.

Chl *c*₃ showed a Fuco and Chl *c*₁ + *c*₂ -independent evolution, with an opposite trend during daylight between HL1 (increase; Fig. 5.32 m) and HL2 condition (decrease; Fig. 5.32 n).

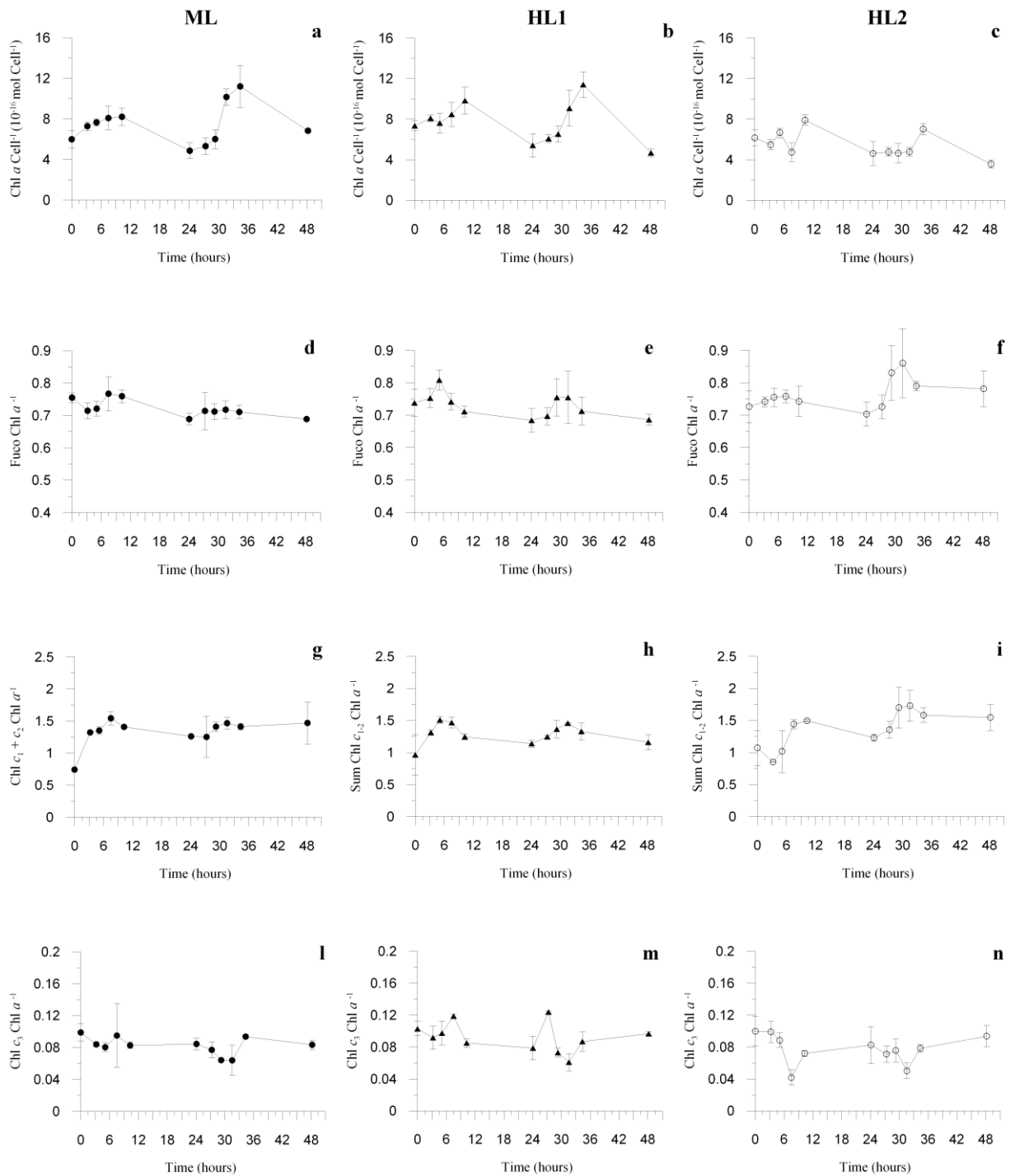


Fig. 5.32: Evolution chlorophyll *a* cell⁻¹ content (10^{-16} mol Chl *a* cell⁻¹; **a**, **b** and **c**), fucoxanthin (**d**, **e** and **f**), chlorophyll *c*₁ + *c*₂ (**g**, **h** and **i**), and chlorophyll *c*₃ Chl *a*⁻¹ ratios (**l**, **m** and **n**), over time, during the two days of the experiment (and one “dawn” sampling on the third day). Data are means with *n* = 3; error bars are SD. ML: filled circles; HL1: filled triangles; HL2: open circles. Chl *a*, *c*₁ + *c*₂, and *c*₃, chlorophyll *a*, *c*₁ + *c*₂, and *c*₃; Fuco, fucoxanthin.

5.5.3 Discussion

In this experiment, after a pre-acclimation period of two weeks under a moderate sine light (SL) climate ($100 \mu\text{mol photons} \cdot \text{m}^{-2} \cdot \text{s}^{-1}$; ML), portions of the culture have been shifted under high SL climates (350 and $650 \mu\text{mol photons} \cdot \text{m}^{-2} \cdot \text{s}^{-1}$; HL1 and HL2). Cells have been followed for two days to study the dynamics of acclimation of *Pseudo-nitzschia multistriata* over the applied irradiance gradient, tackling both the fast (first day) and more long term (second day of the experiment) photoacclimative processes adopted by cells to cope with the increasing irradiances.

During the first day of the experiment, regulative processes occur under both HL regimes. A fast xanthophyll cycle (XC) activation causes the strongest non-photochemical fluorescence quenching (NPQ) development measured at the morning sampling time, under HL1 and HL2 conditions. This result is consistent with the highest decrease in quantum yield of fluorescence on the first day of the experiment, under both HL conditions. The efficient regulation of this fast photoprotective response explains both the fluorescence quantum yield recovery (in the dark hours), and the high growth capacity maintenance from the first to the second day of the experiment (data not shown).

The HL1 regime requires a moderate photoprotective response of cells during the two experimental days, through the regulation of XC activation and consequent NPQ development, as well as the carotenoid biosynthetic pathway modulation. The photosynthetic accessory pigments Chl a^{-1} ratios show a diel cycle periodicity, and either are quite stable (β -carotene and chlorophylls c) or decrease over time (fucoxanthin), in agreement with an efficient XC regulation over time (necessity of a less enhanced response on the second day, than on the first day of the experiment).

The regulative processes activated during the second day of the experiment enable cells to maintain their growth capacity, but not a high photosynthetic rate (more than two-fold lower than HL2 $\text{absETR}_{\text{max}}$ value). This result underlines how a photoprotective response related to the instantaneous XC modulation would be effective in rapidly dissipating the excessive energy of high light events, but not in maintaining a high photosynthetic capacity. Since the P-E curves have been conducted only at peaks, the decrease in absolute electron transport rate ($\text{absETR}_{\text{max}}$) might thus indicate a functional regulation of the photosynthetic machinery to the PFD peak, rather than a net decrease in photosynthetic capacity. This explanation is consistent with the optimal growth capacity of cells subjected to this irradiance regime, compared to the limiting irradiance of the ML condition,

probably revealing the heavy cost of basic processes related to the maintenance respiration rate, under moderate SL climate. The aforementioned result underlines that an efficient regulation of the physiological and biochemical processes, which link photosynthesis and growth, occurs under HL1 condition.

Based upon the fact that only regulative processes are activated under HL1, and that the PFD peak of $350 \mu\text{mol photons} \cdot \text{m}^{-2} \cdot \text{s}^{-1}$ enters the range of values of the saturation irradiance (E_k) measured in the three irradiance conditions (range between 359 and 431 $\mu\text{mol photons} \cdot \text{m}^{-2} \cdot \text{s}^{-1}$; Table 2), it seems that a PFD value higher than the E_k of cells would trigger for photoacclimative changes, as demonstrated by HL2 condition (650 $\mu\text{mol photons} \cdot \text{m}^{-2} \cdot \text{s}^{-1}$).

Under this regime, a fast photoregulative response is found upon the irradiance increase on the first day of the experiment, after which, on the second day of the experiment, a photoacclimative response is needed. PSII structural photoacclimative processes, together with XC and NPQ modulation, are therefore activated to cope with the highest PFD pressure. The less strong NPQ development, on the second day of the experiment rather than on the first day, can be related to these PSII structure modifications, causing a more efficient regulation of the light harvesting capacity of cells under HL2, whereas to XC modulation, under HL1 condition, since the moderately high irradiance.

Our data indicate a one day-long period to activate photoacclimative structural processes, corresponding to one cellular division, during which, thylakoid structure modifications concerning photoprotective and accessory pigments content changes in the light harvesting complexes (LHC) can take place (Raven and Geider, 2003; Brunet *et al.*, 2011). Light induced chloroplast changes (e.g. changes in intracellular self-shading, optical signature properties, optical density, and *in vivo* fluorescence emission) are also likely to occur in response to irradiance changes (Falkowski and Chen, 2003; Sakshaug and Johnsen, 2005; Johnsen and Sakshaug, 2007).

The structural changes adopted by cells under HL2 condition are visible as an $\sim 25\%$ decrease in the cellular Chl *a* content, from HL1 to HL2 conditions, disrupting the diel cycle pattern of Chl *a* synthesis, related to biomass increase (daylight) and cell division (night), whereas evident under ML and HL1 conditions. At the same time, the decrease in Chl *a* cell^{-1} content is balanced by the increase in photosynthetic accessory pigments content (fucoxanthin, β -carotene, and chlorophylls $c_1 + c_2$) over time, during daylight, reflecting both PSII structure changes, and the need for an enhanced light harvesting capacity, contrasting the decrease in Chl *a* cellular content.

Such a decrease in Chl *a* cell⁻¹ content might therefore be related to a decrease in the number of PSII reaction centers (*n*-type photoacclimation strategy; Falkowski and Owens, 1980), a photoacclimative strategy that results in an optimal physiological state of cells under high light, since the highest growth and photosynthetic rates of the three irradiance conditions, reached on the second day of the experiment.

Different studies have already demonstrated how the capacity of large modulations in cellular pool of PSII RC would allow cells for a dynamic regulation of PSII, thus resulting in an advantageous feature for variable light regimes exploitation (Wagner *et al.*, 2006; Six *et al.*, 2008; Dimier *et al.*, 2009a; Giovagnetti *et al.*, 2010). Our finding therefore agrees with *P. multistriata* (coastal) environment of growth, where the light is highly fluctuant and often reaches high intensities.

Our results show the involvement of Vx-cycle and accessory pigments (e.g. fucoxanthin and β -carotene) in the photoacclimative processes related to diel cycle pattern. All these pigments participate to the carotenoids photoprotective biosynthetic pathway, supporting evidences found in previous studies (Lohr and Wilhelm, 1999; Dimier *et al.*, 2009a), and in agreement with results presented in Section 5.3.3.

At the peak of the first day of the experiment, Vx (~ 0.0045) and Dd Chl *a*⁻¹ (~ 0.11) ratios reach quite similar values, between HL1 and HL2 conditions. Under HL conditions, the higher Vx content measured in the first day of the experiment, than in the second day, would indicate both Vx rapid synthesis upon the irradiance increase, and its requirement during the fast regulative photoprotective response occurring on the first day of the experiment. The decrease in Vx content over time might instead suggest a preferential Dd replenishment from Vx mainly when regulative processes are activated (i.e. during the first day of the experiment). This result agrees with an enhancement of Vx flow for Dd accumulation, due to the XC activation feedback-response (see Sec. 5.3.3). At the same time, the fact that, a Vx diel periodicity is evident under the three PFD conditions (also under moderate irradiance), suggests that its increase would not only be induced by a photoprotective response.

Differently, under HL2 condition, the increase in Dd content at the afternoon sampling time of the second day of the experiment might be related to the increase in photosynthetic accessory pigments content (since the slight decrease in Vx Chl *a*⁻¹ at peak), thus showing a distinct modulation of the carotenoid pathway when photoacclimative structural variations occur, with a Dd accumulation mainly due to fucoxanthin (and β -carotene) flow.

Light history affects the photoprotective response of the cells (Anning *et al.*, 2000; Dimier *et al.*, 2007b). Both HL1 and HL2 conditions require an early photoregulative response on the first day of the experiment, based upon XC (and NPQ) modulation. The XC regulation over time (less strong response on the second day of the experiment) enables cells to cope with the moderately high PFD of HL1 condition, and maintain a high growth rate by regulating their photosynthetic capacity. Contrarily, photoacclimative PSII structure changes are needed to efficiently cope with HL2 regime, and maximize growth and photosynthetic rates. In function of the HL-induced regulative or photoacclimative processes adopted by cells, the photoprotective biosynthetic pathway of carotenoids is differently modulated, determining variations in the photoprotective and photosynthetic accessory pigments of cells, under HL conditions.

CHAPTER 6

**Functional relation between growth,
photosynthetic rate and regulation in the coastal
picoeukaryote *Phaeomonas* sp. RCC503
(Pinguiphyceae, Stramenopiles)**

Chapter 6

Functional relation between growth, photosynthetic rate and regulation in the coastal picoeukaryote *Phaeomonas* sp. RCC503 (Pinguiphyceae, Stramenopiles)

This chapter corresponds to a paper published in 2010, in JOURNAL OF PLANKTON RESEARCH, VOLUME 32, NUMBER II, 1501–1511, 2010, doi: 10.1093/plankt/fbq074

Despite their relevance in terms of biomass and production, as well as group diversity/complexity, ecophysiological properties of picoeukaryotes have been only recently studied (see Chapter 3, Sec. 3.4). Being widely distributed in marine ecosystems and adapted to a large variety of light conditions, and being characterized by peculiar biological features (related to their tiny cell size), picoeukaryotes turned out to be valid model organisms to study functional photophysiological properties in relation to aquatic ecosystems adaptation (Dimier *et al.*, 2007a, 2009a; Six *et al.*, 2008, 2009).

The aim of this experiment was to investigate the relation between growth rate, photosynthetic capacity and efficiency of photoacclimative/photoregulative processes, in the picoeukaryote *Phaeomonas* sp. RCC503 (Pinguiphyceae, Stramenopiles). Because of the species ecological adaptation (having been isolated from coastal waters, in the Mediterranean Sea), a strong capacity of photoacclimative and photosynthetic regulation was expected, in agreement with coastal species plasticity (Lavaud *et al.*, 2007; Dimier *et al.*, 2009b).

Physiological response curves (PRC, Peek *et al.*, 2002) were obtained by plotting physiological variables and growth rate against a range of photon flux density (PFD). Cells were subjected to five different sine light climates set to peak at distinct maximal PFD, in order to simulate natural irradiance cycles (with 11 : 13 hours of light : dark photoperiod), and cellular growth was followed over five days.

Multiple reasons motivated the choice of such a species: biological (small cell size), taxonomical (the class of Pinguiphyceae is closely related to Bacillariophyceae, within the Stramenopiles), functional (it displays the Vx cycle, despite belonging to

Stramenopiles) and ecological (coastal species) peculiar aspects. The resulting functional photophysiological flexibility of *Phaeomonas* sp. RCC503 has been interpreted in relation to the species ecological traits.

Functional relation between growth, photosynthetic rate and regulation in the coastal picoeukaryote *Phaeomonas sp.* RCC 503 (Pinguiphyceae, Stramenopiles)

V. GIOVAGNETTI, M. L. CATALDO, F. CONVERSANO AND C. BRUNET*

LABORATORY OF ECOLOGY AND EVOLUTION OF PLANKTON, STAZIONE ZOOLOGICA ANTON DOHRN, VILLA COMUNALE, 80121 NAPLES, ITALY

*: CORRESPONDING AUTHOR: christophe.brunet@szn.it

Received March 31, 2010; accepted in principle May 27, 2010; accepted for publication May 31, 2010

Running head: *Phaeomonas sp.* RCC 503 photoregulation and growth

Abstract

Picoeukaryotes constitute good models for testing photophysiological hypotheses because of constraints as well as opportunities related to their minute size. This study was undertaken to investigate the relation between growth rate and regulation of photosynthesis in a coastal picoeukaryote, using the strain *Phaeomonas* sp. RCC503 as a model. Here we address how photoacclimation responses affect photosynthetic capacity and how growth rate is modulated by photoacclimation and photosynthetic rate variations. Growth of the strain was followed over 5 days under five sinusoidal light regimes set to peak at maximal photon flux densities (PFDs) of 10, 50, 100, 250 and 500 $\mu\text{mol photons} \cdot \text{m}^{-2} \cdot \text{s}^{-1}$. We measured growth rate, pigment composition, variable fluorescence, non-photochemical quenching, electron transport rate, absorption spectrum, cell carbon and nitrogen content one to three times per day under each of these five conditions. Results suggest that *Phaeomonas* sp. RCC503 is a light-adapted species, showing a high physiological plasticity allowing it to grow under a broad range of PFD conditions. The PFD determined the growth rate, the latter being correlated significantly to photosynthetic capacity. Biochemical properties of cells, in term of carbon and nitrogen content were closely correlated to growth rate and PFD. Photoacclimation allows growth to be maintained at low irradiance except at 10 $\mu\text{mol photons} \cdot \text{m}^{-2} \cdot \text{s}^{-1}$, whereas photoprotection efficiency allows enhancement of growth at high PFDs.

Key-words: photoacclimation; picoeukaryote; xanthophyll cycle

Introduction

In the field, maximum light intensity available for photosynthesis varies predictably over daily and annual cycles; and yet, superimposed on these cycles are such factors as cloud cover that affects the amount of incoming light in an unpredictable way. For phytoplankton, and especially coastal phytoplankton, mild turbulence of the water column adds even further to this unpredictability (Lewis *et al.*, 1984; MacIntyre *et al.*, 2000; Litchman and Klausmeier, 2001); one moment a cell finds itself at depth where its photosystems must cope with low light intensity, whereas the next moment it may be transported up to the surface, where its photosystems have to adjust themselves rapidly to conditions approaching full sunlight.

Phytoplankton cells possess a number of physiological acclimation and regulatory responses to cope with these unpredictable, potentially extreme, and often rapid changes in light intensity (MacIntyre *et al.*, 2002; Raven and Geider, 2003).

Acclimation involves net synthesis or breakdown of macromolecules and so changes in pigment quota, stoichiometry of cell components and ultrastructural changes in the cell. Regulation refers to faster processes than acclimatory ones (i.e. time constants of seconds to minutes) acting through the control of enzyme activities and energy dissipation pathways (Raven and Geider, 2003). Regulatory processes therefore allow photosynthesis to react instantaneously and reversibly to the environmental changes occurring. These mechanisms include the Rubisco activity, state transition mechanism and the xanthophyll cycle (XC) (Raven and Geider, 2003).

The XC is one of the main processes involved in the dissipation of excessively absorbed light energy through the non-photochemical quenching (NPQ, Finazzi *et al.*, 2006). In green algae and higher plants, and in other algal groups (i.e. Pinguiphyceae), the XC mechanism is based on the reversible de-epoxidation of violaxanthin (Vx) into zeaxanthin (Zx) through antheraxanthin (Ax). In most chlorophyll *c* (Chl *c*) containing phytoplankton species (e.g. Diatoms), it involves the inter-conversion between diadinoxanthin (Dd) and diatoxanthin (Dt; Stransky and Hager, 1970; Lavaud *et al.*, 2007; Dimier *et al.*, 2007b). Accumulation of Zx or Dt is triggered by the formation of a pH gradient across the thylakoid membrane (e.g. see the review by Goss and Jakob, 2010).

Little is known about the picoeukaryotes with respect to their ecophysiological features (Timmermans *et al.*, 2005; Dimier *et al.*, 2007a, 2009a, b; Six *et al.*, 2008, 2009). These small planktonic photolithotrophs usually dominate oligotrophic water ecosystems,

reaching up to almost 50% of the total biomass and production, while in eutrophic waters their contribution to the phytoplankton community is lower (Not *et al.*, 2005; Worden and Not, 2008). Their small size explains many of their biological and ecological features such as the large surface area per unit volume and minimal diffusion boundary layer (i.e. higher nutrient consumption rates), low sinking rate, low packaging effect and efficient light utilization (Raven, 1998; Raven *et al.*, 2005).

High plasticity in photosynthetic regulation has been described in picoeukaryotes. For instance, Six *et al.* (Six *et al.*, 2008, 2009) highlighted different photoacclimation strategies in three ecotypes of *Ostreococcus* related to their ecological niches. Intraspecific variability has been shown in *Pelagomonas calceolata* (Dimier *et al.*, 2009a), demonstrating different photosynthetic regulation strategies in response to irradiance dynamics.

All these properties make picoeukaryotes interesting models for physiological studies aiming to analyze the functional responses of algae to environmental changes and, for instance, to photon flux density (PFD) variability. The purpose of our experimentation was to investigate the relation between growth rate, photosynthetic capacity and photoacclimative process efficiency in the coastal picoeukaryote *Phaeomonas* sp. (strain RCC503, Pinguiphyceae, Stramenopiles). Physiological response curve (PRC, Peek *et al.*, 2002) experiments were performed plotting physiological variables and growth rate against a range of PFD. The questions behind this work were: what kind of photoresponses are developed by this species when low and high light conditions are experienced? How do these responses explain photosynthetic efficiency changes?

Population growth was investigated over 5 days under five different sinusoidal light regimes set to peak at maximal PFDs of 10, 50, 100, 250 and 500 $\mu\text{mol photons} \cdot \text{m}^{-2} \cdot \text{s}^{-1}$. Pigments, variable fluorescence, NPQ, electron transport rate, absorption spectra, cell carbon and nitrogen content together with size, volume and cell concentrations were measured one to three times per day during the exponential phase.

Method

Algal model and culture conditions

The strain RCC503 of *Phaeomonas* sp. (Pinguiphyceae) was isolated along the Mediterranean Spanish coast and was provided by the Roscoff Culture Collection (Vaultot *et al.*, 2004). The strain was cultivated nonaxenically at 20°C at 100 $\mu\text{mol photons} \cdot \text{m}^{-2} \cdot \text{s}^{-1}$ with a 11 : 13 h light : dark photoperiod in locally obtained, and sterilized seawater amended with *f/2* medium (Guillard and Ryther, 1962) using 225 cm² polystyrene canted-neck flasks (Corning Incorporated, NY, USA). Cultures were continuously aerated and maintained in the exponential phase by daily and semi-continuous dilution (50% of the total volume) over a period of more than 2 weeks before the experiments. Before performing experiments, we checked pre-acclimation of the strain to the light condition, by assessing stability of pigment content and growth rate.

Experimental design and sampling strategy

After 15 days acclimation period at 100 $\mu\text{mol photons} \cdot \text{m}^{-2} \cdot \text{s}^{-1}$, cultures were subjected to five different sinusoidal light (SL, Fig. 6.1 a) regimes, each with a different maximal PFD of 10 (LL1), 50 (LL2), 100 (ML), 250 (HL1) and 500 (HL2) $\mu\text{mol photons} \cdot \text{m}^{-2} \cdot \text{s}^{-1}$, respectively. The mean PFD over the 11 h of illumination ranged between 344 and 7 $\mu\text{mol photons} \cdot \text{m}^{-2} \cdot \text{s}^{-1}$, which is likely similar to the light experienced by cells at a depth of 10 m and at the deep chlorophyll maximum layer in a Mediterranean water column, respectively (Dimier *et al.*, 2009a).

Population growth was followed over 5 days while photophysiological and biochemical properties of *Phaeomonas* sp. were measured during the exponential growth phase. Under the LL conditions, where no exponential phase was observed, sampling of photophysiological and biochemical parameters lasted 5 days.

Each experiment was performed in triplicate. Flasks were illuminated by the light-bulb kit ACLS (Advanced Control Lighting System) and Infinity XR4 (Aquarium Technologies, Sfiligoi S.r.l., Bassano del Grappa, Italy), simulating light–dark sinusoidal cycles, reproducing dawn and sunset. XR4 is equipped with metallic iodur HQI bulbs (10 000 K). The PFD was measured with a 4π quantameter (sensor QSL 2101, Biospherical Instruments Inc., San Diego, CA, USA).

Cultures were sampled three times per day (Fig. 6.1 a). The first sampling was carried out during dawn (for HL2 condition, incident irradiance was below $40 \mu\text{mol photons} \cdot \text{m}^{-2} \cdot \text{s}^{-1}$), while the second corresponded with the irradiance peak. The third one was carried out during sunset (HL2 incident irradiance was below $40 \mu\text{mol photons} \cdot \text{m}^{-2} \cdot \text{s}^{-1}$). Twenty to 50 mL of culture was rapidly taken with a 50 mL syringe during each sampling time, for measuring variable fluorescence, NPQ, electron transport rate and for further analysis of pigments, absorption spectrum, cell size and volume (by Coulter Counter analysis) and cell concentrations (by microscopic counts).

Temperature and pH were controlled daily with an HI-9214-Stick pH meter (Hanna Instruments, Woonsocket, RI, USA). The growth rate was estimated daily from cell abundance measurements using the following equation:

$$\mu = \ln [N_{t_2} : N_{t_1}] : [t_2 - t_1] \quad (6.1)$$

where μ is the growth rate (day^{-1}) and Nt is the mean cell concentration at time t , and t_1 and t_2 correspond to the morning sampling time of Days 1 and 2, respectively. From the growth rate, the number of cell divisions (n) per day was estimated with the following equation:

$$n = \mu : [\ln (2)] \quad (6.2)$$

where n is the number of cell divisions per day and μ is the growth rate.

Pigment analysis

One aliquot of algal culture (10 mL) was filtered onto GF/F glass-fiber filters (Whatman) and immediately stored in liquid nitrogen until analysis. Triplicate samples were taken during each sampling time. Analysis was carried out following the procedure described in Dimier et al. (Dimier *et al.*, 2007a). The pigment extract was injected in a Hewlett Packard series 1100 HPLC (Hewlett Packard) with a C8 BDS 3 mm Hypersil, IP column (Thermo Electron). The mobile phase was composed of two solvent mixtures: methanol and aqueous ammonium acetate (70 : 30) and methanol. Pigments were detected spectrophotometrically at 440 nm using a Model DAD, Series 1100 Hewlett Packard photodiode array detector. Fluorescent pigments were detected in a Hewlett Packard

standard FLD cell series 1100 with excitation and emission wavelengths set at 407 and 665 nm, respectively. Determination and quantification of pigments used pigment standards from D.H.I. Water & Environment (Hørsholm, Denmark).

Variable fluorescence and NPQ

Only during the irradiance peak sampling time, samples for PAM measurements were taken. Photochemical efficiency of PSII was estimated by a Phyto-PAM Fluorometer (Heinz Walz GmbH, Effeltrich, Germany). Triplicate measurements of variable fluorescence were performed on both light- and 15-min dark-acclimated samples. The maximum photochemical efficiency ($F_v : F_m$, with $F_v = F_m - F_o$) was measured on 15-min dark-acclimated sample during the irradiance peak sampling time. F_m and F_m' were measured after a saturating pulse of red light ($2400 \mu\text{mol photons} \cdot \text{m}^{-2} \cdot \text{s}^{-1}$ for 450 ms) causing a complete reduction of the PSII acceptor pool.

The NPQ of fluorescence was quantified by the Stern–Volmer expression:

$$\text{NPQ} = (F_m : F_m') - 1 \quad (6.3)$$

Electron transport rate (ETR) *versus* light curves were determined on 15-min dark-exposed samples applying 10 increasing irradiances (I , from 1 to $1500 \mu\text{mol photons} \cdot \text{m}^{-2} \cdot \text{s}^{-1}$ for 2 min each). The absolute electron transport rate (expressed in $\text{e}^- \text{g Chl } a^{-1} \text{h}^{-1}$) was calculated as follows:

$$\text{absETR} = (F_v' : F_m') \cdot I \cdot (a_{\text{ph}}^* : 2) \quad (6.4)$$

where I is the incident irradiance ($\mu\text{mol photons} \cdot \text{m}^{-2} \cdot \text{s}^{-1}$). The mean absorption value (a_{ph}^*) of phytoplankton was normalized by Chl a ($\text{m}^2 \text{mg Chl } a^{-1}$) and divided by 2 assuming that half of the absorbed light was distributed to PSII.

The ETR-light curves were fitted with the equation of Eilers and Peeters (Eilers and Peeters, 1988) to estimate the photosynthetic parameters α^B , E_k , and $\text{absETR}_{\text{max}}$. The relative electron transport rate ($\text{relETR}_{\text{max}}$) was estimated with equation (4) without Chl a normalization.

Organic carbon and nitrogen

Samples for the determination of particulate organic carbon (POC) and particulate organic nitrogen (PON) were filtered on pre-combusted (450°C, 5 h) glass fiber filters (Whatman GF/F) and immediately stored at -20°C. The analyses were performed with a FlashEA 1112 Series Thermo Electron CHN elemental analyzer (Hedges and Stern, 1984). Cyclohexanone-2,4-dinitrophenyl hydrazone was used as standard.

Absorption spectrum

Ten millilitres samples were filtered onto Whatman GF/F filters and immediately frozen. Measurements were carried out following the procedure described in Dimier *et al.* (Dimier *et al.*, 2007a). Absorption was measured between 280 and 800 nm with 1-nm increments on a spectrophotometer (Hewlett Packard HP-8453E) equipped with an integrating sphere (Labsphere RSA-HP-53). The mean absorption value (a^*) was thus normalized by the Chl *a* concentration of the sample to obtain the Chl *a*-specific absorption coefficient (a^*_{ph} , m² mg Chl *a*⁻¹).

Results

Growth

Phaeomonas sp. was able to grow under the entire range of light conditions with the exception of LL1 (10 $\mu\text{mol photons} \cdot \text{m}^{-2} \cdot \text{s}^{-1}$) and showed the highest growth rate under the highest light regime (Fig. 6.1 b). At the end of the exponential phase for the HL and ML conditions or at Day 5 for LL conditions, where no exponential phase was found, cell concentrations ranged between $1.77 \times 10^4 \pm 1.98 \times 10^3$ and $3.66 \times 10^5 \pm 9.15 \times 10^4$ cells mL⁻¹ following a positive light gradient. The number of divisions per day ranged between 0 and 0.44 day⁻¹. Cell size and volume were $3.27 \pm 0.07 \mu\text{m}$ and $18.65 \pm 0.95 \mu\text{m}^3$, respectively. Only under the lowest PFD, do cells show a decrease of size and volume ($2.86 \pm 0.02 \mu\text{m}$ and $12.28 \pm 0.19 \mu\text{m}^3$).

Photosynthetic pigments

Together with Chl *a*, many accessory pigments were present in the LHCs of *Phaeomonas* sp. and the main ones were the following: chlorophyll (Chl) *c*₂, fucoxanthin (Fuco), *cis*-fucoxanthin (*cis*-Fuco), neoxanthin (Neox), Chl *c*₃ and β -carotene (β -Car).

The mean Chl *a* content per cell was significantly higher in LL conditions compared with the ML or HL ones, ranging between $9.96 \times 10^{-17} \pm 1.93 \times 10^{-17}$ and $2.82 \times 10^{-16} \pm 7.13 \times 10^{-17}$ mol Chl *a* cell⁻¹ (Fig. 6.2 a). It can be seen that a higher Chl *a* cell⁻¹ value was measured under HL2 relative to HL1.

Lowering of the light-harvesting capacity under high light was revealed by the decrease of almost all main accessory pigments (Figs. 6.2 b and c), in agreement with the lower Chl *a*-specific absorption coefficient (a_{ph}^* , data not shown). Following their distribution over the different PFD gradients, three groups of accessory pigments could be defined. The first group was formed by Chl *c*₂ and fucoxanthin (Figs. 6.2 b and c, respectively) as well as violaxanthin and antheraxanthin (see XC paragraph) showing similar values at LL1 and LL2. Minor pigments such as Chl *c*₃, *cis*-fucoxanthin and β -carotene (Figs. 6.2 b and c, respectively) belonged to the second group characterized by an increase from LL2 to LL1, as the Chl *a* pool. Pigments of the third group, neoxanthin (Fig. 6.2 d) and violaxanthin (see XC paragraph), showed a strong increase under HL conditions. The uncoupling between Chl *a* and the main photosynthetic accessory pigments in response to light change could be a signal of a special photoacclimative strategy developed by this species under low light stress.

Organic carbon and nitrogen

Cellular carbon and nitrogen concentrations were significantly correlated ($P < 0.001$) and both strongly related to PFD regimes with lower concentrations under high light and vice versa (Fig. 6.3 a).

The Chl *a* : POC ratio varied slightly, increasing a little from LL to HL regimes (Fig. 6.3 b), mainly due to the decrease of POC along the light gradient.

The POC : PON ratio, ranging between 4.80 ± 0.24 and 6.82 ± 0.08 , increased from low to high PFD regime (Fig. 6.3 c) and was significantly correlated to the growth rate ($R^2 = 0.98$, Fig. 6.3 d).

Photosynthetic parameters

The maximal photosynthetic rate (${}_{\text{abs}}\text{ETR}_{\text{max}}$) increased from the LL to HL regimes, reaching a maximum at HL1 and then decreasing a little under HL2 (Fig. 6.4 a).

A significantly correlated trend between ${}_{\text{abs}}\text{ETR}_{\text{max}}$ and growth rate was observed (Fig. 6.4 b).

Under HL2, Chl *a* enhancement without any related increase in the electron transport rate prevented this light condition fitting a linear regression. Indeed, when ETR was not reported in relation to the Chl *a* concentration, the relationship between $\text{relETR}_{\text{max}}$ and growth rate was highly significant and linear over all the PFD range ($R^2 = 0.92$; Fig. 6.4 c). The photosynthetic efficiency (α^{B} , Fig. 6.4 d) showed a maximum under the ML condition in agreement with the $100 \mu\text{mol photons} \cdot \text{m}^{-2} \cdot \text{s}^{-1}$ pre-acclimation period of cells, and decreased with higher PFDs. Low values of α^{B} under LL1 and LL2 (similar to the HL1 and HL2) might reflect a limited capacity for photosynthetic acclimation at low PFDs. Indeed, the light saturation index (E_k) did not decrease under the value of $200 \mu\text{mol photons} \cdot \text{m}^{-2} \cdot \text{s}^{-1}$, whereas it increased to almost $1000 \mu\text{mol photons} \cdot \text{m}^{-2} \cdot \text{s}^{-1}$ in agreement with the light-acclimated state of this species (Fig. 6.4 e). The high values of E_k indicated that cells were subjected to limiting or suboptimal irradiance during light periods in all the five experimental conditions. The amplitude of light limitation, estimated with the $E_k : \text{PFD}$ ratio, ranged between 24 and 2 (Fig. 6.4 f), with LL1 and LL2 having values higher than 10.

Photophysiology and the xanthophyll cycle

The PSII maximum photochemical efficiency ($F_v : F_m$) showed a small range of variation, with the highest value under LL1 (0.61, Fig. 6.5 a) and the lowest under HL1 (0.56, $250 \mu\text{mol photons} \cdot \text{m}^{-2} \cdot \text{s}^{-1}$). Under HL1 and HL2, *Phaeomonas* sp. developed NPQ (Fig. 6.5 b), while it did not under lower PFD regimes, with the exception of LL1.

A significant linear correlation was found between NPQ and the photoprotective pigment zeaxanthin [$Z_x : (V_x + A_x + Z_x)$], suggesting a relevant role of Z_x in the development of NPQ in *Phaeomonas* sp. (Fig. 6.6 a). Z_x contribution to the XC was low (less than 10%), revealing the limited need for photoprotection, in relation with the gradual PFD increase and the not so extreme irradiance peak applied during the experimental conditions.

The highest values of Zx were found in cultures grown under HL1 and HL2 (Fig. 6.6 b). The two pigments Vx and Ax, expressed per cell (data not shown), followed the same trend of Chl *a* and other accessory photosynthetic pigments cell⁻¹ (Fig. 6.2).

Daily evolution of Zx (Fig. 6.6 c) showed that only under the HL2 condition did this pigment increase significantly at midday. Even though NPQ was similar between the two HLs, Zx concentration differed between the two conditions suggesting that a proportion of zeaxanthin was not involved in NPQ development. The morning value of Zx under the HL2 regime was higher than the values measured during each of the HL1 sampling times, revealing a daily persisting photoprotective state.

Discussion

The Chl *a* content in *Phaeomonas* sp. RCC503 ($\sim 2 \times 10^{-16}$ mol Chl *a* cell⁻¹, cell size ~ 3.3 μm) is in the range of values measured in other small-size algal species (Dimier *et al.*, 2007a, 2009b). Combining this study with data from Dimier *et al.* (Dimier *et al.*, 2009b), a highly significant correlation between the size and the Chl *a* cell⁻¹ content was obtained (six species with the size ranging between 1.8 and 4.0 μm , $R^2 = 0.92$) proving the direct relevance of size in determining pigment content in small species. Taxonomical difference does not affect the relation between size and Chl *a*, while processes such as photoacclimation have a small effect on this relation in picoeukaryotes (Dimier *et al.*, 2009b, this study). Indeed, variations in cell size are so small over the irradiance range that any allometric effect (Finkel *et al.*, 2010) becomes undetectable.

PRCs show that *Phaeomonas* sp. RCC503 grows properly under a broad range of PFD (from 100 to 500 $\mu\text{mol photons} \cdot \text{m}^{-2} \cdot \text{s}^{-1}$), meaning it was able to adequately cope with different light environments owing to efficient photoacclimative processes concerning both cell physiology and biochemistry. This is consistent with its origin from a Mediterranean coastal area, i.e. it is adapted to grow under variable light conditions.

Increase in Chl *c*₃ under low light has been found in many species both in laboratory (Rodriguez *et al.*, 2006; Dimier *et al.*, 2009a) and in field experiments, where higher Chl *c*₃ values were found in the deep chlorophyll maximum layer (Brunet *et al.*, 2007), in agreement with its efficient role in light harvesting (Johnsen and Sakshaug, 1993). Thus, our study reinforces the hypothesis of a photoacclimative role of this pigment and demonstrates that changes in Chl *c*₃ are independent of other pigments, such as

fucoxanthin, Chl c_2 and Chl a . Since Chl c_3 is broadly present in phytoplankton species, and in many picoeukaryotes, this result would further need investigation to understand the ecological advantage in synthesizing such a pigment and how its synthetic pathway would work.

The significant relation between the photosynthetic rate, cell biochemistry changes and growth rate suggests a direct and functional link between the PFD, photoacclimation, photosynthetic and growth rate. In many studies, the variability of the relationship between photosynthetic organic matter production and cell growth has been highlighted (Litchman, 2000), growth and photosynthetic parameters being poorly coupled (van Leeuwe *et al.*, 2005). This variability has been attributed to factors such as variations in respiration rates, dissolved organic matter loss from cells and changed extent of the storage of metabolites such as polysaccharides (van Leeuwe *et al.*, 2005).

The observed result is probably linked to the experimental conditions we applied. Simulating what occurs in nature, the sinusoidal irradiance evolution causes cells to experience a low or moderate daily integrated PFD with a short irradiance peak. Our experimental conditions prevented either continuous high light or continuous limited light stress as occurs under quadratic light evolution. Small cell size limits the intracellular storage of energy (Raven, 1998) that might enhance the coupling of photosynthesis and growth rate, as already discussed by Dimier *et al.* (Dimier *et al.*, 2009a) for the picoeukaryote *Pelagomonas calceolata*.

Growth rate is linearly related to both E_k : PFD ($R^2 = 0.96$, $P < 0.001$) and the POC : PON ratio ($R^2 = 0.98$, $P < 0.001$), these two ratios being correlated ($R^2 = 0.95$, $P < 0.001$). These results indicate a functional and linear link between PFD and growth rate through photosynthetic rate adjustments and consequently changes in cellular biochemistry. The great range of variation of the POC : PON ratio (35%, between 4.80 and 6.50) reveals significant biochemical modifications related to irradiance and growth rate variations (e.g. Finkel *et al.*, 2010).

Higher values of POC : PON obtained under the higher PFD conditions are close to the Redfield ratio, a result that led us to reinforce the hypothesis of an optimal physiological state of cells under high light.

Growth rate being the highest under the HL2 condition, the photoacclimative strategy adopted by *Phaeomonas* sp. is efficient. This species belongs to the 'light adapted' functional category (Falkowski and Owens, 1980; Falkowski, 1983), as also suggested by the high light saturation for photosynthesis (E_k) estimated from the ETR-light curves.

Under the HL2 condition, the small decrease of maximal photosynthetic rate per Chl *a* unit ($_{\text{abs}}\text{ETR}_{\text{max}}$) compared to the HL1 condition while the growth rate still increased relatively could be due to the Chl *a* cell^{-1} increase. Indeed, the relation between $_{\text{rel}}\text{ETR}_{\text{max}}$ and growth rate is linear over the light gradient (Fig. 6.4 c). Increase in both Chl *a* and accessory photosynthetic pigments under the HL2 condition suggests the development of a σ -type photoacclimation strategy aiming to increase the size of light-harvesting antennae (Six *et al.*, 2008; Dimier *et al.*, 2009a). Increase in photosynthetic pigments under the highest PFD condition was surprising since cells developed photoprotection when irradiance reached its maximum. In comparison with the HL1 condition, where no pigment increase was noticeable, pigment enhancement under HL2 condition might be related to the strongest photoprotection. Both the higher level of Zx and its persistent presence in cells growing under the HL2 condition (even before the irradiance peak) indicate a photoprotective state of PSII.

The photoprotective state of HL2 and HL1 cells would also lead to a decreased photosynthetic efficiency, which is demonstrated by the decrease of α^{B} . Since the gradual PFD increase, cells quickly perform photophysiological regulation processes, explaining both the low value of DPS (< 15%) and its efficiency in protecting PSII (Dimier *et al.*, 2009a). The highest NPQ value has been reached already under HL1 and no further increase can be observed under HL2, probably in relation to the development of other photoprotective mechanisms such as PSII conformational changes.

Additional molecules of Zx under the HL2 condition do not have a direct role in NPQ functioning. It is known that Zx molecules are able to indirectly protect PSII through changes in thylakoidal membrane fluidity, or by preventing lipid peroxidation (Goss and Jakob, 2010). The neoxanthin trend is similar to the one of Zx either over the irradiance range (Fig. 6.2 d) or over the day under HL2 (data not shown). This feature might be related to a role of Neox in preserving PSII from photoinactivation and protecting membrane lipids as recently demonstrated in plants (Dall'Osto *et al.*, 2007).

This photoprotective status found in cells grown under HL2 might be explained by the rapid kinetics of PFD increase, also linked to the higher irradiance reached, or also by the increase in accessory photosynthetic pigments, which might have enhanced the sensitivity of PSII to high light. The role of photoprotective pigments as a trap for a part of the harvested electrons would thus decrease the quantum yield leading to an energy-deficient state during low light periods that would in turn require an increase in the light-harvesting pigment content. This last hypothesis supposes a feedback relationship between

photoprotection and photoacclimation aiming to enhance the light-harvesting capacity of cells. Cells would perceive both high light values and low light dose per day (e.g. through the time spent under low light) and respond to both these factors. Such a special physiological plasticity is likely to occur in species growing in coastal waters, where high vertical mixing implies fast shifts between high and low light conditions. This hypothesis agrees with the results obtained by Dimier *et al.* (Dimier *et al.*, 2009b), where it has been shown that coastal species are physiologically ‘intermediary’ compared to surface-offshore and deep water species, in terms of both photosynthetic and photoprotective pigment content. Further studies are needed to test this hypothesis and to obtain clearer knowledge on the ecophysiological capacity of coastal phytoplankton, such as many diatoms, to efficiently photoacclimate and photoprotect themselves.

Phaeomonas sp. is not able to grow under strong light limitation (e.g. for E_k : PFD ratio > 10). The fact that the increase in Chl *a* is not coupled with an increase in photosynthetic accessory pigments might suggest an enhancement in the number of PSII reaction centers more than in the size of the light-harvesting complexes, distinctive of an *n*-type photoacclimation strategy (Six *et al.*, 2008). The heavy nutrient cost for low light growth required by the *n*-type photoacclimation strategy and its higher energy cost (Six *et al.*, 2008) can limit or inhibit growth (Dimier *et al.*, 2009b).

The same photoacclimation strategy has been observed in other picoeukaryotes, the lagoon ecotype of *Ostreococcus tauri* (Six *et al.*, 2008) and the low light-adapted *Pelagomonas calceolata* (Dimier *et al.*, 2009a). The latter (Dimier *et al.*, 2009a) as well as the present study have shown how some species can develop either the σ - or *n*-type photoacclimation strategy in relation to the light conditions experienced. The *n*-type photoacclimation strategy would evolve when the daily PFD dose is very low or when cells spend a long time under low light in order to increase their photochemistry (Dimier *et al.*, 2009a). This result differs from what was shown by Six *et al.* (Six *et al.*, 2008) in two *Ostreococcus* ecotypes (Six *et al.*, 2008), where the *n*-type photoacclimation evolved in the lagoon ecotype with decreasing growth irradiance. The inconsistency between these studies could be related to the differences of experimental design, since the present study (Dimier *et al.*, 2009a) applied a sinusoidal irradiance regime, whereas the work done by Six *et al.* (Six *et al.*, 2008) employed a continuous irradiance over the light period. Supporting such a hypothesis, Dimier *et al.* (Dimier *et al.*, 2009a) showed that the main factor responsible for developing the *n*- or σ -type photoacclimation was the frequency of irradiance variation during the daylight period.

The very low light condition surprisingly induces both NPQ generation and little increase in Zx and Neox. Zx and NPQ formation reveals the development of a trans-thylakoidal proton gradient, probably caused by chlororespiration (Goss and Jakob, 2010, and references therein) or by a putative water–water cycle (Mehler’s reaction, Badger *et al.*, 2000). It is noteworthy that Neox has a role against photo-oxidation and would be particularly active when Mehler’s reaction takes place (Dall’Osto *et al.*, 2007).

Acknowledgements

The authors gratefully acknowledge F. Tramontano for his help during experiments and HPLC analysis. E. Saggiomo and F. Margiotta are acknowledged for helping during the use of the spectrophotometer and the CHN, and for sharing the PAM probe. The authors would like to thank Dr. D. Campbell and the other anonymous referee, for their comments and helpful suggestions for improving the quality of the manuscript.

Funding

This research was funded by the Stazione Zoologica A. Dohrn. V.G.’s PhD was granted by the Stazione Zoologica A. Dohrn.

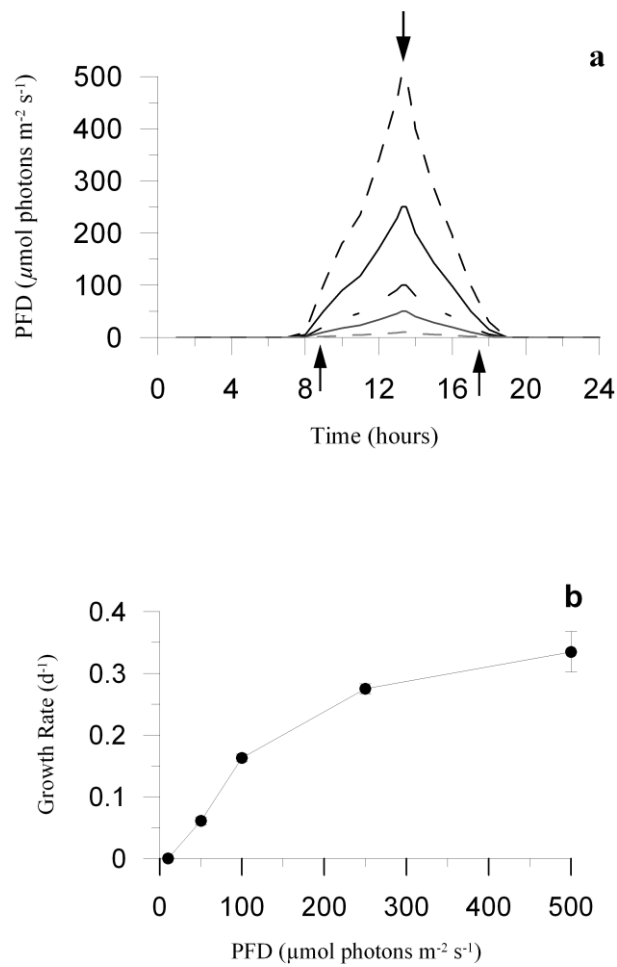


Fig. 6.1: (a) The five sinusoidal light regimes applied during the study, with different maximal PFD peaks (10, 50, 100, 250 and 500 $\mu\text{mol photons m}^{-2} \text{s}^{-1}$, respectively). Arrows indicate sampling. (b) Evolution of growth rate of *Phaeomonas* sp. over the light conditions. Data are the average of three measurements per 3 days (corresponding to the exponential growth phase for HL and ML conditions); error bars are SD.

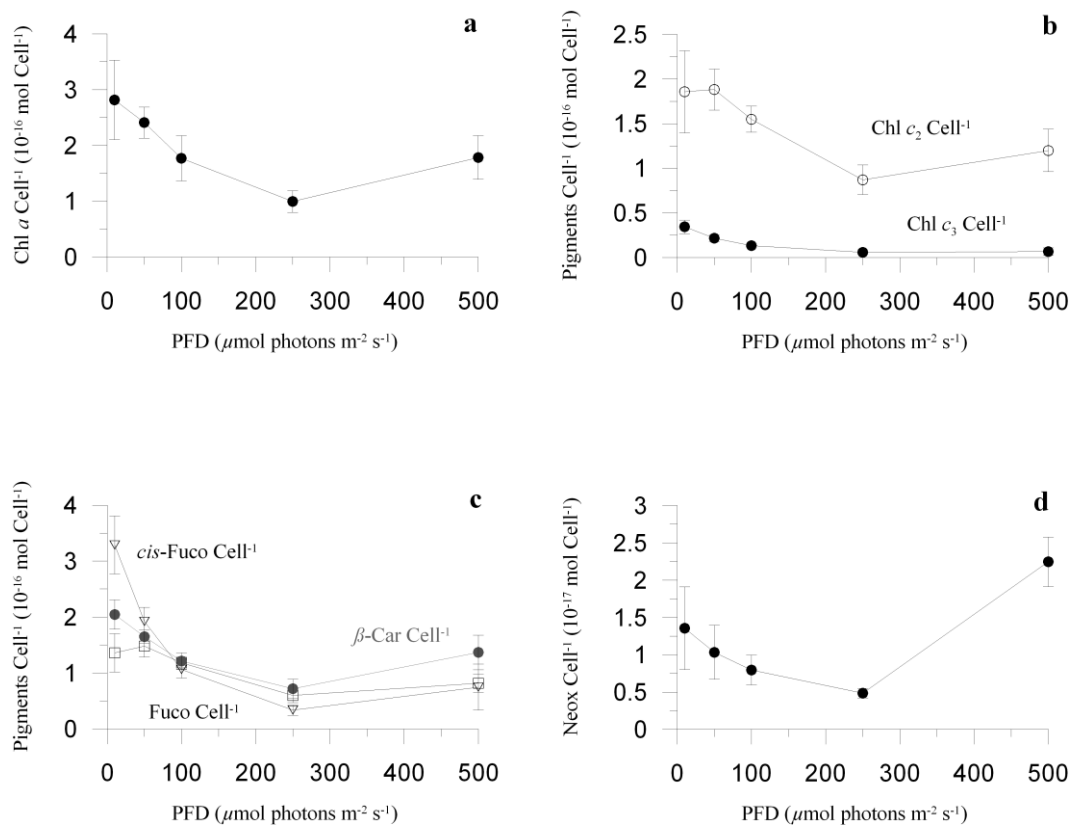


Fig. 6.2: Evolution of: chlorophyll *a* cell⁻¹ expressed in 10⁻¹⁶ mol Chl *a* cell⁻¹ (a), chlorophyll *c*₂ cell⁻¹ (white dots) and chlorophyll *c*₃ cell⁻¹ (black dots) expressed in 10⁻¹⁶ mol pigment cell⁻¹ (b), fucoxanthin cell⁻¹ (white squares), *cis*-fucoxanthin cell⁻¹ (white triangles) and β -carotene cell⁻¹ (grey dots) expressed in 10⁻¹⁶ mol pigment cell⁻¹ (c), and neoxanthin cell⁻¹ content in 10⁻¹⁷ mol pigment cell⁻¹ (d), over the five PFD conditions. Chl *a*, chlorophyll *a*; Chl *c*₂ and *c*₃, chlorophyll *c*₂ and *c*₃; Fuco, fucoxanthin; *cis*-Fuco, *cis*-fucoxanthin; β -Car, β -carotene; Neox, neoxanthin. Data are the average of three measurements per 3 days (corresponding to the exponential growth phase for HL and ML conditions); error bars are SD.

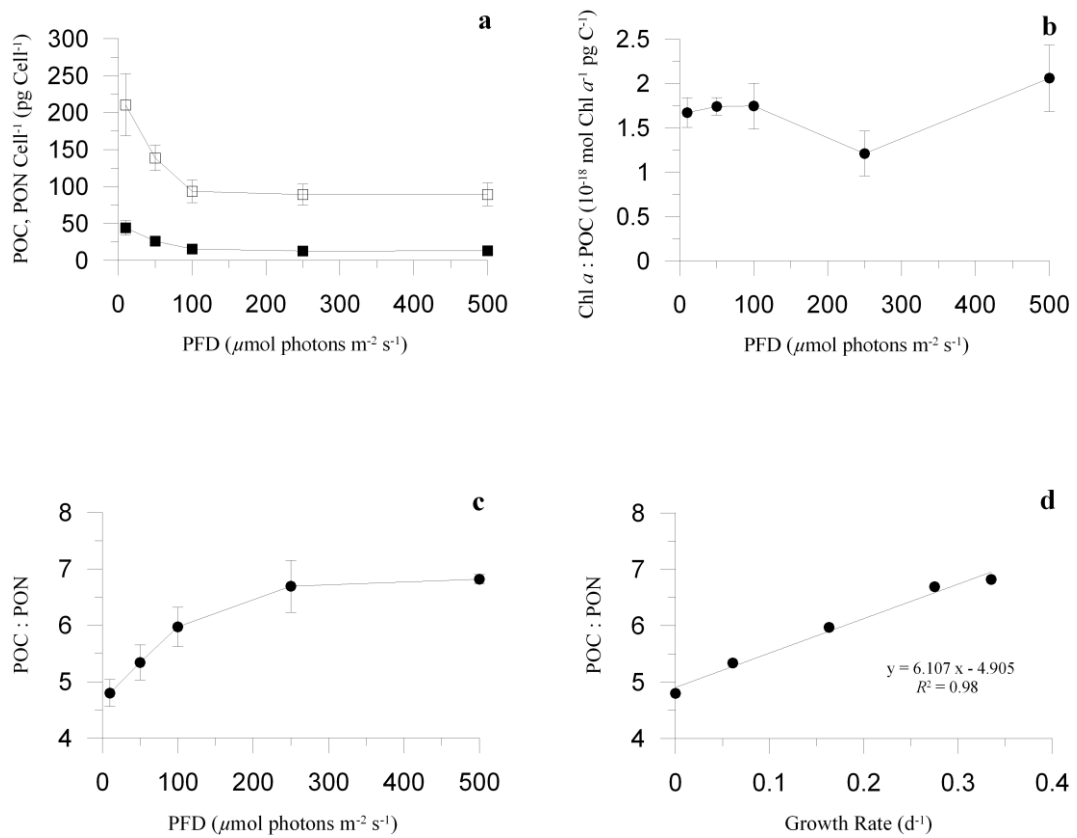


Fig. 6.3: Evolution of: cellular organic carbon (POC, white squares) and nitrogen (PON, black squares) concentrations (pg cell⁻¹) (a), Chl *a* : POC ratio expressed in 10⁻¹⁸ mol Chl *a*⁻¹ pg C⁻¹ (b), and POC : PON ratio (c), over the five PFD conditions. Relationship between POC : PON ratio and growth rate ($R^2 = 0.98$; d). Data are the average of three measurements per 3 days (corresponding to the exponential growth phase for HL and ML conditions); error bars are SD.

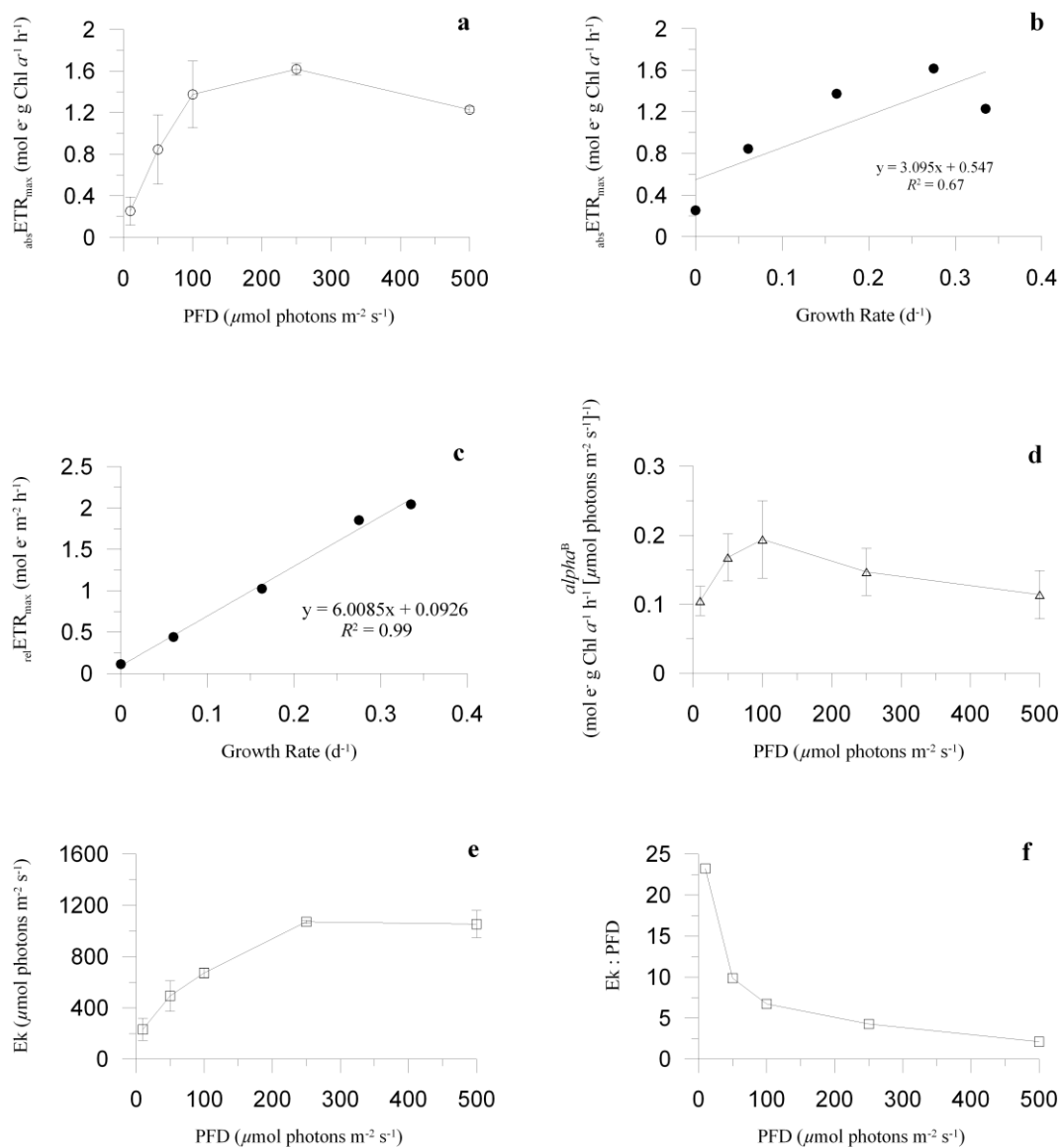


Fig. 6.4: (a) Evolution of the maximal photosynthetic rate $\text{abs ETR}_{\text{max}}$ (in $\text{mol e}^- \text{g Chl a}^{-1} \text{h}^{-1}$) over the five PFD conditions. Relationship between growth rate and $\text{abs ETR}_{\text{max}}$ (b) or $\text{rel ETR}_{\text{max}}$ (c). Evolution of α^B ($\text{mol e}^- \text{g Chl a}^{-1} \text{h}^{-1} [\mu\text{mol photons m}^{-2} \text{s}^{-1}]^{-1}$; d), E_k (in $\mu\text{mol photons m}^{-2} \text{s}^{-1}$; e) and $E_k : \text{PFD}$ ratio (f) over the five PFD conditions. Data are the average of three measurements per 3 days (corresponding to the exponential growth phase for HL and ML conditions); error bars are SD.

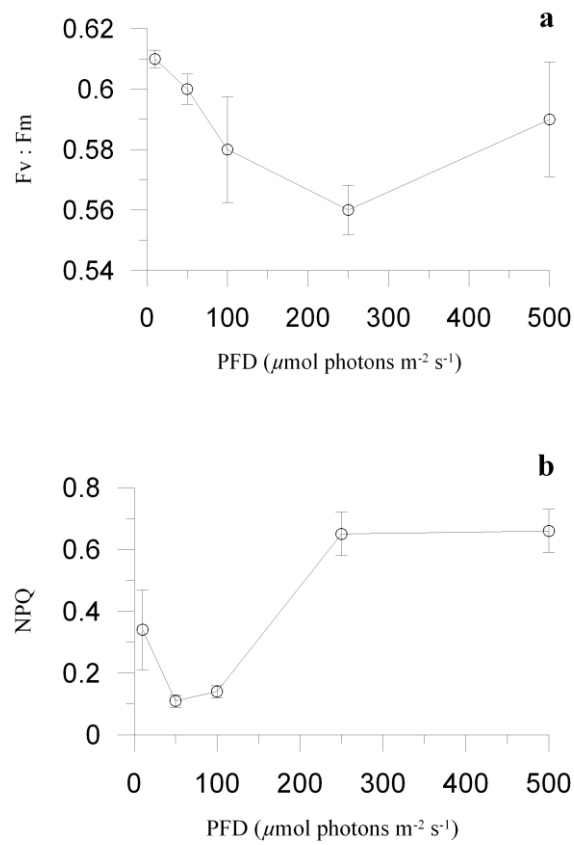


Fig. 6.5: Evolution of the maximal photochemical efficiency (Fv : Fm; **a**) and non-photochemical fluorescence quenching (NPQ; **b**) over the five PFD conditions. Data are the average of three measurements per 3 days (corresponding to the exponential growth phase for HL and ML conditions); error bars are SD.

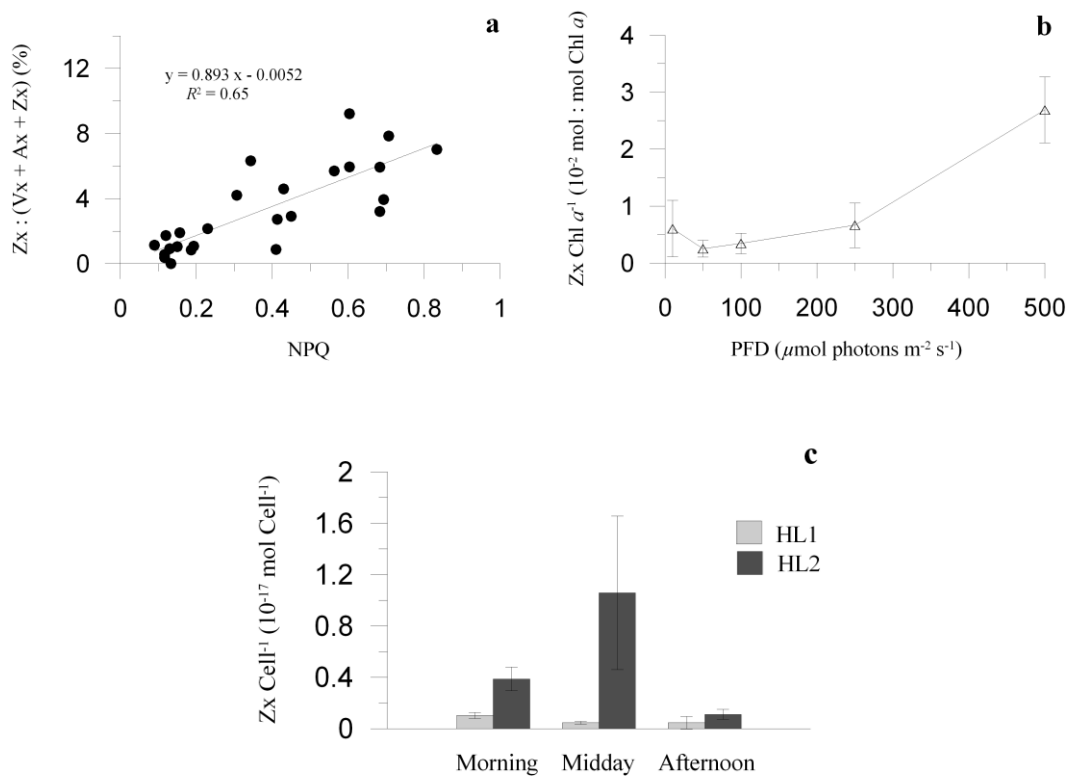


Fig. 6.6: (a) Relationship between Zx : (Vx + Ax + Zx) and NPQ. (b) Evolution of zeaxanthin Chl a^{-1} (Zx Chl a^{-1} in 10^{-2} mol : mol Chl a) over the five PFD conditions. (c) Mean of zeaxanthin cell $^{-1}$ in the three samples of the dawn, irradiance peak and sunset under the HL1 and HL2 regimes. Data are the average of three measurements per 3 days (corresponding to the exponential growth phase for HL and ML conditions), error bars are SD.

CHAPTER 7

**Growth and photophysiological response curves of
the two picoplanktonic *Minutocellus* sp. RCC967
and RCC703 (Bacillariophyceae)**

Chapter 7

Growth and photophysiological response curves of the two picoplanktonic *Minutocellus* sp. RCC967 and RCC703 (Bacillariophyceae)

This chapter corresponds to a paper which has been recently submitted in EUROPEAN JOURNAL OF PHYCOLOGY.

To deepen the knowledge on picoeukaryotes ecophysiology, the relation between photophysiological functional abilities and niche adaptation has been tackled and compared in two picoplanktonic diatoms (Bacillariophyceae, Stramenopiles), isolated from distinct aquatic ecosystems, i.e. upwelling (*Minutocellus* sp. RCC967) and oceanic waters (*Minutocellus* sp. RCC703). The two species underwent the same experimental design described in Chapter 6, allowing for further comparisons on ecophysiological properties, photosynthesis and growth regulation, in the three picoeukaryotic species that have been used to conduct experiments during my PhD (see Chapter 8).

The obtained results were discussed in the light of functional plasticity and marine ecosystem adaptation.

Growth and photophysiological response curves of the two picoplanktonic *Minutocellus* sp. RCC967 and RCC703 (Bacillariophyceae)

V. GIOVAGNETTI, M. L. CATALDO, F. CONVERSANO AND C. BRUNET*

STAZIONE ZOOLOGICA ANTON DOHRN, VILLA COMUNALE, 80121 NAPLES, ITALY

*: CORRESPONDING AUTHOR: christophe.brunet@szn.it

RECEIVED

Short running title: Comparative photophysiology of picoplanktonic diatoms

Abstract

Reaching up to 50 percent of the total biomass in oligotrophic waters, and armed with a set of ecological and biological properties related to their small size, picophytoplankton ($< 3.0 \mu\text{m}$) are a good model to address ecophysiological questions regarding phytoplankton biodiversity. Two picoplanktonic diatoms isolated from an upwelling ecosystem in the Pacific Ocean (*Minutocellus* sp. RCC967), and from oceanic waters in the Indian Ocean (*Minutocellus* sp. RCC703) have been used to test hypothesis on the functional relation between ecological niche adaptation, and photosynthetic regulation capacity and efficiency. Cultures were subjected to five sine irradiance climates each one set to peak at different photon flux densities (PFD) of 10, 50, 100, 250 and 500 $\mu\text{mol photons} \cdot \text{m}^{-2} \cdot \text{s}^{-1}$. Growth rate, photosynthesis, non-photochemical fluorescence quenching (NPQ), pigment composition, elemental composition and macromolecular pools allocation were followed daily during five days. Growth rate and physiological response curves were different in the two species, in agreement with their distinct habitat of origin. Such a difference could be related to the diverse photoacclimative strategies displayed by the two species, revealing a clear adaptative divergence despite their close phylogenetic relationship. Photoacclimative strategies of the two picoplanktonic diatoms are discussed in the light of functional diversity and ecosystem adaptation.

Key words: diatoms, photoacclimation, picoeukaryotes, xanthophyll cycle

Introduction

Diatoms (Bacillariophyceae) are photosynthetic O₂-evolvers ubiquitously widespread over marine ecosystems. They constitute the most prominent and diversified group of eukaryotic phytoplankton populating the ocean, with almost 200,000 different species covering a wide range of cell size and shapes (Kooistra *et al.*, 2007; Armbrust, 2009).

They are approximately responsible for 40% of the oceanic primary production, and hence essential players in the oceanic carbon pump process, as well as in the biogeochemical cycles of silica (compound of their frustule) and nitrogen (Smetacek, 1999; Armbrust, 2009). Being involved in quite all the coastal areas spring blooms and characterized by an impressive ecological and biological diversity, high interest and effort have been led by the scientific community to expand the knowledge of diatoms ecophysiology and biology. Indeed, diversity in diatoms has been also established at a functional level, for instance through their adaptation to the abiotic properties of the ecosystem in which they grow (Strzepek and Harrison, 2004; Lavaud *et al.*, 2007; Dimier *et al.*, 2007b).

Nutrients availability and irradiance, the latter being occasionally limiting or inhibiting, mostly affect phytoplankton growth and thus can be considered as key-factors for algal adaptation to aquatic ecosystems. In the pelagic ecosystem, irradiance is one of the most relevant variables regulating phytoplankton growth rate, and doubtlessly the most fluctuant upon a large range of temporal and spatial scales (MacIntyre *et al.*, 2000). Cells need to continuously adjust their photoacclimative states to cope with irradiance intensity changes, in order to maximize the photosynthetic rate, and prevent photoinhibition or photodamage due to harmful excitation-energy pressure (Raven and Geider, 2003). The fastest photoprotective reaction corresponds to the non-photochemical fluorescence quenching (NPQ), leading to thermal dissipation of excessive irradiance energy in photosystem II (PSII). NPQ development seems to be directly correlated to the xanthophyll cycle activation (XC; Goss and Jakob, 2010). As in most chlorophyll *c* (Chl *c*)–containing phytoplankton species, in diatoms the XC consists of a single and reversible de-epoxidation step in which the epoxy carotenoid diadinoxanthin (Dd) is converted into the epoxy-free carotenoid diatoxanthin (Dt) (Dd cycle; Stransky and Hager, 1970; Goss and Jakob, 2010). This algal group can also contain the violaxanthin (Vx) cycle, concerning the two de-epoxidation steps in which Vx is converted into zeaxanthin (Zx), through antheraxanthin (Ax; Lohr and Wilhelm, 1999, 2001). These pigments are mainly involved

in the photoprotective biosynthetic pathway of the Dd-cycle (Lohr and Wilhelm, 1999, 2001; Dimier *et al.*, 2009a).

The hypothesis of the photosynthetic regulation capacity being a functional trait in algae, i.e. an adaptive trait of the organism to the ecosystem, has already been discussed and partially demonstrated by different authors (Strzepek and Harrison, 2004; Lavaud *et al.*, 2007; Dimier *et al.*, 2009b).

Diatoms have been shown to be highly competitive under fluctuating irradiance, because of very efficient processes of photoprotection operating on a minutes to hour scale (Lavaud *et al.*, 2007; Brunet and Lavaud, 2010). Indeed, NPQ is greatly enhanced in diatoms (Lavaud *et al.*, 2002a, 2002b, 2004, 2007). Together with many biological properties, as well as different shapes, diatoms are also greatly diversified in terms of cell size, ranging from few micrometres to few millimetres (Kooistra *et al.*, 2007; Armbrust, 2009).

Cell size is a key-feature in the ecology of phytoplankton, being one of the most important functional traits (Litchman and Klausmeir, 2008, Finkel *et al.*, 2010). Picophytoplankton ($< 3 \mu\text{m}$, Vaultot *et al.*, 2004) are important contributors to marine primary productivity, being dominant in oligotrophic water ecosystems (up to 50% of the total biomass and organic carbon production; Not *et al.*, 2005; Worden and Not, 2008). The tiny cell size confers picophytoplankton relevant ecological and biological aspects, such as the low sinking rate, the low package effect, and the efficient light utilization (Raven, 1998; Raven *et al.*, 2005). Interest on the diversity and ecology of small-sized organisms is growing (Le Gall *et al.*, 2008; Vaultot *et al.*, 2008; Key *et al.*, 2009; Finkel *et al.*, 2010), as well as ecophysiological studies on picoeukaryotes (Dimier *et al.*, 2007a, 2009a, 2009b; Six *et al.*, 2008, 2009; Giovagnetti *et al.*, 2010). To our knowledge, studies regarding picoeukaryotic diatoms are still lacking.

The photophysiological properties of two small-sized diatoms (same *genus*, but distinct ecological niche) were investigated, comparing the relation between irradiance, growth capacity and photosynthetic regulation in the two species. The general purpose of the work is to better understand how the photophysiological functional diversity relates to niche adaptation. Physiological response curves (PRC) of the two diatoms were studied, by subjecting them to five sine climates, each one set to peak at the maximal photon flux density (PFD) of 10, 50, 100, 250, 500 $\mu\text{mol photons} \cdot \text{m}^{-2} \cdot \text{s}^{-1}$, during five days (Giovagnetti *et al.*, 2010). Growth and photosynthetic rates, together with biochemical properties (carbon and nitrogen concentrations, and macromolecular pools allocation), as

well as pigment changes and non-photochemical fluorescence quenching (NPQ) were daily measured.

Materials and methods

Algal model and culture conditions

The species *Minutocellus* sp. RCC967 (Bacillariophyceae) was isolated at the depth of 40 m from the upwelling waters of the Chile coast (Pacific Ocean), while the species *Minutocellus* sp. RCC703 was isolated at the depth of 100 m near the coast in the Indian Ocean (Le Gall *et al.*, 2008). Both the species were provided by the Roscoff Culture Collection (Vaulot *et al.*, 2004). Ongoing genome sequencing of the species *M.* sp. RCC703 is currently occurring at the Genoscope (Centre National de Séquençage, France; see www.sb-roscoff.fr/Phyto/RCC/).

The strains were nonaxenically grown at 20°C at 100 $\mu\text{mol photons} \cdot \text{m}^{-2} \cdot \text{s}^{-1}$ with a 11 : 13 h light : dark photoperiod, in locally obtained and sterilized seawater amended with f/2 medium (Guillard and Ryther, 1962), using 225 cm^2 polystyrene canted neck flasks (Corning Incorporated, NY, USA). Cells were gently aerated and maintained in the exponential phase by daily and semi-continuous dilution (50% of the total volume), over a period of more than two weeks before the experiment started. Before performing the experiment, the pre-acclimation of the two diatoms to the irradiance climate was checked by assessing pigments content stability and growth rate.

Experimental design and sampling strategy

Experimental conditions and sampling strategy were described in Giovagnetti *et al.* (2010). Once acclimation and stability were asserted, cultures were transferred under five sine irradiance regimes set to peak at the photon flux densities (PFD) of 10 (LL1), 50 (LL2), 100 (ML), 250 (HL1) and 500 (HL2) $\mu\text{mol photons} \cdot \text{m}^{-2} \cdot \text{s}^{-1}$ (Fig. 7.1). These conditions corresponded to a daily-integrated PFD of 0.17, 0.86, 1.71, 4.28 and 8.55 $\text{mol photons} \cdot \text{m}^{-2} \cdot \text{d}^{-1}$, in LL1, LL2, ML, HL1 and HL2 regimes, respectively.

Experiments were conducted using three flasks per condition, during five days, and three samples per day were taken. The first sampling was carried out at dawn (the HL2 incident PFD was lower than 40 $\mu\text{mol photons} \cdot \text{m}^{-2} \cdot \text{s}^{-1}$), the second at the PFD peak, while the

third was taken at sunset (the HL2 incident PFD was lower than $40 \mu\text{mol photons} \cdot \text{m}^{-2} \cdot \text{s}^{-1}$).

Irradiance was provided by the system ACLS (Advanced Control Lighting System) and Infinity XR4 (Aquarium Technologies, Sfiligoi S.r.l., Bassano del Grappa, Italy). XR4 was equipped with a HQI metal halide lamp (10000 K). The irradiance was measured using a laboratory PAR 4 π sensor (QSL 2101, Biospherical Instruments Inc., San Diego, CA, USA).

Temperature and pH were daily controlled by an HI-9214-Stick pH meter (Hanna Instruments, Woonsocket, RI, USA).

Twenty to fifty millilitres of culture were collected during each sampling time to carry out measurements of quantum yield of fluorescence, non-photochemical fluorescence quenching, P-I curves, pigments, absorption spectra, cell concentration and size, carbon and nitrogen concentrations, and macromolecular pools allocation.

Growth rate was estimated from cell concentration measurements using the following equation:

$$\mu = \ln [N_{t_2} : N_{t_1}] : [t_2 - t_1] \quad (7.1)$$

where μ is the growth rate (day^{-1}) and N_t is the mean cell concentration at time t , and t_1 and t_2 correspond to the morning sampling times of days 1 and 2, respectively. From the growth rate, the number of cell divisions (n) per day was estimated using the following equation:

$$n = \mu : [\ln (2)] \quad (7.2)$$

where n is the number of cell divisions per day and μ is the growth rate.

Pigment analysis

A ten millilitres aliquot of algal culture was filtered onto GF/F glass-fiber filters (Whatman) and immediately stored in liquid nitrogen until further analysis. Triplicate samples were taken during each sampling time. Analysis was carried out following the procedure described in Dimier *et al.* (2007a). The pigment extract was injected in a

Hewlett Packard series 1100 HPLC (Hewlett Packard) using a C8 BDS 3 mm Hypersil, IP column (Thermo Electron). The mobile phase was composed of eluent A, a solvent mixtures of methanol and aqueous ammonium acetate (70 : 30, v : v), while eluent B was methanol. Pigments were detected spectrophotometrically at 440 nm using a Model DAD, Series 1100 Hewlett Packard photodiode array detector. Fluorescent pigments were detected in a Hewlett Packard standard FLD cell series 1100 with excitation and emission wavelengths set at 407 and 665 nm, respectively. For determination and quantification of pigments, calibration curves were obtained using pigment standards from D.H.I. Water & Environment (Hørsholm, Denmark).

PAM fluorometer measurements

At the PFD peak, samples were collected for pulse amplitude fluorescence (PAM) measurements. Photochemical efficiency of PSII was estimated by a Phyto-PAM fluorometer (Heinz Walz GmbH, Effeltrich, Germany). Triplicate variable fluorescence analysis was performed on 15-min dark-acclimated samples, to measure the maximal photochemical efficiency ($F_v : F_m$, dark-acclimated samples). F_m was measured after a saturating pulse of red light ($2400 \mu\text{mol photons} \cdot \text{m}^{-2} \cdot \text{s}^{-1}$, lasting 450 ms), causing a complete reduction of the PSII acceptor pool.

The non-photochemical quenching of fluorescence was quantified by the Stern–Volmer expression:

$$\text{NPQ} = (F_m : F_m') - 1 \quad (7.3)$$

Electron transport rate (ETR) versus irradiance curves were determined applying 10 increasing irradiances (I , from 1 to $1500 \mu\text{mol photons} \cdot \text{m}^{-2} \cdot \text{s}^{-1}$ for 2 min each).

The absolute electron transport rate ($_{\text{abs}}\text{ETR}_{\text{max}}$, expressed in $\text{mol e}^- \text{g Chl } a^{-1} \text{ h}^{-1}$) was calculated as follows:

$$_{\text{abs}}\text{ETR}_{\text{max}} = (F_v' : F_m') \cdot I \cdot (a_{\text{ph}}^* : 2) \quad (7.4)$$

where I is the incident irradiance (expressed in $\mu\text{mol photons} \cdot \text{m}^{-2} \cdot \text{s}^{-1}$). The mean absorption value a_{ph}^* of phytoplankton was normalized by Chl a ($\text{m}^2 \text{ mg Chl } a^{-1}$) and divided by 2 assuming that half of the absorbed irradiance was distributed to PSII.

The ETR-irradiance curves were fitted with the equation of Eilers and Peeters (Eilers and Peeters, 1988) to estimate the photosynthetic parameters α^B , E_k and ${}_{\text{abs}}\text{ETR}_{\text{max}}$.

Absorption spectrum

A ten millilitres aliquot of algal culture was filtered onto Whatman GF/F filters and immediately frozen. Measurements were carried out following the procedure described in Giovagnetti *et al.* (2010). Absorption was measured between 280 and 800 nm with 1-nm increments on a spectrophotometer (Hewlett Packard HP-8453E) equipped with an integrating sphere (Labsphere RSA-HP-53). The mean absorption value (a^*) was thus normalized by the Chl *a* concentration of the sample to obtain the Chl *a*-specific absorption coefficient (a^*_{ph} ; $\text{m}^2 \text{mg Chl } a^{-1}$).

Organic carbon and nitrogen content

Samples for the determination of particulate organic carbon (POC) and particulate organic nitrogen (PON) were filtered on pre-combusted (450°C, 5 h) glass-fiber filters (Whatman GF/F) and immediately stored at -20°C. The analyses were performed with a Thermo Scientific FlashEA 1112 automatic elemental analyzer (Thermo Fisher Scientific, MA, USA), following the procedure described by Hedges and Stern (1984). Cyclohexanone-2,4-dinitrophenylhydrazone was used as standard.

Fourier transform infrared (FT-IR) spectroscopy analysis of macromolecular pools

Samples of 30 mL for FT-IR measurements were taken in triplicate in the middle of the exponential growth phase for each irradiance condition, with cell concentration higher than 4×10^6 cells mL^{-1} . Cells were harvested by centrifugation (1800 $\cdot g$ for 15 min) and both culture and blank samples were prepared following the procedure described by Domenighini and Giordano (2009). Culture and blank samples were kept in a desiccator until analyzed.

Spectra were acquired with a Bruker Tensor 27 FT-IR spectrometer (Bruker Optics, Ettlingen, Germany), following the procedure by Domenighini and Giordano (2009), while peak attribution was performed according to Giordano *et al.* (2001). Relative ratios of carbohydrates, lipids, protein, and silica were calculated from the peaks' integrals using

the software OPUS 6.5 (Bruker Optics, 2006). The calculation of the band integrals was done after deconvolution of the spectrum from 1800 cm^{-1} to 1000 cm^{-1} with the ‘peak fit’ function of OPUS 6.5, and the main peaks on which deconvolution was based were identified by applying a second derivative to each spectrum, with nine smoothing points.

Results

Growth and cell parameters

Both *Minutocellus* sp. RCC967 and RCC703 presented a wide range of irradiance conditions suitable for growth. *M. sp.* RCC967 grew optimally under moderate light condition (ML) reaching its highest growth rate (0.82 ± 0.02 ; Fig. 7.2), then decreasing under high irradiances. Differently, *M. sp.* RCC703 growth rate gradually increased over the irradiance range reaching the highest growth rate under 500 $\mu\text{mol photons} \cdot \text{m}^{-2} \cdot \text{s}^{-1}$ condition (1.97 ± 0.15 ; Fig. 7.2). Growth rate was much higher in *M. sp.* RCC703 than in *M. sp.* RCC967 (Fig. 7.2).

A maximal mean cell concentration of $2.26 \times 10^5 \pm 2.07 \times 10^4$ cells mL^{-1} was reached by *M. sp.* RCC967, while *M. sp.* RCC703 maximal mean cell density was $4.35 \times 10^5 \pm 1.20 \times 10^4$ cells mL^{-1} (data not shown). Number of division per day ranged between 0.35 and 1.18 and between 0.65 and 2.84 divisions d^{-1} , in *M. sp.* RCC967 and RCC703, respectively.

Very low variability of cell size and volume was reported without any trend related to the growth rate or irradiance conditions. Cell size ranged between 2.72 ± 0.06 μm and 3.12 ± 0.24 μm , and between 2.66 ± 0.06 μm and 3.11 ± 0.27 μm , in *M. sp.* RCC967 and RCC703 cultures, respectively (data not shown). Volume ranged between 11.20 ± 0.24 μm^3 and 16.19 ± 3.79 μm^3 , and between 9.96 ± 0.70 μm^3 and 16.09 ± 4.36 μm^3 , in *M. sp.* RCC967 and RCC703, respectively (data not shown).

Quantum yield of fluorescence and photosynthetic parameters

The maximal quantum yield of fluorescence ($F_v : F_m$) was stable under LL and ML conditions in both species (Fig. 7.3). The decrease under high light condition was stronger in *M. sp.* RCC967 than in *M. sp.* RCC703.

The $\text{absETR}_{\text{max}}$ of both species increased from LL to ML regime, under which the photosynthetic rate was maximal (Fig. 7.4). Under the lowest irradiance condition, the photosynthetic rate mean value in the species RCC967 was two-fold higher than the value measured in the species RCC703, although the latter performed better under moderate and high irradiance conditions. From ML to HL regimes, the decrease of $\text{absETR}_{\text{max}}$ was much steeper in *M. sp.* RCC967 than in *M. sp.* RCC703, being instead more gradual (Fig. 7.4).

The photosynthetic efficiency (α^{B}) of *M. sp.* RCC703 was stable over the irradiance gradient (Fig. 7.5, $\sim 0.14 \text{ mol e}^- \text{ g Chl } a^{-1} \text{ h}^{-1} [\mu\text{mol photons} \cdot \text{m}^{-2} \cdot \text{s}^{-1}]^{-1}$) with the exception of the increase under LL2 regime ($0.23 \pm 0.091 \text{ mol e}^- \text{ g Chl } a^{-1} \text{ h}^{-1} [\mu\text{mol photons} \cdot \text{m}^{-2} \cdot \text{s}^{-1}]^{-1}$). In *M. sp.* RCC967, α^{B} was higher under the lowest irradiance condition (Fig. 7.5, $\sim 0.20 \text{ mol e}^- \text{ g Chl } a^{-1} \text{ h}^{-1} [\mu\text{mol photons} \cdot \text{m}^{-2} \cdot \text{s}^{-1}]^{-1}$) while it decreased gradually under moderate and high irradiance conditions.

The light saturation index of photosynthesis (E_k) showed a quite opposite trend between the two species (Fig. 7.6), revealing again different physiological responses to irradiance. *M. sp.* RCC967 E_k was stable around ($\sim 130 \mu\text{mol photons} \cdot \text{m}^{-2} \cdot \text{s}^{-1}$) under LL and ML regimes, gradually decreasing with increasing irradiance conditions. In *M. sp.* RCC703, E_k increased from 67.10 ± 3.37 (LL1) to $203.64 \pm 26.01 \mu\text{mol photons} \cdot \text{m}^{-2} \cdot \text{s}^{-1}$ (HL1), only decreasing under the highest irradiance condition ($115.47 \pm 28.74 \mu\text{mol photons} \cdot \text{m}^{-2} \cdot \text{s}^{-1}$).

Chl *a* and accessory pigments

The Chl *a* cell^{-1} content was not significantly different between the two diatoms (Figs. 7.7 and 7.8). Values ranged between $2.32 \times 10^{-16} \pm 4.15 \times 10^{-17}$ and $3.01 \times 10^{-16} \pm 9.47 \times 10^{-17} \text{ mol Chl } a \text{ cell}^{-1}$ in *M. sp.* RCC967 and between $1.26 \times 10^{-16} \pm 1.74 \times 10^{-17}$ and $2.21 \times 10^{-16} \pm 6.09 \times 10^{-17} \text{ mol Chl } a \text{ cell}^{-1}$ in *M. sp.* RCC703. In both species, the low variations in Chl *a* cellular content were independent from cell size or volume changes, since no significant correlation between Chl *a* cell^{-1} content and cell size was found. In the species RCC967, the Chl *a* cell^{-1} content was stable all over the experimental irradiance gradient, while in the species RCC703, Chl *a* cell^{-1} was almost halved under HL2 (Fig. 7.7).

In *M. sp.* RCC703, the main accessory photosynthetic pigments, Chl *c*₁ and *c*₂ and Fucoxanthin (Fuco) per cell were significantly correlated to Chl *a* cell^{-1} (data not shown). This led to a quite stable ratio between accessory pigments and Chl *a*, mainly evident

under moderate and high irradiance intensities (Figs. 7.9 and 7.11). Differently, these pigments independently varied from the Chl *a* cellular content in *M. sp. RCC967*, therefore causing the decrease in accessory pigments to Chl *a* ratios occurring under ML and HL regimes (Figs. 7.10 and 7.12). While in *M. sp. RCC967* the *cis*-fucoxanthin (*cis*-Fuco) : Chl *a* ratio followed the same trend of Fuco over the irradiance gradient (Fig. 7.12), in *M. sp. RCC703* the *cis*-Fuco : Chl *a* ratio was much more variable, with opposed trend in LL and ML with Fuco (Fig. 7.11).

In *M. sp. RCC703*, the β -carotene (β -Car) cell⁻¹ content was stable over the irradiance gradient with the exception of HL2 decrease (Fig. 7.13), while it was higher and more variable under LL and ML regimes in *M. sp. RCC967* (Fig. 7.14).

Interestingly, together with β -Car, α -carotene (α -Car) was also detected (even if in low quantity) in both diatoms (Figs. 7.13 and 7.14). The α -Car cell⁻¹ content slowly decreased from LL to HL in both diatoms (Figs. 7.13 and 7.14). Together with the surprising detection of α -Car, traces of neoxanthin-like were also found in these diatoms. Since the uncertainty of the pigment determination, we did not discuss on this finding, nevertheless considering this as an interesting feature for further investigations.

Photoprotection

In both diatoms, the content of Dt + Dd increased from low to high irradiance conditions (Figs. 7.15 and 7.16), being at least two-fold higher in *M. sp. RCC967* than in *M. sp. RCC703*. In *M. sp. RCC703* the Dd cellular content reached a plateau under HL1 condition, while the Dt cellular content gradually increased over the irradiance gradient (Fig. 7.17). The de-epoxidation state (DPS) reached a maximal 39% in this diatom (Fig. 7.19).

In *M. sp. RCC967*, the XC was differently regulated. While the Dd cellular content was almost stable over the irradiance gradient (Fig. 7.18), the Dt cellular content steeply increased (almost sixty-fold) from ML to HL conditions (Fig. 7.18). Consequently, DPS reached 80% (Fig. 7.20).

These results reflected a much more strongly enhanced photoprotective state of *M. sp. RCC967* cells rather than of *M. sp. RCC703* ones. In both diatoms the NPQ development strongly relied on the de-epoxidation of Dd into Dt ($p < 0.01$; Figs. 7.21 and 7.22). Maximal NPQ mean values of 1.15 ± 0.13 and 0.34 ± 0.02 were reached in *M. sp. RCC703* and *RCC967*, respectively (Figs. 7.23 and 7.24). In both diatoms, NPQ development was

significantly correlated with the decrease in the PSII maximal photochemical efficiency over increasing irradiance conditions ($F_v : F_m$, $p < 0.05$; data not shown).

Another divergence between the two species concerned the presence of the photoprotective xanthophylls of the violaxanthin cycle, antheraxanthin (Ax) and zeaxanthin (Zx) in *M. sp. RCC967*, while it was not the case of *M. sp. RCC703*. Both pigments increased over the irradiance gradient and were significantly correlated to $Dt \text{ cell}^{-1}$ ($p < 0.01$) and NPQ ($p < 0.05$).

Organic Carbon and Nitrogen content

Both the particulate organic carbon (POC) and nitrogen (PON) cellular concentrations and the general trend over the irradiance gradient were quite similar in the two species (Figs. 7.25 and 7.26). In both diatoms, $POC \text{ cell}^{-1}$ increased under LL and HL conditions (Figs. 7.25 and 7.26). POC and $PON \text{ cell}^{-1}$ were significantly correlated together in the species *RCC967* ($p < 0.01$, Fig. 7.28), but not in the species *RCC703* (Fig. 7.27). Indeed, changes in the POC : PON ratio were stronger and related to irradiance gradient in the species *RCC703* (Fig. 7.29) than in the species *RCC967*, in which the ratio was stable (Fig. 7.30). In *M. sp. RCC703*, the POC : PON ratio was correlated to growth rate (Fig. 7.31), which was not true in *M. sp. RCC967* (Fig. 7.32).

Intracellular macromolecular pools allocation

The protein : carbohydrate (Prt : Crb) absorbance ratio was generally greater in *M. sp. RCC703* than in *M. sp. RCC967* (Figs. 7.33 and 7.34). The former presented a Prt : Crb absorbance ratio decreasing trend with increasing PFD - with the exception of the low value found at LL1, while in *M. sp. RCC967* the absorbance ratio was stable over the irradiance gradient. A similar trend occurred in the lipid : carbohydrate (Lp : Crb) absorbance ratio (Figs. 7.35 and 7.36). These results led us to hypothesize that carbohydrates were accumulated - at the expense of protein and lipid allocation - with increasing irradiance conditions, in *M. sp. RCC703*.

In *M. sp. RCC703*, the highest protein : lipid (Prt : Lp) absorbance ratio was found under the moderate irradiance condition ($100 \mu\text{mol photons} \cdot \text{m}^{-2} \cdot \text{s}^{-1}$, Fig. 7.37). The ML condition corresponded to the irradiance of acclimation and of maximal photosynthetic rate, for both species. A higher need of protein biosynthesis can therefore be hypothesized

to sustain a greater activity of the photosynthetic machinery, in *M. sp. RCC703*. A different biochemical response was observed in *M. sp. RCC967*. Indeed, the highest $\text{Prt} : \text{Lp}$ absorbance ratio was reached under LL1 condition (Fig. 7.38) and might be due a higher use of lipids for protein biosynthesis under low irradiance, as similarly described in studies performed on diatoms kept in the dark (see Stehfest *et al.*, 2005).

Discussion

Since the similar cell size and the close phylogenetic relationship, the diversity of the two diatoms in photophysiological responses and growth capacity in relation to a gradient of irradiance intensities might be attributed to distinct ecological niches adaptation.

M. sp. RCC703 is an oceanic species isolated near the coast in the Indian ocean that, considering the obtained results, appears to be an high light adapted species (Falkowski and Owens, 1980; Falkowski *et al.*, 1981), as demonstrated by the highest growth rate reached under the highest irradiance regime. Furthermore, this species performs better than the species *RCC967* under each PFD condition, indicating a more efficient ability in irradiance utilization. *M. sp. RCC967* growth is instead inhibited under the high irradiance regimes underlining how the two diatoms relied upon different ecophysiological requirements and photoacclimation strategies.

Intriguing is the mismatch between the maximal absolute photosynthetic and growth rate in the oceanic species, contrarily to what occurs in the upwelling species (in which both the highest $\text{absETR}_{\text{max}}$ and growth rate are reached under ML condition). This feature indicates that *M. sp. RCC703* growth rate is modulated by irradiance intensity and photosynthetic processes until PFD is limiting ('photosynthetic regulation-dependent growth rate'), and by biochemical machinery adjustments to efficiently use the photons harvested by PSII antenna-complexes, when PFD becomes saturating or even over-saturating during a portion of the day ('biochemical regulation-dependent growth rate').

The significant correlation between POC : PON ratio and growth rate highlights how this species is able to maintain or increase growth under a wide range of PFD by tuning intracellular biochemical properties. The strategy adopted by *M. sp. RCC967* is different, preventing the biochemical properties of cells to evolve over the irradiance gradient, while this species drastically rearranges the PSII structure under high irradiance conditions. The smaller flexibility in facing high light stress might be related to a low light acclimation

state displayed by *M. sp. RCC967*, growing in waters characterized by a high turbidity. It seems that the PFD peak is the main cue determining the physiological state of *M. sp. RCC967* and hence growth capacity, whereas in *M. sp. RCC703* both the PFD *maximum* and daily-light dose trigger the physiological response of cells, affecting growth.

In *M. sp. RCC703*, the lack of significant relationship between POC and PON cellular contents as well as the increase of POC : PON ratio are consistent with a decrease in the cellular amount of proteins, as revealed by the gradual decrease of the Prt : Crb absorbance ratio over increasing irradiance conditions. Decreasing the protein cellular content in favor of a greater allocation of carbohydrates might be justified by the lower amount of electrons per atom of carbon needed in carbohydrates rather than lipids or proteins biosynthesis (i.e. 4 electrons instead of at least 6 electrons per carbon; Kroon and Thoms, 2006). The synthesis of 'low-cost compounds' would thus enable cells to efficiently channel more energy in regulating the photosynthetic mechanisms, and invest in fast-occurring photoprotective processes, as NPQ.

In *M. sp. RCC703*, the decrease of $_{\text{abs}}\text{ETR}_{\text{max}}$ under the HL2 condition would represent a functional regulation of the photosynthetic rate to the high PFD peak, rather than a net decrease of the species photosynthetic capacity due to a stressful irradiance condition. This hypothesis fits the high light enhanced growth rate and photoacclimation strategy of this diatom. As reflected by our results on accessory pigments and Chl *a* variations, a modification in size or number of PSII, i.e. both light-harvesting antenna complexes and reaction centers, occurs under the highest irradiance condition.

The photoacclimative strategy deployed by *M. sp. RCC703* allows this species to keep the photosynthetic efficiency (α^{B}) almost stable over the irradiance gradient (with the exception of LL2 condition), ensuring an effective photosynthetic rate under limiting PFD, which correspond to the large majority of the daylight period (since the applied sine climate).

This photoacclimation strategy and the HL peak short-time negative effect on the species ecophysiology is confirmed by the increase of E_k over the irradiance gradient, excluding the HL2 decrease, which is related to the decrease of photosynthetic pigment content. These results show how this species responds to the high PFD peak with efficient physiological/biochemical changes without compromising growth capacity, confirming the ability to integrate energy-information and adequately respond to both high PFD peak and daily-integrated PFD.

In *M. sp. RCC967*, our results show that this species is negatively affected by high irradiance condition, i.e. over a daily PFD dose of $2 \text{ mol photons} \cdot \text{m}^{-2} \cdot \text{d}^{-1}$. This low value confirms this species as low light acclimated, in agreement with its habitat (upwelling water) and depth (40 m) of isolation. Moreover, under the very low irradiance (LL1) condition, *M. sp. RCC967* photosynthetic rate is two-fold greater than *M. sp. RCC703*. This result might be explained by the higher α^B value in *M. sp. RCC967* than in *M. sp. RCC703* under LL1 condition, bearing a greater photon flux in the PSII antenna, as also suggested by the higher pigment content in this species than in *M. sp. RCC703*.

M. sp. RCC967 mainly responds to the PFD peak, entering a photoprotective state that reduces the photosynthetic efficiency for light harvesting, as the decrease in α^B , which then causes a state of light-limitation for cells growth, during the largest portion of the day (when PFD is limiting).

M. sp. RCC967 photoprotective strategy probably relies on a σ -type photoacclimation strategy (Six *et al.*, 2008; Dimier *et al.*, 2009a; Giovagnetti *et al.*, 2010), regulating the energy flux by decreasing the accessory photosynthetic pigments content (i.e. the size of the PSII antenna) to achieve a lower light harvesting capacity. This feature is further enhanced by the huge synthesis of Dt, which greatly persists in cells even under low PFD. In fact, the content of Dd and Dt measured in this species at sunset and dawn is two-fold higher than the content measured in *M. sp. RCC703* ($1.5 - 2 \times 10^{-16}$ versus $4 - 5 \times 10^{-16}$ mol (Dt + Dd) cell⁻¹, in *M. sp. RCC703* and *RCC967*, respectively), mainly due to the strong increase in Dt ($0.25 - 0.50 \times 10^{-16}$ versus $0.50 - 1.00 \times 10^{-16}$ mol Dt cell⁻¹, in *M. sp. RCC703* and *RCC967*, respectively). This photoacclimative strategy is probably possible because of the higher content of Dd and β -Car in PSII of *M. sp. RCC967* than of *M. sp. RCC703*, as well as of the presence of the xanthophylls antheraxanthin (Ax) and zeaxanthin (Zx), as intermediate products taking part of the Dd cycle pigments biosynthetic pathway (Goss and Jakob, 2010). Whereas Dd and Dt increased together with increasing irradiance intensities in *M. sp. RCC703*, their trends become opposite under HL regimes in *M. sp. RCC967*, revealing that for a certain PFD and/or Dt content threshold, Dt still increases without any replenishment of Dd. A similar strategy with a very high Dt synthesis has been observed also in the low-light acclimated *Skeletonema marinoi* when subjected to PFD increase (Dimier *et al.*, 2007b). Such strong increase, together with the probable low accessibility to the Dt-epoxidase and low level of NPQ would be related to a photoprotective role of Dt at the level of the thylakoid membrane lipids, against

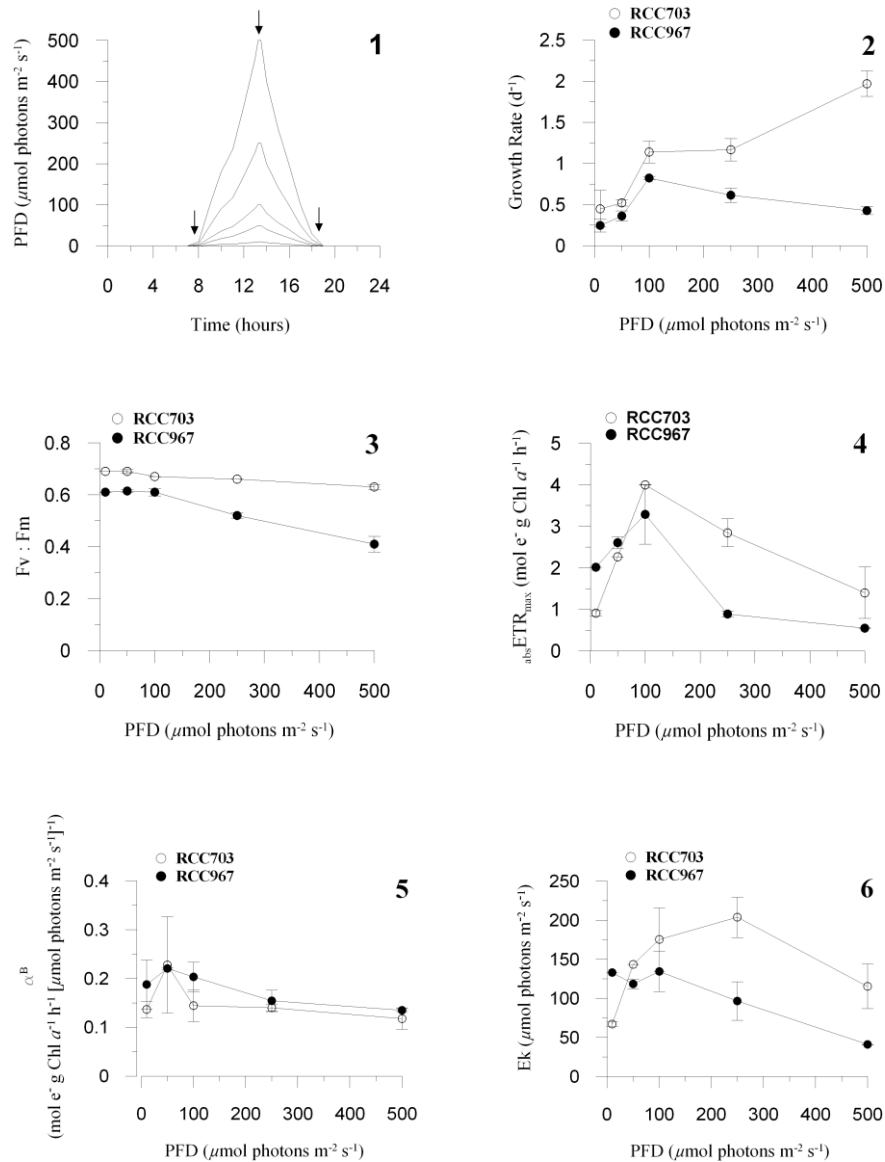
peroxidative stress during excessive irradiance exposure, as also demonstrated for zeaxanthin in higher plants (Havaux and Niyogi, 1999).

The two photoacclimative strategies afore-documented differ from the strategy deployed by another picoeukaryote, *Phaeomonas* sp. RCC503 subjected to identical experimental conditions (Giovagnetti *et al.*, 2010). Under high irradiance, despite the photoprotective state of cells, *P.* sp. RCC503 increases the size of the light-harvesting antenna complexes (by increasing both Chl *a* and accessory photosynthetic pigments content) to overcome the loss of photosynthetic efficiency. The synergetic match between photoprotection and irradiance-harvesting enhancement has been explained by the species adaptation to the coastal environment (Giovagnetti *et al.*, 2010). The reason of this finding might reside in the fact that cells experience multiple and rapid PFD variations in a basically low-irradiance climate, linked to water column turbulence, low depth and turbidity of the coastal ecosystem. Comparison of the three picoeukaryotes fits the results obtained by Dimier and coauthors (2009b), comparing the ecophysiological properties of seven phytoplanktonic species. During this study, three photophysiological groups (the high light-, low light- and variable light-adapted species) have been discriminated on the basis of the species properties concerning the xanthophyll cycle ecophysiology and photosynthetic pigments.

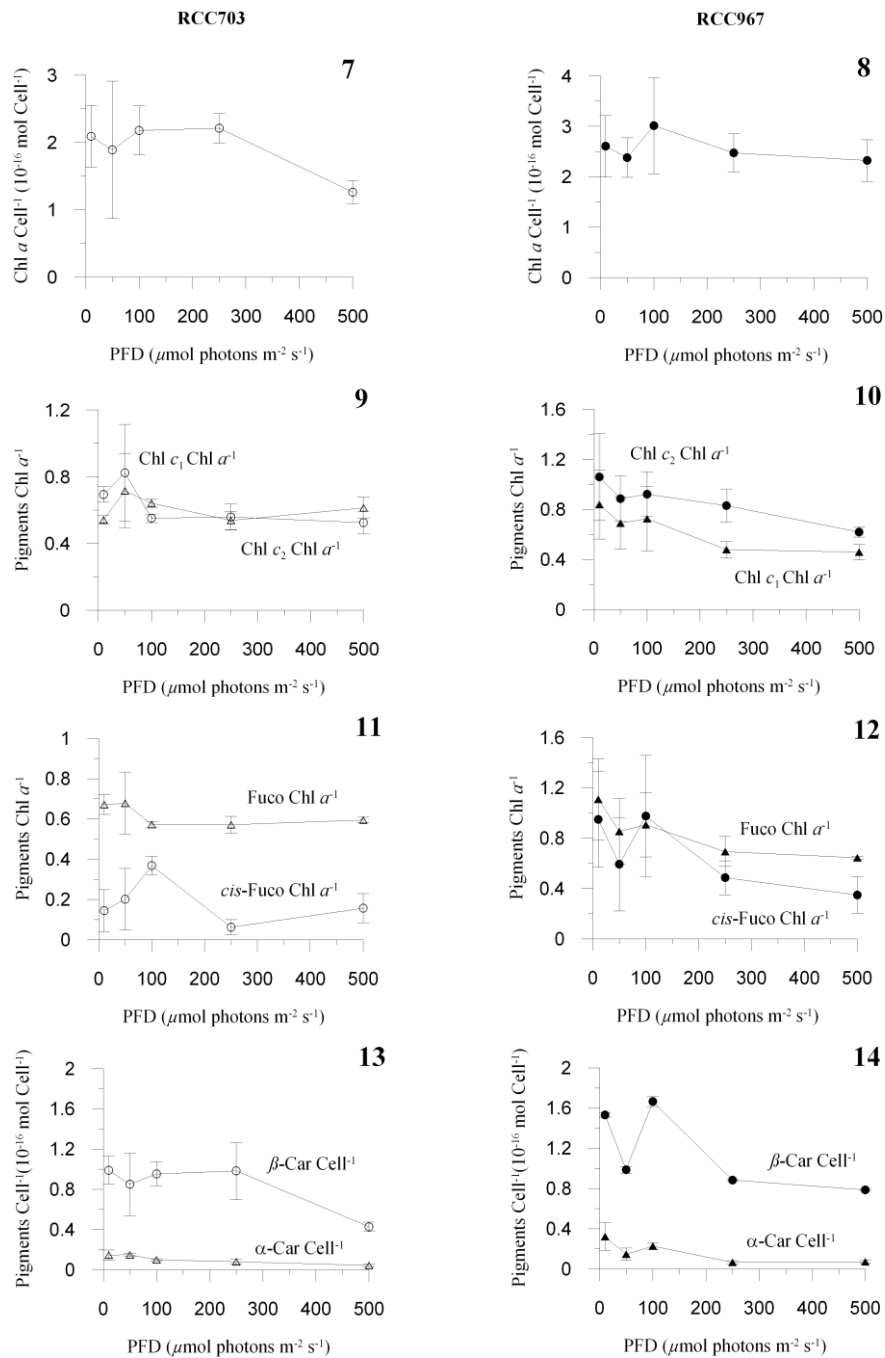
Despite the ecophysiological diversity, growth rate and $_{\text{abs}}\text{ETR}_{\text{max}}$ are significantly correlated ($p < 0.025$), by pooling the three species data set, with a linear regression slope value of 0.26 (Fig. 7.39). Such finding might suggest that 25% of the absolute electron transport rate is conveyed to growth maintenance in picoeukaryotes. Interestingly is the fact that this percentage is close to the value of the quantum yield of oxygen formation (0.25) during photosynthesis. This result therefore emphasizes how energy losses (e.g. cell respiration rate and catabolism) might be narrowly confined, in picophytoplankton.

Acknowledgments

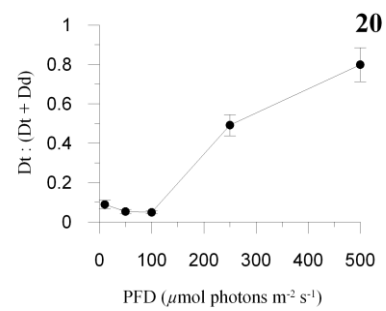
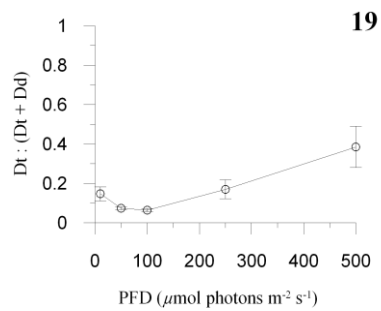
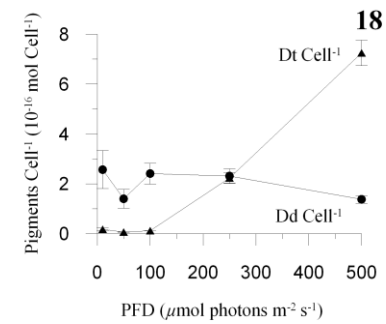
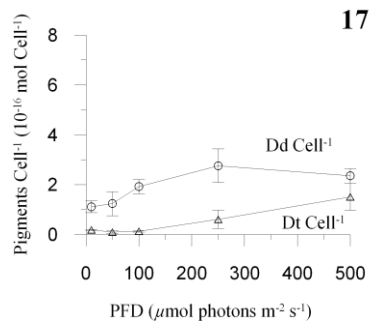
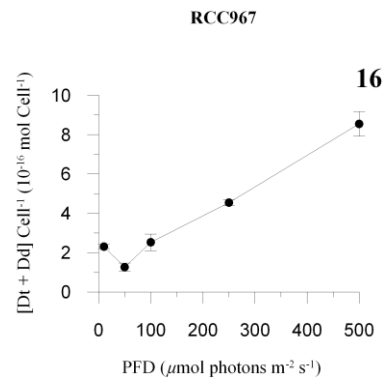
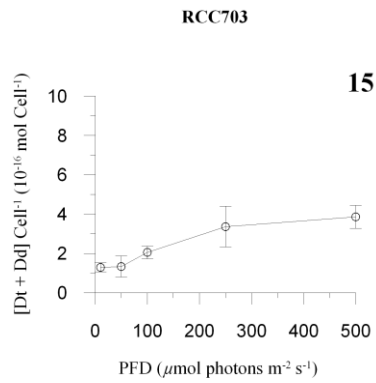
We wish to gratefully acknowledge M. Giordano, S. Ratti and M. Palmucci for the access to FT-IR spectrometer and their kind help during samples analysis. Help from F. Tramontano, during experiments and HPLC analysis, is greatly acknowledged. V. Saggiomo and F. Margiotta are acknowledged for CHN analysis, and for sharing the PAM fluorometer. V.G.'s PhD was supported by the Stazione Zoologica A. Dohrn.



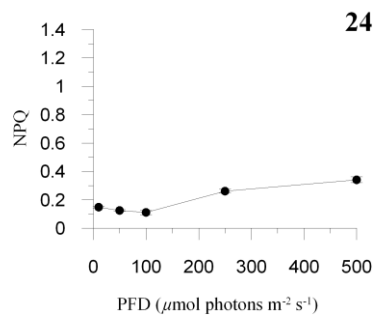
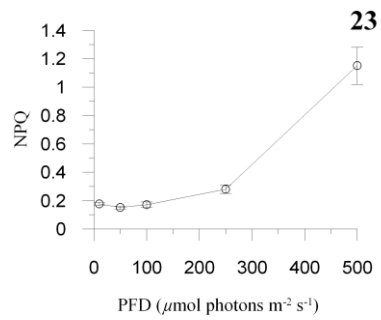
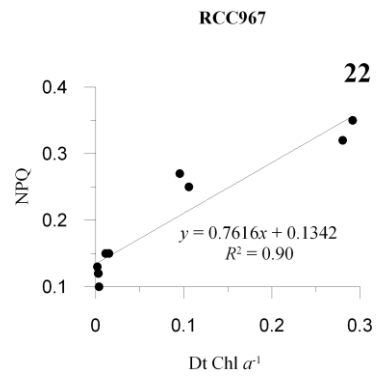
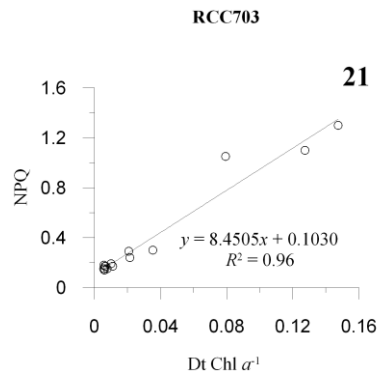
Figs. 7.1–7.6: Fig. 1. Scheme of the five sine irradiance conditions, peaking at maximal PFD of 10, 50, 100, 250 and 500 $\mu\text{mol photons m}^{-2} \text{s}^{-1}$ (arrows indicate sampling times). Figs 2-6. Evolution of the growth rate (d^{-1} ; Fig. 2), PSII maximal photochemical efficiency ($F_v : F_m$; Fig. 3), maximal absolute electron transport rate ($_{\text{abs}}\text{ETR}_{\text{max}}$, in $\text{mol e}^{-} \text{g Chl a}^{-1} \text{h}^{-1}$; Fig. 4), photosynthetic efficiency (α^B , in $\text{mol e}^{-} \text{g Chl a}^{-1} \text{h}^{-1} [\mu\text{mol photons m}^{-2} \text{s}^{-1}]^{-1}$; Fig. 5), and irradiance saturation index (E_k , in $\mu\text{mol photons m}^{-2} \text{s}^{-1}$; Fig. 6) in the two species. *Minutocellus* sp. RCC703: open circles; *Minutocellus* sp. RCC967: filled circles. Data are means with $n = 3$; error bars are SD.



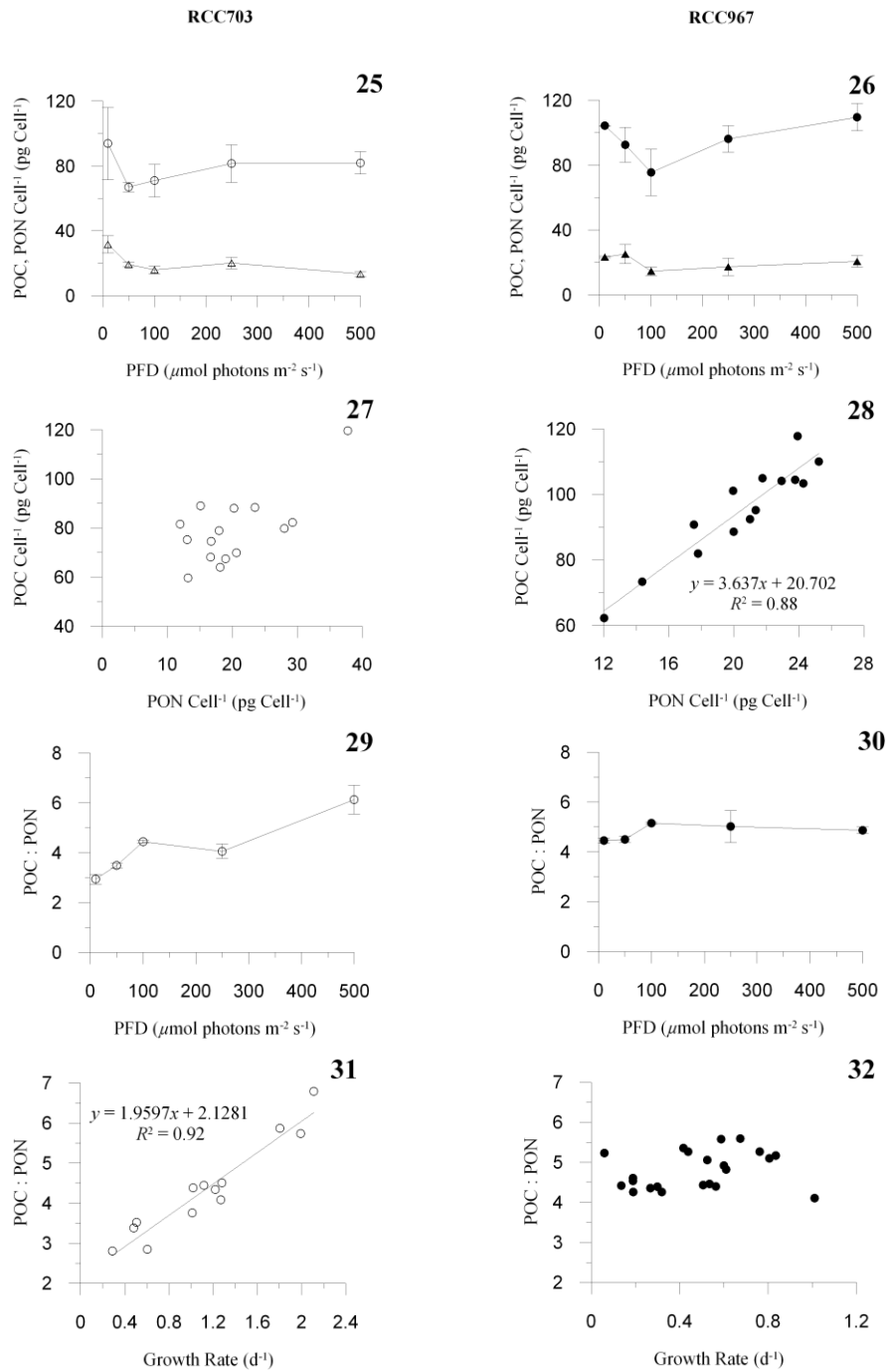
Figs. 7.7–7.14: Evolution of chlorophyll *a* cellular content (10^{-16} mol Chl *a* cell⁻¹; Figs 7, 8), chlorophyll *c*₁ and *c*₂ Chl *a*⁻¹ (Figs 9, 10), fucoxanthin and *cis*-fucoxanthin : Chl *a* (Figs 11, 12), and α - and β -carotene cellular content (10^{-16} mol pigment cell⁻¹; Figs 13, 14), over the irradiance conditions. Chl *a*, chlorophyll *a*; Chl *c*₁, chlorophyll *c*₁; Chl *c*₂, chlorophyll *c*₂; Fuco, fucoxanthin; *cis*-Fuco, *cis*-fucoxanthin; α -Car, α -carotene; β -Car, β -carotene. *Minutocellus* sp. RCC703: open circles and triangles; *Minutocellus* sp. RCC967: filled circles and triangles. Data are means with n = 3; error bars are SD.



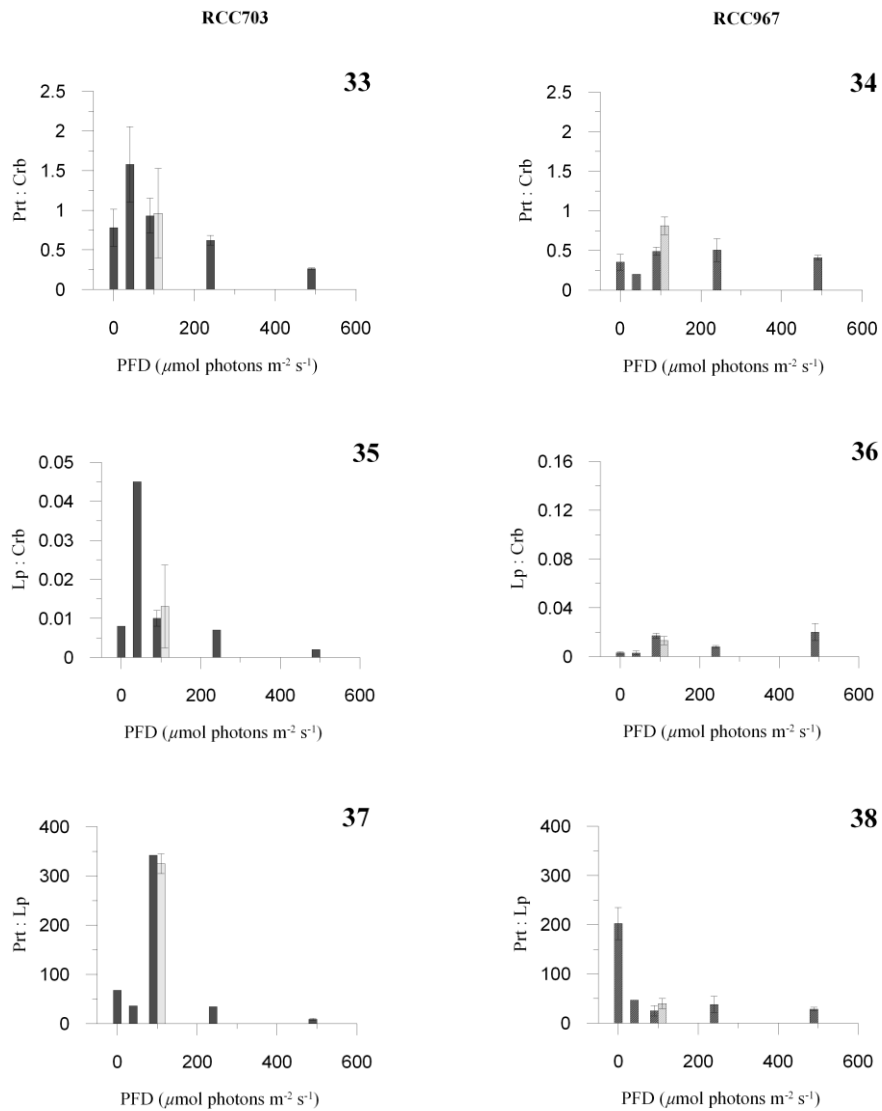
Figs. 7.15–7.20: Evolution of (Dt + Dd) cell⁻¹ (10⁻¹⁶ mol pigment Chl *a* cell⁻¹; Figs 15, 16), Dt and Dd cell⁻¹ (10⁻¹⁶ mol pigment cell⁻¹; Figs 17, 18), [Dt : (Dt + Dd)] DPS (DPS; Figs 19, 20), over the irradiance conditions. Chl *a*, chlorophyll *a*; Dt, diatoxanthin; Dd, diadinoxanthin. *Minutocellus* sp. RCC703: open circles and triangles; *Minutocellus* sp. RCC967: filled circles and triangles. Data are means with n = 3; error bars are SD.



Figs 7.21–7.24: Figs 21, 22. Relationship between NPQ and Dt Chl a^{-1} . Figs 23, 24. Evolution of NPQ over the irradiance conditions. Data are means with $n = 3$; error bars are SD. NPQ, non-photochemical fluorescence quenching. *Minutocellus* sp. RCC703: open circles; *Minutocellus* sp. RCC967: filled circles.



Figs 7.25–7.32: Figs 25, 26. Evolution of particulate organic carbon (POC) and nitrogen (PON) concentrations (pg cell^{-1}) over the irradiance conditions. Data are means with $n = 3$; error bars are SD. Figs 27, 28. Relationship between POC and PON cell^{-1} . Figs 29, 30. Evolution of the POC : PON ratio over the irradiance conditions. Data are means with $n = 3$; error bars are SD. Figs 31, 32. Relationship between growth rate (d^{-1}) and POC : PON ratio. *Minutocellus* sp. RCC703: open circles and triangles; *Minutocellus* sp. RCC967: filled circles and triangles.



Figs 7.33–7.38: Evolution of the protein : carbohydrate absorbance ratio (Figs 33, 34), lipid : carbohydrate absorbance ratio (Figs 35, 36), and protein : lipid over the irradiance conditions (Figs 37, 38). Data are means with $n = 3$; error bars are SD. *Minutocellus* sp. RCC703: black and grey bars; *Minutocellus* sp. RCC967: black and grey striped bars. Grey bars represent control samples, measured at 100 $\mu\text{mol photons m}^{-2} \text{s}^{-1}$ (ML condition). Crb, carbohydrate; Lp, lipid; Prt, protein.

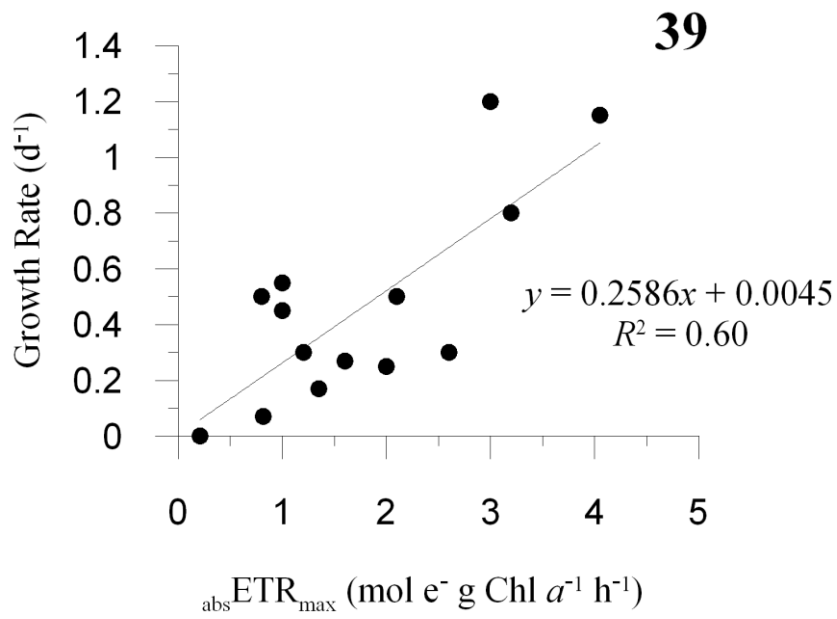


Fig. 7.39: Relationship between maximal absolute electron transport rate (${}_{\text{abs}}\text{ETR}_{\text{max}}$, expressed in $\text{mol e}^- \text{g Chl } a^{-1} \text{h}^{-1}$) and growth rate (d^{-1}), by pooling the data set of three picoeukaryotic species: *Minutocellus* sp. RCC703, RCC967, and *Phaeomonas* sp. RCC503 (data from Giovagnetti *et al.*, 2010).

CHAPTER 8

General discussion and conclusions

Chapter 8

General discussion and conclusions

Recent studies report that the flexibility in photophysiological responses to light climate fluctuations might correspond to a functional trait in phytoplankton (Strzepek and Harrison, 2004; Dimier *et al.*, 2007b, 2009b; Lavaud *et al.*, 2007), a key-feature that would affect the competition behavior of cells, and then the spatial co-existence and/or temporal succession of species in marine ecosystems.

The main goal of my PhD was to investigate if the species photophysiology is functionally related to its ecological traits. This has been done by characterizing the ecophysiology of four species belonging to the *phylum* Stramenopiles, focusing on the xanthophyll cycle (XC) and the non-photochemical fluorescence quenching (NPQ) activities. The ecophysiological approach allows us to get reliable information for ecological interpretation and studies, as well as to test the ‘sensitivity’ of different biological parameters that respond to light variations. This is a relevant point for ecological studies, since such type of approach would tell us the temporal scale and the functioning of different photoresponses, then possibly used for in field studies and modeling exercises.

The experiments have been conducted using the following species: *Pseudo-nitzschia multistriata* (Takano) Takano (Bacillariophyceae), *Phaeomonas* sp. RCC503 (Pinguicophyceae), *Minutocellus* sp. RCC967 and RCC703 (Bacillariophyceae).

These species provided a high degree of diversity that was investigated in my PhD work. High diversity of ecological niches (i.e. different mixing pressure and thus photon flux density infra-diel variability) has been taken into account, investigating species isolated either from coastal (*P. multistriata* and *P. sp.* RCC503, Mediterranean Sea), or oceanic (*M. sp.* RCC703, Indian Ocean), or upwelling regions (*M. sp.* RCC967, Pacific Ocean). Furthermore, particular attention has been paid to ‘cell size constraints’ and their potential influence on the species photophysiology, by deepening the ecophysiological plasticity of one microplanktonic (i.e. *P. multistriata*) and three picoplanktonic species (precisely, picoeukaryotes).

Lastly, despite the phylogenetic proximity of the four species, *P. sp.* RCC503 contains the violaxanthin (Vx)-cycle, whereas the three diatoms display the diadinoxanthin (Dd)-cycle.

Results obtained in this study confirm the hypothesis that photophysiological plasticity is a functional trait in phytoplankton ecology. A large diversity in regulation and capacity/efficiency of photoprotective responses (XC and NPQ) are reported, with each species photoacclimative strategy related to its ecological niche.

Even if a deep comparison is not possible, because of different experimental designs and high light (HL) peaks, in the two coastal species, *P. multistriata* and *P. sp. RCC503*, the photoprotective response is activated after a moderate light threshold is exceeded, in agreement with the light threshold for a significant photoprotective pigment synthesis of the coastal species *Phaeocystis cordata* (Prymnesiophyceae, Stramenopiles; Dimier *et al.*, 2009b). The highest NPQ values are reached under moderately high irradiances, with a maximal NPQ value of 1.05 ± 0.09 measured in *P. multistriata* at the photon flux density (PFD) of $164 \mu\text{mol photons} \cdot \text{m}^{-2} \cdot \text{s}^{-1}$, and of 0.66 ± 0.07 in *P. sp. RCC503* at the PFD of $250 \mu\text{mol photons} \cdot \text{m}^{-2} \cdot \text{s}^{-1}$. The PFD at which the maximal NPQ occurs is in the range of values of the photosynthetic light saturation values (Ek, retrieved from the P–E curve), that might indicate that the photoprotective response developed by algae anticipates the ‘photoinhibition portion’ of the P–E curve.

Besides this similarity, the microplanktonic coastal diatom is apparently able of a much stronger photoprotective response than the picoplanktonic species, with *P. multistriata* being able to reach a much higher DPS than *P. sp. RCC503* (i.e. 78 versus 9%), under HL. Such an impressive difference might be in part explained, mainly, by the distinct functioning of the two types of XC displayed by the two species, as well as by cell size- and taxonomy-related aspects.

The results that have been achieved through three specific experiments clearly demonstrate that *P. multistriata* photoacclimative characteristics fit with the life in turbulent environments. This diatom can efficiently and rapidly cope with increasing irradiance climate (up to $650 \mu\text{mol photons} \cdot \text{m}^{-2} \cdot \text{s}^{-1}$), being able to develop a multi-component NPQ and efficiently regulate/activate the biosynthetic pathway of carotenoids, in function of XC requirements. The multi-component NPQ is a synergetic process resulting from the main Dd cycle-dependent NPQ development (which relies upon a finely regulated XC modulation), and Dd cycle-independent NPQ components (especially, an initial transient mechanism based upon the Dt content present within the cell, and a PSII-detached FCP antennae aggregation mechanism). The Dd cycle-independent NPQ mechanisms are clearly activated when the irradiance quantity per unit of time becomes excessive (i.e. in

relation to irradiance increase velocity), and its contribution to the total NPQ development is significant, especially under moderate PFD (maximal contribution has been estimated to 65%, at $123 \mu\text{mol photons} \cdot \text{m}^{-2} \cdot \text{s}^{-1}$).

An interesting point highlighted in this study is the occurrence of Dt-epoxidase (DEP) activity under HL ($300 \mu\text{mol photons} \cdot \text{m}^{-2} \cdot \text{s}^{-1}$) in *P. multistriata*, a feature that has already been recently reported for a coastal (*Phaeocystis cordata*), deep chlorophyll maximum (DCM; *Pelagomonas calceolata*) and surface isolated species (*Mesopedinella arctica*), exposed to gradually increasing light intensities (Dimier *et al.*, 2009b). Differently to what has been described by Dimier *et al.* (2009b), in our study DEP activity has been measured while applying a sudden light change (i.e. from 37 to $300 \mu\text{mol photons} \cdot \text{m}^{-2} \cdot \text{s}^{-1}$). This increasing kinetics of epoxidation from Dt to Dd might represent an ecological competitive advantage, to limit the loss of energy when light becomes less excessive, and thus rapidly increase the photosynthetic quantum yield. These results, together with the short activation time for Dt *de-novo* synthesis measured in this diatom, are consistent with the strong photoacclimative flexibility of species growing in coastal regions (Lavaud *et al.*, 2007; Dimier *et al.*, 2009b).

Despite the apparently modest photoprotective capacity when compared to the microplanktonic diatom, *P. sp. RCC503* ability of adopting distinct photoacclimation strategies, in relation to low or high light conditions, supports its great ecophysiological capacity allowing to gradually increase its growth rate over the irradiance range. Such a great photophysiological plasticity might thus be very favourable in responding to rapid light fluctuations of coastal waters.

The modest NPQ development and low DPS of *P. sp. RCC503*, when compared to *P. multistriata*, reflect the particular photoacclimative strategy deployed by this picoeukaryote under HL. A simplistic generalization concerning an eventual lower photoprotective capacity of Vx cycle-containing species, relative to Dd cycle-containing ones, does not seem to be the case. In fact, comparing our results on *P. sp. RCC503* with the results presented by Dimier and co-authors (2009b) on the surface-isolated species, *Ochromonas sp. (RCC480, Chrysophyceae, Stramenopiles)*, despite showing similar xanthophyll Chl a^{-1} ratio values (ranging between $\sim 0.10 - 0.14 \text{ Vx Chl } a^{-1}$ and $\sim 0.005 - 0.021 \text{ Zx Chl } a^{-1}$, in *O. sp. RCC480*, and between $\sim 0.12 - 0.23 \text{ Vx Chl } a^{-1}$ and $\sim 0.002 - 0.028 \text{ Zx Chl } a^{-1}$, in *P. sp. RCC503*, expressed in mol : mol), NPQ development and DPS are much higher in *O. sp. RCC480* (NPQ = 1.5 and DPS = 50%) than in *P. sp. RCC503* (NPQ = 0.66 and DPS = 9%).

This comparison reveals how diverse adaptive strategies to different ecosystems greatly affect the photophysiological responses functioning, even in Vx cycle-containing species. Undergoing the same experimental conditions of *P. sp. RCC503*, photoacclimation and photoprotection distinct abilities, and capacities of regulation, are described in the two picoplanktonic diatoms, in relation to the physical and chemical characteristics of the water masses of isolation, i.e. upwelling (*M. sp. RCC967*) and oceanic areas (*M. sp. RCC703*).

The upwelling species is a low light-adapted species, in relation to the high turbidity of upwelling waters, with its physiological state being determined by the HL PFD peak. Indeed, under HL, this species adopts a σ -type photoacclimation strategy, lowering its light-harvesting capacity through a decrease in the PSII antenna size, coupled with a huge Dt synthesis (even persisting under low light). This strategy is not advantageous to cope with high light climate variability, as already suggested by other studies (Behrenfeld *et al.*, 1998; Kana *et al.*, 2002; Six *et al.*, 2008), and eventually causes a decrease in growth rate, under HL regimes.

Consistently with its ecological characteristics, the high light-adapted oceanic diatom can instead efficiently cope with HL, and maximize its growth rate over increasing irradiance. In comparison with the upwelling diatom, despite the much lower Dt cellular content and DPS of the oceanic diatom (i.e. $\sim 7.2 \times 10^{-16}$ versus $\sim 1.2 \times 10^{-16}$ Dt cell⁻¹, and DPS of 80 versus 39%, in *M. sp. RCC967* and *RCC703*, respectively), NPQ development is much stronger in the HL-adapted (1.15 ± 0.13 , in *M. sp. RCC703*) than in the LL-adapted species (0.34 ± 0.02 , in *M. sp. RCC967*). *M. sp. RCC703* ecophysiological features prove its adaptation to the surface layer light climate, consistently with similar photoadaptive ability of the aforementioned *O. sp. RCC480*, which has been isolated from the surface layer of Indian Ocean (Dimier *et al.*, 2009b).

In comparison to the oceanic diatom, while the upwelling diatom larger pool of photosynthetic carotenoids probably fits the light-harvesting properties of the low- and variable-light functional groups (as proposed in Dimier *et al.*, 2009b), the much greater cellular content of Dt does not. A possible explanation to this result might reside in the experimental light climate, and particularly in the high PFD peaks, causing a strong XC activation in this low-light adapted diatom, while subjected to a stressful (for this species) light energy pressure. Indeed, in this species, the functionally active photoprotection due to NPQ development is quite low, possibly revealing a photoprotective role of Dt at the level

of the thylakoid membrane lipids, against peroxidation during excessive light exposure, as it has been demonstrated for zeaxanthin in higher plants (Havaux and Niyogi, 1999).

Together with a great physiological diversity in relation to species-specific ecological properties, further complexity is added by the light conditions of the experimental approach (Wagner *et al.*, 2006). The difficulty in comparing results obtained on different species might come from multiple factors affecting the light regime experienced by cells, such as the photoperiod, the light curve, the maximal PFD peaks and the irradiance quantity integrated per unit of time. In this context, the use of continuous (Lavaud *et al.*, 2007; Six *et al.*, 2008) or fluctuant light climate, either sinusoidal (Dimier *et al.*, 2009a; Giovagnetti *et al.*, 2010) or highly fluctuating regimes (van Leeuwe *et al.*, 2005; Wagner *et al.*, 2006; van de Poll *et al.*, 2007; Dimier *et al.*, 2009a), might result in different ecophysiological response to high light. For all the aforementioned reasons, and since one of the main purpose of this study was to investigate the relation between phytoplankton photophysiological functional diversity and ecological adaptation, a gradually increasing sine light climate (whose maximal intensity corresponded to a PFD of 500 or 650 $\mu\text{mol photons} \cdot \text{m}^{-2} \cdot \text{s}^{-1}$) has been applied to all the experiments, to limit the eventual physiological stress due to continuous or largely excessive irradiance, and to facilitate ecological interpretations.

One of our interests has been to dissect the XC ecophysiology investigating it in relation with light velocity increase (i.e. the integrated irradiance intensity per unit of time), to test if this variable parameter would affect the XC/NPQ dynamics. Experiments have been conducted on the diatom *P. multistriata*, that underwent three kinetics of light increase (same maximal PFDs, but reached in 5, 3 and 2 hours), to simulate three mixing events. In our opinion, the achieved results are very interesting, they stimulate our curiosity and deserve a deeper study. The slowest kinetics (i.e. 5 hours) seems to cause a photoresponse that we can call normal- diel response, in fact, the time of light increase is almost equal to the diel cycle of light. The relatively low velocity of this irradiance increase allows for an effective photoprotective response, relying upon the most intense and efficient XC activation and photoprotective biosynthetic pathway regulation, with no need for a strong NPQ enhancement.

Faster shifts from low to high light are instead perceived as far from a potential diel cycle of light, and thus induce peculiar photoprotective response dynamics. A strong carotenoid biosynthesis and XC activation are prevented, while a higher NPQ development (through a

multi-component mechanism) is required, until the integrated irradiance quantity per unit of time becomes stressful (i.e. the 2 hours kinetic), and the velocity of light change overcomes the species capacity to cope with light increase.

Since phytoplankton great complexity and variability of photoprotective and photoacclimative responses, modelling approaches might represent a further and interesting tool, to tackle the XC ecophysiology. Recent studies underline the importance of implementing the formulations of theoretical models in the light of the actual knowledge of the physiological processes, moving away from parameterization based on empirically derived functions (Flynn, 2010; Allen and Polimene, 2011). In such modeling framework, the XC ecophysiology might be questioned and its regulation/modulation deepened in response to simulated natural irradiance conditions, to better understand the XC impact on NPQ extent and modulation (in terms of Dd cycle dependent or independent contributions), as well as on photosynthetic and growth rate maintenance/maximization. Building appropriate theoretical models would also permit to test different variables, known to affect the light climate, and to extract the essence out of the obtained results, in order to design laboratory experiments and zoom-in on precise questions concerning phytoplankton photophysiology. Few steps have been recently taken in this direction, with a mathematical model quantitatively describing the generic NPQ *versus* E curve, and its relationship with the photoacclimation of studied organisms (via light–response curves of the PSII ETR; Serôdio and Lavaud, 2011), and a numerical model describing the xanthophyll-mediated photoprotective activity in phytoplankton, to study cellular photoprotective responses (Polimene *et al.*, submitted).

The study of one micro- and three picoplanktonic species enabled us to draw some considerations on the biological and ecological advantages and disadvantages related to small cell size.

The Chl *a* cellular content of the three picoeukaryotes (cell size range between 2.6 and 3.3 μm) fits the range of values measured in other small-sized species (Dimier *et al.*, 2007a, 2009b; Giovagnetti *et al.*, 2010), ranging between ~ 1 and $\sim 3 \times 10^{-16}$ mol Chl *a* cell $^{-1}$, demonstrating the relevance of size in pigment content determination.

Due to an almost ten-fold larger cell size, relative to the size of picoplanktonic species, the microplanktonic diatom (*P. multistriata*) has a higher Chl *a* cellular pool (ranging between ~ 3 and $\sim 12 \times 10^{-16}$ mol Chl *a* cell $^{-1}$), being able of greater changes in content of Chl *a*

and photosynthetic accessory pigments than the two picoplanktonic diatoms, in agreement with its adaptation to coastal waters. To a lower extent, this flexibility is also found in *Phaeomonas* sp. RCC503, with a higher variability in Chl *a* (between $\sim 1 - 3 \times 10^{-16}$ mol Chl *a* cell⁻¹) and accessory pigments pool, than the two picoplanktonic diatoms.

Minute cell-sized species present a set of features significantly affecting the acquisition and use of resources (nutrient and light energy). The greater picoeukaryotes efficiency in resources acquisition and use, rather than larger species, is supported by the greater absolute maximal electron transport rate ($_{\text{abs}}\text{ETR}_{\text{max}}$) values measured in the picoeukaryotic (from three- to ten-fold greater values), than in the microplanktonic species. Furthermore, a significant correlation occurs when the growth rate and $_{\text{abs}}\text{ETR}_{\text{max}}$ values of the three picoeukaryotes are pooled together, thus underlining the narrow relationship that links photosynthesis regulation and growth capacity in these small organisms. The higher photosynthetic efficiency (α^{B}) of picoeukaryotes (ranging between ~ 0.11 and ~ 0.23 mol e⁻ g Chl *a*⁻¹ h⁻¹ [$\mu\text{mol photons} \cdot \text{m}^{-2} \cdot \text{s}^{-1}$]⁻¹), than *P. multistriata* (ranging between ~ 0.005 and ~ 0.008 mol e⁻ g Chl *a*⁻¹ h⁻¹ [$\mu\text{mol photons} \cdot \text{m}^{-2} \cdot \text{s}^{-1}$]⁻¹), might be due to the higher Chl *a* cellular content and package effect of bigger than smaller species, but also to picoeukaryotes greater acclimation capacity in coping with low light environment. This feature would fit with the higher efficiency, of smaller than larger cells, in exploiting resource-poor (i.e. oligotrophic and low light) environments, and maintaining the growth by restraining energy-losses.

The smaller package effect and lower sinking rate, in smaller than larger cells, involve a greater potential for photosynthetic reactions saturation, and eventually photodamage, by photosynthetically active and UV-B radiation (Raven, 1998). By comparing xanthophylls to Chl *a* ratio values, DPS, and NPQ, in the four species, no major differences can be discerned in function of the size physical constraints. The distinct experimental approaches used for the two size-classes make a precise comparative effort as very difficult. For this reason, further studies on the role played by cell size, on the capacity of XC and NPQ regulation, are requested to deeply understand how cell size would shape the intracellular energetic fluxes in function of photoregulation, photosynthesis and growth.

* * *

BIBLIOGRAPHY

- AHRENS, M. A. AND PETERS, R. H. (1991). Patterns and limitations in limnoplankton size spectra. *Can. J. Fish. Aquat. Sci.*, **48**: 1967–1978.
- AKSNES, D. L. AND EGGE, J. K. (1991). A theoretical model for nutrient uptake in phytoplankton. *Mar. Ecol. Prog. Ser.*, **70**: 65–72.
- ALLEN, J. I. AND POLIMENE, L. (2011). Linking physiology to ecology: towards a new generation of plankton models. *J. Plankton Res.*, **33**: 989–997.
- ALTABET, M.A. (1990). Organic C, N and stable isotope composition of particulate matter collected on glass-filter and aluminium oxide filters. *Limnology and Oceanography* **35**: 902–909.
- ANDERSEN, R.A., BIDIGARE, R.R., KELLER, M.D., AND LATASA, M. (1996). A comparison of HPLC pigment signatures and electron microscopic observations for oligotrophic waters of the North Atlantic and Pacific Oceans. *Deep-Sea Res. Pt. II, Topical Studies in Oceanography* **43**: 517–537.
- ANDERSEN, R. A., SAUNDERS, G. W., PASKIND, M. P. AND SEXTON, J. (1993). Ultrastructure and 18S rRNA gene sequence for *Pelagomonas calceolata* gen. and sp. nov. and the description of a new algal class, the Pelagophyceae *classis* nov. *J. Phycol.*, **29**: 701–715.
- ANDERSON, J. M., GOODCHILD, D. AND BOARDMAN, N. (1973). Composition of the photosystems and chloroplast structure in extreme shade plants. *Biochim. Biophys. Acta*, **325**: 573–585.
- ANDERSON, J. A., CHOW, W. S. AND PARK, Y. I. (1995). The grand design of photosynthesis: acclimation of the photosynthetic apparatus to environmental stress. *Photosynth. Res.*, **46**: 129–139, 1995.

- ANNING, T., MACINTYRE, H. L., PRATT, S. M., SAMMES, P. J., GIBB, S. AND GEIDER, R. J. (2000). Photoacclimation in the marine *Skeletonema costatum*. *Limnol. Oceanogr.*, **45**: 1807–1817.
- APT, K. E., CLENDENNEN, S. K., POWERS, D. A. AND GROSSMAN, A. R. (1995). The gene family encoding the fucoxanthin chlorophyll proteins from the brown alga *Macrocystis pyrifera*. *Molecular Genetics and Genomics* **246**: 445-464.
- ARMBRUST, E. V. (2009). The life of diatoms in the world's oceans. *Nature*, **459**: 185–192.
- ARMBRUST, E. V., BERGES, J. A., BOWLER, C. ET AL. (2004). The genome of the diatom *Thalassiosira pseudonana*: Ecology, evolution, and metabolism. *Science*, **306**: 79–86.
- ARMSTRONG, R. A. (2003). A hybrid spectral representation of phytoplankton growth and zooplankton response: the 'control rod' model of plankton interaction. *Deep-Sea Res. Pt. II*, **50**: 2895–2916.
- ARSALANE, W., ROUSSEAU, B. AND DUVAL, J.-C. (1994). Influence of the pool size of the xanthophyll cycle on the effects of light stress in a diatom: competition between photoprotection and photoinhibition. *Photochem. Photobiol.*, **60**: 237–243.
- AZAM, F., FENCHEL, T., FIELD, J. G., GRAY, J. S., MEYER-REIL, L. A. AND THINGSTAD, F. (1983). The ecological role of water column microbes in the sea. *Mar. Ecol. Prog. Ser.*, **10**: 257–263.
- BADGER, M.R., CAEMMERER, VON, S., RUUSKA, S. AND NAKANO, H. (2000). Electron flow to oxygen in higher plants and algae: rates and control of direct photoreduction (Mehler reaction) and rubisco oxygenase. *Phil. Trans. R. Soc. Lond. B.*, **355**: 1433-1446.
- BAILEY, S. AND GROSSMAN, A. (2008) Photoprotection in cyanobacteria: regulation of light harvesting. *Photochem. Photobiol.*, **84**: 1410–1420.
- BAILEY, S., MANN, N.H., ROBINSON, C. AND SCANLAN, D.J. (2005). The occurrence of rapidly reversible non-photochemical quenching of chlorophyll a fluorescence in cyanobacteria. *FEBS Letters*, **579**: 275-280.
- BAILEY-WATTS, A.E., BINDLESS, M.E. AND BELCHER, J.H. (1968). Freshwater primary productivity by a blue-green alga of bacterial size. *Nature*, **220**: 1344–1345.
- BAILLEUL, B., ROGATO, A., DE MARTINO, A., COESEL, S., CARDOL, P., BOWLER, C., FALCIATORE, A. AND FINAZZI, G. (2010). An atypical member of the light-harvesting complex stress-related protein family modulates diatom responses to light. *Proc. Natl. Acad. Sci. U.S.A.*, **107**: 18214–18219.

- BAKER, N.R. AND HORTON, P. (1987). Physiological factors associated with fluorescence quenching during photoinhibition. In: Arntzen C.J., Kyle D.J. and Osmond C.B. (Eds.), *Topics in Photosynthesis, Photoinhibition, vol. 9*. Elsevier, Amsterdam, 145–168.
- BALLOTTARI, M., GIRARDON, J., DALL'OSTO, L. AND BASSI, R. (2011). Evolution and functional properties of Photosystem II light harvesting complexes in eukaryotes. *Biochim. Biophys. Acta*, doi: 10.1016/j.bbabi.2011.06.005.
- BANSE, K. (1976). Rates of growth, respiration and photosynthesis of unicellular algae as related to cell size - a review. *J. Phycol.*, **12**: 135–140.
- BASSHAM, J. A. (2003). Mapping the carbon reduction cycle, a personal retrospective. *Photosynth. Res.*, **76**: 35-52.
- BASSI, R. AND CAFFARRI, S. (2000). Lhc proteins and the regulation of photosynthetic light harvesting function by xanthophylls. *Photosynth. Res.*, **64**: 243–256.
- BEARDALL, J., ALLEN, D., BRAGG, J., FINKEL, Z. V., FLYNN, K. J., QUIGG, A., REES, T. A. V., RICHARDSON, A. AND RAVEN, J. A. (2009). Allometry and stoichiometry of unicellular, colonial and multicellular phytoplankton. *New Phytol.*, **181**: 1–15.
- BEARDALL, J. AND STOJKOVIC, S. (2006). Microalgae under global environmental change: implications for growth and productivity, populations and trophic flow. *ScienceAsia*, **32**: 1–10.
- BEARDALL, J. AND RAVEN, J. A. (2004). The potential effects of global climate change on microalgal photosynthesis, growth and ecology. *Phycologia*, **43**: 26–40.
- BEARDALL, J. AND MORRIS, I. (1976). The concept of light intensity adaptation in marine phytoplankton: some experiments with *Phaeodactylum tricornutum*. *Mar. Biol.*, **37**: 377–387.
- BECKER, F. AND RHIEL, E. (2006). Immuno-electron microscopic quantification of the fucoxanthin chlorophyll *a/c*-binding polypeptides Fcp2, Fcp4, and Fcp6 of *Cyclotella cryptica* grown under low and high-light intensities. *Int. Microbiol.*, **9**: 29–36.
- BEER, A., GUNDERMANN, K., BECKMANN, J. AND BÜCHEL, C. (2006). Subunit composition and pigmentation of fucoxanthin-chlorophyll proteins in diatoms: evidence for a subunit involved in diadinoxanthin and diatoxanthin binding. *Biochemistry*, **45**: 13046–13053.
- BEHRENFELD, M. J., PRASIL, O., BABIN, M. AND BRUYANT, F. (2004). In search of a physiological basis for covariations in light-limited and light-saturated photosynthesis. *J. Phycol.*, **40**: 4–25.
- BÉJÀ, O., ARAVIND, L., KOONIN, E. V. ET AL. (2000). Bacterial rhodopsin: evidence for a new type of phototrophy in the sea. *Science*, **289**: 1902–1906, 2000.

- BEKKER, A., HOLLAND, H. D., WANG, P.-L. *ET AL.* (2004). Dating the rise of atmospheric oxygen. *Nature*, **427**: 117–120.
- BENSON, A. A. (2002). Paving the path. *Annu. Rev. Plant Biol.*, **53**: 1–23.
- BERNER, T., DUBINKSKY, Z., WYMAN, K. AND FALKOWSKI, P. G. (1989). Photoadaptation and the package effect in *Dunaliella tertiolecta* (Chlorophyceae). *J. Phycol.*, **25**: 70–78.
- BERTHOS, N.R. AND GIBBS, S.P. (1998). Evidence for a lack of photosystem segregation in *Chlamydomonas reinhardtii* (Chlorophyceae). *J. Phycol.*, **34**: 1009–1016.
- BERTRAND, M. (2010). Carotenoid biosynthesis in diatoms. *Photosynth. Res.*, **106**: 89–102.
- BERTRAND, M., SCHOEFS, B., SIFFEL, P., ROHACEK, K. AND MOLNAR, I. (2001). Cadmium inhibits epoxidation of diatoxanthin to diadinoxanthin in the xanthophyll cycle of the marine diatom *Phaeodactylum tricornutum*. *FEBS Lett.*, **508**: 153–156.
- BIDIGARE, R. R., R. C. SMITH, K. S. BAKER AND MARRA, J. (1987). Oceanic primary production estimates from measurements of spectral irradiance and pigment concentration. *Global Biogeochem. Cycles*, **1**: 171–186.
- BIEGALA, I. C., NOT, F., VAULOT, D. AND SIMON, N. (2003). Quantitative assessment of picoeucaryotes in the natural environment using taxon specific oligonucleotide probes in association with TSA-FISH (tyramide signal amplification-fluorescent *in situ* hybridization) and flow cytometry. *Appl Environ. Microbiol.*, **69**: 5519–5529.
- BILGER, W., BJÖRKMAN, O. AND THAYER, S. S. (1989). Light-induced spectral absorbance changes in relation to photosynthesis and the epoxidation state of xanthophyll cycle components in cotton leaves. *Plant Physiol.*, **91**: 542–551.
- BINDER, B. J., CHISHOLM, S. W., OLSON, R. J., FRANKEL, S. L. AND WORDEN, A. Z. (1996). Dynamics of pico-phytoplankton, ultra-phytoplankton, and bacteria in the central equatorial Pacific. *Deep-Sea Res. Pt. II*, **43**: 907–931.
- BJÖRNLAND, T. AND LIAAEN-JENSEN, S. (1989). Distribution patterns of carotenoids in relation to chromophyte phylogeny and systematics. In: Green, J., Leadbeater, B. and Driver, W.(Eds.), *The Chromophyte algae: problems and perspectives*. Volume 38, pages 37–60. Clarendon Press, Oxford.
- BLANCHOT, J. AND RODIER, M. (1996). Picophytoplankton abundance and biomass in the western tropical Pacific Ocean during the 1992 El Niño year: Results from flow cytometry. *Deep-Sea Res. Pt. I*, **43**: 877–895.
- BLANCHOT, J., ANDRE, J. M., NAVARETTE, C., NEVEUX, J. AND RADENAC, M. H. (2001). Picophytoplankton in the equatorial Pacific: vertical distributions in the warm pool and in high nutrient low chlorophyll conditions. *Deep-Sea Res. Pt. I*, **48**: 297–314.

- BLATT, M. R., WEISENSEEL, M. H. AND HAUPT, W. (1981). A light-dependent current associated with chloroplast aggregation in the alga *Vaucheria sessilis*. *Planta*, **152**: 513–526.
- BOULAY, C., WILSON, A., D'HAENE, S. AND KIRILOVSKY, D. (2010). Identification of a protein required for recovery of full antenna capacity in OCP-related photoprotective mechanism in cyanobacteria. *Proc. Natl. Acad. Sci. U.S.A.*, **107**: 11620–11625.
- BOULAY, C., ABASOVA, L., SIX, C., VASS, I. AND KIRILOVSKY, D. (2008). Occurrence and function of the orange carotenoid protein in photoprotective mechanisms in various cyanobacteria. *Biochim. Biophys. Acta*, **1777**: 1344–1354.
- BOUVIER, F., D'HARLINGUE, A., HUGUENEY, P., MARIN, E., MARION-POLL, A. AND CAMARA, B. (1996). Xanthophyll biosynthesis: cloning, expression, functional reconstitution, and regulation of *b*-cyclohexenyl carotenoid epoxidase from pepper (*Capsicum annuum*). *J. Biol. Biochem.*, **271**: 28861–28867.
- BOWLER, C., ALLEN, A. E., BADGER, J. H. ET AL. (2008). The *Phaeodactylum* genome reveals the evolutionary history of diatom genomes. *Nature*, **456**: 239–244.
- BRATT, C. E., ARVIDSSON, P. O., CARLSSON, M. AND AKERLUND, H. E. (1995). Regulation of violaxanthin de-epoxidase activity by pH and ascorbate concentration. *Photosynth. Res.*, **45**: 169–175.
- BROWN, J. H., GILLOOLY, J. F., ALLEN, A. P., SAVAGE, V. M. AND WEST, G. B. (2004). Toward a metabolic theory of ecology. *Ecology*, **85**: 1771–1789.
- BROWN, S. L., LANDRY, M. R., BARBER, R. T., CAMPBELL, L., GARRISON, D. L. AND GOWING, M. M. (1999). Picophytoplankton dynamics and production in the Arabian Sea during the 1995 Southwest Monsoon. *Deep-Sea Res. Pt. II*, **46**: 1745–1768.
- BRUNET, C., JOHNSEN, G., LAVAUD, J. AND ROY, S. (2011). Selected pigment applications in oceanography. Pigments and photoacclimation processes. In: Roy, S., Johnsen, G., Llewellyn, C. and Skarstad, E. (Eds), *Phytoplankton Pigments in Oceanography: Guidelines to Modern Methods, Series: Oceanographic Methodologies*. Vol. 2. SCOR-UNESCO Publishing, Cambridge University Press.
- BRUNET, C. and LAVAUD, J. (2010). Can the xanthophyll cycle help extract the essence of the microalgal functional response to a variable light environment? *J. Plankton Res.*, **32**: 1609–1617.
- BRUNET, C., CASOTTI, R., VANTREPOTTE, V. AND CONVERSANO, F. (2007). Vertical variability and diel dynamics of picophytoplankton in the Strait of Sicily (Mediterranean Sea) in summer. *Mar. Ecol. Prog. Ser.*, **346**: 15–26.

- BRUNET, C., CASOTTI, R., VANTREPOTTE, V., CORATO, F. AND CONVERSANO, F. (2006). Picophytoplankton diversity and photophysiology in the Strait of Sicily (Mediterranean Sea) in summer. I. Mesoscale variations. *Aquat. Microbiol. Ecol.*, **44**: 127–141.
- BRUNET, C., CASOTTI, R., ARONNE, B. AND VANTREPOTTE, V. (2003). Measured photophysiological parameters used as tools to estimate vertical water movements in the coastal Mediterranean. *J. Plankton Res.*, **25**: 1413–1425.
- BRUNET, C., DAVOULT, D. AND CASOTTI, R. (1996). Physiological reactions to a change in light regime in cultured *Skeletonema costatum* (Bacillariophyta): implications to estimation of phytoplankton biomass. *Hydrobiologia*, **333**: 87–94.
- BRUNET, C., BRYLINSKY, J. M. AND LEMOINE, Y. (1993). *In situ* variations of the xanthophylls diatoxanthin and diadinoxanthin: photoadaptation and relationships with a hydrodynamical system in the Eastern English Channel. *Mar. Ecol. Prog. Ser.*, **102**: 69–77.
- BRUNET, C., BRYLINSKY, J. M. AND FRONTIER, S. (1992). Productivity, photosynthetic pigments and hydrology in the coastal front of the Eastern English Channel. *J. Plankton Res.*, **14**: 1541–1552.
- BÜCH, K., STRANSKY, H. AND HAGER, A. (1995). FAD is a further essential cofactor of the NAD(P)H and O₂-dependent zeaxanthin-epoxidase. *FEBS Lett.*, **376**: 45–48.
- BÜCHEL, C. (2003). Fucoxanthin–chlorophyll proteins in diatoms: 18 and 19 kDa subunits assemble into different oligomeric states. *Biochemistry*, **42**: 13027–13034.
- BÜCHEL, C. AND WILHELM, C. (1993). Isolation and characterization of a photosystem I-associated antenna (LHC I) and a photosystem I-core complex from the chlorophyll *c*-containing alga *Pleurochloris meiringensis*. *J. Photochem. Photobiol.*, **20**: 87–93, 1993.
- BÜCHEL, C. AND WILHELM, C. (1992). Evidence for a lateral heterogeneity by patchwork-like areas enriched with photosystem I complexes in the three thylakoid lamellae of *Pleurochloris meiringensis* (Xanthophyceae). *Journal of Cryptogam Botany*, **2**: 375–386.
- BUGOS, R. C., HIEBER, A. D. AND YAMAMOTO, H. Y. (1998). Xanthophyll cycle enzymes are members of the lipocalin family, the first identified from plants. *J. Biol. Chem.*, **273**: 15321–15324.
- BUGOS, R. C. AND YAMAMOTO, H. Y. (1996). Molecular cloning of violaxanthin de-epoxidase from romaine lettuce and expression in *Escherichia coli*. *Proc. Natl. Acad. Sci. U.S.A.*, **93**: 6320–6325.

- BUMA, A. G. J., MOORDELOOS, A. A. M. AND LARSEN, J. (1993). Strategies and kinetics of photoacclimation in three Antarctic nanophytoflagellates. *J. Phycol.*, **29**: 407–417.
- BUTCHER, R. (1952). Contributions to our knowledge of the smaller marine algae. *J. Mar. Biol. Assoc. UK*, **31**: 175–191.
- CAMPBELL, L. AND VAULOT, D. (1993). Photosynthetic picoplankton community structure in the subtropical North Pacific Ocean near Hawaii (Station ALOHA). *Deep-Sea Res.*, **40**: 2043–2060.
- CARDOL, P., BAILLEUL, B., RAPPAPORT, F. ET AL. (2008). An original adaptation of photosynthesis in the marine green alga *Ostreococcus*. *Proc. Natl. Acad. Sci. U.S.A.*, **105**: 7881–7886.
- CARON, L., REMY, R. AND BERKALOFF, C. (1988). Polypeptide composition of light-harvesting complexes from some algae and diatoms. *FEBS Lett.*, **229**: 11–15.
- CASOTTI, R., MAZZA, S., BRUNET, C., VANTREPOTTE, V., IANORA, A. AND MIRALTO, A. (2005). Growth inhibition and toxicity of the diatom aldehyde 2-*trans*,4-*trans*-decadienal on *Thalassiosira weissflogii* (Bacillariophyceae). *J. Phycol.*, **41**: 7–20.
- CASPER-LINDLEY, C. AND BJORKMAN, O. (1998). Fluorescence quenching in 4 unicellular algae with different light-harvesting and xanthophyll-cycle pigments. *Photosynth. Res.*, **56**: 277–289.
- CHISHOLM, S.W. (1992). Phytoplankton size. In: Falkowski, P. G. and Woodhead, A. D. (Eds.), *Primary Productivity and Biogeochemical Cycles in the Seas*. Plenum Press, New York, 213–237.
- CHISHOLM, S. W., OLSON, R. J., ZETTLER, E. R., WATERBURY, J., GOERICKE, R. AND WELSCHMEYER, N. (1988). A novel free-living prochlorophyte occurs at high cell concentrations in the oceanic euphotic zone. *Nature*, **334**: 340–343.
- CHRÉTIENNOT-DINET, M. J., COURTIES, C., VAQUER, A., NEVEUX, J., CLAUSTRE, H., LAUTIER, J. AND MACHADO, M. C. (1995). A new marine picoeukaryote: *Ostreococcus tauri* gen. et sp. nov. (Chlorophyta, Prasinophyceae). *Phycologia*, **34**: 285–292.
- CLAUSTRE, H., KERHERVÉ, P., MARTY, J. C. AND PRIEUR, L. (1994). Phytoplankton photoadaptation related to some frontal physical processes. *J. Mar. Syst.*, **5**: 251–265.
- CLEVELAND, J. S. AND WEIDEMANN, A. D. (1993). Quantifying absorption by aquatic particles: A multiple scattering correction for glass-fiber filters. *Limnol. Oceanogr.*, **38**: 1321–1327.
- COGDELL, R. J. (2006). The structural basis of non-photochemical quenching revealed? *Trends in plant science* 11: 59-60.

- CONAN, P., SONDERGAARD, M., KRAGH, T. *ET AL.* (2007). Partitioning of organic production in marine plankton communities: the effects of inorganic nutrient ratios and community composition on new dissolved organic matter. *Limnol. Oceanogr.*, **52**: 753–765.
- CORATO, F., BRUNET, C. AND DIMIER C. (2007). Sviluppo ed applicazioni in fotobiologia algale di un sistema ad illuminazione variabile. *Biologia dei Sistemi Acquatici*, **2**: 37–43.
- CONSALVEY, C., PERKINS, R. G. AND PATERSON, D. M. (2005). PAM fluorescence: a beginners guide for benthic diatomists. *Diatom Res.*, 20:1–22.
- COUNTWAY, P. D. AND CARON, D. A. (2006). Abundance and distribution of *Ostreococcus* sp. in the San Pedro Channel, California, as revealed by quantitative PCR. *Appl. Environ. Microbiol.*, **72**: 2496–2506.
- COURTIES, C., VACQUER, A., TROUSSELLIER, M., LAUTIER, J., CHRÉTIENNOT-DINEL, M. J., NEVEUX, J., MACHADS, C. AND CLAUSTRE, H. (1994). Smallest eukaryotic organism. *Nature*, **370**: 255.
- CROCE, R., BRETON, J. AND BASSI, R. (1996). Conformational changes induced by phosphorylation in the CP29 subunit of photosystem II. *Biochemistry*, **35**: 11142–11148.
- CULLEN, J. J. (1990). On models of growth and photosynthesis in phytoplankton. *Deep-Sea Res.*, **37**: 667–683.
- CULLEN, J. J., FRANK, P. J. S., KARL, D. M. AND LONGHURST, A. (2002). Physical influences on marine ecosystem dynamics. In: Robinson, A., McCarthy, J. and Rothschild, B. (Eds.), *The Sea*, Volume 12, pages 297–336. John Wiley and Sons, New York.
- CULLEN, J. J. AND LEWIS, M. R. (1988). The kinetics of algal photoadaptation in the context of vertical mixing. *J. Plankton Res.*, **10**: 1039–1063.
- D’ALELIO, D., D’ALCALÀ, M. R., DUBROCA, L., SARNO, D., ZINGONE, D. AND MONTRESOR, M. (2010). The time for sex: A biennial life cycle in a marine diatom. *Limnol. Oceanogr.*, **55**: 106–114.
- D’ALELIO, D., AMATO, A., LUEDEKING, A. AND MONTRESOR, M. (2009). Sexual and vegetative phases in the planktonic diatom *Pseudo-nitzschia multistriata*. *Harmful Algae*, **8**: 225–232.

- DALL'OSTO, L., CAZZANIGA, S., NORTH, H., MARION-POLL, A. AND BASSI, R. (2007). The *Arabidopsis aba4-1* mutant reveals a specific function for neoxanthin in protection against photo-oxidative stress. *Plant Cell*, **19**: 1048–1064.
- DE MARTINO, A., DOUADY, D., QUINET-SZELY, M., ROUSSEAU, B., CRÉPINEAU, F., APT. K. E. AND CARON, L. (2000). The light-harvesting antenna of brown algae. Highly homologous proteins encoded by a multigene family. *Eur. J. Biochem.*, **267**, 5540–5549.
- DEMERS, S., ROY, S., GAGNON, R. AND VIGNAULT, C. (1991). Rapid light-induced changes in cell fluorescence and in xanthophyll-cycle pigments of *Alexandrium excavatum* (Dinophyceae) and *Thalassiosira pseudonana* (Bacillariophyceae): a photo-protection mechanism. *Mar. Ecol. Prog. Ser.*, **76**: 185–193.
- DEMMIG-ADAMS, B. (1990). Carotenoids and photoprotection in plants: a role for the xanthophyll zeaxanthin. *Biochim. Biophys. Acta*, **1020**: 1–24.
- DEMMIG-ADAMS, B. AND ADAMS, W. W. III (2006). Photoprotection in an ecological context: the remarkable complexity of thermal energy dissipation. *New Phytol.*, **172**: 11–21.
- DEMMIG-ADAMS, B. AND ADAMS, W. W. III (2000). Harvesting sunlight safely. *Nature*, **403**: 371–374.
- DEMMIG-ADAMS, B. AND ADAMS, W. W. III (1996). The role of xanthophyll cycle carotenoids in the protection of photosynthesis. *Trends Plant Sci.*, **1**: 21–26.
- DERELLE, E., FERRAZ, C., ROMBAUTS, S. ET AL. (2006). Genome analysis of the smallest free-living eukaryote *Ostreococcus tauri* unveils many unique features, *Proc. Natl. Acad. Sci. U.S.A.*, **103**: 11647–11652.
- DÍEZ, B., PEDRÓS-ALIÓ, C. AND MASSANA, R. (2001b). Study of genetic diversity of eukaryotic picoplankton in different oceanic regions by small-subunit rRNA gene cloning and sequencing. *Appl. Environ. Microbiol.*, **67**: 2932–2941.
- DIMIER, C., BRUNET, C., GEIDER, J. R. AND RAVEN, J. A. (2009a). Growth and photo-regulation dynamics of the picoeukaryote *Pelagomonas calceolata* in fluctuating light. *Limnol. Oceanogr.*, **54**: 823–836.
- DIMIER, C., SAVIELLO, G., TRAMONTANO, F. AND BRUNET, C. (2009b). Comparative ecophysiology of the xanthophyll cycle in six marine phytoplanktonic species. *Protist*, **160**: 397–411.

- DIMIER, C., CORATO, F., TRAMONTANO, G. AND BRUNET, C. (2007a). Photophysiological properties of the marine picoeukaryote *Picochlorum* RCC237 (Trebouxiophyceae, Chlorophyta). *J. Phycol.*, **43**: 275–283.
- DIMIER, C., CORATO, F., TRAMONTANO, F. AND BRUNET, C. (2007b). Photoprotection and xanthophyll cycle activity in three diatoms. *J. Phycol.*, **43**: 937–947.
- DINER, B. A. AND G. T. BABCOCK (1996). Structure, dynamics and energy conversion efficiency in photosystem II. In: Ort, D. and Yocum, C. (Eds.), *Oxygenic photosynthesis: the light reactions*. Pages 137–164. Kluwer Academic Publishers, Dordrecht.
- DITTAMI, S. M., MICHEL, G., COLLÉN, J., BOYEN, C. AND TONON, T. (2010). Chlorophyll-binding proteins revisited – a multigenic family of light-harvesting and stress proteins from a brown algal perspective. *BMC Evol. Biol.*, **10**: 1–14.
- DOMENIGHINI, A. AND GIORDANO, M. (2009). Fourier transform infrared spectroscopy of microalgae as a novel tool for biodiversity studies, species identification, and the assessment of water quality. *J. Phycol.*, **45**: 522–531.
- DUBINSKY, Z. AND SCHOFIELD, O. (2010). From the light to the darkness: thriving at the light extremes in the oceans. *Hydrobiologia*, **639**: 153–171.
- DUBINSKY, Z., FALKOWSKI, P. G. AND WYMAN, K. (1986). Light harvesting and utilization by phytoplankton. *Plant Cell Physiol.*, **27**: 1335–1349.
- DUFRESNE, A., GARZAREK, L. AND PARTENSKY, F. (2005). Accelerated evolution associated with genome reduction in a free-living prokaryote. *Genome Biol.*, **6**: R14.1-R14.10.
- DUFRESNE, A., SALANOUBAT, M., PARTENSKY, F. ET AL. (2003). Genome sequence of the cyanobacterium *Prochlorococcus marinus* SS120, a nearly minimal oxyphototrophic genome. *Proc. Natl. Acad. Sci. U.S.A.*, **100**: 10020–10025.
- DURNFORD, D. G., PRICE, J. A., MCKIM, S. AND SARCHFIELD, M. L. (2003). Light-harvesting complex gene expression is controlled by both transcriptional and post-transcriptional mechanisms during photoacclimation in *Chlamydomonas reinhardtii*. *Physiol. Plant.*, **118**: 193–205.
- DURNFORD, D. G. AND FALKOWSKI, P. G. (1997). Chloroplast redox regulation of nuclear gene transcription during photoacclimation. *Photosynth. Res.*, **52**: 229–241.
- DUSENBERRY, J. A., OLSON, R. J. AND CHISHOLM, S. W. (1999). Frequency distributions of phytoplankton single cell fluorescence and vertical mixing in the surface ocean. *Limnol. Oceanogr.*, **44**: 431–435.

- EILERS, P.H.C. AND PEETERS, J.C.H. (1988). A model for the relationship between light intensity and the rate of photosynthesis in phytoplankton. *Ecol. Model.* **42**: 199–215.
- EISENSTADT, D., OHAD, I., KEREN, N. AND KAPLAN, A. (2008). Changes in the photosynthetic reaction centre II in the diatom *Phaeodactylum tricornutum* result in non-photochemical fluorescence quenching. *Environ. Microbiol.*, **10**: 1997–2007.
- EISENSTADT, D., BARKAN, E., LUZ, B. AND KAPLAN, A. (2010). Enrichment of oxygen heavy isotopes during photosynthesis in phytoplankton. *Photosynth. Res.*, **103**: 97–103.
- EGELAND, E. S., EIKREM, W., THRONSEN, J., WILHELM, C., ZAPATA, M., AND LIAAEN-JENSEN, S. (1995). Carotenoids from further prasinophytes. *Biochem. Syst. Ecol.*, **23**: 747–55.
- EL-BISSATI, K., DELPHIN, E., MURATA, N., ETIENNE, A.-L. AND KIRILOVSKY, D. (2000). Photosystem II fluorescence quenching in the cyanobacterium *Synechocystis* sp. PCC 6803: involvement of two different mechanisms. *Biochim. Biophys. Acta*, **1457**: 229–242.
- ENGELKEN, J., BRINKMANN, H. AND ADAMSKA, I. (2010). Taxonomic distribution and origins of the extended LHC (light-harvesting complex) antenna protein superfamily. *BMC Evol. Biol.*, **10**: 233.
- EPPARD, M., KRUMBEIN, W. E., VON HAESLER, A. AND RHIEL, E. (2000). Characterization of fcp4 and fcp12, two additional genes encoding light harvesting proteins of *Cyclotella cryptica* (Bacillariophyceae) and phylogenetic analysis of this complex gene family. *Plant Biol.*, **2**: 283–289.
- EVENS, T. J., KIRKPATRICK, G. J., MILLIE, D. F., CHAPMAN, D. J. AND SCHOFIELD, O. M. E. (2001). Photophysiological responses of the toxic red-tide dinoflagellate *Gymnodinium breve* (Dinophyceae) under natural sunlight. *J. Plankton Res.*, **23**: 1177–1193.
- FALKOWSKI, P. G. (1994). The role of phytoplankton photosynthesis in global biogeochemical cycles. *Photosynth. Res.*, **39**: 235–258.
- FALKOWSKI, P. G. (1983). Light-shade adaptation and vertical mixing of marine phytoplankton: a comparative field study. *J. Mar. Res.*, **41**: 215–237.
- FALKOWSKI, P. G. (1981). Light-shade adaptation and assimilation numbers. *J. Plankton Res.*, **3**: 203–216.
- FALKOWSKI, P.G. AND RAVEN, J.A. (2007). *Aquatic Photosynthesis*. Princeton, Princeton University Press.
- FALKOWSKI, P. G., SCHOFIELD, O., KATZ, M. E., VAN DE SCHOOTBRUGGE, B. AND KNOLL, A. H. (2004a). Why is the land green and the ocean red? In: Theirstein, H. and Young,

- J. (Eds.), *Coccolithophores – from molecular processes to global impact*. Pages: 429–453. Elsevier, Amsterdam.
- FALKOWSKI, P. G., KATZ, M. E., KNOLL, A. H., QUIGG, A., RAVEN, J. A., SCHOFIELD, O. AND TAYLOR, F. R. J. (2004b). The evolution of modern eukaryotic phytoplankton. *Science* **305**, 354–360.
- FALKOWSKI, P. G. AND CHEN, Y-B. (2003). Photoacclimation of light harvesting systems in eukaryotic algae. In: Beverley, R. and Parson, W. W. (Eds.), *Light harvesting antennas in photosynthesis*, 423–447.
- FALKOWSKI, P. G. AND LAROCHE, J. (1991). Acclimation to spectral irradiance in algae. *J. Phycol.*, **27**: 8–14.
- FALKOWSKI, P. G., DUBINSKY, Z. AND WYMAN, K. (1985). Growth-irradiance relationship between light intensity and the rate of photosynthesis in phytoplankton. *Limnol. Oceanogr.*, **30**: 311–321.
- FALKOWSKI, P.G., OWENS, T.G., LEY, A.C. AND MAUZERALL, D.C. (1981). Effects of growth irradiance levels on the ratio of reaction centers in two species of marine phytoplankton. *Plant Physiol.*, **68**: 969–973.
- FALKOWSKI, P. G. AND OWENS, T. G. (1980). Light-shade adaptation: two strategies in marine phytoplankton. *Plant Physiol.*, **66**: 592–595.
- FARQUHAR, J., BAO, H. AND THIEMENS, M. (2000). Atmospheric influence of Earth's earliest sulfur cycle. *Science*, **289**: 756–758.
- FERREIRA, K. N., IVERSON, T. M., MAGHLAOU, K., BARBER, J. AND IWATA, S. (2004). Architecture of the photosynthetic oxygen-evolving center. *Science*, **303**: 1831–1838.
- FIELD, C. B., BEHRENFELD, M. J., RANDERSON, J. T. AND FALKOWSKI, P. G. (1998). Primary production of the biosphere: integrating terrestrial and oceanic components. *Science*, **281**: 237–240.
- FINAZZI, G., JOHNSON, G. N., DALL'OSTO, L., ZITO, F., BONENTE, G., BASSI, R. AND WOLLMAN, F. A. (2006). Non-photochemical quenching of chlorophyll fluorescence in *Chlamydomonas reinhardtii*. *Biochemistry*, **45**: 1490–1498.
- FINKEL, Z. V. (2007). Does phytoplankton cell size matter? The evolution of modern marine food webs. In: Falkowski, P. G. and Knoll, A. H. (Eds.), *Evolution of Aquatic Photoautotrophs*. Academic Press, San Diego, 333–350.
- FINKEL, Z. V. (2001). Light absorption and size scaling of light-limited metabolism in marine diatoms. *Limnol. Oceanogr.*, **46**: 86–94.

- FINKEL, Z. V., BEARDALL, J., FLYNN, K. J., QUIGG, A., REES, T. A. AND RAVEN, J. A. (2010). Phytoplankton in a changing world: cell size and elemental stoichiometry. *J. Plankton Res.*, **32**: 119–137.
- FINKEL, Z. V. AND IRWIN, A. J. (2000). Modeling size-dependent photosynthesis: light absorption and the allometric rule. *J. Theor. Biol.*, **204**: 361–369.
- FINKEL, Z. V., IRWIN, A. J. AND SCHOFIELD, O. (2004). Resource limitation alters the 3/4 size scaling of metabolic rates in phytoplankton. *Mar. Ecol. Prog. Ser.*, **273**: 269–279.
- FISHER, T., SCHURTZ-SWIRSKI, R., GEPSTEIN, S. AND DUBINSKY, Z. (1989). Changes in the levels of ribulose-1,5-biphosphate carboxylase/oxygenase (Rubisco) in *Tetraedron minimum* (Chlorophyta) during light and shade adaptation. *Plant Cell Physiol.*, **30**: 221–228, 1989.
- FLÖDER, S. U. J. AND KAWABATA, Z.-I. (2002). The influence of fluctuating light intensities on species composition and diversity of natural phytoplankton communities. *Oecologia*, **133**: 395–401.
- FLYNN, K. J. (2010). Ecological modelling in a sea of variable stoichiometry: disfunctionality and the legacy of Redfield and Monod. *Progress Oceanogr.*, **84**: 52–56.
- FOGG, G.E. (1986). Picoplankton. *Proceedings of the Royal Society of London B*, **228**: 1–30.
- FRANK, H.A., BAUTISTA, J.A., JOSUE, J.S. AND YOUNG, A. J. (2000). Mechanism of Nonphotochemical quenching in green plants: energies of the lowest excited singlet states of violaxanthin and zeaxanthin, *Biochemistry*, **39**: 2831–2837.
- FRANK, H., CUA, A., CHYNWAT, V., YOUNG, A., GOSZTOLA, D. AND WASIELEWSKI, M. (1994). Photophysics of the carotenoids associated with the xanthophyll cycle in photosynthesis. *Photosynth. Res.*, **41**: 389–395.
- FRYXELL, G. A. AND HASLE, G. R. (2003). Taxonomy of harmful diatoms. In: Hallegraeff, G. M., Anderson, D. M. and Cembella, A. D. (Eds.), *Manual on harmful marine microalgae*. UNESCO, 465–509.
- FUJIKI, T. AND TAGUCHI, S. (2001). Relationship between light absorption and the xanthophyll-cycle pigments in marine diatoms. *Plankton Biol. Ecol.*, 48:96–103, 2001.
- FUHRMAN, J. (2003). Genome sequences from the sea. *Nature*, **424**: 1001–1002.
- FULLER, N. J., CAMPBELL, C., ALLEN, D. J., PITT, F. D., LE GALL, F., VAULOT, D. AND SCANLAN, D. J. (2006a). Analysis of photosynthetic picoeukaryote diversity at open ocean sites in the Arabian Sea using a PCR biased towards marine algal plastids. *Aquat. Microb. Ecol.*, **43**: 79–93.

- FULLER, N. J., TARRAN, G., CUMMINGS, D. *ET AL.* (2006b). Molecular analysis of photosynthetic picoeukaryote community structure along an Arabian Sea transect. *Limnol. Oceanogr.*, **51**: 2502–2514.
- GEIDER, G. AND MACINTYRE, H. L. (2002). Physiology and biochemistry of photosynthesis and algal carbon acquisition. In: Williams, P. J., Thomas, D. R. and Reynolds, C. S. (Eds.), *Phytoplankton productivity and carbon assimilation in marine and freshwater ecosystems*. Blackwell Science, London.
- GEIDER, R. J., MACINTYRE, H. L. AND KANA, T. M. (1997). A dynamic model of phytoplankton growth and acclimation: responses of the balanced growth rate and chlorophyll a:carbon ratio to light, nutrient limitation and temperature. *Mar. Ecol. Prog. Ser.*, **148**: 187–200.
- GEIDER, R. J., H. L. MACINTYRE AND T.M. KANA (1996). A dynamic model of photoadaptation in phytoplankton. *Limnol. Oceanogr.*, **41**: 1–15.
- GENTY, B. B., BRIANTAIS, J. M. AND BAKER, N. R. (1989). The relationship between the quantum yield of photosynthetic electron transport and quenching of chlorophyll fluorescence. *Biochim. Biophys. Acta*, **990**: 87–92.
- GILLOOLY, J. F., BROWN, J. H., WEST, G. B. *ET AL.* (2001). Effects of size and temperature on metabolic rate. *Science*, **293**: 2248–2251.
- GILMORE, A. M. (1997). Mechanistic aspects of xanthophyll cycle-dependent photoprotection in higher plant chloroplasts and leaves. *Physiol. Plant.*, **99**: 197–209.
- GILMORE, A. M. AND YAMAMOTO, H. (1993). Linear models relating xanthophylls and lumen acidity to non-photochemical fluorescence quenching. Evidence that antheraxanthin explains zeaxanthin-independent quenching. *Photosynth. Res.*, **35**: 67–78.
- GIORDANO, M., BEARDALL, J. AND RAVEN, J. A. (2005). CO₂ concentrating mechanisms in algae: mechanisms, environmental modulation and evolution. *Annu. Rev. Plant Biol.*, **56**: 641–658.
- GIORDANO, M., KANSIZ, M., HERAUD, P., BEARDALL, J., WOOD, B. AND MCNAUGHTON, D. (2001). Fourier transform infrared spectroscopy as a novel tool to investigate changes in intracellular macromolecular pools in the marine microalga *Chaetoceros muellerii* (Bacillariophyceae). *J. Phycol.*, **37**: 271–279.
- GIOVAGNETTI, V., CATALDO, M.L., CONVERSANO, F. AND BRUNET, C. (2010). Functional relation between growth, photosynthetic rate and regulation in the coastal picoeukaryote

- Phaeomonas* sp. RCC 503 (Pinguiphyceae, Stramenopiles). *J. Plankton Res.*, **32**: 1501–1511.
- GIOVANNONI, S. J., TRIPP, H. J., GIVAN, S. *ET AL.* (2005). Genome streamlining in a cosmopolitan oceanic bacterium. *Science*, **309**: 1242–1245.
- GIOVANNONI, S. J., BRITSCHGI, T. B., MOYER, C. L. AND FIELD, K. G. (1990). Genetic diversity in Sargasso Sea bacterioplankton. *Nature*, **345**: 60–63.
- GOEDHEER, J. C. (1970). On the pigment system of brown algae. *Photosynthetica*, **4**: 97–106.
- GOERICKE, R. AND MONTROYA, J. P. (1998). Estimating the contribution of microalgal taxa to chlorophyll a in the field - variations of pigment ratio under nutrient and light-limited growth. *Mar. Ecol. Prog. Ser.*, **169**: 97–112.
- GOERICKE, R. AND WELSCHMEYER, N. A. (1992). Pigment turnover in the marine diatom *Thalassiosira weissflogii*. II. The ¹⁴CO₂-labeling kinetics of carotenoids. *J. Phycol.*, **28**: 507–517.
- GORBUNOV, M. Y., KUZMINOV, F. I., FADEEV, V. V., KIM, J. D. AND FALKOWSKI, P. G. (2011). A kinetic model of non-photochemical quenching in cyanobacteria. *Biochim. Biophys. Acta*, **1807**: 1591–1599.
- GOSS, R. AND JAKOB, T. (2010). Regulation and function of xanthophyll cycle-dependent photoprotection in algae. *Photosynth. Res.*, **106**: 103–122.
- GOSS, R. AND WILHELM, C. (2009). Lipids in algae, lichens and mosses. In: Wada, H., Murata, N. and Govindjee (Eds.), *Lipids in photosynthesis: essential and regulatory functions*. Vol. 5. Springer Science. Business Media B, Dordrecht, The Netherlands, Pages: 117–137.
- GOSS, R., LATOWSKI, D., GRZYB, J., VIELER, A., LOHR, M., WILHELM, C. AND STRZALKA, K. (2007). Lipid dependence of diadinoxanthin solubilization and de-epoxidation in artificial membrane systems resembling the lipid composition of the natural thylakoid membrane. *Biochim. Biophys. Acta*, **1768**: 67–75.
- GOSS, R., LEPETIT, B. AND WILHELM, C. (2006a). Evidence for a rebinding of antheraxanthin to the light-harvesting complex during the epoxidation reaction of the violaxanthin cycle. *J. Plant Physiol.*, **163**: 585–590.
- GOSS, R., ANN PINTO, E., WILHELM, C. AND RICHTER, M. (2006b). The importance of a highly active and ΔpH-regulated diatoxanthin epoxidase for the regulation of the PS II antenna function in diadinoxanthin cycle containing algae. *J. Plant Physiol.*, **163**: 1008–1021.

- GOSS, R., LOHR, M., LATOWSKI, D., GRZYB, J., VIELER, A., WILHELM, C. AND STRZALKA, K. (2005). Role of hexagonal structure-forming lipids in diadinoxanthin and violaxanthin solubilization and de-epoxidation. *Biochemistry*, **44**: 4028–4036.
- GOSS, R. (2003). Substrate specificity of the violaxanthin de-epoxidase of the primitive green alga *Mantoniella squamata* (Prasinophyceae). *Planta*, **217**: 801–812.
- GOSS, R. AND GARAB, G. (2001). Non-photochemical chlorophyll fluorescence quenching and structural rearrangements induced by low pH in intact cells of *Chlorella fusca* (Chlorophyceae) and *Mantoniella squamata* (Prasinophyceae). *Photosynth. Res.*, **67**: 185–197.
- GOSS, R., BÖHME, K. AND WILHELM, C. (1998). The xanthophyll cycle of *Mantoniella squamata* converts violaxanthin into antheraxanthin but not to zeaxanthin: consequences for the mechanism of enhanced non-photochemical energy dissipation. *Planta*, **205**: 613–621.
- GOSS, R., RICHTER, M. AND WILD, A. (1995). Role of Δ pH in the mechanism of zeaxanthin-dependent amplification of qE. *J. Photochem. Photobiol. B.*, **27**: 147–152.
- GREEN, B. R. (2007). Evolution of light-harvesting antennas in an oxygen world. In: Falkowski P. G. and Knoll, A. H. (Eds.), *Evolution of primary producers in the sea*. Elsevier, Burlington, USA, pages: 37–53.
- GREEN, B. R. (2003). The evolution of light-harvesting antennas. In: Green, B. R. and Parson, W. W. (Eds.), *Light-Harvesting Antennas in Photosynthesis*. Kluwer Academic Publishers, Dordrecht, The Netherlands, Pages: 129–168.
- GREEN, B. R., ANDERSON, J. M. AND PARSON, W. W. (2003). Photosynthetic membranes and their light-harvesting antennas. In: Green, B.R. and Parson, W.W. (Eds.), *Light-harvesting antennas in photosynthesis*, Kluwer Academic Publishers, Dordrecht, the Netherlands, Pages: 1–28.
- GREEN, B. R. AND DURNFORD, D. G. (1996). The chlorophyll-carotenoid proteins of oxygenic photosynthesis. *Annu. Rev. Plant Physiol. Plant Mol. Biol.*, **47**: 685–714.
- GROTZ, B., MOLNAR, P., STRANSKY, H. AND HAGER, A. (1999). Substrate specificity and functional aspects of violaxanthin-de-epoxidase, an enzyme of the xanthophyll cycle. *J. Plant Physiol.*, **154**: 437–446.
- GROUNOVA, I., JAKOB, T., WILHELM, C. AND GOSS, R. (2009). The regulation of xanthophyll cycle activity and non-photochemical fluorescence quenching by two different types of alternative electron flow in the diatoms *P. tricornutum* and *C. meneghiniana*. *Biochim. Biophys. Acta*, **1787**: 929–938.

- GROUNOVA, I., JAKOB, T., WILHELM, C. AND GOSS, R. (2008). A new multicomponent NPQ mechanism in the diatom *Cyclotella meneghiniana*. *Plant Cell Physiol.*, **49**: 1217–1225.
- GROUNOVA, I., JAKOB, T., WILHELM, C. AND GOSS, R. (2006). Influence of ascorbate and pH on the activity of the diatom xanthophyll cycle-enzyme diadinoxanthin de-epoxidase. *Physiol. Plant*, **126**: 205–211.
- GRUSZECKI, W. I. AND STRZALKA, K. (1991). Does the xanthophyll cycle take part in the regulation of fluidity of the thylakoid membrane? *Biochim. Biophys. Acta*, **1060**: 310–314.
- GUILLARD, R. R. AND RYTHER, J. H. (1962). Studies of marine planktonic diatoms. I. *Cyclotella nana* Hustedt and *Detonula confervacea* (Cleve) Gran. *Can. J. Microbiol.*, **8**: 229–238.
- GUILLOU, L., CHRÉTIENNOT-DINET, M.-J., MEDLIN, L. K., CLAUSTRE, H., LOISEAUX-DE GOËR, S. AND VAULOT, D. (1999a). Bolidomonas: a new genus with two species belonging to a new algal class, the Bolidophyceae (Heterokonta). *J. Phycol.*, **35**: 368–381.
- GUILLOU, L., MOON-VAN DER STAAY, S. Y., CLAUSTRE, H., PARTENSKY, F. AND VAULOT, D. (1999b). Diversity and abundance of Bolidophyceae (Heterokonta) in two oceanic regions. *Appl. Environ. Microbiol.*, **65**: 4528–4536.
- GUILLOU, L., EIKREM, W., CHRÉTIENNOT-DINET, M.-J. ET AL. (2004) Diversity of picoplanktonic prasinophytes assessed by direct nuclear SSU rDNA sequencing of environmental samples and novel isolates retrieved from oceanic and coastal marine ecosystems. *Protist*, **155**: 193–214.
- GUNDERMANN, K. AND BÜCHEL, C. (2008). The fluorescence yield of the trimeric fucoxanthin chlorophyll-protein FCPa in the diatom *Cyclotella meneghiniana* is dependent on the amount of bound diatoxanthin. *Photosynth. Res.*, **95**: 229–235.
- HAGER, A. (1980). The reversible, light-induced conversions of xanthophylls in the chloroplast. In: Czygan, F. C. (Ed.), *Pigments in plants*. Gustav Fischer Verlag, Stuttgart. Pages: 57–79.
- HAGER, A. (1975). Die reversiblen, lichtabhängigen Xanthophyllumwandlungen im Chloroplasten. *Ber. Deutsch Bot. Ges.*, **88**: 27–44.
- HAGER, A. (1969). Lichtbedingte pH-Erniedrigung in einem Chloroplasten Kompartiment als Ursache der enzymatischen Violaxanthin-Zeaxanthin-Umwandlung: Beziehungen zur Photophosphorylierung. *Planta*, **89**: 224–243.

- HAGER, A. (1967a). Untersuchungen über die lichtinduzierten reversible Xanthophyllumwandlungen an *Chlorella* und *Spinacia*. *Planta*, **74**: 148–172.
- HAGER, A. (1967b). Untersuchungen über die Rückreaktionen im Xanthophyll-Cyclus bei *Chlorella*, *Spinacia* und *Taxus*. *Planta*, **76**: 138–148.
- HAGER, A. AND HOLOCHER, K. (1994). Localization of the xanthophyll-cycle enzyme violaxanthin de-epoxidase within the thylakoid lumen and abolition of its mobility by a (light-dependent) pH decrease. *Planta*, **192**: 581–589.
- HALDANE, J. B. S. (1928). *Possible Worlds and Other Papers*. Harper & Brothers, New York.
- HAMILTON, A. K., LOVEJOY, C., GALAND, P. E. AND INGRAM, R. G. (2008). Water masses and biogeography of picoeukaryote assemblages in a cold hydrographically complex system. *Limnol. Oceanogr.*, **53**: 922–935.
- HARRIS, G. N., SCANLAN, D. J. AND GEIDER, R. J. (2005). Acclimation of *Emiliania huxleyi* (Prymnesiophyceae) to photon flux density. *J. Phycol.*, **41**: 851–862.
- HASLE, G. R. (2002). Are most of the domoic acid-producing species of the diatom genus *Pseudo-nitzschia* cosmopolites? *Harmful Algae*, **1**: 137–146.
- HAVAUX, M. AND NIYOGI, K. K. (1999). The violaxanthin cycle protects plants from photo-oxidative damage by more than one mechanism. *Proc. Natl. Acad. Sci. U.S.A.*, **96**: 8762–8767.
- HAVELKOVÁ-DOUSOVÁ, H., PRÁŠIL, O. AND BEHRENFELD, M. J. (2004). Photoacclimation of *Dunaliella tertiolecta* (Chlorophyceae) under fluctuating irradiance. *Photosynthetica*, **42**: 273–281.
- HEDGES, J. I. AND STERN, J. H. (1984). Carbon and nitrogen determination of carbonate-containing solids. *Limnol. Oceanogr.*, **29**: 657–663.
- HEIN, M., FOLAGER PEDERSEN, M. AND SAND-JENSEN, K. (1995). Size-dependent nitrogen uptake in micro- and macroalgae. *Mar. Ecol. Prog. Ser.*, **118**: 247–253.
- HEMMINGSSEN, A. M. (1960). Energy metabolism as related to body size and respiratory surfaces, and its evolution. *Rep. Steno. Mem. Hosp.*, **9**: 15–22.
- HERNDL, G. J., AGOGUÉ, H., BALTAR, F., REINTHALER, T., SINTES, E. AND VARELA, M. M. (2008). Regulation of aquatic microbial processes: the ‘microbial loop’ of the sunlit surface waters and the dark ocean dissected. *Aquat. Microb. Ecol.*, **53**: 59–68.
- HILLER, R. G., WRENCH, P. M., GOOLEY, A. P., SHOEBRIDGE, G. AND BRETON, J. (1993). The major intrinsic light-harvesting protein of *Amphidinium*: characterization and relation to the other light harvesting proteins. *J. Photochem. Photobiol.*, **57**: 125–131.

- HOBBIE, J. E., DALEY, R. J. AND JASPER, S. (1977). Use of Nuclepore filters for counting bacteria by fluorescence microscopy. *Appl. Environ. Microbiol.*, **33**: 1225–1228.
- HOFSTRAAT, J. W., PEETERS, J. C. H., SNEL, J. F. H. AND GEEL, C. (1994). Simple determination of photosynthetic efficiency and photoinhibition of *Dunaliella tertiolecta* by saturating pulse fluorescence measurements. *Mar. Ecol. Prog. Ser.*, **103**: 187–196.
- HOLDEN, H., RYPNIEWSKI, W., LAW, J. AND RAYMENT, I. (1987). The molecular structure of insecticyanin from the tobacco hornworm *Manduca sexta* L. at 2.6 Å resolution. *EMBO J.*, **6**: 1565–1570.
- HOLT, N. E., ZIGMANTAS, D., VALKUNAS, L., LI, X., NIYOGI, K. K. AND FLEMING, G. R. (2005). Carotenoid cation formation and the regulation of photosynthetic light harvesting. *Science*, **307**: 433–436.
- HOLT, N. E., FLEMING, G. R. AND NIYOGI, K. K. (2004). Toward an understanding of the mechanism of the non-photochemical quenching in green plants. *Biochemistry*, **43**: 8281–8289.
- HOLZWARTH, A. R., MILOSLAVINA, Y., NILKENS, M. AND JAHNS, P. (2009). Identification of two quenching sites active in the regulation of photosynthetic light-harvesting studied by time-resolved fluorescence. *Chem. Phys. Lett.*, **483**: 262–267.
- HORTON, P., JOHNSON, M. P., PEREZ-BUENO, M. L., KISS, A. Z. AND RUBAN, A. V. (2008). Photosynthetic acclimation: does the dynamic structure and macroorganisation of photosystem II in higher plant grana membranes regulate light harvesting states? *FEBS J.*, **275**: 1069–1079.
- HORTON, P., WENTWORTH, M. AND RUBAN, A. V. (2005). Control of the light harvesting function of chloroplast membranes: the LHCII aggregation model for non-photochemical quenching. *FEBS Lett.*, **579**: 4201–4206.
- HORTON, P., RUBAN, A. V. AND WALTERS, R. (1996). Regulation of light harvesting in green plants. *Annu. Rev. Plant Biol.*, **47**: 655–684.
- HORTON, P. AND RUBAN A. V. (1992). Regulation of photosystem II. *Photosynth. Res.*, **34**: 375–385.
- HORTON, P., RUBAN, A. V., REES, D., PASCAL, A. A., NOCTOR, G. AND YOUNG, A. J. (1991). Control of the light-harvesting function of chloroplast membranes by aggregation of the LHCII chlorophyll-protein complex. *FEBS Lett.* **292**: 1–4.
- HOOKE, C.E., BIDIGARE, R. R., KELLER, M. D. AND GUILLARD, R. R. L. (1988). Coccoid eukaryotic marine ultraplankters with four different HPLC pigment signatures. *J. Phycol.* **24**: 571–580.

- HUGUENEY, P., BOUVIER, F., BADILLO, A., QUENNEMET, J., D'HARLINGUE, A. AND CAMARA, B. (1996). Developmental and stress regulation of gene expression for plastid and cytosolic isoprenoid pathways in pepper fruit. *Plant Physiol.*, **111**: 2619–2626.
- HUISMAN, J., JOHANSSON, A. M., FOLMER, E. O. AND WEISSING, F. J. (2001). Towards a solution of the plankton paradox: the importance of physiology and life history. *Ecol. Lett.*, **4**: 408–411.
- HUTCHINSON, G. E. (1961). The paradox of the plankton. *Am. Natur.*, **95**: 137–145.
- IGLESIAS-PRIETO, R. AND TRENCH, R. K. (1994). Acclimation and adaptation to irradiance in symbiotic dinoflagellates. I. Responses of photosynthetic unit to changes in photon flux density. *Mar. Ecol. Prog. Ser.*, **113**: 163–175.
- IRIARTE, A. AND PURDIE, D. A. (1993). Photosynthesis and growth response of the oceanic picoplankter *Pycnococcus provasolii* Guillard (clone Omega 48-23) (Chlorophyta) to variations in irradiance, photoperiod and temperature. *J. Exp. Mar. Biol. Ecol.*, **168**: 239–257.
- IRIGOIEN, X., HUISMAN, J. AND HARRIS, R. P. (2004). Global biodiversity patterns of marine phytoplankton and zooplankton. *Nature*, **429**: 863–867.
- IRWIN, A. J., FINKEL, Z. V., SCHOFIELD, O. M. E. AND FALKOWSKI, P. G. (2006). Scaling-up from nutrient physiology to the size-structure of phytoplankton communities. *J. Plankton Res.*, **28**: 459–471.
- JAHNS, P. AND HOLZWARTH, A. R. (2011). The role of the xanthophyll cycle and of lutein in photoprotection of photosystem II. *Biochim. Biophys. Acta*, doi: 10.1016/j.bbabi.2011.04.012.
- JAHNS, P., KRAUSE, G. H. (1994). Xanthophyll cycle and energy-dependent fluorescence quenching in leaves from pea plants grown under intermittent light. *Planta*, **192**: 176–182.
- JAKOB, T., GOSS, R. AND WILHELM, C. (1999). Activation of diadinoxanthin de-epoxidase due to a chlororespiratory proton gradient in the dark in the diatom *Phaeodactylum tricorutum*. *Plant Biol.* **1**: 76–82.
- JAKOB, T., GOSS, R. AND WILHELM, C. (2001). Unusual pH-dependence of diadinoxanthin de-epoxidase activation causes chlororespiratory induced accumulation of diatoxanthin in the diatom *Phaeodactylum tricorutum*. *J. Plant Physiol.* **158**: 383–390.
- JARDILLIER, L., ZUBKOV, M. V., PEARMAN, J. AND SCANLAN, D. J. (2010). Significant CO₂ fixation by small prymnesiophytes in the subtropical and tropical northeast Atlantic Ocean. *ISME J.*, **4**: 1180–1192.

- JEFFREY, S.W. (1969). Properties of two spectrally different components in chlorophyll *c* preparations. *Biochim. Biophys. Acta*, **177**: 456–467.
- JING, H., LIU, H., BIRD D. F., WONG, T. H. C., CHEN, X. AND CHEN, B. (2010). Composition and seasonal variability of picoeukaryote communities at two subtropical coastal sites with contrasting trophic conditions. *J. Plankton Res.*, **32**: 565–573.
- JOHNSEN, G. AND SAKSHAUG, E. (2007). Bio-optical characteristics of PSII and PSI in 33 species (13 pigment-groups) of marine phytoplankton, and the relevance for PAM and FRR fluorometry. *J. Phycol.* **43**: 1236–1251.
- JOHNSEN, G., DALLØKKEN, R., EIKREM, W., LEGRAND, C., AURE, J. AND SKJOLDAL, H. R. (1999). Eco-Physiology, bio-optics and toxicity of the ichthyotoxic *Chrysochromulina leadbeateri* (Prymnesiophyceae). *J. Phycol.* **35**: 1465–1476.
- JOHNSEN, G., PRÉZELIN, B. B. AND JOVINE, R. V. M. (1997). Fluorescence excitation spectra and light utilization in two red tide dinoflagellates. *Limnol. Oceanogr.*, **42**: 1166–1177.
- JOHNSEN, G., AND SAKSHAUG, E. (1993). Bio-optical characteristics and photoadaptive responses in the toxic and bloomforming dinoflagellates *Gyrodinium aureolum*, *Gymnodinium galatheanum*, and two strains of *Prorocentrum minimum*. *J. Phycol.*, **29**: 627-642.
- JOHNSEN, G., SAKSHAUG, E. AND VERNET, M. (1992). Pigment composition, spectral characterization and photosynthetic parameters in *Chrysochromulina polylepis*. *Mar. Ecol. Progr. Ser.*, **83**: 241–249.
- JOSHI-DEO, J., SCHMIDT, M., GRUBER, A., WEISHEIT, W., MITTAG, M., KROTH, P. G. AND BÜCHEL, C. (2010). Characterization of a trimeric light-harvesting complex in the diatom *Phaeodactylum tricornutum* built of FcpA and FcpE proteins. *J. Exp. Bot.*, **61**: 3079–3087.
- JOSUE, J. S. AND FRANK, H. A. (2002). Direct determination of the S-1 excited-state energies of xanthophylls by low-temperature fluorescence spectroscopy. *J. Phys. Chem. A*, **106**: 4815–4824.
- KALITUHO, L., BERAN, K.C. AND JAHNS, P. (2007). The transiently generated non-photochemical quenching of excitation energy in *Arabidopsis* leaves is modulated by zeaxanthin. *Plant Physiol.*, **143**: 1861–1870.
- KANA, R., LAZAR, D., PRAŠIL, O. AND NAUS, J. (2002). Experimental and theoretical studies on the excess capacity of Photosystem II. *Photosynth. Res.*, **72**: 271–284.

- KANA, T. D., GEIDER, R. J. AND CRITCHLEY, C. (1997). Regulation of photosynthetic pigments in micro-algae by multiple environmental factors: a dynamic balance hypothesis. *New Phytol.*, **137**: 407–424.
- KARAPETYAN, N.V. (2007). Non-photochemical quenching of fluorescence in cyanobacteria, *Biochemistry (Mosc)*, **72**: 1127–1135.
- KASHINO, Y. AND KUDOH, S. (2003). Concerted response of xanthophyll-cycle pigments in a marine diatom, *Chaetoceros gracilis*, to shifts in light condition. *Phycol. Res.*, **51**: 168–172.
- KATZ, M. E., FINKEL, Z. V., GRYZEBEK, D., KNOLL, A. H. AND FALKOWSKI, P. G. (2004). Evolutionary trajectories and biogeochemical impacts of eukaryotic phytoplankton. *Annu. Rev. Ecol. Evol. Systemat.*, **35**: 523–556.
- KAWACHI, M., INOUE, I., HONDA, D., O'KELLY, C. J., BAILEY, J. C., BIDIGARE, R. R. AND ANDERSEN, R. A. (2002). The Pinguiphyceae *classis nova*, a new class of photosynthetic stramenopiles whose members produce large amounts of omega-3 fatty acids. *Phycol. Res.*, **50**: 31–47.
- KELLER, M. D., SELVIN, R. C., CLAUS, W. AND GUILLARD, R. R. L. (1987). Media for the culture of oceanic ultraphytoplankton. *J. Phycol.*, **23**: 633–638.
- KERR, S. R. AND DICKIE, L. M. (2001) The biomass spectrum: a predator–prey theory of aquatic production. Complexity in Ecological Systems Series. Columbia University Press, New York.
- KEY, T., MCCARTHY, A., CAMPBELL, D. A., SIX, C., ROY, S. AND FINKEL, Z. V. (2009). Cell size trade-offs govern light exploitation strategies in phytoplankton. *Environ. Microbiol.*, doi:10.1111/j.1462–2920.2009.02046.x.
- KIRILOVSKY, D. (2007). Photoprotection in cyanobacteria: the orange carotenoid protein (OCP)-related non-photochemical-quenching mechanism. *Photosynth. Res.*, **93**: 7–16.
- KIRK, J. T. O. (1983). Light and photosynthesis in aquatic systems. Cambridge University Press.
- KIRK, J. T. O. AND TILNEY-BASSETT, R. A. E. (1978). The Plastids. Their chemistry, structure, growth and inheritance. Elsevier/North-Holland Biomedical Press, Amsterdam. 2nd Edition. 960 pp.
- KIRK, J. T. O. (1977). Thermal dissociation of fucoxanthin protein binding in pigment complexes from chloroplasts of *Hormosira* (Phaeophyta). *Plant Sci. Lett.*, **9**: 373–380.
- KLEIBER, M. (1947). Body size and metabolic rate. *Physiol. Rev.*, **27**: 511–541.

- KNIGHT-JONES, E. W. (1951). Preliminary studies of nanoplankton and ultraplankton systematics and abundance by a quantitative culture method. *Extrait J. Conseil Int. Exploration*, **17**: 139–155.
- KNIGHT-JONES, E. W., AND WALNE, P. R. (1951). *Chromulina pusilla* Butcher, a dominant member of the ultraplankton. *Nature*, **167**: 445–446.
- KNOLL, A. H. (2003). *Life on a Young Planet*. Princeton University Press, Princeton, NJ, USA.
- KOCH, A. L. (1996). What size should a bacterium be? A question of scale. *Annual Review of Microbiology* **50**, 317–348.
- KOHFELD, K., LE QUÉRÉ, C., HARRISON, S. P. ET AL. (2005). Role of marine biology in glacial-interglacial CO₂ cycles. *Science*, **308**: 74–78.
- KOLBER, Z. S., VAN DOVER, C. L., NIEDERMAN, R. A. AND FALKOWSKI, P. G. (2000). Bacterial photosynthesis in surface waters of the open ocean. *Nature*, **407**: 177–179.
- KOLBER, Z. AND FALKOWSKI, P. G. (1993). Use of active fluorescence to estimate phytoplankton photosynthesis *in situ*. *Limnol. Oceanogr.*, **38**: 1646–1665.
- KOOISTRA, W.H.C.F., GERSONDE, R., MEDLIN, L.K. AND MANN, D.G. (2007). The origin and evolution of the diatoms: their adaptation to a planktonic existence. In Falkowski, P. G. and Knoll, A. H., (Eds.), *Evolution of Primary Producers in the Sea*. Pages: 207–249. Elsevier Academic Press, Burlington, MA.
- KOZIOL, A. G., BORZA, T., ISHIDA, K. I., KEELING, P., LEE, R. W. AND DURNFORD, D. G. (2007). Tracing the evolution of the light-harvesting antennae in chlorophyll *a/b*-containing organisms. *Plant Physiol.*, **143**: 1802–1816.
- KROON, B.M.A. AND THOMS, S. (2006). From electron to biomass: a mechanistic model to describe phytoplankton and steady-state growth rates. *J. Phycol.*, **42**: 593–609.
- KROMKAMP, J. C. AND FORSTER, R. M. (2003). The use of variable fluorescence measurements in aquatic ecosystems: differences between multiple and single turnover measuring protocols and suggesting terminology. *Eur. J. Phycol.*, **38**: 103–112.
- KROPUENSKE, L. R., MILLS, M. M., VAN DIJKEN, G. L., ALDERKAMP, A.-C., BERG, G. M., ROBINSON, D. H., WELSCHMEYER, N. A. AND ARRIGO, K. R. (2010). Strategies and rates of photoacclimation in two major Southern Ocean phytoplankton taxa: *Phaeocystis antarctica* (Haptophyta) and *Fragilariopsis cylindrus* (Bacillariophyceae). *J. Phycol.*, **46**: 1138–1151.
- KROPUENSKE, L. R., MILLS, M. M., VAN DIJKEN, G. L., BAILEY, S., ROBINSON, D. H., WELSCHMEYER, N. A. AND ARRIGO, K. R. (2009). Photophysiology in two major

- Southern Ocean phytoplankton taxa: photoprotection in *Phaeocystis antarctica* and *Fragilariopsis cylindrus*. *Limnol. Oceanogr. Methods*, **54**: 1176–1196.
- KROTH, P. G. AND STROTMANN, H. (1999). Diatom plastids: secondary endocytobiosis, plastid genome and protein import. *Physiol. Plant.*, **107**: 136–141.
- LANDRY, M. R., KIRSHEIN, J. AND CONSTANTINOU, J. (1996). Abundance and distributions of picoplankton populations in the central equatorial Pacific from 128N to 128S, 1408W. *Deep-Sea Res. Pt. II*, **43**: 871–890.
- LARKUM A. W. D. AND KÜHL, M. (2005). Chlorophyll *d*: the puzzle resolved. *Trends Plant Sci.*, **10**: 355–357.
- LARKUM, A. W. D. AND VESK, M. (2003). Algal plastids: Their fine structure and properties. In: Larkum, A. W. D., Douglas, S. E. and Raven, J. A. (Eds), *Photosynthesis in algae*. Kluwer Academic Publ., Dordrecht, The Netherlands, Pages: 11–28.
- KUHLBRANDT, W., WANG, D. N. AND FUJIYOSHI, Y. (1994). Atomic model of plant light-harvesting complex by electron crystallography. *Nature*, **367**: 614–621.
- LATOWSKI, D., KRUK, J., BURDA, K., SKRZYNECKA-JASKIER, M., KOSTECKA-GUGALA, A. AND STRZALKA, K. (2002). Kinetics of violaxanthin de-epoxidation by violaxanthin de-epoxidase, a xanthophyll cycle enzyme, is regulated by membrane fluidity in model lipid bilayers. *Eur. J. Biochem.*, **269**: 4656–4665.
- LATOWSKI, D., KOSTECKA, A. AND STRZALKA, K. (2000). Effect of monogalactosyldiacylglycerol and other thylakoid lipids on violaxanthin de-epoxidation in liposomes. *Bioch. Soc. Trans.*, **28**: 810–812.
- LAURION, I. AND ROY, S. (2009). Growth and photoprotection in three dinoflagellates (including two strains of *Alexandrium tamarense*) and one diatom exposed to four weeks of natural and enhanced ultraviolet-B radiation. *J. Phycol.*, **45**: 16–33.
- LAVAUD, J. (2007). Fast regulation of photosynthesis in diatoms: mechanisms, evolution and ecophysiology. *Funct. Plant Sci. Biotech.*, **1**: 267–287.
- LAVAUD, J., STRZEPEK, R. F. AND KROTH, P. G. (2007). Photoprotection capacity differs among diatoms: possible consequences on the spatial distribution of diatoms related to fluctuations in the underwater light climate. *Limnol. Oceanogr.*, **52**: 1188–1194.
- LAVAUD, J. AND KROTH, P. G. (2006). In diatoms, the transthylakoid proton gradient regulates the photoprotective non-photochemical fluorescence quenching beyond its control on the xanthophyll cycle. *Plant Cell Physiol.*, **47**: 1010–1016.

- LAVAUD, J., ROUSSEAU, B. AND ETIENNE, A.-L. (2004). General Features of Photoprotection By Energy Dissipation in Planktonic Diatoms (Bacillariophyceae)1. *J. Phycol.*, **40**: 130–137.
- LAVAUD, J., ROUSSEAU, B. AND ETIENNE, A.-L. (2003). Enrichment of the light-harvesting complex in diadinoxanthin and implications for the non-photochemical quenching fluorescence quenching in diatoms. *Biochemistry*, **42**: 5802–5808.
- LAVAUD, J., ROUSSEAU, B., VAN GORKOM, H. J. V. AND ETIENNE, A.-L. (2002a). Influence of the diadinoxanthin pool size on photoprotection in the marine planktonic diatom *Phaeodactylum tricornutum*. *Plant Physiol.*, **129**: 1398–1406.
- LAVAUD, J., ROUSSEAU, B. AND ETIENNE, A.-L. (2002b). In diatoms, a transthylakoidal proton gradient alone is not sufficient for non-photochemical fluorescence quenching. *FEBS Lett.*, **523**: 163–166.
- LAVAUD, J., VAN GORKOM, H. J. AND ETIENNE, A.-L. (2002c). Photosystem II electron transfer cycle and chlororespiration in planktonic diatoms. *Photosynth. Res.*, **74**: 51–59.
- LAWS, E. A., FALKOWSKI, P. G., SMITH, W. O. J., DUCKLOW, H. AND MCCARTHY J. J. (2000). Temperature effects on export production in the open ocean. *Global Biogeochem. Cycles*, **14**: 1231–1246.
- LEE, R. E. (1980). Prymnesiophyceae. Cambridge University Press.
- LE GALL, F., RIGAUT-JALABERT, F., MARIE, D., GARCZARECK, L., VIPREY, M., GODET, A. AND VAULOT, D. (2008). Picoplankton diversity in the South-East Pacific Ocean from cultures. *Biogeosciences*, **5**: 203–214.
- LEPERE, C., DEMURA, M., KAWACHI, M., ROMAC, S., PROBERT, I., AND VAULOT, D. (2011). Whole-genome amplification (WGA) of marine photosynthetic eukaryote populations. *FEMS Microbiol. Ecol.*, **76**: 513–23.
- LEPETIT, B., GOSS, R., JAKOB, T. AND WILHELM, C. (2011). Molecular dynamics of the diatom thylakoid membrane under different light conditions. *Photosynth. Res.*, DOI 10.1007/s11120-011-9633-5.
- LEPETIT, B., VOLKE, D., GILBERT, M., WILHELM, C. AND GOSS, R. (2010). Evidence for the existence of one antenna-associated, lipid-dissolved, and two protein-bound pools of diadinoxanthin cycle pigments in diatoms. *Plant Physiol.*, **154**: 1905–1920.
- LEPETIT, B., VOLKE, D., SZÁBO, M., HOFFMANN, R., GARAB, G., WILHELM, C. AND GOSS, R. (2008). The oligomeric antenna of the diatom *P. tricornutum*—localisation of diadinoxanthin cycle pigments. In: Allen, J. F., Gantt, E., Golbeck, J. H. and Osmond, B. (Eds.), *Energy from the sun*. Springer, Dordrecht, The Netherlands, Pages: 283–286.

- LEPETIT, B., VOLKE, D., SZÁBO, M., HOFFMANN, R., GARAB, G., WILHELM, C. AND GOSS, R. (2007). Spectroscopic and molecular characterization of the oligomeric antenna of the diatom *Phaeodactylum tricorutum*. *Biochemistry*, **46**: 9813–9822.
- LETÉLIER, R. M., BIDIGARE, R. R., HEBEL, D. V., ONDRUSEK, M. E., WINN, C. D. AND KARL, D. M. (1993). Temporal variability of phytoplankton community structure based on pigment analyses. *Limnol. Oceanogr.*, **38**: 1420–1437.
- LEWIS, M. R., HORNE, E. P. W., CULLEN, J. J., OAKEY, N. S. AND PLATT, T. (1984). Turbulent motions may control phytoplankton photosynthesis in the upper ocean. *Nature*, **311**: 49–50.
- LEWIS, M. R., CULLEN, J. J. AND PLATT, T. (1984). Relationships between vertical mixing and photoadaptation of phytoplankton: similarity criteria. *Mar. Ecol. Prog. Ser.*, **15**: 141–149.
- LI, Z., WAKAO, S., FISCHER, B. B. AND NIYOGI, K. (2009). Sensing and responding to excess light. *Annu. Rev. Plant Biol.*, **60**: 239–260.
- LI, W. K. W. (2002). Macroecological patterns of phytoplankton in the northwestern North Atlantic Ocean. *Nature*, **419**: 154–157.
- LI, W. K. W. (1994). Primary production of prochlorophytes, cyanobacteria, and eukaryotic ultraplankton: Measurements from flow cytometric sorting. *Limnol. Oceanogr.*, **39**: 169–175.
- LI, W. K. W., DICKIE, P. M., IRWIN, B. D. AND WOOD, A. M. (1992). Biomass of bacteria, cyanobacteria, prochlorophytes and photosynthetic eukaryotes in the Sargasso Sea. *Deep-Sea Res.*, **39**: 501–519.
- LI, X., MÜLLER-MOULÉ, P., GILMORE, A. M. AND NIYOGI, K. K. (2002). PsbS-dependent enhancement of feedback de-excitation protects photosystem II from photoinhibition. *Proc. Natl. Acad. Sci. U.S.A.*, **99**: 15222–15227.
- LI, X., BJÖRKMAN, O., SHIH, C. ET AL. (2000). A pigment-binding protein essential for regulation of photosynthetic light harvesting. *Nature*, **403**: 391–395.
- LISS, A., LANGE, K., SCHULZ, F. ET AL. (2009). Light, nutrients and grazing interact to determine diatom species richness via change to productivity, nutrient state and grazing activity. *J. Ecol.*, doi: 10.1111/j.1365-2745.2008.01463.x.
- LICHTENTHALER, H., BUSCHMANN, C., DÖLL, M., FIETZ, H., BACH, T., KOZEL, U., MEIER, D. AND RAHMSDORF, U. (1981). Photosynthetic activity, chloroplast ultrastructure, and leaf characteristics of high-light and low-light plants and of sun and shade leaves. *Photosynth. Res.*, **2**: 115–141.

- LICHTLÉ, C., SPILAR, A. AND DUVAL, J.-C. (1992). Immunogold localization of light-harvesting and photosystem I complexes in the thylakoids of *Fucus serratus* (Phaeophyceae). *Protoplasma* **166**: 99–106.
- LICHTLÉ, C., ARSALANE, W., DUVAL, J.-C. AND PASSAQUET, C. (1995). Characterization of the light-harvesting complex of *Gyraudyopsis stellifer* (Chrysophyceae) and effect of light stress. *J. Phycol.*, **31**: 380–387.
- LIGNELL, R. (1990). Excretion of organic carbon by phytoplankton: its relation to algal biomass, primary productivity and bacterial secondary productivity in the Baltic Sea. *Mar. Ecol. Prog. Ser.*, **68**: 85–99.
- LITCHMAN, E. (2000). Growth rate of phytoplankton under fluctuating light. *Freshwater Biol.*, **44**: 223–235.
- LITCHMAN, E. AND KLAUSMEIER, C. A. (2008). Trait-based community ecology of phytoplankton. *Annu. Rev. Ecol. Evol. Syst.*, **39**: 615–639.
- LITCHMAN, E. AND KLAUSMEIER, C. A. (2001). Competition of phytoplankton under fluctuating irradiance. *Am. Nat.*, **157**: 170–187.
- LOHR, M. AND WILHELM, C. (1999). Algae displaying the diadinoxanthin cycle also possess the violaxanthin cycle. *Proc. Natl. Acad. Sci. U.S.A.*, **96**: 8784–8789.
- LOHR, M. AND WILHELM, C. (2001). Xanthophyll synthesis in diatoms: quantification of putative intermediates and comparison of pigment conversion kinetics with rate constants derived from a model. *Planta*. **212**: 382–391.
- LOGAN, B. A., PARKER, D. H., DEMMIG-ADAMS, B. AND ADAMS, W. W. III (1996). Acclimation of leaf carotenoid composition and ascorbate levels to gradients in the light environment within an Australian rain forest. *Plant Cell Environ.*, **19**: 1083–1090.
- LÓPEZ-GARCÍA, P., RODRIGUEZ-VALERA, F., PEDRÓS-ALIÓ, C. AND MOREIRA, D. (2001). Unexpected diversity of small eukaryotes in deep-sea Antarctic plankton. *Nature*, **409**: 603–607.
- LÓPEZ-URRUTIA, A., SAN MARTIN, E., HARRIS, R. P. AND IRIGOIEN, X. (2006). Scaling the metabolic balance of the oceans. *Proc. Natl. Acad. Sci. U.S.A.*, **103**: 8739–8744.
- MACINTYRE, H. L., KANA, T. M. AND GEIDER, R. J. (2000). The effect of water motion on short-term rates of photosynthesis by marine phytoplankton. *Trends Plant Sci.*, **5**: 12–17.
- MACPHERSON, A. N. AND HILLER, R. G. (2003). Light-harvesting systems in chlorophyll *c*-containing algae. In: Green B. R. and Parson, W. W. (Eds.), *Light-Harvesting Antennas*

- in *Photosynthesis*, Kluwer Academic Publishers, Dordrecht, The Netherlands, Pages: 325–352.
- MANTON, I. AND PARKE, M. (1960). Further observations on small green flagellates with special reference to possible relatives of *Chromulina pusilla* Butcher. *J. Mar. Biol. Assoc. UK*, **39**: 275–298.
- MANTOURA, R. F. C. AND LLEWELLYN, C. A. (1983). The rapid determination of algal chlorophyll and carotenoid pigments and their breakdown products in natural waters by reverse-phase high-performance liquid chromatography. *Analyt. Chim. Acta*, **151**: 297–314.
- MARAÑÓN, E. (2008). Inter-specific scaling of phytoplankton production and cell size in the field. *J. Plankton Res.*, **30**: 157–163.
- MARAÑÓN, E. (2005). Phytoplankton growth rates in the Atlantic subtropical gyre. *Limnol. Oceanogr.*, **50**: 299–310.
- MARAÑÓN, E., HOLLIGAN, P. M., BARCIELA, R., ET AL. (2001). Patterns of phytoplankton size structure and productivity in contrasting open-ocean environments. *Mar. Ecol. Prog. Ser.*, **216**: 43–56.
- MARIE, D., SHI, X., RIGAUT-JALABERT, F. AND VAULOT, D. (2010). Diversity of small photosynthetic eukaryotes in the English Channel from samples sorted by flow cytometry. *FEMS Microbiol. Ecol.*, **72**: 165–178.
- MARIE, D., ZHU, F., BALAGUÉ, V., RAS, J., AND VAULOT, D. (2006). Eukaryotic picoplankton communities of the Mediterranean Sea in summer assessed by molecular approaches (DGGE, TTGE, QPCR). *FEMS Microbiol. Ecol.*, **55**: 403–415.
- MASSANA, R., CASTRESANA, J., BALAGUE, V., GUILLOU, L., ROMARI, K., ET AL. (2004). Phylogenetic and ecological analysis of novel marine stramenopiles. *Applied and Environmental Microbiology*, **70**: 3528–3534.
- MATSUMOTO, K., FURUYA, K. AND KAWANO, T. (2004). Association of picophytoplankton distribution with ENSO events in the equatorial Pacific between 1458E and 1608W. *Deep-Sea Res. Pt. I*, **51**: 1851–1871.
- MEI, Z.-P., FINKEL, Z. V. AND IRWIN, A. J. (2009). Growth rate Allometry in response to light and nutrient limitation in phytoplankton. *J. Theor. Biol.*, **259**: 582–588.
- Melis, A. (1991). Dynamics of photosynthetic membrane composition and function. *Biochim. Biophys. Acta*, **1058**: 87–106.

- MEYER, A. A., TACKX, M. AND DARO, N. (2000). Xanthophyll cycling in *Phaeocystis globosa* and *Thalassiosira* sp.: a possible mechanism for species succession. *J. Sea Res.*, **43**: 373–384.
- MEWES, H. AND RICHTER, M. (2002). Supplementary ultraviolet-B radiation induces a rapid reversal of the diadinoxanthin cycle in the strong light-exposed diatom *Phaeodactylum tricorutum*. *Plant Physiol.*, **130**: 1527–1535.
- MILLER, S. R., AUGUSTINE, S., OLSON, T. L., BLANKENSHIP, R. E., SELKER, J. AND WOOD, A.M. (2005). Discovery of a free-living chlorophyll *d*-producing cyanobacterium with a hybrid proteobacterial-cyanobacterial small-subunit rRNA gene. *Proc. Nat. Acad. Sci. U.S.A.*, **102**: 850–855.
- MILLS, M. M., KROPUENSKE, L. R., VAN DIJKEN, G. L., ALDERKAMP, A.-C., BERG, G. M., ROBINSON, D. H., WELSCHMEYER, N. A., AND ARRIGO, K. R. (2010). Photophysiology in two southern ocean phytoplankton taxa: photosynthesis of *Phaeocystis Antarctica* (Prymnesiophyceae) and *Fragilariopsis Cylindrus* (Bacillariophyceae) under simulated mixed-layer irradiance. *J. Phycol.*, **46**: 1114–1127.
- MILOSLAVINA, Y., GROUNOVA, I., LAMBREV, P. H., LEPETIT, B., GOSS, R., WILHELM, C. AND HOLZWARTH, A. R. (2009). Ultrafast fluorescence study on the location and mechanism of non-photochemical quenching in diatoms. *Biochim. Biophys. Acta*, **1787**: 1189–1197.
- MILOSLAVINA, Y., WEHNER, A., LAMBREV, P. H., WIJNTJES, E., REUS, M., GARAB, G., CROCE, R. AND HOLZWARTH, A. R. (2008). Far-red fluorescence: A direct spectroscopic marker for LHCII oligomer formation in non-photochemical quenching. *FEBS Lett.*, **582**: 3625–3631.
- MITROVIC, S. M., HOWDEN, C. G., BOWLING, L. C. ET AL. (2003) Unusual allometry between in situ growth of freshwater phytoplankton under static and fluctuating light environments: possible implications for dominance. *J. Plankton Res.*, **25**: 517–526.
- MOISAN, T. A. AND MITCHELL, B. G. (1998). Xanthophyll cycling in *Phaeocystis antarctica*: changes in cellular fluorescence. *Mar. Ecol. Prog. Ser.*, **169**: 113–121.
- MOISAN, T. A. AND MITCHELL, B. G. (1999). Photophysiological acclimation of *Phaeocystis antarctica* Karsten under light limitation. *Limnol. Oceanogr.*, **44**: 247–258.
- MOLINE, M. (1998). Photoadaptive response during the development of a coastal Antarctic bloom and relationship to water column stability. *Limnol. Oceanogr.*, **43**: 146–153.

- MOLONEY, C. L. AND FIELD, J. G. (1991). The size-based dynamics of plankton food webs. I. A simulation model of carbon and nitrogen flows. *J. Plankton Res.*, **13**: 1003–1038.
- MOLONEY, C. L., FIELD, J. G. AND LUCAS, M. I. (1991). The size-based dynamics of plankton food webs. II. Simulations of three contrasting southern Benguela food webs. *J. Plankton Res.*, **13**: 1039–1092.
- MOLONEY, C. L. AND FIELD, J. G. (1989). General allometric equations for rates of nutrient uptake, ingestion, and respiration in plankton organisms. *Limnol. Oceanogr.*, **34**: 1290–1299.
- MONTSANT, A., JABBARI, K., MAHESWARI, U. AND BOWLER, C. (2005). Comparative genomics of the pennate diatom *Phaeodactylum tricorutum*. *Plant Physiol.*, **137**: 500–513.
- MOON-VAN DER STAAY, S. Y., DE WACHTER, R. AND VAULOT, D. (2001). Oceanic 18S rDNA sequences from picoplankton reveal unsuspected eukaryotic diversity. *Nature*, **409**: 607–610.
- MOON-VAN DER STAAY, S. Y., VAN DER STAAY, G., GUILLOU, L., VAULOT, D., CLAUSTRE, H. AND MEDLIN, L. (2000). Abundance and diversity of prymnesiophytes in the picoplankton community from the equatorial Pacific Ocean inferred from 18S rDNA sequences. *Limnol. Oceanogr.*, **45**: 98–109.
- MOREIRA, D. AND LÓPEZ-GARCÍA, P. (2002). The molecular ecology of eukaryotes unveils a hidden world. *Trends Microbiol.*, **10**: 31–38.
- MORIN, P. J. AND FOX, J. W. (2004). Diversity in the deep blue sea. *Nature*, **429**: 814.
- MOUGET, J. L., TREMBLIN, G., MORANT-MANCEAU, A., MORANCAIS, M. AND ROBERT, J. M. (1999). Long-term photoacclimation of *Haslea ostrearia* (Bacillariophyta): effect of irradiance on growth rates, pigment content and photosynthesis. *Eur. J. Phycol.*, **34**: 109–115.
- MOUSTAFA, A., BESZTERI, B., MAIER, U.-G., BOWLER, C., VALENTIN, K. AND BHATTACHARYA, A. (2009). Genomic footprints of a cryptic plastid endosymbiosis in diatoms. *Science*, **324**: 1724–1726.
- MULLINEAUX, C. W. AND EMLYN-JONES, E. (2004). State-transitions: an example of acclimation to low-light stress. *J. Exp. Bot.*, **56**: 389–393.
- NAGAO, R., TOMO, T., NOGUCHI, E., NAKAJIMA, S., SUZUKI, T., OKUMURA, A., KASHINO, Y., MIMURO, M., IKEUCHI, M. AND ENAMI, I. (2010). Purification and characterization of a stable oxygen-evolving Photosystem II complex from a marine centric diatom, *Chaetoceros gracilis*. *Biochim. Biophys. Acta*, **1797**: 160–166.

- NAGAO, R., ISHII, A., TADA, O., SUZUKI, T., DOHMAE, N., OKUMURA, A., IWAI, M., TAKAHASHI, T., KASHINO, Y. AND ENAMI, I. (2007). Isolation and characterization of oxygen-evolving thylakoid membranes and Photosystem II particles from a marine diatom *Chaetoceros gracilis*. *Biochim. Biophys. Acta*, **1767**: 1353–1362.
- NAGATA, T. (2000). Production mechanisms of dissolved organic matter. In: Kirchman DL (Ed.), *Microbial ecology of the oceans*. Wiley-Liss, New York, Pages: 121–152.
- NÄGELI, C. (1849). Gattungen einzelliger Algen physiologisch und systematisch bearbeitet. Zürich.
- NELSON, N. AND BEN-SHEM, A. (2004). The complex architecture of oxygenic photosynthesis. *Nature*, **5**: 1–12.
- NEWCOMER, M., JONES, T., AQVIST, J., SUNDELIN, J., ERIKSSON, U., RASK, L. AND PETERSON, P. (1984). The three-dimensional structure of retinolbinding protein. *EMBO J.*, **3**: 1451–1454.
- NEWTON, P. P. AND LISS, P. S. (1990). Particles in the oceans (and other natural waters). *Science Progress Oxford* **74**, 91–114.
- NIYOGI, K. (1999). Photoprotection revisited: genetic and Molecular Approaches. *Annu. Rev. Plant. Phys.*, **50**: 333–359.
- NIELSEN, M. AND SAKSHAUG, E. (1993). Adaptation to spectrally different light regimes: Studies of the growth rate and Carbon to Chlorophyll *a* ratio of the marine diatom *Skeletonema costatum*. *Limnol. Oceanogr.* **38**: 1576–1581.
- NISBET, E. G. AND SLEEP, N. H. (2001). The habitat and nature of early life. *Nature*, **409**: 1083–1091.
- NOT, F., LATASA, M., SCHAREK, R. ET AL. (2008). Protistan assemblages across the Indian Ocean, with a specific emphasis on the picoeukaryotes. *Deep-Sea Res. Pt. I*, **55**: 1456–1473.
- NOT, F., GAUSLING, R., AZAM, F., HEIDELBERG, J. F. AND WORDEN, A. Z. (2007a). Vertical distribution of picoeukaryotic diversity in the Sargasso Sea. *Environ. Microbiol.*, **9**: 1233–1252.
- NOT, F., VALENTIN, K., ROMARI, K. ET AL. (2007b). Picobiliphytes, a new marine picoplanktonic algal group with unknown affinities to other eukaryotes. *Science*, **315**: 252–254.
- NOT, F., MASSANA, R., LATASA, M. ET AL. (2005). Late summer community composition and abundance of photosynthetic picoeukaryotes in Norwegian and Barents Seas. *Limnol. Oceanogr.*, **50**: 1677–1686.

- NOT, F., LATASA, M., MARIE, D., CARIOU, T., VAULOT, D. AND SIMON, N. (2004). A single species *Micromonas pusilla* (Prasinophyceae) dominates the eukaryotic picoplankton in the western English Channel. *Appl. Environ. Microbiol.*, **70**: 4064–4072.
- NYMARK, M., VALLE, K. C., BREMBU, T., HANCKE, K., WINGE, P., ANDRESEN, K., JOHNSEN, G. AND BONES, A. M. (2009). An integrated analysis of molecular acclimation to high light in the marine diatom *Phaeodactylum tricorutum*. *PLoS One*, **4**: e7743.
- OLAIZOLA, M., LAROCHE, J., KOLBER, Z. AND FALKOWSKI, P.G. (1994). Nonphotochemical fluorescence quenching and the diadinoxanthin cycle in a marine diatom. *Photosynth. Res.*, **41**: 357–370.
- OLAIZOLA, M. AND YAMAMOTO, H. Y. (1994). Short-term response of the diadinoxanthin cycle and fluorescence yield to high irradiance in *Chaetoceros muelleri* (Bacillariophyceae). *J. Phycol.*, **30**: 606–612.
- OLAIZOLA, M., BIENFANG, P.K. AND ZIEMANN, D.A. (1992). Pigment analysis of phytoplankton during a subarctic bloom: xanthophyll cycling. *J. Exp. Mar. Biol. Ecol.*, **158**: 59–74.
- ONDRUSEK, M.E., BIDIGARE, R.R., SWEET, S.T., DEFREITAS, D.A. AND BROOKS, J.M. (1991). Distribution of phytoplankton pigments in the North Pacific Ocean in relation to physical and optical variability. *Deep-Sea Res. Pt. II Topical Studies in Oceanography*, **38**: 243–266.
- ORR, L. AND GOVINDJEE (2010). Photosynthesis on line. *Photosynth. Res.*, **105**: 167–200.
- OUDOT-LE SECQ, M. P., GRIMWOOD, J., SHAPIRO, H., ARMBRUST, E. V., BOWLER, C., AND GREEN, B. R. (2007). Chloroplast genomes of the diatoms *Phaeodactylum tricorutum* and *Thalassiosira pseudonana*: comparison with other plastid genome of the red lineage. *Mol. Genet. Genomics*, **277**: 427–439.
- OWENS, T. G. (1988). Light-harvesting antenna systems in the chlorophyll *a/c*-containing algae. In: Stevens, C. and Bryant, D. (Eds.), *Light-energy transduction in photosynthesis*. Pages 122–136. Am. Soc. Plant physiologists, Rockville, Maryland.
- OWENS, T. G. (1986). Light-harvesting function in the diatom *Phaeodactylum tricorutum*: II. Distribution of excitation energy between the photosystems. *Plant Physiol.*, **80**: 739–746.
- PALENIK, B., BRAHAMSHA, B., LARIMER, F. W. ET AL. (2003). The genome of a motile marine *Synechococcus*. *Nature*, **424**: 1037–1042.

- PALENIK, B., GRIMWOOD, J., AERTS, A. *ET AL.* (2007). The tiny eukaryote *Ostreococcus* provides genomic insights into the paradox of plankton speciation. *Proc. Natl. Acad. Sci. U.S.A.*, **104**: 7705–7710.
- PARK, S., JUNG, G., HWANG, Y. S. AND JIN, E. (2010). Dynamic response of the transcriptome of a psychrophilic diatom, *Chaetoceros neogracile*, to high irradiance. *Planta*, **231**: 349–360.
- PARTENSKY, F., BLANCHOT, J. AND VAULOT, D. (1999). Differential distribution and ecology of *Prochlorococcus* and *Synechococcus* in oceanic waters: A review. In: Charpy, L. and Larkum, A. W. D. (Eds.), *Marine Cyanobacteria*. Bulletin de L'Institut Oceanographique, Monaco, Special Paper 19.
- PASCAL, A. A., LIU, Z., BROESS, K. *ET AL.* (2005). Molecular basis of photoprotection and control of photosynthetic light-harvesting. *Nature*, **436**: 134–137.
- PASCAL, A. A., CARON, L., ROUSSEAU, B., LAPOUGE, K., DUVAL, J. C. AND ROBERT, B. (1998). Resonance Raman spectroscopy of a light-harvesting protein from the brown alga *Laminaria saccharina*. *Biochemistry*, **37**: 2450–2457.
- PEEK, M. S., RUSSEK, E., WAIT, C. D. A. AND FORSETH, I. N. (2002). Physiological response curve analysis using nonlinear mixed models. *Oecologia*, **132**: 175–180.
- PEERS, G., TRUONG, T. B., OSTENDORF, E. *ET AL.* (2009). An ancient light-harvesting protein is critical for the regulation of algal photosynthesis. *Nature*, **462**: 518–521.
- PÉREZ, V., FERNANDEZ, E., MARAÑÓN, E. *ET AL.* (2005). Latitudinal distribution of microbial plankton abundance, production and respiration in the Equatorial Atlantic in autumn 2000. *Deep-Sea Res.*, **52**: 861–880.
- PERRY, M., TALBOT, M. AND ALBERTE, R. (1981). Photoadaptation in marine phytoplankton: response of the photosynthetic unit. *Mar. Biol.*, **62**: 91–101.
- PESARESI, P., HERTLE, A., PRIBIL, M. (2009). Arabidopsis STN7 kinase provides a link between short- and long-term photosynthetic acclimation. *Plant Cell*, **21**: 2402–2423.
- PETROU, K., HILL, R., DOBLIN, M. A., MCMINN, A., JOHNSON, R., WRIGHT, S. W. AND RALPH, P. J. (2011a). Photoprotection of Sea-Ice Microalgal Communities From the East Antarctic Pack Ice1. *J. Phycol.*, **47**: 77–86.
- PETROU, K., DOBLIN, M. A. AND RALPH, P. J. (2011b). Heterogeneity in the photoprotective capacity of three Antarctic diatoms during short-term changes in salinity and temperature. *Mar. Biol.*, **158**: 1029–1041.

- PFANNSCHMIDT, T., BRAUTIGAM, K. AND WAGNER, R. (2009). Potential regulation of gene expression in photosynthetic cells by redox and energy state: approaches towards better understanding. *Ann Bot Lond*, **103**: 599–607.
- PFANNSCHMIDT, T., NILSSON, A. AND ALLEN, J. F. (1999) Photosynthetic control of chloroplast gene expression. *Nature*, **397**: 625–628.
- PFÜNDEL, E., RENGANATHAN, M., GILMORE, A. M., YAMAMOTO, H. Y. AND DILLEY, R. A. (1994). Intrathylakoid pH in isolated pea chloroplasts as probed by violaxanthin de-epoxidation. *Plant Physiol.*, **106**: 1647–1658.
- PIRIE, N.W. (1964). The size of small organisms. *Proceedings of the Royal Society of London B*, **160**: 149–166.
- PIRIE, N.W. (1973). ‘On being the right size’. *Annu. Rev. Microbiol.*, **27**: 119–132.
- PLATT, T., DENMAN, K. L. AND JASSBY, A. D. (1977). Modeling the productivity of phytoplankton. In: Goldberg, E. (Eds.), *The Sea*, pages 807–856. John Wiley, New York.
- POLIMENE, L., BRUNET, C., ALLEN, J. I., BUTENSCHÖN, M., WHITE, D. AND LLEWELLYN, C. (2011). Modelling xanthophyll photoprotective activity in Phytoplankton. *J. Plankton Res.*, submitted.
- POLIVKA, T., HEREK, J. H., ZIGMANTAS, D. AKERLUND, H. E. AND SUNDSTROM, V. (1999). Direct observation of the (forbidden) S1 state in carotenoids. *Proc. Natl. Acad. Sci. U.S.A.*, **96**: 4914–4917.
- POMEROY, L. R. (1974). The ocean’s food web, a changing paradigm. *Bioscience*, **24**: 499–504.
- POST, A. F., DUBINSKY, Z., WYMAN, K. AND FALKOWSKI, P. G. (1984). Physiological responses of a marine planktonic diatom to transitions in growth irradiance. *Mar. Ecol. Prog. Ser.*, **25**: 141–149.
- PREMVARDHAN, L., ROBERT, B., BEER, A. AND BÜCHEL, C. (2010). Pigment organization in fucoxanthin chlorophyll *a/c*(2) proteins (FCP) based on resonance Raman spectroscopy and sequence analysis. *Biochim. Biophys. Acta*, **1797**: 1647–1656.
- PRICE, C. A., GILLOOLY, J. F., ALLEN, A. P., WEITZ, J. S. AND NIKLAS, K. J. (2010). Tansley review. The metabolic theory of ecology: prospects and challenges for plant biology. *New Phytol.*, **188**: 696–710.
- PYSZNIAC, A. M. AND GIBBS, S. P. (1992). Immunocytochemical localization of photosystem I and the fucoxanthin-chlorophyll *a/c* light-harvesting complex in the diatom *Phaeodactylum tricorutum*. *Protoplasma*, **166**: 208–217.

- RANIELLO, R., LORENTI, M., BRUNET, C., BUIA, M. C. (2006). Photoacclimation of the invasive alga *Caulerpa racemosa* var. *cylindrica* to depth and daylight patterns and a putative role for siphonaxanthin. *Mar. Ecol.*, **27**: 20–30.
- RASCHER, U. AND NEDBAL, L. (2006). Dynamics of photosynthesis in fluctuating light. *Curr. Opin. Plant. Biol.*, **9**: 671–678.
- RAVEN, J. A., FINKEL, Z. V. AND IRWIN, A. J. (2005). Picophytoplankton: bottom-up and top-down controls on ecology and evolution. *Vie et Milieu*, **55**: 209–215.
- RAVEN, J. A. AND WAITE, A. (2004). Tansley review. The evolution of silicification in diatoms: inescapable sinking and sinking as escape? *New Phytol.*, **162**: 45–61.
- RAVEN, J. A. AND GEIDER, R. J. (2003). Adaptation, acclimation and regulation in algal photosynthesis. In: Larkum, W. D., Douglas, S. E. and Raven, J. A. (Eds.), *Photosynthesis in Algae*. Kluwer Academic Publishers, Dordrecht, The Netherlands, 385–412.
- RAVEN, J. A. AND KÜBLER, J. A. (2002). New light on the scaling of metabolic rate with the size of algae. *J. Phycol.*, **38**: 11–16.
- RAVEN, J. A. (1999). Picophytoplankton. *Progress in Phycological Research* **13**: 33–106.
- RAVEN, J. A. (1998). The twelfth Tansley lecture. Small is beautiful: the picophytoplankton. *Funct. Ecol.*, **12**: 503–513.
- RAVEN, J. A. (1986). Physiological consequences of extremely small size for autotrophic organisms in the sea. *Photosynthetic Picoplankton* (Eds. Platt, T. and Li, W. K. W.). *Can. B. Fish. Aquat. Sci.*, **214**: 1–70.
- RAVEN, J. A. (1994a). Photosynthesis in aquatic plants. In: Schulze, E. D. and Caldwell, M. H., (Eds.), *Ecophysiology of Photosynthesis*, pp. 299–318. Springer Verlag, Berlin.
- RAVEN, J. A. (1994b). Why are there no picoplanktonic O₂-evolvers with volumes less than 10⁻¹⁸ m³? *J. Plankton Res.*, **16**: 565–580.
- REGER, B. J. AND KRAUSS, R. W. (1970). The photosynthetic response to a shift in the chlorophyll a to chlorophyll b ratio of *Chlorella*. *Plant Physiol.*, **46**: 568–575.
- RICHARDSON, K., BEARDALL, J. AND RAVEN, J. A. (1983). Adaptation of unicellular algae to irradiance: an analysis of strategies. *New Phytologist*, **93**: 157–191.
- RITZ, M., NEVEROV, K. V. AND ETIENNE, A. L. (1999). ΔpH-dependent fluorescence quenching and its photoprotective role in the unicellular red alga *Rhodella violacea*. *Photosynthetica*, **37**: 267–280.

- ROCAP, G., LARIMER, F. W., LAMERDIN, J. *ET AL.* (2003). Genome divergence in two *Prochlorococcus* ecotypes reflects oceanic niche differentiation. *Nature*, **424**: 1042–1047.
- RODRÍGUEZ, F., DERELLE, E., GUILLOU, L., LE GALL, F., VAULOT, D. AND MOREAU, H. (2005). Ecotype diversity in the marine picoeukaryote *Ostreococcus* (Chlorophyta, Prasinophyceae). *Environ Microbiol.*, **7**: 853–859.
- RODRÍGUEZ, F., CHAUTON, M., JOHNSEN, G., ANDRESEN, K., OLSEN, L. M. AND ZAPATA, M. (2006). Photoacclimation in phytoplankton: implications for biomass estimates, pigment functionality and chemotaxonomy. *Mar. Biol.*, **148**: 963-971.
- ROMARI, K. AND VAULOT, D. (2004). Composition and temporal variability of picoeukaryote communities at a coastal site of the English Channel from 18S rDNA sequences. *Limnol Oceanogr.*, **49**: 784–798.
- RUBAN, A. V., JOHNSON, M. P. AND DUFFY, C. D. P. (2011). The photoprotective molecular switch in the photosystem II antenna. *Biochim. Biophys. Acta*, doi: 10.1016/j.bbabi.2011.04.007.
- RUBAN, A. V. AND JOHNSON, M. P. (2009). Dynamics of higher plant photosystem cross-section associated with state-transitions. *Photosynth. Res.*, **99**: 173–183.
- RUBAN, A. V., BERERA, R., ILIOAIA, C. *ET AL.* (2007). Identification of a mechanism of photoprotective energy dissipation in higher plants. *Nature*, **450**: 575–578.
- RUBAN, A. V., LAVAUD, J., ROUSSEAU, B., GUGLIELMI, G., HORTON, P. AND ETIENNE, A-L. (2004). The super-excess energy dissipation in diatom algae: comparative analysis with higher plants. *Photosynth. Res.*, **82**., 165–175.
- RUBAN, A. V. AND HORTON, P. (1999). The xanthophyll cycle modulates the kinetics of non-photochemical energy dissipation in isolated light-harvesting complexes, intact chloroplasts and leaves. *Plant Physiol.*, **119**: 531–542.
- RUBAN, A. V., WENTWORTH, M., YOUNG, A. J. AND HORTON, P. (1999). Determination of the stoichiometry and strength of binding of xanthophylls to the photosystem II light-harvesting complexes. *J. Biol. Chem.*, **274**:10458–10465.
- RUBAN, A. V. AND HORTON, P. (1995). An investigation of the sustained component of non-photochemical quenching of chlorophyll fluorescence in isolated chloroplasts and leaves of spinach, *Plant Physiol.*, **108**: 721–726.
- RUBAN, A. V., YOUNG, A. J., PASCAL, A. A. AND HORTON, P. (1994). The effects of illumination on the xanthophyll composition of the photosystem II light-harvesting complexes of spinach thylakoid membranes. *Plant Physiol.*, **104**: 227–234.

- RUBAN, A. V., YOUNG, A.J. AND HORTON, P. (1993). Induction of nonphotochemical energy dissipation and absorbance changes in leaves. Evidence for changes in the state of the light-harvesting system of photosystem II in vivo. *Plant Physiol.*, **102**: 741–750.
- RYTHER, J. H. AND MENZEL, D. W. (1959). Light adaptation by marine phytoplankton. *Limnol. Oceanogr.*, **4**: 492–497.
- SAKSHAUG, E. AND JOHNSEN, G. (2005). Absorption, fluorescence excitation and photoacclimation in phytoplankton. In: Rao, S. (Eds.), *Algal cultures, Analogues of Blooms and Applications*. Pages 687–714. Science Press Publ.
- SAKSHAUG, E., BRICAUD, A., DANDONNEAU, Y., FALKOWSKI, P. G., KIEFER, D. A., LEGENDRE, L., MOREL, A., PARSLow, J. AND TAKAHASHI, M. (1997). Parameters of photosynthesis: definitions, theory and interpretation of results. *J. Plankton Res.*, **19**: 1637–1670.
- SAKSHAUG, E., DEMERS, S. AND YENTSCH, C. M. (1987). *Thalassiosira oceanica* and *T. pseudonana*: Two different photoadaptational responses. *Mar. Ecol. Prog. Ser.*, **41**: 275–282.
- SANDMANN, G. AND BOGER, P. (1989). Inhibition of carotenoid biosynthesis by herbicides. In Boger, P. and G. Sandman, (Eds.), *Target sites of herbicides action*. Pages: 25–44. CRC Press, Boca Raton FL.
- SAPOZHNIKOV, D. I., KRASOVSKAYA, T. A. AND A. N. MAEVSKAYA, A. N. (1957) Change in the interrelationship of the basic carotenoids of the plastids of green leaves under the action of light. *Dokl. Akad. Nauk. USSR*, **113**: 465–467.
- SARMIENTO, J. L. AND WOFsy, S. C. (1999). A US Global Cycle Science Plan. Carbon and climate working group. 69 pp.
- SARNO, D. AND DAHLMAN, J. (2000). Production of domoic acid in another species of *Pseudo-nitzschia*: *P. multistriata* in the Gulf of Naples (Mediterranean Sea). *Harmful Algae News.*, **21**: 5.
- SARRY, J.E., MONTILLET, J.L., SAUVAIRE, Y. AND HAVAUX, M. (1994). The protective function of the xanthophyll cycle in photosynthesis. *FEBS Lett.*, **353**: 147–150.
- SARTHOU, G., TIMMERMANS, K. R., BLAIN, S. AND TRE'GUER, P. (2005). Growth physiology and fate of diatoms in the ocean: a review. *J Sea Res.*, **53**: 25–42.
- SCHLESINGER, D. A., MOLOT, L. A. AND SHUTER, B. J. (1981). Specific growth rate of freshwater algae in relation to cell size and light intensity. *Can. J. Fish. Aquat. Sci.*, **38**: 1052–1058.

- SCHREIBER, U., BILGER, W. AND NEUBAUER, C. (1994). Chlorophyll fluorescence as a non-intrusive indicator for rapid assessment of in vivo photosynthesis. *Ecol. Studies.*, **100**: 49–70.
- SCHUBERT, H. AND FORSTER, R. M. (1997). Sources of variability in the factors used for modelling primary productivity in eutrophic waters. *Hydrobiologia*, **349**: 75–85.
- SCHUMANN, A., GOSS, R., JAKOB, T. AND WILHELM, C. (2007). Investigation of the quenching efficiency of diatoxanthin in cells of *Phaeodactylum tricoratum* (Bacillariophyceae) with different pool sizes of xanthophyll cycle pigments. *Phycologia*, **46**: 113–117.
- SERÔDIO, J. AND LAVAUD, J. (2010). A model for describing the light response of the non-photochemical quenching of chlorophyll fluorescence. *Photosynth. Res.*, **108**: 61–76.
- SERÔDIO, J., CRUZ, S., VIEIRA, S. AND BROTA, V. (2005). Non-photochemical quenching of chlorophyll fluorescence and operation of the xanthophyll cycle in estuarine microphytobenthos. *J. Exp. Mar. Biol. Ecol.*, **326**: 157–169.
- SHALAPYONOK, A., OLSON, R. J. AND L. S. SHALAPYONOK, L. S. (2001). Arabian Sea phytoplankton during South West and Northeast Monsoons 1995: Composition, size structure and biomass from individual cell properties measured by flow cytometry. *Deep-Sea Res. Pt. II*, **48**: 231–261.
- SIEBURTH, J. M., SMETACEK, V. AND LENZ, J. (1978). Pelagic ecosystem structure: Heterotrophic compartments of plankton and their relationship to plankton size fractions. *Limnol. Oceanogr.*, **33**: 1225–1227.
- SIEFERMANN, D. AND AMOTO, H. (1975). NADPH and oxygen-dependent epoxidation of zeaxanthin in isolated chloroplasts. *Biochem. Biophys. Res. Co.*, **62**: 456–461.
- SIX, C., SHERRARD, R., LIONARD, M., ROY, S. AND CAMPBELL, D. A. (2009). Photosystem II and pigment dynamics among ecotypes of the Green Alga *Ostreococcus*. *Plant Physiol.*, **151**: 379–390.
- SIX, C., FINKEL, Z. V., RODRIGUEZ, F., MARIE, D., PARTENSKY, F. AND CAMPBELL, D. A. (2008). Contrasting photoacclimation costs in ecotypes of the marine eukaryote picoplankton *Ostreococcus*. *Limnol. Oceanogr.*, **53**: 255–265.
- SIX, C., FINKEL, Z. V., IRWIN, A. J. AND CAMPBELL, D. A. (2007). Light variability illuminates niche partitioning among marine picocyanobacteria. *PLoS ONE*, **2**: e134, DOI: 10.1371/journal.pone.0001341
- SMETACEK, V. (1999). Diatoms and the ocean carbon cycle. *Protist*, **150**: 25–32.

- SOMMER, U. (1989). Maximal growth rates of Antarctic phytoplankton: Only weak dependence on cell size. *Limnol. Oceanogr.*, **34**: 1109–1112.
- SPRULES, W. G. AND MUNAWAR, M. (1986). Plankton size spectra in relation to ecosystem productivity, size and perturbation. *Can. J. Fish. Aquat. Sci.*, **43**: 1789–1794.
- STAEHR, P. A., HENRIKSEN, P. AND MARKAGER, S. (2002). Photoacclimation of four marine phytoplankton species to irradiance and nutrient availability. *Mar. Ecol. Prog. Ser.*, **238**: 47–59.
- STAUBER, J. L. AND JEFFREY, S. W. (1988). Photosynthetic pigments in fifty-one species of marine diatoms. *J. of Phycol.*, **24**: 158–172.
- STEHFEST, K., TOEPEL, J. AND WILHELM, C. (2005). The application of micro-FTIR spectroscopy to analyze nutrient stress-related changes in biomass composition of phytoplankton algae. *Plant Physiol. Biochem. (Paris)*, **43**: 717–726.
- STEMMANN, L., JACKSON, G. A. AND IANSON, D. (2004). Vertical model of particle size distributions and fluxes in the midwater column that includes biological and physical process – Part I. Model formulation. *Deep Sea Res. I*, **51**: 856–884.
- STEMMANN NIELSEN, E. AND V. K. HANSEN, V. K. (1959). Light adaptation in marine phytoplankton population and its interrelation with temperature. *Physiol. Plant.*, **14**: 595–613.
- STERNER, R. W. AND ELSER, J. J. (2002). *Ecological Stoichiometry: The Biology of the Elements from Molecules to the Biosphere*. Princeton University Press, Princeton.
- STODEREGGER, K. E. AND HERNDL, G. J. (1999). Production of exopolymer particles by marine bacterioplankton under contrasting turbulence conditions. *Mar. Ecol. Prog. Ser.*, **189**: 9–16.
- STODEREGGER, K. AND HERNDL, G. J. (1998). Production and release of bacterial capsular material and its subsequent utilization by marine bacterioplankton. *Limnol. Oceanogr.*, **43**: 877–884.
- STOLTE, W., KRAAY, G. W., NOORDELOOS, A. A. M. AND RIEGMAN, R. (2000). Genetic and physiological variation in pigment composition of *Emiliania huxleyi* (prymnesiophyceae) and the potential use of its pigment ratios as a quantitative physiological marker. *J. Phycol.*, **36**: 529–539.
- STOMP, M., HUISMAN, J., DE JONGH, F., VERAART, A., GERLIA, D., RIJKBOER, M., IBELINGS, B. W., WOLFFENZIE, U. I. A. AND STAL, L. J. (2004). Adaptive divergences in pigment composition promotes phytoplankton biodiversity. *Nature*, **432**: 104–107.

- STRANSKY, H. AND HAGER, A. (1970). Das Carotinoidmuster und die Verbreitung des lichtinduzierten Xanthophyll-Cyclus in verschiedenen Alganklassen. VI Chemosystematische Betrachtung. *Arkiv für Mikrobiologie*, **75**: 315–323.
- STRZALKA, K., KOSTECKA-GUGALA, A. AND LATOWSKI, D. (2003). Carotenoids and environmental stress in plants: significance of carotenoid-mediated modulation of membrane physical properties. *Russian J. Plant Physiol.*, **50**: 168–172.
- STRZEPEK, R. F. AND HARRISON, P. J. (2004). Photosynthetic architecture differs in costal and oceanic diatoms. *Nature*, **431**: 689–692.
- SUGGETT, D., PRÁŠIL, O. AND BOROWITZKA, M. (2010). *Chlorophyll a fluorescence in aquatic sciences: methods and applications*. Springer, UK.
- SUKENIK, A., BENNETT, J. AND FALKOWSKI, P. G. (1987). Light-saturated photosynthesis-limitation by electron transport or carbon fixation? *Biochim. Biophys. Acta*, **891**: 205–215.
- SULLIVAN, M. B., COLEMAN, M. L., WEIGELE, P., ROHWER, F. AND CHISHOLM, S. W. (2005). Three *Prochlorococcus* cyanophage genomes: signature features and ecological interpretations. *PLoS Biology*, **3**: 0790–0806.
- SUZUKI, K., MINAMI, C., LIU, H. AND SAINO, T. (2002). Temporal and spatial patterns of chemotaxonomic algal pigments in the subarctic Pacific and the Bering Sea during the early summer of 1999. *Deep Sea Res. Pt. II*, **49**: 5685–5704.
- SZÁBO, I., BERGANTINO, E. AND GIACOMETTI, G. M. (2005). Light and oxygenic photosynthesis: energy dissipation as a protection mechanism against photo-oxidation. *EMBO reports*, **6**: 629–634.
- TAGUCHI, S. (1976). Relationship between photosynthesis and cell size of marine diatoms. *J. Phycol.*, **12**: 185–189.
- TAKEGUCHI, C. A. AND YAMAMOTO, H. Y. (1968). Light-induced $^{18}\text{O}_2$ uptake by epoxy xanthophylls in New Zealand spinach leaves *Tetragonia expansa*. *Biochim. Biophys. Acta*, **153**: 459–465.
- TAKISHITA, K., ISHIDA, K. I., MARUYAMA, T. (2004). Phylogeny of nuclear-encoded plastid-targeted GAPDH gene supports separate origins for the peridinin and the fucoxanthin derivative containing plastids of dinoflagellates. *Protist*, **155**: 447–458.
- TASSAN, S. AND FERRARI G. M. (1995). An alternative approach to absorption measurements of aquatic particles retained on filters. *Limnol. Oceanogr.*, **40**: 1358–1368.

- TAYLOR, F. J. R. (1976). Flagellate Phylogeny: A Study in Conflicts. *Journal of Protozoology*, **23**: 28–40.
- TELFER, A. (2002). What is carotene doing in the photosystem II reaction centre? *Philos. Trans. R. Soc. Lond.*, **357**: 1431–1440.
- TESSON, S. V. M. (2010). Population genetic structure of a planktonic diatom in the Gulf of Naples: *Pseudo-nitzschia multistriata*. O.U. PhD Thesis.
- THOMSEN, H. A. (1986). A survey of the smallest eukaryotic organisms of the marine phytoplankton. *Can. B. Fish. Aquat. Sci.*, **214**: 121–158.
- TIMMERMANS, K. R., VAN DER WAGT, B., VELDHUIS, M. J. W., MAATMAN, A. AND DE BAAR, H. J. W. (2005). Physiological responses of three species of marine picophytoplankton to ammonium, phosphate, iron and light limitation. *J. Sea Res.*, **53**: 109–120.
- TRANTAPHYLLIDES, C. AND HAVAUX, M. (2009). Singlet oxygen in plants: production, detoxification and signaling. *Trends Plant Sci.*, **14**: 219–228.
- URSI, S., PEDERSÉN, M., PLASTINO, E. AND SNOEIJIS, P. (2003). Intraspecific variation of photosynthesis, respiration and photoprotective carotenoids in *Gracilaria birdie* Gracilariales (Rhodophyta). *Mar. Biol.*, **142**: 997–1007.
- VAN AMERONGEN, H. AND DEKKER, J. P. (2003). Light-harvesting in photosystem II. In: Green, B. and Parson, W. W. (Eds.), *Light-Harvesting Antennas in Photosynthesis: Advances in Photosynthesis and Respiration*. Pages: 219–251, Dordrecht, Kluwer.
- VAN DE POLL, W. H., BUMA, A. G. J., VISSER, R. J. W. ET AL. (2010). Xanthophyll cycle activity and photosynthesis of *Dunaliella tertiolecta* (Chlorophyceae) and *Thalassiosira weissflogii* (Bacillariophyceae) during fluctuating solar radiation. *Phycologia*, **49**: 249–259.
- VAN DE POLL, W. H., VISSER, R. J. W. AND BUMA, A. G. J. (2007). Acclimation to a dynamic irradiance regime changes excessive irradiance sensitivity of *Emiliana huxleyi* and *Thalassiosira weissflogii*. *Limnol. Oceanogr.*, **52**: 1430–1438.
- VAN LEEUWE, M. A., BROUWER, V., CONSALVEY, M. ET AL. (2008). Photoacclimation in microphytobenthos and the role of the xanthophylls cycle. *Eur. J. Phycol.*, **43**: 123–132.
- VAN LEEUWE, M. A., VAN SIKKELERUS, B., GIESKES, W. W. C. AND STEFELS, J. (2005). Taxon specific differences in photoacclimation to fluctuating irradiance in an Antarctic diatom and a green flagellate. *Limnol. Oceanogr.*, **288**: 9–19.

- VAULOT, D., EIKREM, W., VIPREY, M., AND MOREAU, H. (2008). The diversity of small eukaryotic phytoplankton ($\leq 3 \mu\text{m}$) in marine ecosystems. *FEMS Microbiol. Rev.*, **32**: 795–820.
- VAULOT, D., LE GALL, F., MARIE, D., GUILLOU, L. AND PARTENSKY, F. (2004). The Roscoff Culture Collection (RCC): a collection dedicated to marine picoplankton. *Nova Hedwigia*, **79**: 49–70.
- VAULOT, D, ROMANI, K., NOT, F. (2002). Are autotrophs less diverse than heterotrophs in marine picoplankton? *Trends Microbiol.*, **10**: 266–267.
- VEITH, T. AND BÜCHEL, C. (2007). The monomeric photosystem I complex of the diatom *Phaeodactylum tricornutum* binds specific fucoxanthin chlorophyll proteins (FCPs) as light-harvesting complexes. *Biochim. Biophys. Acta*, **1767**: 1428–1435.
- VEITH, T., BRAUNS, J., WEISHEIT, W., MITTAG, M. AND BÜCHEL, C. (2009). Identification of a specific fucoxanthin chlorophyll protein in the light harvesting complex of photosystem I in the diatom *Cyclotella meneghiniana*. *Biochim. Biophys. Acta*, **1787**: 905–912.
- VELDHUIS, M. J. W., TIMMERMANS, K. R., CROOT, P. AND VAN DER WAGT, B. (2005). Picophytoplankton a comparative study of their biochemical composition and photosynthetic properties. *J. Sea Res.*, **53**: 7–24.
- VELDHUIS, M. J. W. AND KRAAY, G. (2004). Phytoplankton in the subtropical Atlantic Ocean: towards a better assessment of biomass and composition. *Deep-Sea Res. I*, **51**: 507–530.
- VENTER, J. C., REMINGTON, K., HEIDELBERG, J. F. ET AL. (2004). Environmental genome shotgun sequencing of the Sargasso Sea. *Science*, **304**: 66–74.
- VERMAAS, W. (1993). Molecular-biological approaches to analyze photosystem II structure and function. *Annu. Rev. Plant Physiol. Plant Mol. Biol.*, **44**: 457–481.
- VIDUSSI, F., CLAUSTRE, H., BUSTILLOS-GUZM'AN, J., CAILLIAU, C. AND. MARTY, J. C. (1996). Determination of chlorophylls and carotenoids of marine phytoplankton: separation of chlorophyll *a* from divinyl-chlorophyll *a* and zeaxanthin from lutein. *J. Plankton Res.*, **18**: 2377–2382.
- VOLK, T. AND HOFFERT, M. I. (1985). Ocean carbon pumps: analysis of relative strengths and efficiencies in ocean-driven atmospheric CO₂ exchanges. In: Sunquist, E.T. and Broecker, W.S. (Eds.), *The Carbon Cycle and Atmospheric CO₂: Natural Variations Archean to Present*. Pages: 99–110. American Geophysical Union, Washington, DC, USA.

- WAGNER, H., JAKOB, T. AND WILHELM, C. (2006). Balancing the energy flow from captured light to biomass under fluctuating light conditions. *New Phytol.*, **169**: 95–108.
- WALTERS, R. G., RUBAN, A. V. AND HORTON, P. (1994). Higher plant light harvesting complexes LHCIIa and LHCIIc are bound by dicyclohexylcarbodiimide during inhibition of energy dissipation. *Eur. J. Biochem.*, **226**: 1063–1069.
- WATERBURY, J. B., WATSON, S. W., GUILLARD, R. R. L. AND BRAND, L. E. (1979). Widespread occurrence of a unicellular, marine planktonic, cyanobacterium. *Nature*, **277**: 293–294.
- WATSON, A. J. AND LISS, P. S. (1998). Marine biological controls on climate via the carbon and sulphur geochemical cycles. *Phil. Trans. R. Soc. Lond. B*, **353**: 41–51.
- WESTERMANN, M. AND RHIEL, E. (2005). Localisation of fucoxanthin chlorophyll *a/c* binding polypeptides of the centric diatom *Cyclotella cryptica* by immuno-electron microscopy. *Protoplasma*, **225**: 217–223.
- WHITE, A. J. AND CRITCHLEY, C. (1999). Rapid light curves: a new fluorescence method to assess the state of the photosynthetic apparatus. *Photosynth. Res.*, **59**: 63–72.
- WHITMARSH, J. AND GOVINDJEE (1999). The photosynthetic process. In: Singhal, G. S., Renger, G., Sopory, S. K., Irrgang, K. D. and Govindjee (Eds.), *Concepts in photobiology: Photosynthesis and photomorphogenesis*. Page: 11–51. Narosa Publishers and Kluwer Academic Publishers, Dordrecht, The Netherlands.
- WILHELM, C. (1993). Some critical remarks on the suitability of the concept of the photosynthetic unit in photosynthesis research and phytoplankton ecology. *Bot Acta*, **106**: 287–293.
- WILHELM, C. (1990). The biochemistry and physiology of light-harvesting processes in chlorophyll *b*- and chlorophyll *c*-containing algae. *Plant Physiol. and Biochem*, **28**: 293–306.
- WILSON, A., PUNGINELLI, C., GALL, A. ET AL. (2008). A photoactive carotenoid protein acting as light intensity sensor. *Proc. Natl. Acad. Sci. U. S. A.*, **33**: 12075–12080.
- WILSON, A., BOULAY, C., WILDE, A., KERFELD, C. A. AND KIRILOVSKY, D. (2007). Light-induced energy dissipation in iron-starved cyanobacteria: roles of OCP and IsiA proteins. *Plant Cell*, **19**: 656–672.
- WILSON, A., AJLANI, G., VERBAVATZ, J.-M., VASS, I., KERFELD, C. A. AND KIRILOVSKY, D. (2006). A soluble carotenoid protein involved in phycobilisome-related energy dissipation in cyanobacteria. *Plant Cell*, **18**: 992–1007.

- WILSON, W. H., SCHROEDER, D. C., ALLEN, M. J ET AL. (2005). Complete genome sequence and lytic phase transcription profile of a *Coccolithovirus*. *Science*, **309**: 1090–1092.
- WORDEN, A. Z., LEE, J. H., MOCK, T. ET AL. (2009). Green evolution and dynamic adaptations revealed by genomes of the marine picoeukaryotes *Micromonas*. *Science*, **324**: 268–272.
- WORDEN, A. Z. AND NOT, F. (2008). Ecology and diversity of picoeukaryotes. In: Kirchman D. L. (Ed.), *Microbial Ecology of the Oceans* (2nd Ed.). Pages: 159–205. Wiley & Sons.
- WORDEN, A. Z., NOLAN, J. K., AND PALENIK, B. (2004). Assessing the dynamics and ecology of marine picophytoplankton: The importance of the eukaryotic component. *Limnol. Oceanogr.*, **49**: 168–179.
- XIONG, J., SUBRAMANIAM, S. AND GOVINDJEE. (1996). Modeling of the D1/D2 proteins and cofactors of the photosystem II reaction center: Implications for herbicides and bicarbonate binding. *Prot. Sci.*, **5**: 2054–2073.
- YAMAMOTO, H. Y. AND BASSI, R. (1996). Carotenoids: Localization and function. In Ort, D. and Yokum, C. (Eds.), *Advances in photosynthesis. Oxygenic photosynthesis: The light reactions*. Pages: 539–563. Kluwer Academic Publishers, The Netherlands.
- YAMAMOTO, H. Y., BUGOS, R. C. AND HIEBER, A. D. (1996). Biochemistry and molecular biology of the xanthophylls cycle. In Frank, A., A. Young, A., Britton, G. and R. Cogdell, R. (Eds.), *The photochemistry of carotenoids*. Kluwer Academic Publishers, Dordrecht.
- YAMAMOTO, H. AND HIGASHI, R. (1978). Violaxanthin de-epoxidase. Lipid composition and substrate specificity. *Arch Biochem Biophys*, **90**: 514–522.
- YAMAMOTO, H. Y., CHENCHIN, E. E. AND YAMADA, D. K. (1974). Effect of chloroplast lipids on violaxanthin de-epoxidase activity. In Proceedings of the 3rd International Cong. Photosyn., Pages: 1999–2006. Elsevier, Amsterdam.
- YAMAMOTO, H.Y. AND KAMITE, L. (1972). The effects of dithiothreitol on violaxanthin de-epoxidation and absorbance changes in the 500- nm region. *Biochim. Biophys. Acta*, **267**: 538–543.
- YAMAMOTO, H., NAKAYAMA, T. AND CHICHESTER, C. (1962). Studies on the light and dark interconversions of leaf xanthophylls. *Arch. Biochem. Biophys.*, **97**: 168–173.
- ZAPATA, M., JEFFREY, S. W., WRIGHT, S. W., RODRIGUEZ, F., GARRIDO, J. L. AND CLEMENTSON, L. (2004). Photosynthetic pigments in 37 species (65 strains) of

- Haptophyta: implications for oceanography and chemotaxonomy. *Mar. Ecol. Prog. Ser.* **270**: 83–102.
- ZINGONE, A., BORRA, M., BRUNET, C., FORLANI, G., KOOISTRA, W. H. C. F. AND PROCACCINI, G. (2002). Phylogenetic position of *Crustomastix stigmatica* sp. nov. and *Dolichomastix tenuilepsis* in relation to the mamiellales (Prasinophyceae, Chlorophyta). *J. Phycol.*, **38**: 1024–1039.
- ZHU, S. H. AND GREEN, B. R. (2010). Photoprotection in the diatom *Thalassiosira pseudonana*: role of LI818-like proteins in response to high light stress. *Biochim. Biophys. Acta*, **1797**: 1449–1457.
- ZUBKOV, M. V., M. A. SLEIGH, G. A. TARRAN, P. H. BURKILL, AND R. J. G. LEAKEY. (1998). Picoplankton community structure on an Atlantic transect from 508N to 508S. *Deep-Sea Res.*, **45**: 1339–1355.